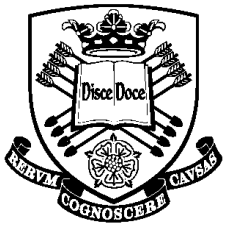

The University Of Sheffield.

Department of Mechanical Engineering

PISA Block Copolymers prepared via RAFT Polymerisation for use as Friction Modifiers

Liam **Pratt**

JULY 2022

Professor Rob Dwyer-Joyce, Professor Steve Armes

Thesis submitted to the Department of Mechanical Engineering, University of Sheffield in partial fulfilment of the requirements for the degree of PhD

[Page intentionally left blank]

Contents

Acknowledgments

I'd like to give all my thanks to all the people who have supported me throughout my PhD. My supervisors: Rob, Steve, and Matt for your support throughout, your knowledge and feedback has been invaluable. To my examiners, who have provided me with expertise to ensure this thesis is as good as possible. Also thanks to the EPRSC for their funding throughout.

Thanks to all those in the iT-CDT and the tribology department who supported me with my work, provided me with insight, and supported me emotionally throughout the process. In particular thanks to Rodders and Will who had to put up with me throughout the various Covid lockdowns and helped support me throughout.

Thank you to my Mum, Dad, and Izzie Johnson who supported me through large chunks of my PhD. Finally and perhaps the greatest thanks to Izzie Blood, you supported me when times were toughest and helped keep me going when I was struggling. I wouldn't have completed this thesis without your support and I can't thank you enough.

Abstract

Friction modifiers are chemical additives for motor oils, they are used to reduce frictional losses within an engine in order to improve it's efficiency. Poly(Stearylmethacrylate)-Poly(Benzylmethacrylate) (PSMA-PBzMA) nanoparticles were synthesised via a one-pot polymerisation-induced self assembly reaction using a RAFT control group and tested for use as friction modifiers. 11 different sized nanoparticles were synthesised with and without ethylene glycol dimethacrylate cross-linking. These were synthesised with good chain length control, as measured by GPC, and formed stable spherical nanoparticles with small variance in nanoparticle diameter, as measured by DLS, TEM and SAXS.

These nanoparticles were tested in a variety of different tribological contacts in order to establish their effect on friction within a contact, these include across all sliding:rolling ratios as well as in a linear and reciprocating contact. These tests show that small nanoparticles ($PSMA_{30}PBzMA_{40}$ primarily tested) show reduced friction across all contact environments and speeds, with particularly large friction reduction in the boundary regime, with cross-linking of these nanoparticles appearing to improve their long term friction reduction. Larger nanoparticles ($PSMA_{30}PBzMA_{200}$ primarily tested) show larger friction reduction in the boundary lubrication regime in some contact environments, in particular the cross-linked equivalent. This effect though is not present across all types of contact, e.g. high sliding:rolling ratios. This shows that small cross-linked PSMA-PBzMA nanoparticles (23-30nm) can be effective friction modifiers in an internal combustion engine, while larger nanoparticles are likely only effective in niche environments. These nanoparticles also have no effect on wear of the contact or viscosity of the oil and were shown to be stable long term upon completion of tribological testing, indicating these nanoparticles can be effective long term friction modifiers with little effect on other tribological properties within an ICE.

Mechanistic analysis of how these nanoparticles reduce friction within a contact was undertaken by analysing the film generation and nanocompression. These showed that these nanoparticles rapidly formed a stable tribofilm upon the contact, these nanoparticles are then easily compressed within a contact while being soft and easily sheared, resulting in a very low friction contact by preventing contact of the hard steel surfaces. Upon exiting the contact they then display an elastic property to rebound back to their original shape, allowing for long term friction reduction.

Testing of PDMAC-PDAAM water soluble nanoparticles also displayed friction reduction in the boundary lubrication regime, indicating that this friction reducing effect is common across a wide variety of polymerisation induced self assembled nanoparticles.

List of Figures

List of Tables

Acronyms

ICE	Internal Combustion Engine
MoDTC	Molybdenum Dithiocarbonate
SMA	Stearyl Methacrylate
PSMA	Polymerised Stearyl Methacrylate
BzMA	Benzyl Methacrylate
PBzMA	Polymerised Benzyl Methacrylate
OFM	Organic Friction Modifier
DP	Degree of Polymerisation
CTA	Chain Transfer Agent
TEMPO	(2,2,6,6-Tetramethylpiperidin-1-yl)oxyl
ATRP	Atom Transfer Radical Polymerisation
RAFT	Reversible Addition-Fragmentation Chain-Transfer
PISA	Polymerisation Induced Self-Assembly
GMO	Glycerol Monooleate
DLC	Diamond-like Carbon
PE	Polyethylene
IL	Ionic Liquid
ZDDP	Zinc Dialkyldithiophosphates
AFM	Atomic Force Microscopy
MoDPP	Molybdenum Diakyldithiophosphate
XPS	X-ray Photoelectron Spectroscopy

ToF-Sims	Time-of-Flight Secondary Ion Mass Spectrometry
IF	Inorganic Fullerene
TEM	Transmission Electron Microscopy
SEM	Scanning Electron Microscopy
PAO	Polyalphaolefin
EDS	Energy Dispersive Spectroscopy
PVP	Polyvinylpyrrolidone
PETTC	Cyano-4-(Phenylcarbonothioylthio) Pentanoic acid
T21S	Tert-Butyl Peroxy-2-Ethylhexanoate
EGDMA	Ethylene Glycol Dimethacrylate
PEGDMA	Polymerised Ethylene Glycol Dimethacrylate
NMR	Nuclear Magnetic Resonance
GPC	Gel Permeation Chromotography
THF	Tetrahydrofuran
DLS	Dynamic Light Scattering
SAXS	Small Angle X-ray Scattering
MTM	Mini Traction Machine
S:R	Sliding:Rolling ratio
UMT	Universal Machine Tribometer
ASTM	American Society for Testing Materials
SLIM	Spacial Layer Imaging
RGB	Red Green Blue
QCM	Quartz Crystal Microbalance
DDMAT	2-(Dodecylthiocarbonothioylthio)-2-Methylpropionic Acid
DMAC	Dimethylacetamide
PDMAC	Polymerised Dimethylacetamide
AIBN	Azobisisobutyronitrile

DAAM	Diacetone Acrylamide
PDAAM	Polymerised Diacetone Acrylamide
ADH	Adipic Acid Dihydrazide
ACVA	4,4'-Azobis(4-Cyanovaleric Acid)
DMF	Dimethylformamide

Nomenclature

η	Dynamic Viscosity (Pas)
λ	Lambda ratio
λ	Wavelength
μ	Friction Coefficient
ν	Poissons Ratio
ρ	Density (Kg/m^3)
σ	Surface Roughness (nm)
θ	Half Scattering Angle
A_r	Contact Area
alpha	Pressure-Viscosity Coefficient (mm^2/N)
E	Young's Modulus
E^*	Effective Reduced Modulus
F	Load (N)
G	Material Parameter
H	Dimensionless Film Thickness
h	Film Thickness (nm)
k	Thermal Conductivity ($W/m.K$)
l_f	Equivalent Linear Heat Diffusion
P	Pressure (Pa)
R	Reduced radius
R_a	Mean Surface Roughness Amplitude (nm)
t	Time (s)
T_b	Bulk Temperature ($°C$)
T_f	Flash Temperature ($°C$)
U	Dimensionless Speed
u	Entrainment speed (m/s)
v	Velocity (m/s)
W	Dimensionless Load
$\mathrm{D_{int}}$	Mean distance between adjacent chains at core-shell interface
$\mathrm{D_s}$	Spherical Core Diameter
$\mathrm{M_i}$	Molecular Weight of a Polymer Chain
$\mathrm{M_n}$	Number Average Molecular Weight
$\mathrm{M_w}$	Weight Average Molecular Weight
$\mathrm{N_{agg}}$	Mean Aggregation Number
$\mathrm{N_i}$	Number of Polymer Chains
q	Scattering vector
$\mathrm{S_{agg}}$	Number of Copolymers per surface area

Chapter 1

Introduction

1.1 Statement of the Problem

With the increasing drive to a more environmentally friendly and sustainable future the improved efficiency of all motors is of vital importance. In cars 17% of energy produced by the ICE is lost due to friction within the engine and transmission.(Holmberg et al., 2012) Reducing this frictional loss, in particular in the boundary lubrication regime where friction is highest, would improve efficiency of vehicles and allow for less fuel to be required to generate the same amount of power to the wheels. This strive for decreased friction loss continues to drive the development of motor oils and the additives within them, in particular friction modifier additives.

Friction modifiers are oil additives that act to reduce friction of the contact by reducing the contact between hard metal surfaces. There are a large number of commercially viable friction modifiers such as glycerol monooleate and MoDTC have displayed the ability to reduce friction in the boundary lubrication regime but these friction modifiers often have some issues such as being ineffective in some contact environments, long term ineffectiveness or environmental impact. This means the continued research and development of friction modifiers is necessary to provide optimal friction reduction in all ICEs and machines.

A novel look into friction modifiers is the use of nanoparticle friction modifiers. Here a nano-sized molecule enters the contact and prevents surface contact and in doing so

reduces friction of the contact. These nanoparticles though often are expensive to produce, not soluble within mineral oil and have high hardness; making them not appropriate as commercial friction modifiers.

This means that the development of a inexpensive, soft, readily soluble nanoparticle as a friction modifier would potentially allow for the reduction of friction within an ICE without the drawbacks of other nanoparticle additives. One potential solution to this is the use of polymeric nanoparticles that are synthesised in situ of the mineral oil. This is achieved by polymerisation-induced self assembly. Here a block copolymer is synthesised where one block is soluble within the oil and the other is insoluble. This results in the soluble block surrounding the insoluble block and forming a nanoparticle. These nanoparticles should then be capable of entering a contact, preventing surface contact and maintaining or reforming their shape to allow for prolonged friction reduction.

1.2 Aims and Objectives

1.2.1 Project Aim

The aim of this project is to develop an effective friction modifier using PISA PSMA-PBzMA block copolymers and establish the mechanism by which they act to reduce friction.

1.2.2 Project Objectives

- Synthesise PSMA-PBzMA nanoparticles via a one-pot protocol within mineral oil.
- Establish the effects of PSMA-PBzMA nanoparticles on friction of a number of contact types.
- Establish the effects PSMA-PBzMA nanoparticles on other tribological properties e.g. wear and viscosity
- Establish the long term stability of PSMA-PBzMA nanoparticles within an contact.

- Establish the mechanism by which PSMA-PBzMA interact within a tribological contact.
- Investigate other PISA nanoparticles to develop a thorough understanding of their effect on tribological contacts.

1.3 Thesis Layout

- **Chapter 2: Theory of Lubrication**

  This chapter will describe how lubrication affects a tribological contact and how the addition of friction modifiers such as the polymer nanoparticles described in this thesis can affect this.

- **Chapter 3: Theory of Polymerisation**

  This chapter will describe the fundamentals of polymers and their formation and allow for an understanding of the formation of the nanoparticles described in this thesis.

- **Chapter 4: Literature Review**

  This chapter will provide an analysis on the current state of research into friction modifiers. This will allow for investigation into the benefits and drawbacks of currently available friction modifiers as well as display the reasoning for the testing of the nanoparticle friction modifiers described in this thesis.

- **Chapter 5: Synthesis and Chemical Analysis of Nanospheres**

  This chapter will describe how the nanoparticles described in this thesis are synthesised and the effectiveness of this polymerisation, both in terms of the formation of polymer chains and also the formation of nanoparticles.

- **Chapter 6: Methodology for Tribological Testing**

  This chapter will detail the experiments that were undertaken throughout the tribological testing of these nanoparticles.

- **Chapter 7: Tribological Testing of Nanospheres**

  This chapter will provide the testing results to establish the ability of these nanoparticles as friction modifiers, as well as their long term stability upon completion of this testing.

- **Chapter 8: Mechanistic Analysis**

  This chapter will investigate how the nanoparticles described in the thesis act within a contact, both their ability to form a film within the contact and also how they respond to the pressure associated with a tribological contact.

- **Chapter 9: Water Soluble Nanoparticles**

  This chapter investigates different chemistry nanoparticles PDMAC-PDAAM that are formed in a similar manner to the PSMA-PBzMA nanoparticles descibed in this thesis. These nanoparticles are soluble in water rather than oil and as such will provide insight into if any friction reduction is a chemistry specific or more universal to polymerisation-induced self-assembled nanoparticles.

- **Chapter 10: Conclusions and Future Work**

  This chapter will summarise the findings of this thesis as well as stating the potential gaps in the research that could be further investigated.

Chapter 2

Theory of Lubrication

2.1 Introduction

This chapter will underline the basic principle of liquid lubrication and the additives that enable the effective running of an engine or transmission system. Particular focus of this thesis will be put onto friction modifiers which are oil additives which act to reduce friction within an engine or transmission system.

2.2 Introduction To Lubrication

Lubrication is the addition of a third body to a contact; this separates the contacting surfaces and allows for smoother movement. Lubrication can have many effects on the system: including reducing friction and wear, cooling the surfaces or removing impurities from the contact. There are two main types of lubrication, solid and liquid, but this thesis will focus on liquid lubrication.

Modern-day liquid lubricants comprise two parts: the base oil, which comprises the long-chain carbons extracted from oil and chemical additives. Base oils were selected since they meet all of the required characteristics of a lubricant: they have a high boiling point and low freezing point, high viscosity index; high thermal stability; high hydraulic stability, are insoluble in water; prevent corrosion and are highly resistant to oxidation.(Hutchings and Shipway, 2017) Common types of oils are shown in Figure 2.1.

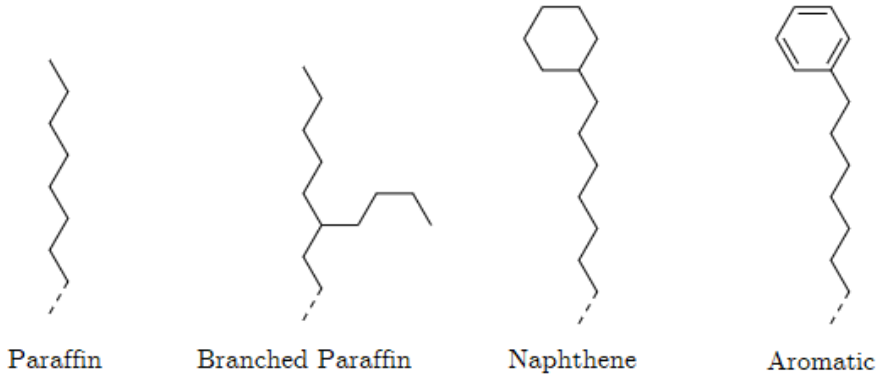

Figure 2.1: Common types of Lubricating Oil

Chemical additives typically make up approximately 10-30% of the lubricant and are a variety of compounds that are added to give the lubricant different chemical and physical properties. These additives are typically split into three main areas. Lubrication protective additives are additives that act to protect and maintain the lubricant quality; these prevent any breakdown or accumulation of the lubricant chains and, as such, allow them to maintain their lubricating properties. Examples of this include anti-foaming agents, which prevent foam formation within the lubricant; anti-oxidants, which prevent any oxidative decomposition of the lubricant; and metal deactivators, which prevent metals present from having a catalytic effect on lubricant oxidation. Performance additives act to improve the ability of the lubricant to perform its function. The primary examples of this are: pour point depressants, these improve the flow of lubricant at lower temperatures; seal swell agents, these act to increase the size of the seals within the engine, thus preventing oil leakage, and viscosity modifiers which act to prevent the decrease in oil viscosity as the temperature of the oil increases. Surface protecting additives adsorb or bond to the contact surface and act to protect the contact surfaces. Examples of this are anti-wear agents; these form a hard film that lowers friction and wear of a contact. Corrosion and rust inhibitors; detergents keep surfaces free of deposits and neutralise acids at the surface. Dispersants that keep insoluble wear particles in solution and as such prevent them from wearing the contact. Finally, friction modifiers that are the main focus of this thesis and will be discussed further in this chapter. Some common oil additives are shown in Figure

$$HerseyNumber = \frac{\eta.N}{P} \tag{2.1}$$

2.1: Equation for the calculation of the Hersey Number. η is the viscosity of the oil, N is the speed of the contact and P is the linear load upon the contact.

2.2.

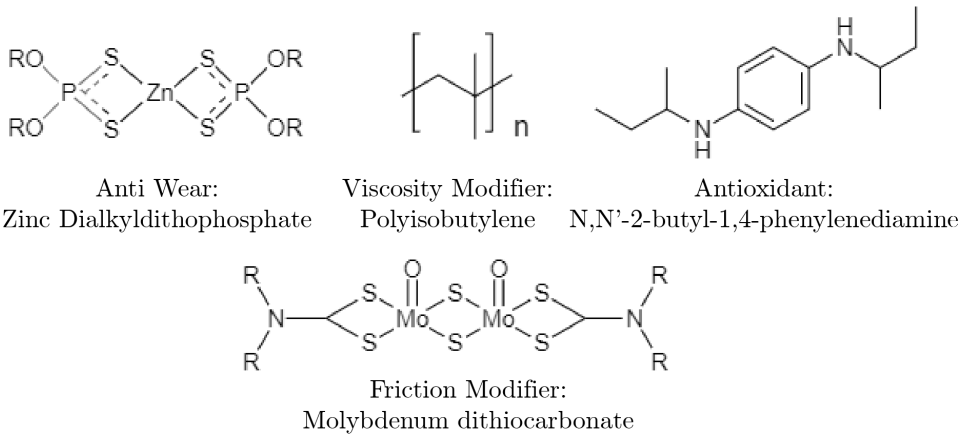

Anti Wear: Zinc Dialkyldithophosphate

Viscosity Modifier: Polyisobutylene

Antioxidant: N,N'-2-butyl-1,4-phenylenediamine

Friction Modifier: Molybdenum dithiocarbonate

Figure 2.2: Common Oil Additives

Development of these additives is of utmost importance for the continued improvement of the efficiency and lifetime of an ICE and many other types of machinery. There is also a large amount of research into decreasing the adverse effects of these additives, e.g. cost of production and the environmental effect of production, with substantial amounts of current research looking into reducing the environmental effects of additive presence in oil, e.g. reducing sulphur and heavy metal content of oil.

2.3 Friction in a Lubricated Contact

Unlike friction in an unlubricated contact, where the friction coefficient is proportional to only the load upon the contact, the addition of lubrication results in the friction coefficient varying depending upon various factors. These factors are described via Hersey number, which is shown in equation 2.1.

Hersey's number states the coefficient of friction of a lubricated contact is proportional to the lubrication's dynamic viscosity and contact speed but inversely proportional to the

load of the contact. These factors affect the ability of the lubricant to keep the contact separated; increasing the viscosity of the lubricant means it is less likely to be forced out of the contact, and increasing the speed means that more lubricant is pulled into the contact. Increasing the contact load means the lubricant is more likely to be pushed out of the contact. The Hersey number can be plotted against the coefficient of friction of a contact to show how the friction coefficient varies in a lubricated contact; this is known as the Stribeck curve and generally looks like Figure 2.3.

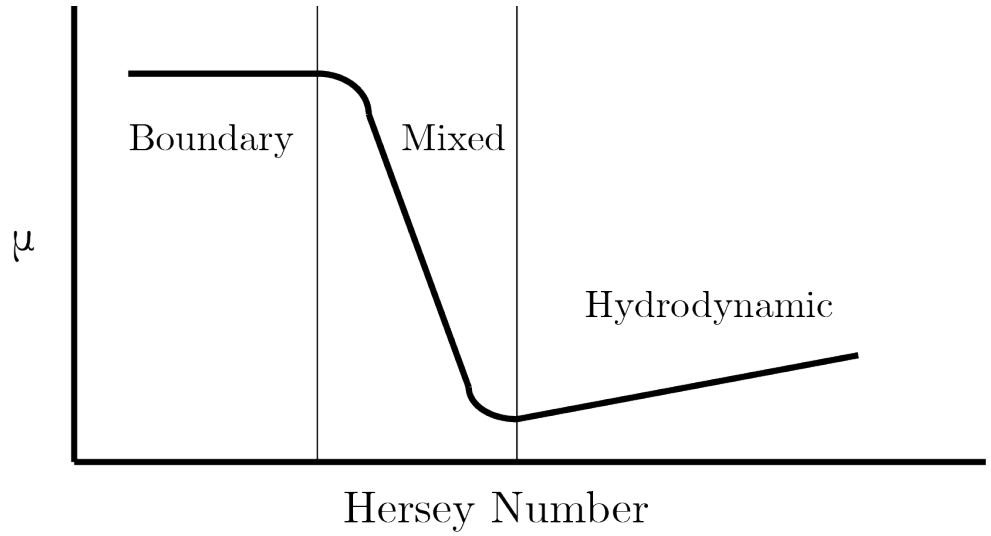

Figure 2.3: Typical Stribeck Curve

As shown in Figure 2.3, there are three distinct areas of the Stribeck curve. These are known as the lubrication regimes and are the boundary, mixed and hydrodynamic lubrication regimes.

2.3.1 Boundary Lubrication - High Asperity Pressure

Boundary lubrication is the area in which the friction coefficient is at its highest. Here there is insufficient lubricant to separate the contact resulting in a large amount of surface contact. This surface contact leads to a high amount of friction, and the coefficient of friction is high. A schematic for this is displayed in Figure 2.4.

Since the friction of a system is at its highest in the boundary lubrication regime, and that the majority of the friction effects are due to surface contact, this is the area in which

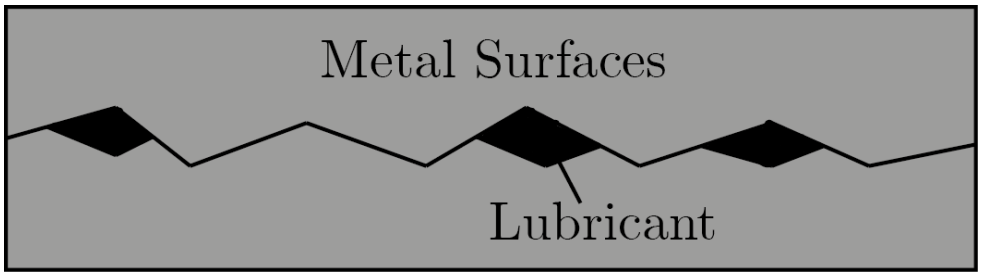

Figure 2.4: Schematic for Boundary Lubrication of a Contact

friction modifiers can have the most significant effect in reducing the friction of the system.

2.3.2 Mixed Lubrication- Asperity and Hydrodynamic Pressure

Mixed lubrication occurs when there is sufficient enough lubricant within the contact to begin to separate the surfaces, this results in less surface contact, and as a result, the friction begins to reduce. As the Hersey number increases, the degree of separation between surfaces also increases, resulting in the coefficient of friction decreasing.

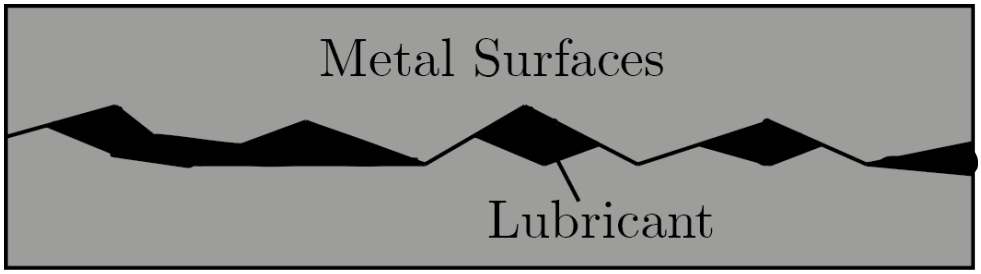

Figure 2.5: Schematic for Mixed Lubrication of a Contact

2.3.3 Elastohydrodynamic Lubrication

Elastohydrodynamic lubrication occurs when the pressure of the contact results in sufficient elastic deformity of the contacting surfaces asperities to allow a film of lubricant to separate the contact. This lubricant will be in a high pressure environment and such lubricant will sufficiently separate the contacts resulting in very low friction as no fluid friction is able to occur like in the hydrodynamic lubrication regime.

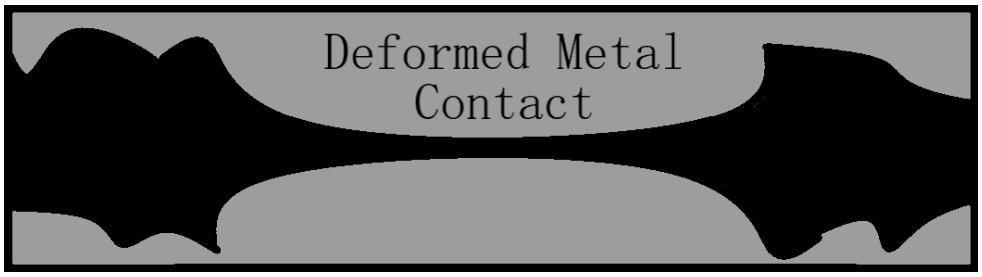

Figure 2.6: Schematic for Elastohydrodynamic Lubrication of a Contact

2.3.4 Hydrodynamic Lubrication- Hydrodynamic Pressure

Hydrodynamic lubrication occurs once the oil is capable of fully separating the contacting surfaces without the need for any surface deformation. As more oil enters the contact, there is an increase in the friction associated with the fluid particles passing past one another, or fluid friction. This fluid friction explains the increase in friction coefficient that is observed in the Stribeck curve, Figure 2.3, as the Hersey number increases.

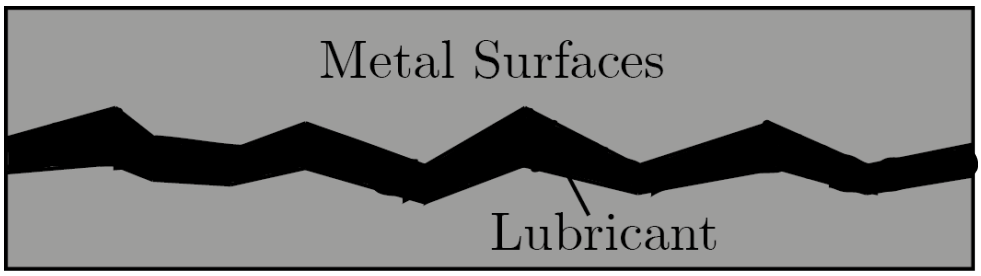

Figure 2.7: Schematic for Hydrodynamic Lubrication of a Contact

2.3.5 Lambda Ratio

It is possible to calculate the lubrication regime that a lubricated contact. This calculation is known as the lambda ratio. This is the ratio of lubricant film thickness compared to the contact surface roughness, as shown in Equation 2.2 here h is the film thickness and σ is the surface roughness. If the value of the lambda ratio is > 3 then the contact is in

$$\lambda = \frac{h}{\sigma} \tag{2.2}$$

2.2: Equation for calculation of the lambda ratio, here h is the film thickness and σ is the surface roughness.

the hydrodynamic regime, 1-3 is the mixed regime and < 1 is the boundary regime.

The film thickness is calculated using the Dowson and Hamrock solution as shown in Equation 2.3.(Dowson and Higginson, 1959).

$$
\begin{aligned}
H_{\mathrm{c}} = 2.69.U^{0.68}.G^{0.53}.W^{\text{-}0.067}.(1 - 0.61\exp -0.73k) \\
\frac{1}{R_{\mathrm{x}}} = \frac{1}{R_{1\mathrm{x}}} + \frac{1}{R_{2\mathrm{x}}} \\
\frac{1}{R_{\mathrm{y}}} = \frac{1}{R_{1\mathrm{y}}} + \frac{1}{R_{2\mathrm{y}}} \\
H = \frac{h}{R_{\mathrm{x}}} \\
U = \frac{\eta_0 u}{2.E^*.R_{\mathrm{x}}} \\
G = 2.\alpha.E^* \\
W = \frac{P}{2.E^*.{R_{\mathrm{x}}}^2} \\
\frac{1}{E^*} = (\frac{1-{\nu_1}^2}{E_1} + \frac{1-{\nu_2}^2}{E_2}) \\
k \approx 1.03(\frac{R_{\mathrm{y}}}{R_{\mathrm{x}}})^{0.64}
\end{aligned}
\tag{2.3}
$$

2.3: Equations for the calculation of Film thickness. R_{x} is the reduced radius in the x direction. R_{y} is the reduced radius in the y direction, u is the entrainment speed, η_0 is the viscosity of the oil as it enters the contact, α is the pressure viscosity coefficient, P is the normal load and E^* is the reduced modulus.

2.4 Friction in the Boundary Lubrication Regime

In the boundary lubrication regime the lubricant is unable to adequately separate the contact, this means the friction of the contact is predominantly influenced by solid contact mechanics. This means that friction is influenced by many factors such as the hardness, elasticity, pressure and size of the contact.

2.4.1 Contact Mechanics-Hertzian Contact

The fundamental theory for understanding the size and stresses within a solid contact is the Hertz theory of elastic contact, with Johnson et al. showing a similar theory for adhesive

contacts.(Hertz, 1881; Johnson et al., 1971) This thesis will focus on the solution for a non-adhesive contact or the traditional Hertz theory. This theory makes multiple assumptions about a contact, firstly that The strains of the material are small and within the elastic limit, meaning that the materials are not permanently deformed. Another assumption is that the surfaces are continuous and non-conforming meaning that the contact area is much smaller that the dimensions of the contact. Thirdly that each body can be considered an elastic half-space, meaning that the contact is made up of homogenous perfectly elastic body with is infinitely large above the plane Finally the surfaces are frictionless meaning there are no forces perpendicular to the normal force upon the contact. While these assumptions lead to inaccuracies the use of a these calculations for a hertzian contact allow for approximation of the size and stresses of a contact. This thesis will predominantly focus on a point contact, associated with Mini Traction Machine and Universal Mechanical Tester, and an elliptical contact, associated with TE54. These equations for these contacts are shown in Equations 2.4 and Equation 2.5 respectively.

$$\begin{aligned} \frac{1}{R'} &= \frac{1}{R_1} + \frac{1}{R_2} \\ \frac{1}{E^*} &= \left(\frac{1-{\nu_1}^2}{E_1} + \frac{1-{\nu_2}^2}{E_2}\right) \\ a &= \sqrt[3]{\frac{3.P.R'}{4E^*}} \\ p_0 &= \frac{3P}{2.\pi.a^2} \\ p_{\text{avg}} &= \frac{P}{\pi.a^2} \\ p(r) &= p_0\sqrt{1-\frac{r^2}{a^2}} \end{aligned} \tag{2.4}$$

2.4: Equations for the calculation of contact area and pressures of a Hertzian point contact. R' is the reduced radius of the bodies of radii R_1 and R_2, a is the radius of the contact area, P is applied load, E^* is the effective elastic modulus of the surfaces who's elastic modulus is referred to as E_1 and E_2, ν_1 and ν_2 are the Poisson's ratio of the two surfaces, p_0 is the maximum contact pressure and p_{avg} is the average contact pressure, p(r) is the contact pressure distribution,

The assumptions made by the Hertz equations are incorrect in most engineering contacts where some friction and surface roughness will occur, the Hertz equations though

$$
\begin{aligned}
\frac{1}{R'} &= \frac{1}{R_x} + \frac{1}{R_y} \\
\frac{1}{R_x} &= \frac{1}{R_{1x}} + \frac{1}{R_{2x}} \\
\frac{1}{R_y} &= \frac{1}{R_{1y}} + \frac{1}{R_{2y}} \\
a &= \sqrt[3]{\frac{3.E.P.R'}{\pi.E^*}} \\
b &= \sqrt[3]{\frac{3.E.P.R'}{\pi.k.E^*}} \\
k &= 1.0339(\frac{R_y}{R_x})^{0.636} \\
E &= 1.0003 + \frac{0.5968.R_x}{R_y} \\
p_0 &= \frac{3P}{2\pi.a.b} \\
p_{avg} &= \frac{P}{\pi.a.b} \\
p(x,y) &= p_0(1 - \frac{x^2}{a^2} - \frac{y^2}{b^2})^{0.5}
\end{aligned}
\tag{2.5}
$$

2.5: Equations for the calculation of contact area and pressures of a Hertzian elliptical contact. where R' is the reduced radius of the bodies of radii R_1 and R_2, a is the radius of the contact area in one direction and b is the radius perpendicular to this, P is applied load, E^* is the effective elastic modulus of the contacts who's surfaces elastic modulus is referred to as E_1 and E_2, ν_1 and ν_2 are the Poisson's ratio of the two surfaces, p_0 is the maximum contact pressure and p_{avg} is the average contact pressure, p(r) is the contact pressure distribution

form a good approximation of the pressures and size of a contact and will form the basis of all calculations in this thesis. Understanding how surface topography affects the contact and the friction associated with it is of vital importance.

2.4.2 Surface Topography

Almost no engineering materials are perfectly smooth and as such there will be some deviation in the surface height from a perfectly flat plane, these deviations are known as surface topography.

Surface Roughness is a form of surface topography and can either be natural or the

result of machining of materials. Surface roughness can be measured by a number of parameters such as amplitude of the asperities, distance between asperities, slope of asperities, cumulative probability density of the surface and are often measured using either profilometry methods e.g. profilometer, AFM etc or by optical methods e.g. Microscopy.

One of the most common methods for measuring surface roughness is the average deviation from a smooth surface or Ra. This can be calculated via equation 2.6 and gives the average asperity height for the surface.

$$Ra = \frac{1}{l}\int_0^l |z(x)|\, dx \tag{2.6}$$

2.6: Equation for the calculation of mean surface roughness amplitude. l is the evaluation length and z(x) is the profile height

Roughness of the contact can have a large effect on the contact mechanics. This is due to the fact that asperities from each surface are the first to come in contact and as such in relatively stiff materials the size and distribution of these asperities has a large effect on the properties of the contact e.g. friction, wear.

This is very important in the boundary lubrication as the breaking of physical and chemical bonds between the two surfaces asperities are what result in friction within the contact. Surfaces with high levels of roughness often have the largest amount of asperity to asperity contact, as a result a greater number of bonds need to be broken resulting in a greater amount of surface friction and wear associated with the potential breaking of these asperities. This high friction is particularly likely in unpolished and unmachined components that are often prevelant in a ICE and as such preventing asperity contact is often of vital importance for the reduction of friction in the boundary regime.

2.4.3 Flash Temperature and Tribochemistry

The coming together, bonding and subsequent bond breaking of the surfaces asperities can also result in large amounts of energy in the form of heat being released. This heat release is of vital importance for a variety of tribological processes and is referred to as the flash temperature of the contact. This heat is generated rapidly at the asperity point

due to friction and is often poorly dissipated across the full contact, this results in areas of much higher temperature at the asperity contact, often hundreds of degrees higher, than in the bulk contact. These elevated temperatures last very short amounts of time but can lead to changes in the chemical and mechanical structure of the asperity and as such can have a great effect on the contact environment.

Due to the fact that these elevated temperatures exist for very short periods of time and over very small regions, the measurement of the flash temperature is very difficult and as such theoretical estimates are sought. This is difficult though as there is often great variation between these theoretical models with Ashby et al. providing one such model as shown in equation 2.7.

$$\begin{aligned} x &= l_{1\mathrm{f}} + \frac{k_2}{l_{2\mathrm{f}}} \\ y &= A_{\mathrm{r}}(\frac{1}{k_1}) \\ B &= \frac{y}{x} \\ T_{\mathrm{f}} - T_{\mathrm{b}} &= \frac{\mu.F.\upsilon}{B} \end{aligned} \tag{2.7}$$

2.7: Ashby Equation for Flash Temperature. $\mathrm{T_f}$ is the flash temperature, $\mathrm{T_b}$ is the bulk fluid temperature, μ is the coefficient of friction, F is the Load, υ is the contact speed, $\mathrm{A_r}$ is the contact area, k is the thermal conductivity of the surfaces and $\mathrm{l_f}$ is the equivalent linear heat diffusion distances for the surfaces.

These elevated temperatures can result in significant changes in the contact, either from localised changes in the physical properties such as changes in the hardness and elasticity of the material at these elevated temperature or changes in the chemical properties such as through oxidation, removal of surface chemistry or through the formation of tribofilms at these elevated temperatures. This is referred to as tribochemistry and is often fundamental for a large number of surface modifying oil additives such as friction modifiers and anti-wear additives. Here these high temperatures result in the breakdown of the additives into a more reactive state to allow for bonding to the contact surface.

In order to reduce the friction within an ICE, there has been an increasing move towards less viscous lubricants; this effectively reduces the Hersey number while in the

hydrodynamic regime. However, this lower viscosity increases the friction within the boundary lubrication regime, so the development of friction modifiers to reduce this friction has also increased.

2.5 Friction Modifiers

Friction modifiers are chemical additives that decrease the amount of friction within a contact. They work by preventing surface contact when there is not enough lubricant to separate the contacting surfaces effectively. They do this by forming a physical barrier that is softer and more easily sheared than the contacting surfaces. There are two main types of friction modifiers, organic and inorganic, although other more novel types of friction modifiers have been researched in recent years.

2.5.1 Organic Friction Modifiers

OFM's are friction modifiers that are made up of predominantly carbon. They are made up of a polar head group and a long non-polar chain. One example of this is glycerol monooleate which is shown in Figure 2.8. The polar head group of the compound is attracted to the polar metal surface via hydrogen bonding, while the non-polar chains are attracted to each other via Van der Waals and, as a result, form a tribofilm. This tribofilm helps separate the contacting surfaces and, as a result, lowers the coefficient of friction.(Ratoi et al., 2014) This is shown in Figure 2.9.

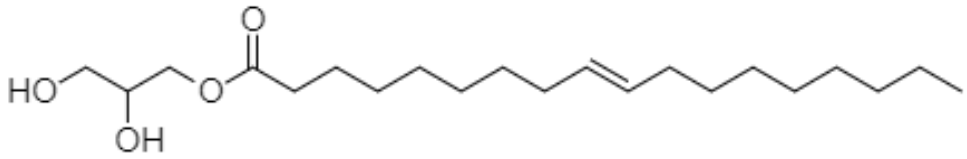

Figure 2.8: Glycerol Monooleate

These self assembled monolayers act to sterically hinder the coming together of the contacting surfaces and form an imcompressible film, as such act to reduce asperity contact and as such reducing friction.

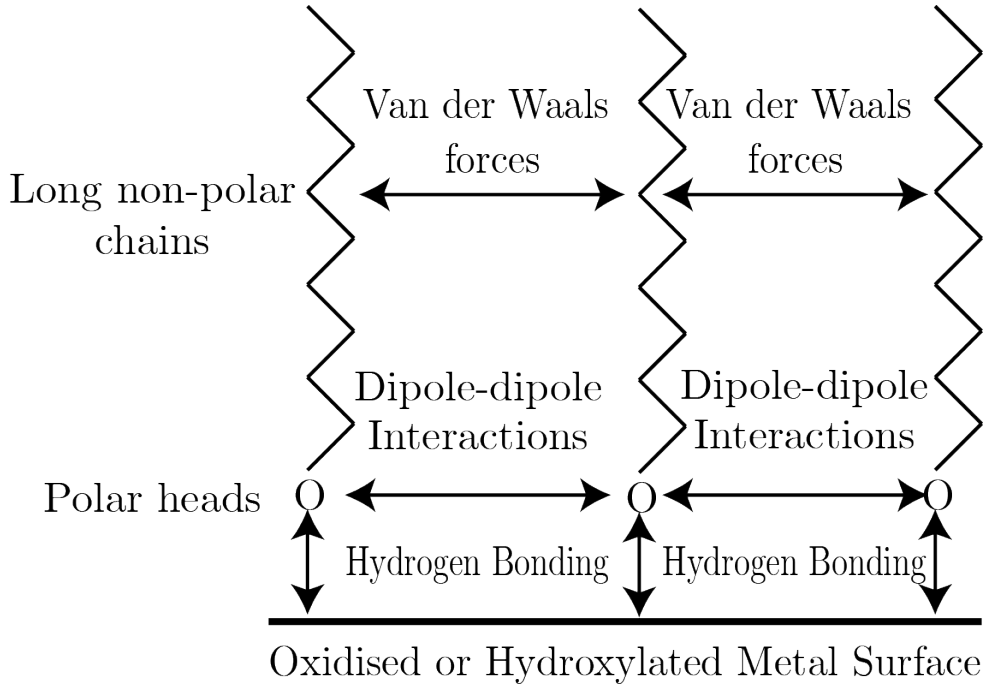

Figure 2.9: Formation of OFM Tribofilms, adapted from (Abdel-Hameed et al., 2015)

There are, however, some disadvantages of OFM's. Firstly the tribofilms take some time to establish; this means that the friction reduction effect of these tribofilms does not come into effect for some time within a system.(Spikes, 2015) Secondly, due to the weak adsorption of the films, they are easily removed in more extreme lubrication conditions, e.g. high pressures, shear rates or sliding:rolling ratios.(Guegan et al., 2019) These films will not then be re-established and will not reduce the friction of these contacts. This film removal is of particular importance as these contact conditions are observed in the boundary lubrication regime, which means that OFM's may be less effective in high friction conditions.

2.5.2 Inorganic Friction Modifiers

Inorganic friction modifiers are compounds that contain little to no carbon, typically metal salts. These compounds chemically decompose within the contact to form products that can chemisorb onto the contacting surfaces, producing a tribofilm of low shear strength that prevents surface contact and lowers the friction within the contact. The most common inorganic friction modifiers are molybdenum based salts, with the most

common commercially being Molybdenum dithiocarbonate (MoDTC), as shown in Figure 2.10. Here MoDTC breaks down to form MoS_2 nanosheets on the contact asperities; this is believed to occur due to a friction activated decomposition mechanism and only forms on the contacting asperities to form a low friction surface.(Grossiord et al., 1998) This proposed mechanism is displayed in Figure 2.11 although other mechanisms have been suggested for the nanosheet formation.

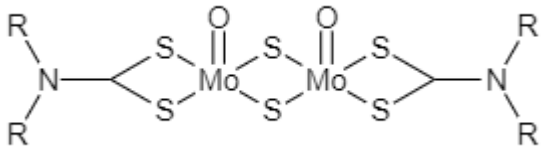

Figure 2.10: Molybdenum Dithiocarbonate

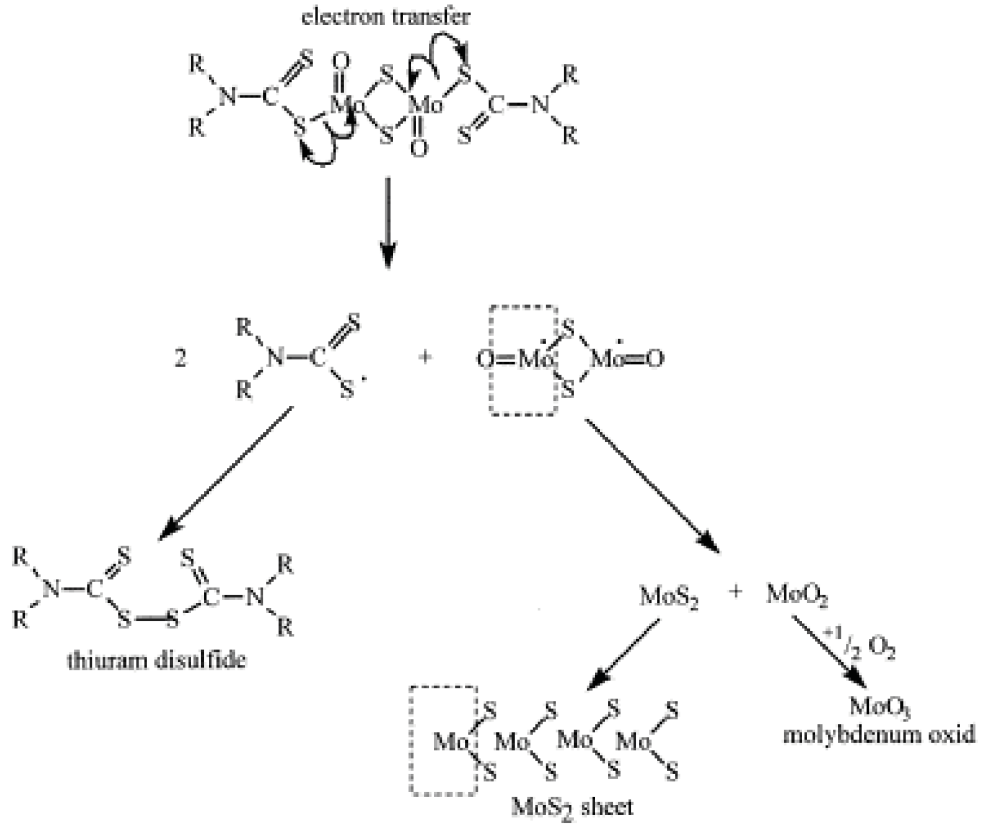

Figure 2.11: Formation of MoS_2 nanosheets from MoDTC.(Grossiord et al., 1998) Reprinted with permission, Copyright ©1999 Elsevier Science Ltd.

This friction activated formation of the tribofilm means that inorganic friction mod-

ifiers are often very efficient and effective, particularly when friction is highest in the boundary lubrication regime. With lower costs than organic friction modifiers, these are very common commercially. There are some issues; however, the metals involved in these films often have multiple oxidation states. Multiple oxidation states mean the metal can donate electrons to the contact for the formation of metal oxides. This metal oxide formation leads to the breakdown of the tribofilm over time, but also these oxides are often hard particles and can increase the amount of friction and wear within the system over time. Secondly, high sulphur content within oil can lead to a number of negative consequences both to the ICE and the environment. The presence of sulphur in the engine leads to the formation of hydrogen sulphide, this is a highly acidic compound and can lead to corrosion of metals within an engine as well as being one of the major causes of acid rain. Sulphur in oils can also lead to the formation of ash in the exhausts of engines, this ash can build up in the filters of the engine and lead to reduced performance of engines as well as poisoning of the catalytic converter in the exhaust.(Miller et al., 2007; Liati et al., 2013) These particulates can also have large effect on human health such as leading to cancer and lung disease.(Zhang et al., 2019) The result of these negative consequences has led to a move towards reducing sulfur content within motor oils and as a result a move towards a reduction in sulphur containing additives in an engine.

2.5.3 Nanoparticle Friction Modifiers

Nanoparticles are defined as particles that are smaller than 100nm in at least one direction. In recent years more research has been undertaken to establish the effects of the addition of nanoparticles to lubricants on the friction of a contact. Early research suggests that various nanoparticles can be used to decrease friction and wear within a contact effectively. However, due to the still early nature of the research, there is no consensus on how this friction reduction occurs. These friction modifiers will be discussed further in chapter 4.

2.6 Other Oil Additives

2.6.1 Anti-Wear Additives

Anti-wear additives are surface modification additives that act to prevent surface contact and as a result reduce the wear upon the surfaces. These molecules are tribochemically active, meaning that the extremely high temperatures associated with surface contact result in the formation of an anti-wear film. These anti-wear films form by the breakdown of the additives on the asperities and the formation of soft and easily malleable lamellar films upon the surface. These lamellar films protect the contact materials and act to spread the load of the contact across a larger area and prevent adhesion of the contact reducing the pressure upon the contact and as a result reduce wear in the contact. One of the most common types of anti-wear additives is Zinc dialkyl dithiophosphate or ZDDP, although other Zinc phosphates are also commonly used. These additives break down to form a zinc polyphosphate film upon the surface which acts to prevent contact of the asperities.

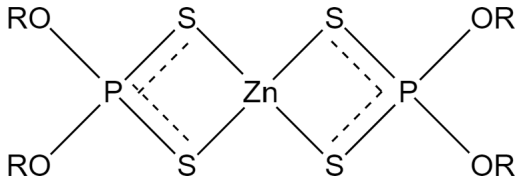

Figure 2.12: Structure of Zinc Dialkyl Dithiophosphate

As previously stated there has been a move away from sulphur containing compounds and oils and this is also the case with phosphorus. Phosphorus has been shown to reduce the efficiency of catalytic converters and as such increase the release of toxic gases and pollutants into the atmosphere from ICE emissions. This has led to a drive to reduce the amounts or find alternative anti-wear additives to ZDDP and other polyphosphate compounds.

As a result of these negative effects of sulphur ash, phosphates and sulphur (SAPS) there has been a push towards low SAPS oils. This involves the reduction of these compounds from the base oil and their reduction as additives. These fully synthetic oils will

reduce the negative consequences of SAPS while maintaining high performance within an engine and requires the increased understanding of SAPS containing additives and also the development of suitable alternatives.

2.6.2 Viscosity modifiers

The viscosity of oil within an engine is of upmost importance. Too thick and the engine can be highly inefficient with large amounts of energy loss due to viscous drag or possibly result in oil starvation of the contact, too thin and the oil is unable to adequately prevent surface contact or may begin to leak from the engine seals. Viscosity modifiers act to reduce the effect of temperature and shear on the viscosity of an oil, this means the viscosity of the oil remains consistent regardless of conditions and so can maintain optimal performance. These viscosity modifiers are polymeric compounds, these occupy large volumes within the oil and as such act to thicken the oil and prevent flow within the contact at high temperatures and low shear rates but due to their reorientation at high shear rates result in them occupying a smaller cross-section and result in lower viscosity at these higher shear rates. Figure 2.13 shows how viscosity modifiers act to alter the viscosity within an engine.

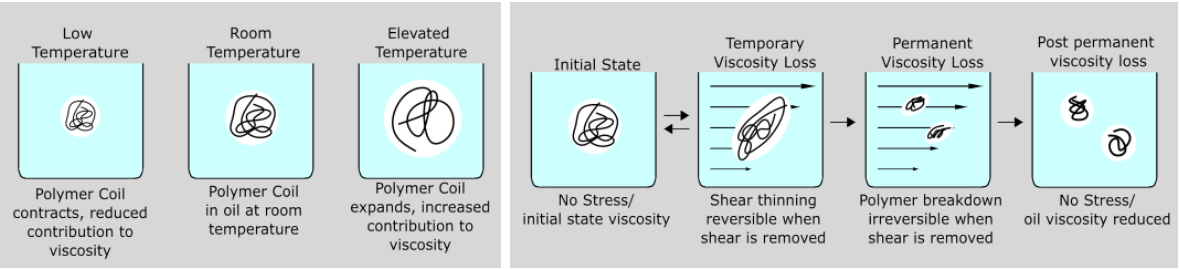

Figure 2.13: Schematic of the mechanism by which viscosity modifiers work to negate temperature (left) and shear effects (right). Redrawn from (Chevron, 2022)

2.6.3 Anti-Oxidants

Anti-oxidants are additives that increase the lifetime of motor oils by preventing their oxidation within an engine. Oil oxidation results in the formation of oil radicals or peroxides, these are highly unstable compounds and as such will react readily resulting in

polymerisation of the oil. This results in thickening of the oil or sludge formation and as a result is no longer able to perform it's role as a motor oil. Anti-oxidants are compounds that react rapidly with oxidation radicals or peroxides, this prevents the propagation of the oil polymerisation reaction and as such no oil thickening occurs.

ZDDP while also an anti-wear additive can also act as an anti-oxidant but the move towards low sulphur and phosphorus additives has also lead to other compounds such as aminics and phenolics to be widely used as anti-oxidants in ICE oils. A mechanism for a phenolic reaction with a peroxide radicals is shown in Figure 2.14.

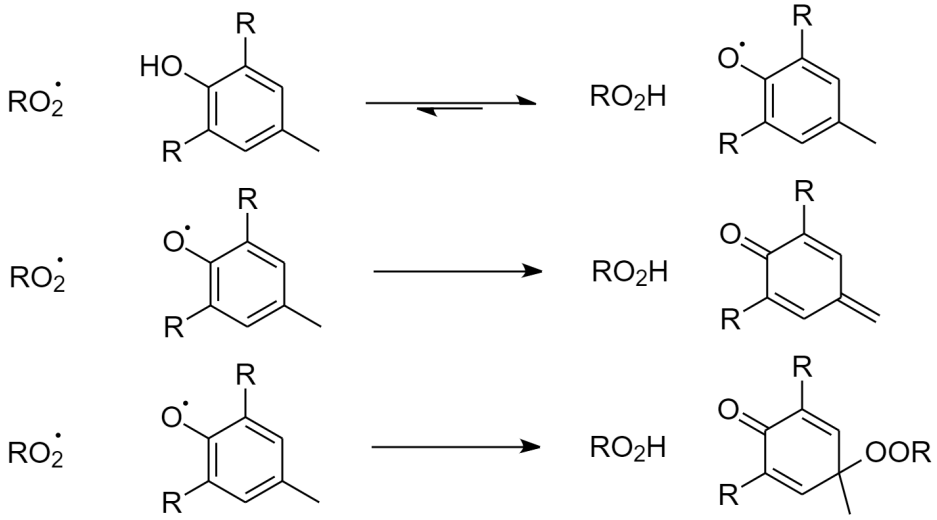

Figure 2.14: Mechanism for anti-oxidative properties of phenolic compounds, adapted from (Mitchell R.Dorfman, 2012)

2.6.4 Rust and Corrosion Inhibitors

These additives act to reduce rust and corrosion within an engine by protecting the metal surfaces. They can do this by two potential mechanisms, either by neutralising any corrosive compounds within the oil such as acidic groups such as a number of amines, or by forming a protective coating upon the surface, ZDDP is effective in this regards.

2.6.5 Detergents

Detergents are additives that act to keep the metal surfaces free from deposits and also act to neutralise acids within the oil. This prevents 3rd body abrasive wear upon the surface and ensures a longer lifetime for the engine. An example of a detergent is shown in Figure 2.15.

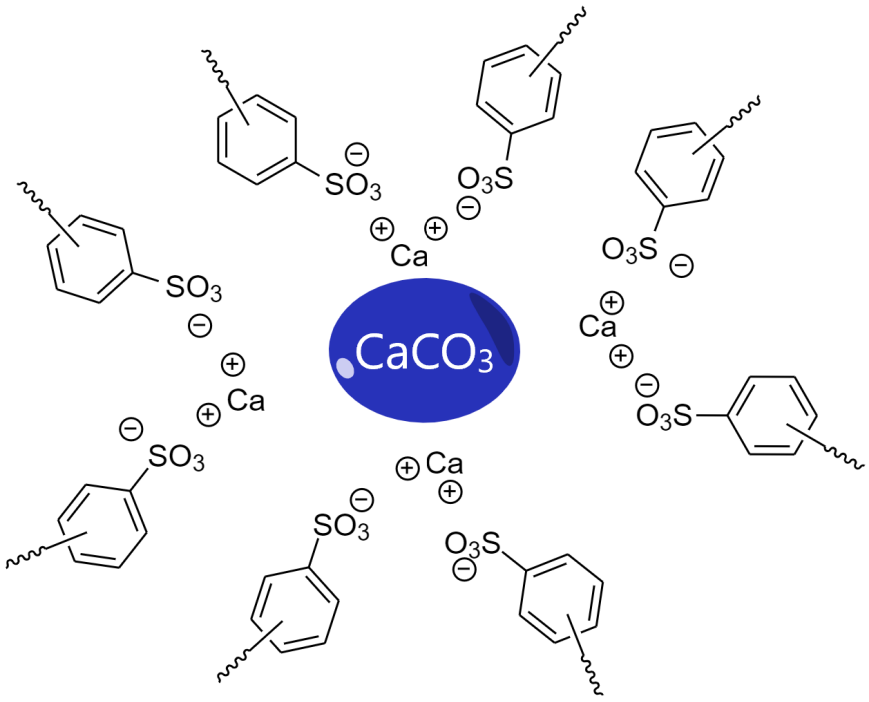

Figure 2.15: Example of a detergent oil additive, adapted from (Tang and Jao, 2013)

2.6.6 Dispersants

Dispersants are often chemically similar to detergents. These act to keep contact surfaces clean by keeping large particles in solution within the oil. As a result these objects do not deposit upon the surface and so prevents 3rd body abrasive wear. These are often made up of a compound with a polar group that is attracted to the particle and a non-polar chain that is soluble within the oil. These act by the mechanism shown in Figure 2.16.

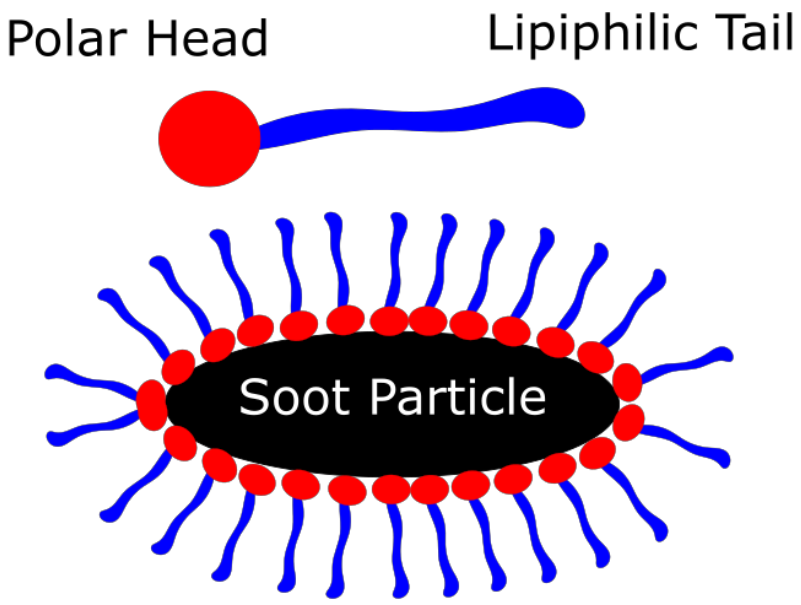

Figure 2.16: Mechanism for dispersants in motor oils, adapted from (Tang and Jao, 2013)

2.7 Conclusion

Lubrication is of vital importance for the correct running of ICE and a variety of other machines. Understanding the effect of lubrication and the additives within them on friction within a contact allows us to understand the effects that the additives studied within this thesis have on a contact.

This thesis will investigate a polymer-based nanoparticle as friction modifiers. Chapter 3 will provide the background for polymerisation reactions and detail the method by which polymer nanoparticles can form.

Chapter 3

Theory of Polymerisation

3.1 Introduction

This chapter provides a background for how polymers are formed via polymerisation processes. It will show how these reactions are controlled and provide the mechanism for forming the nanoparticles discussed in this thesis.

3.2 Introduction to Polymerisation

Polymerisation is the chemical reaction that describes the formation of large chain molecules (polymers) from a series of smaller molecules (monomers). These polymers can be anywhere from tens to millions of monomer lengths. Equation 3.1 shows a typical polymerisation reaction where n of monomer A react to form a polymer of n units of A.

$$nA \rightarrow A_{\mathrm{n}} \tag{3.1}$$

There are two main ways in which this polymerisation occurs step-growth polymerisation and chain growth polymerisation.

Step-growth polymerisations occur when the polymerisation reaction results in the formation of a byproduct. Step-growth polymerisation typically requires two different monomers to react with each other. One example of this is the formation of polyamides.

Here a diacid monomer and a diamine monomer react with each other to form a polyamide. This reaction is shown in Figure 3.1. This type of polymerisation is often called step-growth; here, the polymer grows via independent reactions between the reactive sites on the monomers. These reactive sites are functional groups and could be due to a polarity within the bond or delocalisation of the electron density. In the polyamide example in Figure 3.1 the functional groups are the amine group and the C=O group within the acid. Step growth polymerisations result in the polymer growing slowly, with a significant increase in size observed at high conversions.

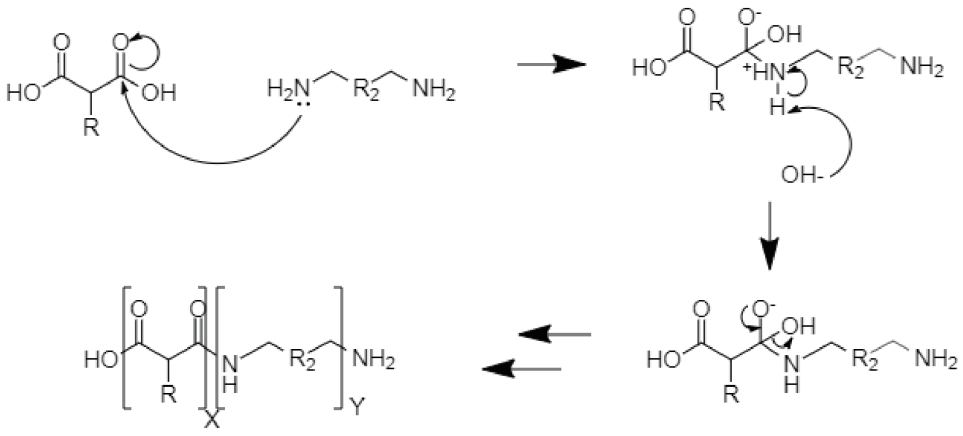

Figure 3.1: Polyamide Formation Mechanism

Chain growth polymerisation, by comparison, occurs when the monomers react with each other without any byproducts of the reaction. Chain growth polymerisation typically requires a catalyst to break down a functional group within the monomer; this allows for a reaction with another monomer to form a polymer. One example of this is the formation of polystyrene, shown in Figure 3.2. Here the polymer grows in a chain from an active centre. This reaction is rapid and results in large chains early in the reaction.

The polymers discussed in this thesis are a form of chain growth polymerisation using radicals to catalyse the reaction.

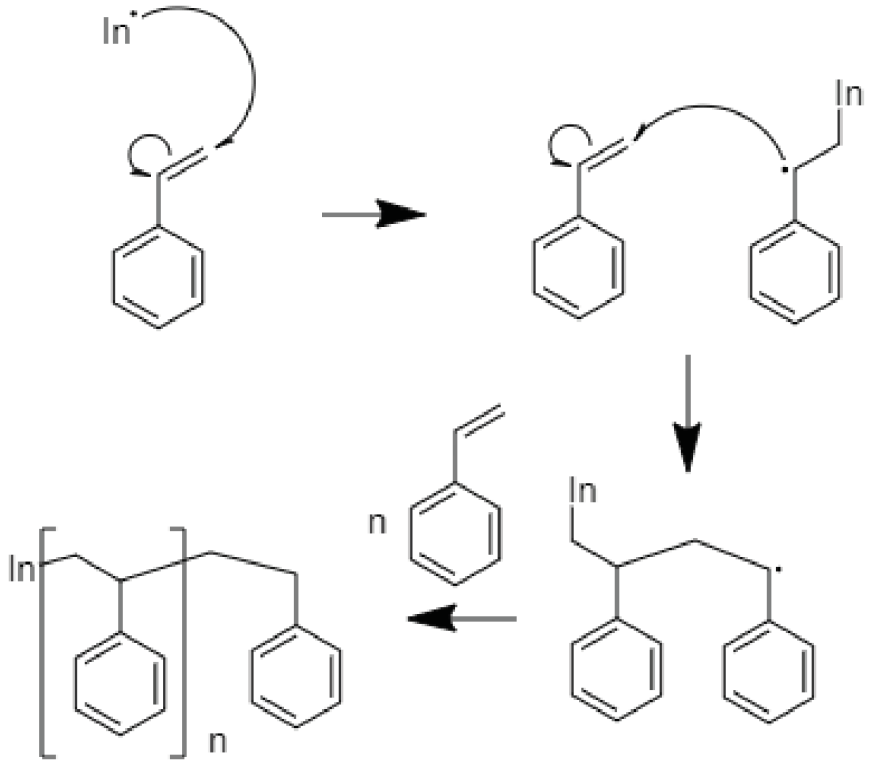

Figure 3.2: Polystyrene Formation

3.3 Radical Polymerisation

A radical is an atom, molecule, or ion with an unpaired electron in its outer or valence shell. These radicals are typically unstable due to the high energy associated with the unpaired electron. This energy will be decreased by forming a bond that pairs this electron. Meaning a reaction will occur as chemical reactions will always go from high energy to low energy equilibrium.

The instability of radicals means that they can be used to catalyse and then maintain a polymerisation. Adding radicals to our monomer mixture will result in this radical reacting with a monomer to generate a monomer radical. This monomer radical can then react with other monomer groups to generate the polymer. The formation of a monomer radical and then its propagation to form a polymer is displayed in Figure 3.3.

The issue with radical polymerisation is also linked to the instability of the radical.

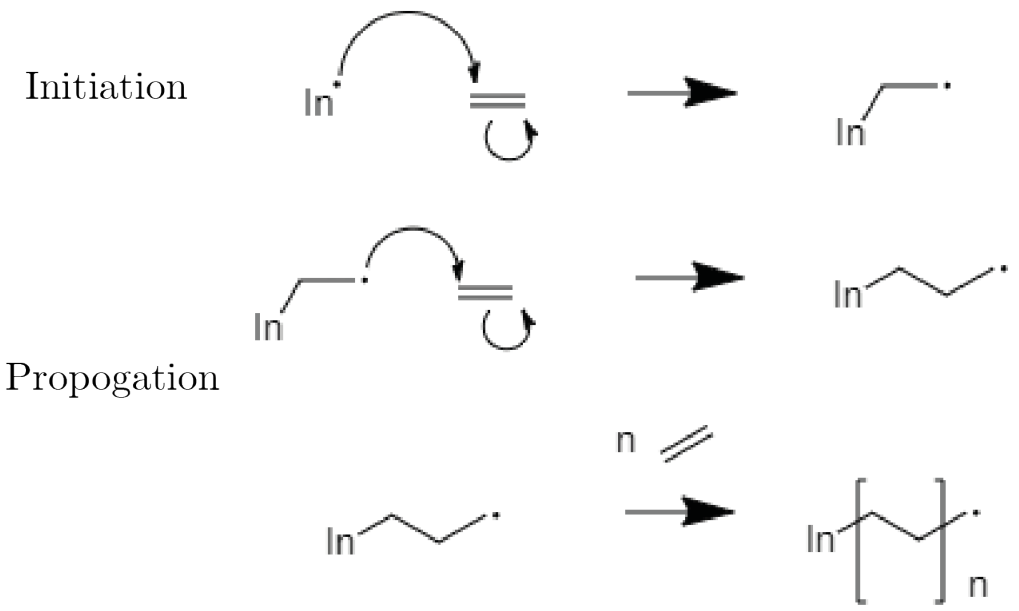

Figure 3.3: Initiation and Propogation of a Radical Polymerisation Reaction

Although the radical stability does increase slightly as the propagation reaction occurs due to steric stabilisation, this increase is slight, and as a result, the radical often seek to become more stable. The most effective way to do this is to react with another compound within the system; this will result in an electron pair, destroy the polymer radical, and end the polymerisation reaction. This is called termination and can occur in a variety of ways.

Firstly the presence of dioxygen, the oxygen that we breathe in the atmosphere, within the reaction will result in termination of the reactive radical. Dioxygen is stable as a diradical; it consists of two oxygen atoms connected by a single bond with the final electron on each atom, forming a radical rather than a double bond as expected. This radical oxygen can react with the polymer radical to form a more stable radical so that the polymerisation will terminate. This mechanism is shown in Figure 3.4. This oxygen termination means that any radical polymerisation must be performed in an inert atmosphere, typically using nitrogen or argon. Dioxygen is not the only impurity that can terminate a radical polymerisation, but it is the most common in most reactions.

Beyond impurities within the reaction, there are multiple ways that the radical poly-

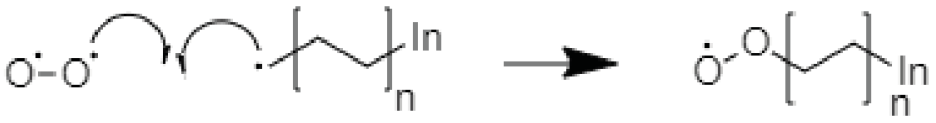

Figure 3.4: Mechanism for Termination of Polymerisation by Dioxygen

merisation reaction can terminate. The polymer radical can react with another radical to form a bond, removing any unstable unpaired electron. These are shown in Figure 3.5.

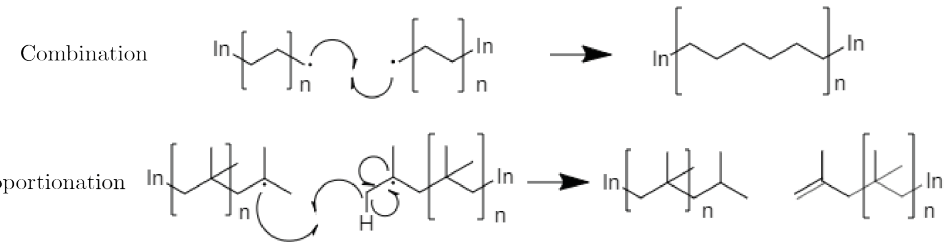

Figure 3.5: Termination of Radical Polymerisation

There is also the possibility of a chain transfer reaction occurring. These are reactions that result in the formation of a second radical while still terminating the polymer radical. This termination is similar to the disproportionation reaction shown in Figure 3.5, but instead of generating a double bond, a radical is produced. This is shown in Figure 3.6. This chain transfer is common if the chain transfer agent has a weak bond; examples of this are carbon to halogen (except fluorines) or sulphur bonds. Although these reactions are often unwanted within a polymerisation, the addition of chain transfer agents such as thiols can target shorter polymers without adding extra initiator or limiting the amount of monomer within the reaction.(Henriquez et al., 2003)

It is often vital to control the extent of polymerisation or degree of polymerisation, DP. DP is defined as the number of monomer groups within a polymer and is essential as

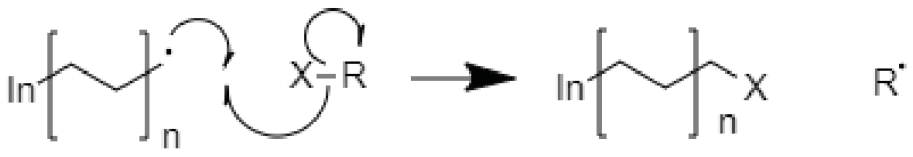

Figure 3.6: Chain Transfer Mechanism

a polymers physical properties are often heavily related to its DP. The level of control on the DP that is achieved in polymerisation is known as dispersity. Here a perfect polymer, where all the chains are the same weight and have the same DP, is said to have a dispersity of 1, and this gets larger as the variance in DP increases and the control of the reaction decreases. The dispersity of a polymer is calculated by dividing the mass average molar mass, Mw, by the Number average molar mass, Mn. The Mn of a polymer is the mean weight of the polymer chains, while the Mw considers that larger polymer chains contain a higher proportion of the polymers total mass. The way these values are calculated is shown in equation 3.2 and 3.3, as well as being shown on a typical polymer mass distribution curve in Figure 3.7. There are multiple ways to do this, including control of polymerisation conditions, e.g. solvents, or addition of control chemicals to the reaction.

$$M_{\mathrm{n}} = \frac{\Sigma M_{\mathrm{i}}.N_{\mathrm{i}}}{\Sigma N_{\mathrm{i}}} \tag{3.2}$$

$$M_{\mathrm{w}} = \frac{\Sigma M_{\mathrm{i}}{}^{2}.N_{\mathrm{i}}}{\Sigma M_{\mathrm{i}}.N_{\mathrm{i}}} \tag{3.3}$$

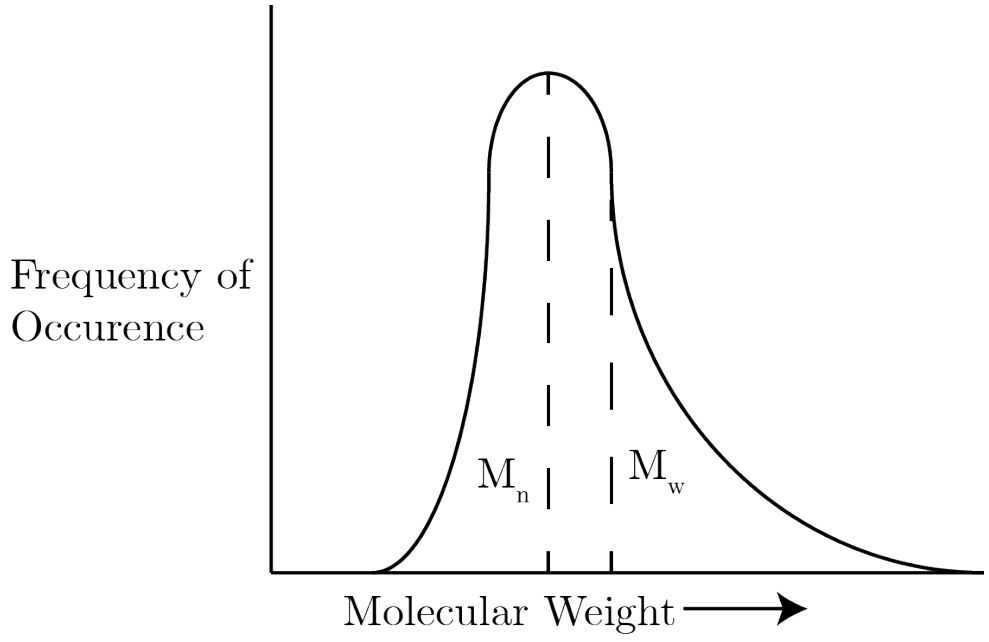

Figure 3.7: Typical Molecular Weight Distribution of Polymer Synthesis

Control of solvent is important to control the polymerisation termination. Firstly the

solvent must not have any weak bonds within it; this prevents any chain transfer reactions occurring that would result in the premature termination of the polymerisation. Secondly, there is a strong link between the viscosity of the solvent and the rate of termination. Here the rate of termination is inversely proportional to the viscosity of the solvent at low conversion rates; this is referred to as the solvent cage effect. Here the solvent surrounds the initiator or small polymer radicals preventing the radical from interacting with another radical within the solvent. This solvent cage lowers the rate of termination of a reaction at low conversions. This cage is more robust at higher viscosity's as the solvent molecules are more resistant to flow, resulting in the radicals being unable to diffuse. As conversion increases, this is not the case, as the solution becomes homogeneous.(Ito, 1969) This solvent cage, however, also results in a decrease in initiator efficiency. Here the cage will effectively trap both the initiator radicals, increasing the likelihood of them recombining. This recombination will significantly decrease the rate of polymerisation due to the rate of initiation being decreased.(Boodhoo and Jachuck, 2000) Solvents can have a significant effect on a variety of other factors, but these effects often vary depending on the chemistry of the monomer, polymer and solvent, as well as the type of polymerisation that is occurring.

The second and most commonly used methods of controlling radical polymerisation are adding chemicals to the reaction. These chemicals allow for radicals to be reversibly terminated, reducing the radical concentration within the reaction and decreasing the termination rate. This is known as living polymerisation.

3.4 Living Radical Polymerisation

Many different chemicals can be added to radical polymerisation reactions that can control them and ensure that the termination rate is lowered. These chemicals though effectively fall into two main categories: reversible trapping or degenerative transfer. Reversible trapping works by a reversible reaction occurring between the propagating radical and the chemical that is added. Although this terminates the reaction momentarily, the reversible nature of the reaction allows the propagating radical to be rereleased and allow the reaction

to continue further, as shown in Figure 3.8.

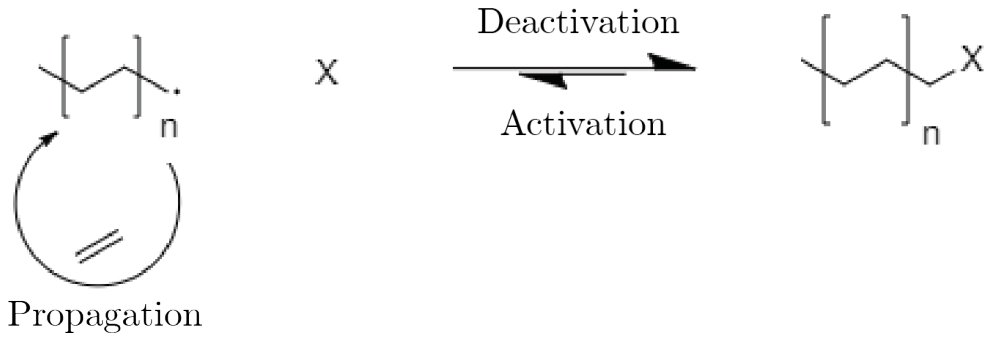

Figure 3.8: Control of Radical Polymerisation by Reversible Trapping

Degenerative transfer, however, involves the use of a chain transfer agent, CTA. This CTA reacts with the propagating radical and, in doing so, produces a different propagating radical while making the original radical dormant. If this CTA is present at much larger proportions than the initiator, this allows for control of the radical termination. The mechanism is shown in Figure 3.9.

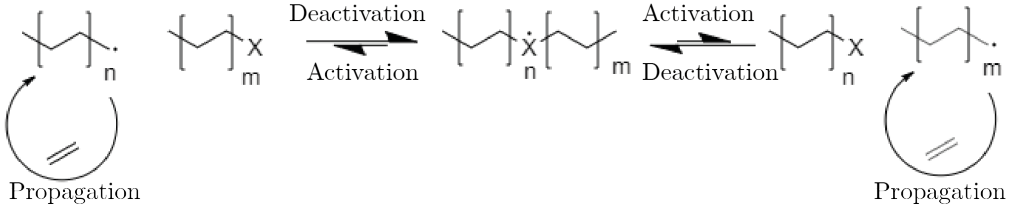

Figure 3.9: Control of Radical Polymerisation by Degenerative Transfer

The most important thing to consider when adding a control method to radical polymerisation is the reversible reaction kinetics between the propagating radical and the chemicals that generate this control. To effectively reduce the radical concentration and reduce the rate of termination of the radical, the polymer must be much more stable once reacted with the control chemical. This higher stability ensures that the addition of the control chemical does effectively reduce the radical concentration. If the radical is too stable while dormant, however, the reaction will not be reversed, and the control chemical effectively terminates the polymerisation. These control chemicals have to be carefully selected to ensure the kinetics of the reaction are sufficient to allow the reaction to be controlled without reducing the rate of propagation.

3.4.1 Stable Free Radical Polymerisation

One example of radical polymerisation control via a reversible trapping mechanism is stable free radical control. Here a more thermodynamically stable radical is added to the reaction and reacts reversibly with the propagating radical. The most common example is nitroxide mediated polymerisation, which was first discovered using a molecule called TEMPO, whose structure is found in Figure 3.10. TEMPO and other similar nitroxide radicals are stable due to their resonance structures. This resonance means the radical can either be found on the oxygen group, or by transfer of electrons within the structure, or the nitrogen with a double bond occurring between the nitrogen and oxygen. This resonance increases the stability of the radical, but the severe steric hindrance of the neighbouring groups, in TEMPO's case the methyl groups, means that the reactivity of the radical is reduced. This resonance and steric hindrance mean that TEMPO and similar nitroxides are relatively stable in radical form and can be used for reversible trapping control. This reaction for TEMPO is shown in Figure 3.11.

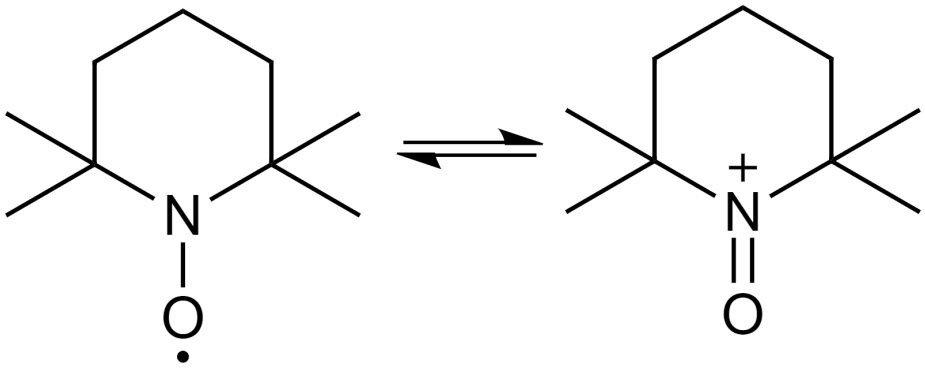

Figure 3.10: Structure of TEMPO

3.4.2 Atom Transfer Radical Polymerisation

ATRP is another example of reversible trapping control that involves the use of a transition metal-based catalyst. This catalyst can reversibly add or subtract a halide group from the propagating radical due to its different oxidation states. The oxidation state of the metal is defined as the metals ability to donate electrons to form a compound. Copper

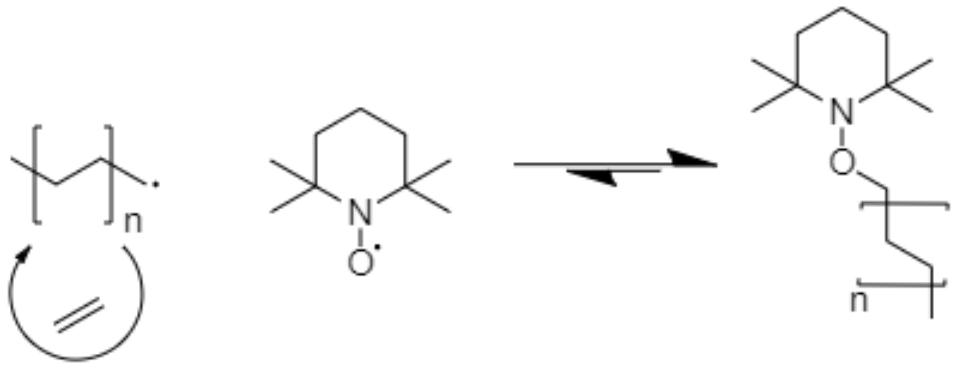

Figure 3.11: Mechanism of Nitroxide Mediated Polymerisation

can go from donating one electron to donating two electrons to remove the halide from the propagating radical. As this process is reversible, this halide group can reversibly cap the propagating radical and, as a result, control the polymerisation. The mechanism for a copper-based ATRP is shown in Figure 3.12

Figure 3.12: Mechanism for ATRP Controlled Polymerisation

One other important part of the catalyst is the ligand that is attached to the metal centre. Ligands are typically molecules that donate both the electrons to the central metal to form a bond. This ligand can alter the performance of the catalyst in multip le ways. Firstly, it can help control the catalyst's solubility, but it can also affect the metal catalysts' ability to change oxidation state or redox potential. These ligand affects the kinetics of the reaction shown in Figure 3.12 and therefore affects the degree to which the catalyst can control the reaction. Meaning the ATRP catalyst and ligand have to be carefully selected based on the polymerisation reaction that is being undertaken.

3.4.3 Reversible Addition Fragmentation Chain Transfer Polymerisation

The method that will be used as a part of this thesis is known as RAFT polymerisation. RAFT involves using a sulphur-based compound that acts as a CTA in a degenerative transfer method of polymerisation control. A RAFT agent comprises a compound that contains a carbon atom bonded to two sulphur atoms. These sulphur to carbon bonds can flip between being a double bond and a single bond, this change in bond type allows for the propagating radical to bond to one of these sulphur atoms and, as a result, control the propagation reaction. A typical RAFT agent and the mechanism by which they work are shown in figure 3.13 and 3.14 respectively.

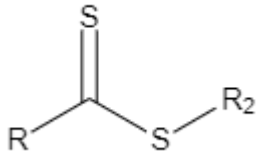

Figure 3.13: Typical RAFT Agent

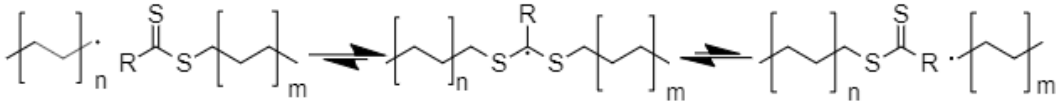

Figure 3.14: Mechanism for RAFT Controlled Polymerisation

The design of the RAFT agent needs to vary depending on the polymerisation that is being performed. The R group shown in Figure 3.13 is essential as it helps to affect the stability of the intermediate in Figure 3.14. This effect is because of the proximity of the R group to the radical in the intermediate, meaning it can significantly affect the stability of the radical, for example, allowing the formation of resonance structures to stabilise the radical. This intermediate stability affects the polymerisation kinetics, as we need to generate an intermediate that is more stable than the propagating radicals but not sufficiently so that the propagating radicals do not form. Secondly, the R_2 group on the RAFT agent has a significant effect on the polymer formed; because this group will be

removed from the RAFT agent to generate a new propagating radical. The R_2 group caps the majority of the polymer chains, as the concentration of the RAFT agent is significantly higher than that of the initiator. This group can be used to tune the characteristics of the polymer, e.g. adding a reactive group to allow surface grafting.

The polymers described in this thesis are prepared via RAFT dispersion polymerisation. Here the monomers are soluble within the solvent used, in this case, Benzyl methacrylate and mineral oil, respectively. Undergo the polymerisation reaction to form an insoluble polymer, allowing for the formation of separate dissolved polymer particles within the solution via copolymerisation.

3.5 Copolymerisation

3.5.1 Introduction to Copolymerisation

Copolymerisation is the act of forming a polymer chain made up of more than one type of monomer. Although in some polymerisations, e.g. step-growth polymerisations as discussed in section 3.2, this is necessary to generate the polymer chain. In radical chain polymerisation, this requires adding two or more monomers to the reaction vessel. Copolymerisation can be done in many ways, for example, adding all the monomers at once or systematically adding them to the reaction, and as a result, a large variety of copolymers can be formed.

3.5.2 Statistical Copolymers

Statistical copolymers are the most simple form of copolymer. Here the location and number of the monomer groups are determined by the relative proportions within the reaction medium and is often called random polymerisation as if all else is equal; the monomers are randomly added to the polymer chain. This random addition will not be the case as the kinetics of the reactions between the propagating radicals and monomer and their concentrations within the medium will vary somewhat. Statistical copolymers occur when all the monomers are added to the reaction vessel at the start of the reaction.

$$nA + nB \rightarrow A - B - A - A - B - A - B - B - A - A - A - B - A - B - B...$$

Figure 3.15: Formation of a Statistical Copolymer

3.5.3 Alternating Copolymers

Alternating copolymers are formed when the monomers attach in an alternating manner. Although this is most common in step-growth polymerisations, it is possible to achieve alternating copolymerisation via chain polymerisation. One example of this is the formation of the styrene-maleic anhydride copolymer, shown in Figure 3.16. This polymer is formed due to the reactivity of the radical of one monomer reacting with the second monomer is significantly higher than reacting with the same monomer. This difference in reactivity means that the reaction is much quicker in an alternating manner than in any other manner. In the case of the styrene-maleic anhydride copolymer, this is believed to be due to the electron-rich styrene being electrostatically attracted to the electron-poor maleic anhydride. However, the presence of charge transfer complexes from the comonomers means that these may be a part of the mechanism.(Klumperman, 2010)(Hill et al., 1985)(Tsuchida and Tomono, 1971)

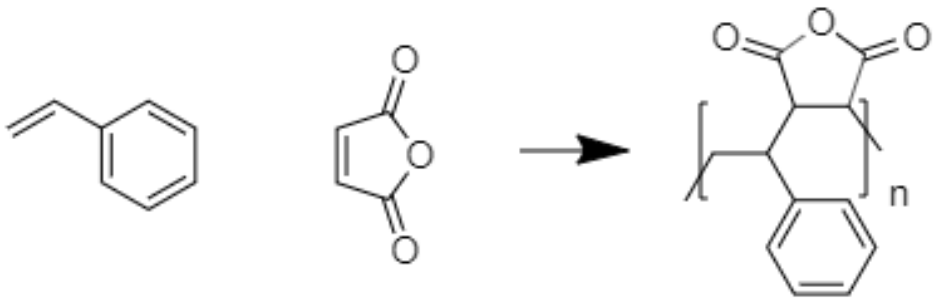

Figure 3.16: Formation of Styrene Maleic Anhydride Alternating Copolymer

3.5.4 Block Copolymers

Block copolymers are formed when the different monomers with the copolymer are organised into distinct blocks. These typically occur if the reactivity of one monomer is significantly higher with itself than the other monomer or when the second monomer is added as the first monomer is nearing the end of its polymerisation reaction. The characteristics of these polymers are determined by the DP of the blocks and the chemistry of the monomers. By carefully tuning these blocks, the chemical and physical properties of the polymer can be controlled. One way in which these block copolymers can be used is to form distinct structures within a solution known as polymerisation induced self-assembly (PISA).

$$nA + nB \rightarrow [A]_{\mathrm{n}} - [B]_{\mathrm{n}}$$

Figure 3.17: Formation of a Block Copolymer

3.5.5 Polymerisation Induced Self Assembly

PISA is a method of forming distinct particles of block copolymers that are dissolved within the solution. This method is achieved by forming a block copolymer where one of the blocks is soluble within the solution and formed via solvent polymerisation, and the other block is insoluble and formed by dispersion polymerisation. Due to the insolubility of the second block of the copolymer, they will be attracted to other insoluble blocks on other polymer chains and surrounded by the solvent stable blocks. This process will take place as the polymerisation reaction occurs, and as a result, stable particles will be formed within the solution. These polymerisations can only be performed in living conditions. Once the insoluble block begins to form and the particles begin to form, all the further chain polymerisation will occur within these particles. As these particles form, there will be a significant increase in the local concentration of both the monomer and the propagating radicals resulting in a significant increase in termination rate without a method of control. Several different shape and size particles can be produced by controlling the size of the

two blocks; this is shown in Figure 3.18 where the red block is the soluble block, and the blue block is insoluble.

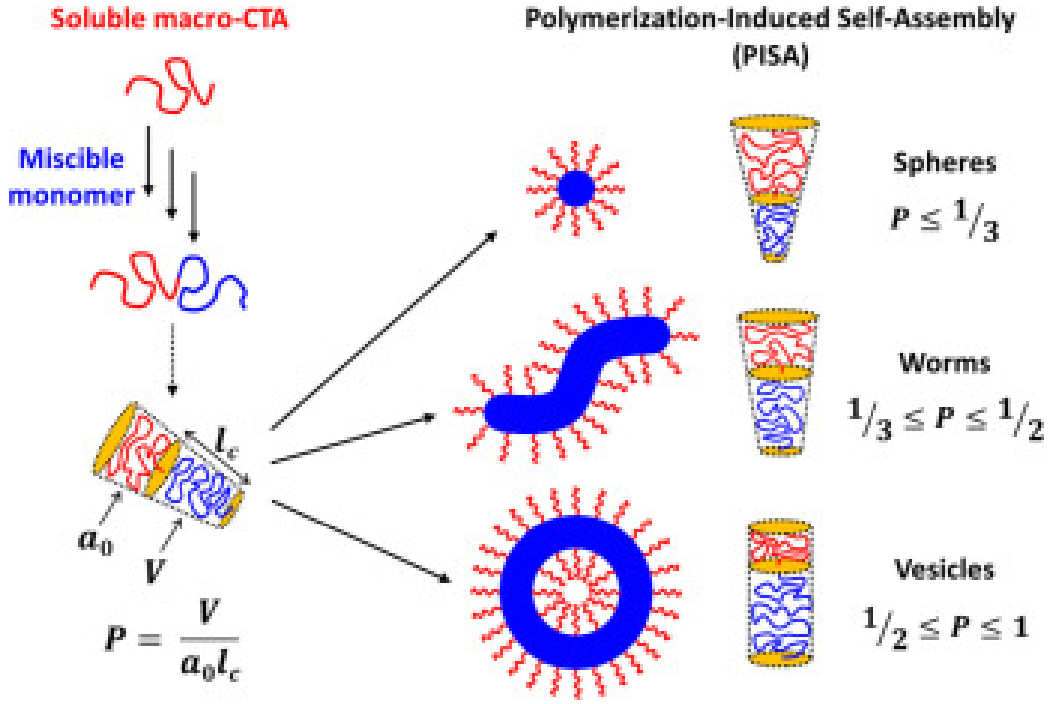

Figure 3.18: PISA of Block Copolymers.(Derry et al., 2016a) Reprinted with permission, Copyright ©2015 Elsevier Ltd

The primary way to determine the shape achieved during PISA is by altering the block volume fractions; this is done simply by varying the DP of the blocks or by varying the size of the monomers.

If the volume fractions are similar for both the insoluble block or core block and the soluble or stabiliser block, then vesicles are formed as shown in Figure 3.18. Here, the stabiliser block surrounds both the inside and outside of the core block, creating a solvent core to the vesicles, which allows for vesicles to have a wide range of uses. From being used as delivery methods, in particular in drug delivery, to being used as nanoreactors.(Discher and Eisenberg, 2002)(Brinkhuis et al., 2011) In both these cases, the vesicle contains a compound within the inner solvent as the core block prevents easy movement of the stored compound into the surrounding solvent.

Worms are formed when the core block's volume fraction is lower than that of the stabilising block. These worms have a broad range of uses, but their predominant use is

as a viscosity modifier. Here, the long and thin nature of the worms means that as the shear rate of the liquid increases, they interact more with each other, forming different structures as a result. These different structures are due to the shear-induced gelation of the ends of the worms and effectively thicken the fluid, giving a shear thickening property.(Van Egmond, 1998) In recent years, it has also been shown that some polymer worms could have potential use as a method of energy storage and conversion. Here films of polymers containing TEMPO have been shown to have very high redox potential and high conductivity.(Zhang et al., 2017)(Joo et al., 2018) The worms can effectively act to form a more significant conductive ability even at lower amounts of active material and requiring less post polymerisation processing.(Hatton et al., 2019) One other potential use of worms that is more relevant to the topic discussed as part of this thesis is their potential use to increase the viscosity of a liquid at high temperatures. Derry et al. found that a $PSMA_{13}$-$PBzMA_{96}$ block copolymer, prepared via RAFT dispersion polymerisation, undergoes a change from vesicles to worms at around 135°C in mineral oil.(Derry et al., 2017) This is of particular importance as the move towards lower viscosity liquids in motor vehicles leads to poor friction and wear performance at high temperatures.

Spheres are formed when the core block volume is significantly lower than the stabilising block. These are the nanoparticles that will be discussed in this thesis as having potential use as friction modifiers.

3.6 Conclusions

Understanding the theory behind polymerisation reactions, control of the reaction and formation of PISA particles is of utmost importance for the synthesis design of the PSMA-PBzMA nanoparticles described in this thesis. This chapter underlines the methodologies that will be used to ensure the successful and correct synthesis of nanospheres. From the use of nitrogen atmosphere, using RAFT control through to ensuring the PSMA stabiliser shell has a larger volume than the PBzMA core.

In Chapter 4 the academic research of alternative friction modifiers will be reviewed, with particular attention paid to nanoparticle friction modifiers. Allowing for the iden-

tification of limitations with currently available research allows this thesis to attempt to resolve these limitations.

Chapter 4

Literature Review

4.1 Introduction

This chapter will investigate the current academic research in friction modifiers for motor oils. This review will follow friction modifier research through time: investigating their mechanism, initial development and more modern research, focussing on three main types of friction modifier: organic, inorganic and nanoparticles.

4.2 Organic Friction Modifiers

4.2.1 Mechanism of Organic Friction Modifiers

Initial research into the effects of lubrication within a contact displayed that lubricants can separate rubbing surfaces. This research, though, suggested that the viscosity of a lubricant alone was responsible for this separation, meaning all lubricants with the same viscosity should be equally effective lubricants.(Reynolds, 1886) It took until 1920 to disprove this theory. Wells and Southcombe showed that adding a low concentration of vegetable oil-based fatty acids to a mineral oil would reduce the friction and wear of a contact.(Wells and Southcombe, 1920) This discovery showed that the chemistry of lubricant affected its lubrication properties. There were many theories for why this occurred; Langmuir showed that oleic acid monolayers on a glass surface could substantially reduce

friction within the contact.(Langmuir, 1920) This occurred by a physical attraction of a single atom of the acid to the surface, rather than the whole compounds attraction, resulting in only a monolayer will be forming a schematic of this is shown in Figure 4.1. Hardy then showed that the relationship between fatty acids and alcohols on a glass to steel contact to decrease the friction coefficient was proportional to the chain length.(Hardy and Doubleday, 1922) The discovery and mechanism by which OFMs reduce friction has been known for some time, and as such, the research and commercial availability into these compounds is very advanced. With compounds such as carboxylic acid derivatives, amide derivatives, phosphoric acid derivatives being shown to be effective OFMs.(Herdan, 2000; Khalkar et al., 2013; Doig et al., 2014; Eriksson, 2014; Ratoi et al., 2014; Spikes, 2015)

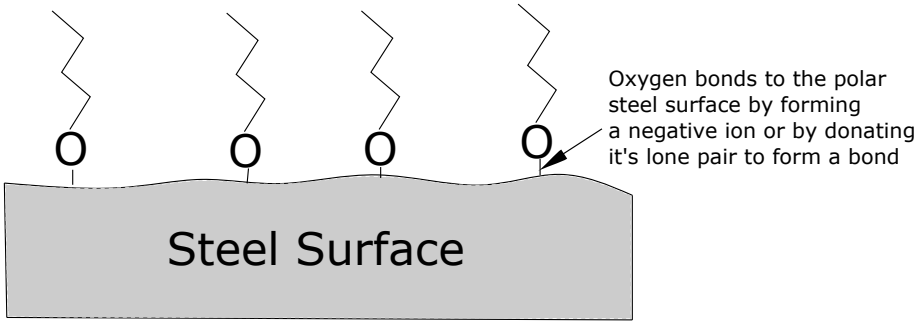

Figure 4.1: Adsorption of acid groups to steel surface via single oxygen atom to form a monolayer

As well as reducing friction in the boundary lubrication regime, recent research has shown that these compounds can also affect the hydrodynamic lubrication regime. Choo et al. showed that stearic acid effectively decreased the friction coefficient of a contact in the hydrodynamic regime.(Choo et al., 2007) Here, the stearic acid monolayer adsorbed to the surface and promoted liquid slip of the lubricant at the surface of the contact, a schematic for this is shown in Figure 4.2. This paper may provide a somewhat flawed view; firstly, this slip was only observed when the contact had been exposed to the stearic acid for a prolonged amount of time, 96 hours. This exposure time does not give a realistic picture of what would occur in reality. The contact was also only very lightly loaded, with a maximum load of 0.3N in the testing. This light load is well below anything that would be observed within a typical engine. However, it is worth noting that this friction reduction did improve as the load was increased, but this could be caused by a decrease

liquid to liquid friction due to a decrease in the Hersey number. Finally, these results were only observed on a very smooth sapphire surface with an increase in roughness of the surface, removing any effect of the stearic acid additive. These rougher sapphire surfaces with a root mean square roughness of 7.39 nm are still substantially smoother than would occur within an engine, where a surface roughness of approximately 0.8 μm would be expected.(Mezghani et al., 2013)

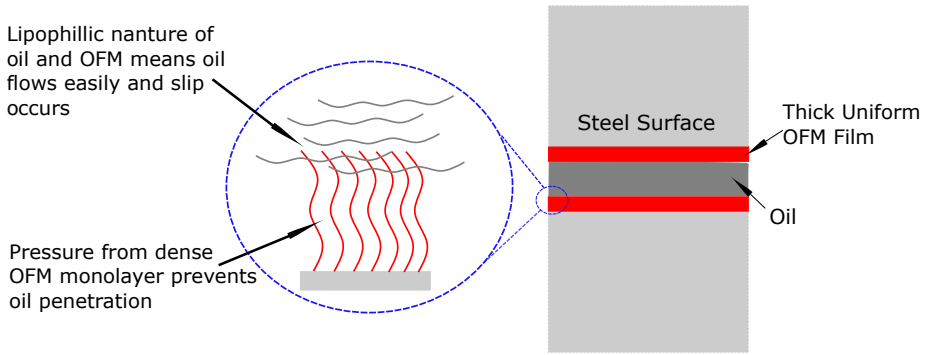

Figure 4.2: Schematic of liquid slip of oils in contacts with OFM films

These results contradict the long-held convention that no slip occurs within a contact in the boundary regime, meaning the Reynolds equation is no longer valid.(Reynolds, 1886) An altered Reynolds equation was derived by Spikes known as the half-wetted bearing.(Spikes, 2003) This calculation assumes that slip only occurs at one surface of the contact, and these calculations show that these contacts can support a significantly larger load than a traditional non-slip bearing as well as leading to a significant friction reduction, similar to those observed by Choo et al. This was due to the contact exhibiting no Couette friction as the contact converges. Couette friction means that the lubricant flow is pressure-based rather than drag-based, resulting in significantly reduced friction. This phenomenon is likely to only occur in low load contacts, and it is questionable the effect in higher load contacts.

Based on the current literature available for the effects of OFM induced sliding to reduce friction within a contact, it is impossible to say that these hydrodynamic effects would occur in an ICE. More tests would be required to confirm this. However, the results are positive and suggest that there could be other mechanisms than just monolayer separation of surfaces that could decrease friction within a contact.

4.2.2 Development of Organic Friction Modifiers

The research around OFM development has primarily centred around two different areas: the length of the hydrocarbon chain and functional groups for adsorption to the contact. These are particularly important as they define the stability and the size of the monolayer formed by the OFM, and these determine their ability to reduce friction.

Hardy was the first to investigate boundary lubrication systematically. He measured the static friction of surfaces using a series of fatty acids, alcohols and paraffins to establish the effect of chemistry and chain length on the friction of the contact.(Hardy and Doubleday, 1922) It was found that the coefficient of friction was inversely proportional to chain length for all compounds, as well as show the relationship between the solid surface and the chemistry of the lubricant. He put this down to the formation of a monolayer film that helped promote slip at the surface. Although this research gave the initial understanding of how the chain length of a friction modifier was able to affect the friction of the contact but the exact results he obtained, where friction decreased linearly with chain length, has not been repeated since; with most research showing a much sharper decrease at smaller chain lengths before plateauing at longer chain lengths.

Jahanmir studied carboxylic acids and alcohols with 12-18 carbon atom chains as additives in hexadecane base lubricant.(Jahanmir, 1985) He found that for both types of additive, the friction coefficient of the contact was inversely proportional to the chain length, as shown in Figure 4.3.

He also found that as the temperature of the oil increased the organic friction modifier additive mix reached a transition temperature. At this temperature, the friction coefficient began to increase and a second higher temperature, increasing rapidly. Both of these temperatures increase with the increased chain length, as shown in Figure 4.4. This temperature increase is the result of longer chain friction modifiers having stronger intramolecular bonds between the carbon chains. The energy to break these bonds is greater and as a result a higher temperature is required to break down the organic friction modifier film. These experiments were undertaken at 0.0005 ms^{-1}, while at higher speeds of 0.01 ms^{-1} longer acid chains ($>C_{16}$) display no increase in friction with temperature. This indicates that these longer chain acids, and likely other adsorbant molecules that are

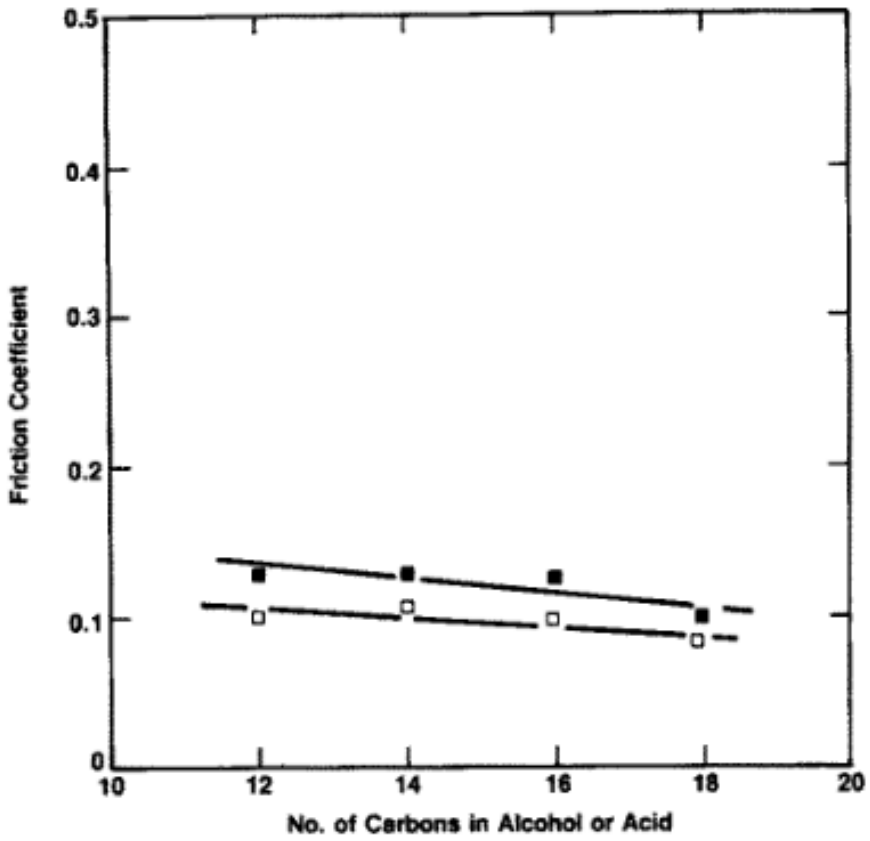

Figure 4.3: Effect of chain length of alcohols and acids on friction coefficient of n-hexadecane containing 1% additive 10mm s^{-1}.(Jahanmir, 1985) Reprinted with permission, Copyright ©1985 Elsevier B.V.

typical in OFMs, are effective friction modifiers within ICE temperature environments.

This research shows that longer chain lengths up to 18 carbons long are more effective at reducing a contact's friction coefficient and maintaining this friction reduction capability to higher temperatures than shorter carbon chains.

Further research by Studt confirmed the findings of Jahanmir.(Studt, 1989) With an almost identical trend observed with zinc di-n-alkyl dithiophosphates, which is a commonly used anti-wear additive. This trend shows that the size of the film, and as a result, the friction reduction capability of a compound is directly proportional to chain length.

Both of these papers performed experiments on pure sliding contacts; this is an important test to undertake and will give an idea of the performance of friction modifiers. However, pure sliding testing does not allow us to fully represent the types of contact

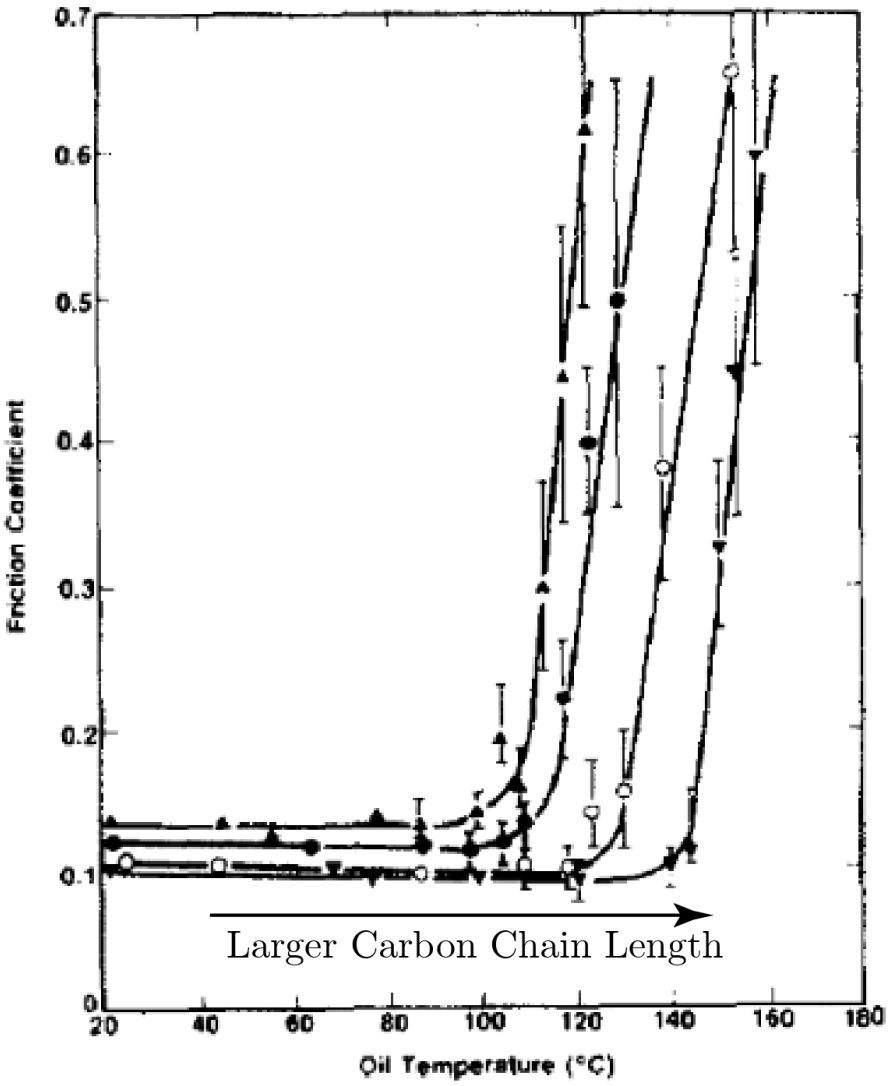

Figure 4.4: Effect of oil temperature on friction coefficient at low speeds for a series of fatty acids (1%) in n-hexadecane.(Jahanmir, 1985) Reprinted with permission, Copyright ©1985 Elsevier B.V.

in which a friction modifier will be present. Jahanmir also only performs tests up to a maximum of 60 turns of the ball on cylinder apparatus. Sixty turns is a relatively short test and, as a result, may not show the long term performance of these friction modifiers. Studt, however, does not provide information on the length of the test that was undertaken, meaning that the results of this paper could be at any time from machine startup. We also do not know the contact pressure within the Studt experiments as the pin diameter is not detailed. This lack of detail means that although the Studt experiments show the same trend as that by Jahanmir. We cannot tell if this is because they have undertaken an

almost identical experiment or that this is a general trend across various contact pressures and times. Although the Studt paper confirms the general trend of OFM's being more effective at higher chain lengths and that the bonding between the contact surface and the friction modifiers functional group is crucial, we can draw little else from the results detailed.

Other work has also investigated the effect of chain length on the performance of OFM style additives. Cameron and Crouch performed experiments on various OFM additives in different hydrocarbon oils to establish the scuffing load of a contact; this is the point where the OFM film fails, and as a result, the friction of the contact increases rapidly. They found that the scuffing point increased as the carbon chain length of the OFM increased, up until the length of the OFM is the same length as the hydrocarbon oil, this is shown in Figure 4.5. (Cameron and Crouch, 1963) They found this to be the case for multiple different hydrocarbon oils.

Further work by Askwith et al. confirms these findings and shows that the matching of the oil chain length to the OFM length results in a high surface viscosity film, as shown in Figure 4.6.(Askwith et al., 1966) This results in a stronger thin film, and as a result, the scuffing load increases. Scuffing is likely due to the stronger intermolecular bonds between the oil and the additive when their chain length matches.

Matching friction modifier and oil chain length, however, likely has limited engineering applications. Most commercially used oils are a mixture of different hydrocarbons with similar viscosities rather than pure chemicals. Making it almost impossible to match an additive to the oil components, and this has limited applications, which means that as a general rule, the development of OFM chain length has followed the research of Jahanmir and Studt, where larger chains are better with a plateau of around C18 being observed. Rather than the chain matching reported by Cameron and Askwith.

Another critical aspect of the design of OFM's is the chemistry of the polar head. The polar head affects the strength of bonding between the contact surface and the OFM and affects the stability of the film formed. All of the previous papers were undertaken on various functional groups, a reactive site resulting in a polar bond. All these results show that a more polar functional group leads to improved friction reduction performance.

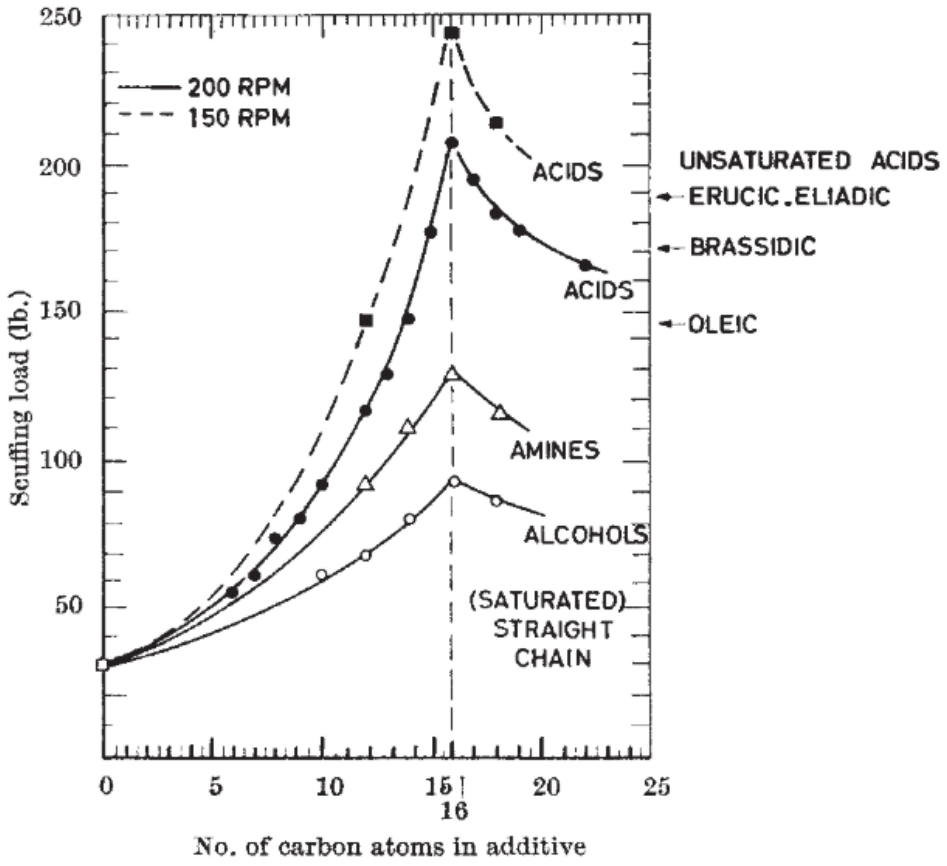

Figure 4.5: Scuffing Load vs OFM chain length for Hexadecane (C16) oil.(Cameron and Crouch, 1963) Reprinted with permission, Copyright ©1963 Nature Publishing Group

Leading to the general observation of most systematic papers that carboxylic acids are the most effective friction modifiers followed by alcohols and then amines with paraffins being the least effective.

Jahanmir et al. were able to model the effect of the head group on frictional performance.(Jahanmir, 1985) They showed that heads with larger free energy of adsorption to the surface would result in more considerable friction reduction capabilities. This effect is due to either increased hydrogen bonding at the surface or attraction between the chains, meaning the surface coverage and the film strength improved. As a result, most OFM's contain head groups that form as strong a bond as possible with the surface while avoiding any other adverse effects, e.g. corrosion due to acid groups.

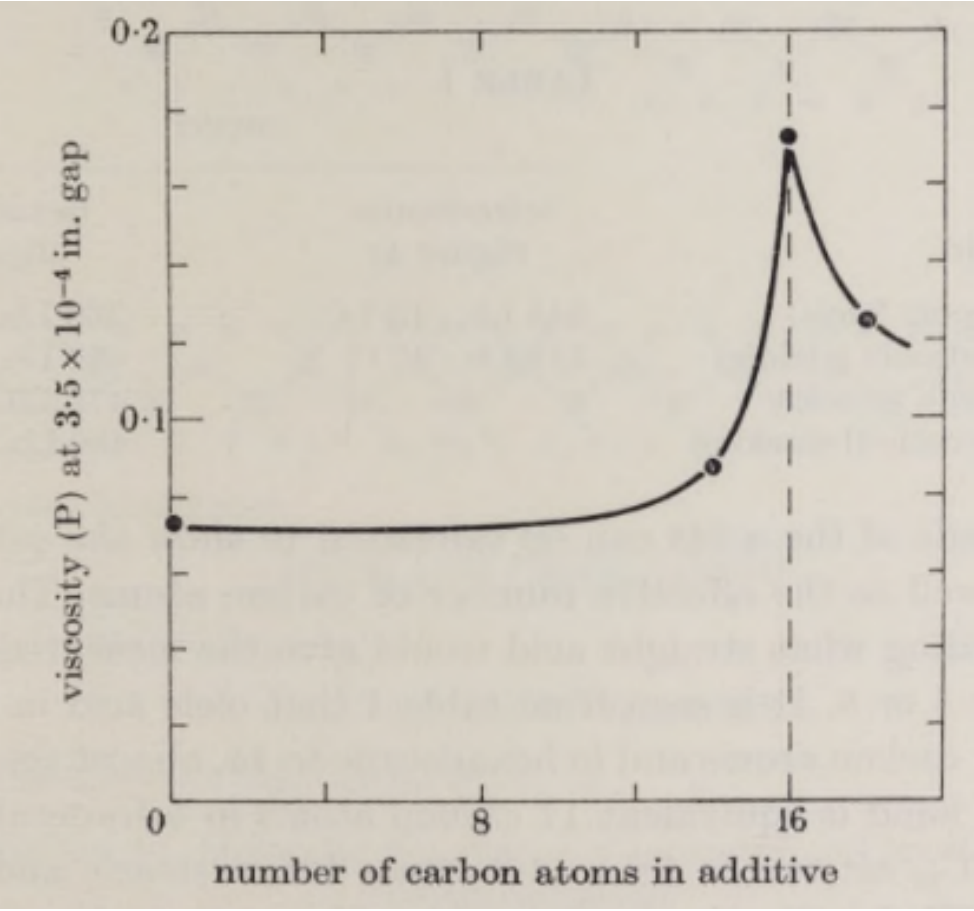

Figure 4.6: Viscosity of thin film of cetane (C16) containing additives.(Askwith et al., 1966) Reprinted with permission, Copyright ©1966 The Royal Society(U.K.)

4.2.3 Modern Organic Friction Modifier Research

Modern research into organic friction modifiers has primarily focused on a few main areas: the continued development of single-chain compounds through the study of different polar heads, the development of polymeric additives and the development of ionic liquids.

In recent years, demand for more environmentally friendly lubricants has led to a move away from petroleum-based lubricants and towards more polar biodegradable or synthetic oils. This increase in polarity of the solvent has meant that the adsorption of traditional acid-based friction modifiers is insufficient to reduce friction. Meaning that recent research has involved the addition of more than one functional group to make the friction modifier more polar and, as a result, improve their friction reduction performance.(Minami and Mori, 2007) One example of this is the development of glycerol monooleate (GMO),

see Figure 4.7, a long chain ester. GMO adsorbs to the surface and displays significant friction reduction on various surfaces, including steel and DLC, and has shown that it can perform this friction reduction by a different mechanism depending on the surface. GMO can hydrolyse to form a straight chain acid and adsorb to more polar surfaces such as steel or adsorb to less polar surfaces, such as DLC, in its ester form. The formation of the carboxylic acid group has been known for some time, but Topolovec-Miklozic et al. described the ester bonding method.(Topolovec-Miklozic et al., 2008) This was shown due to GMO's ability to significantly reduce friction in the mixed lubrication regime on DLC coatings. Indicating that either GMO can form a weakly adsorbed film that is stable in the lower pressure environment of the mixed lubrication regime but not higher pressures associated with boundary lubrication or that an adsorbed layer generates a more viscous liquid around it and is more able to prevent surface contact. The fact that this phenomenon was also observed with glycerol indicates a specific glycerol interaction with the DLC taking place.(Kano, 2006)

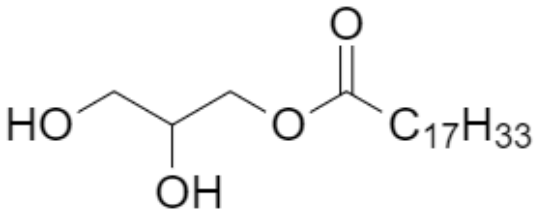

Figure 4.7: Structure of Glycerol Monooleate

There are some issues, however, with GMO and other alcohol derivative friction modifiers. The hydroxylation of them requires an oxidising or hydrolysing agent to be present either within the oil or on the surface of the metal; this can often require additive addition or coatings to be applied to the surface. (Yazawa et al., 2014) They can also undergo thermal breakdown or oxidative polymerisation at high temperatures, which reduces their lubricity properties. (Kenbeek et al., 2000) Some acid groups can also be corrosive enough to result in corrosion of the engine, meaning their long term use is not viable.

Although a large number of amine groups are effective at reducing friction in typical ICE conditions.(Zhao et al., 2012; Colucci and Fricke, 2007; Saccomando et al., 2012)

Primary amines, where only one carbon chain is attached to the nitrogen atom, cannot be used as friction modifiers, this is because they are shown to prevent the formation of anti-wear films and also act to degrade elastomers.(Spikes, 2015) This means secondary or tertiary amines, two or three carbons are attached to the nitrogen atom. This leads to shielding of the polar group, and they are often less effective friction modifiers.

One way in which non-primary amines can still be effective polar heads is through the use of cyclens. Here several amine groups are bonding together to form a spherical structure as the polar head. This clumping of polar groups allows for a strong polar head without the use of primary amines. Desanker et al. showed that 1,4,7,10-Tetra(dodecyl)-1,4,7,10-tetraaza-cyclododecane, structure and surface bonding, shown in Figure 4.8, was able to reduce friction and wear of a steel contact at temperatures up to 200°c by a greater amount than other commercially available primary amines.(Desanker et al., 2017) This result, though has only been shown to occur in a sliding contact with a relatively low contact pressure of 700MPa. This is a limited test, so it is not easy to know if these additives will be effective across the broad range of environments experienced in an ICE.

Recent research has been undertaken on borates as they display a wide variety of favourable properties such as being anti-wear, anti-oxidant, reducing friction, and their low toxicity and biodegrade-ability.(Erdemir, 2008) This was shown when Lovell et al. found that nanoscale boric acid provided was able to improve friction and wear performance by filling the surface asperities.(Lovell et al., 2010) This led to the development of organic compounds containing boron for use as friction modifiers. Philippon et al. showed that borate esters broke down within the contact to form a BO_3^{3-} which then reacts with an iron oxide surface to form a boron glass network, as shown in Figure 4.9. This boron glass significantly reduces the friction and wear of the contact.(Philippon et al., 2011) This has led to the development of many alkylborate compounds as potential friction modifiers.(Shah et al., 2012, 2011)

Much modern research on OFM's has evolved beyond single-chain compounds towards more polymeric based compounds. Many of these compounds also have the dual advantage of acting as viscosity index improvers within the oil. These so-called multifunctional polymers contain multiple adsorption points throughout the polymer chain. They can

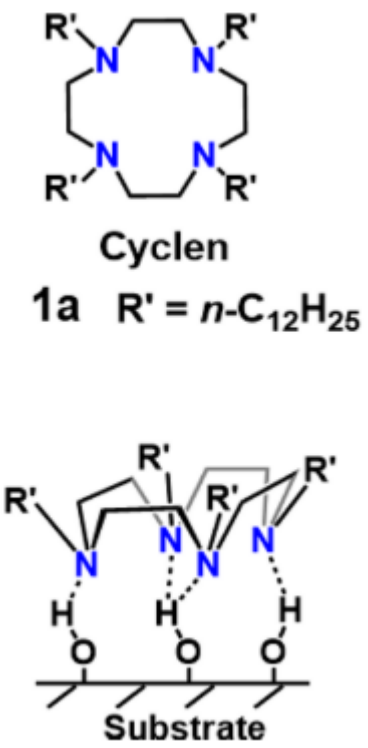

Figure 4.8: Structure and surface bonding of 1,4,7,10-Tetra(dodecyl)-1,4,7,10-tetraaza-cyclododecane.(Desanker et al., 2017) Reprinted with permission, Copyright ©2017 American Chemical Society

form a film in multiple different ways, as shown in Figure 4.10 as described by Brittain et al.(Brittain and Minko, 2007) The pancake configuration occurs when the polymer chain arranges across the surface and is expected when there are multiple bonding points along the chain. The mushroom and brushes occur when the bonding sites are concentrated towards the end of the polymer; here mushrooms typically occurs early during the adsorption process, while brushes form when the adsorption densities begin to increase.

Multiple pieces of work have investigated the effect of the location of the functionalised monomer within the polymer on its ability to reduce friction effectively.(Müller et al., 2006; Fan et al., 2007) These studies show that the polymers more effectively reduce friction when the functionalised, or polar, groups are concentrated to one end of the polymer in the form of a block copolymer, see Figure 4.11. This polar block generates a large polar head to the polymer and, as a result, will adsorb much rapidly and much more firmly than a statistical copolymer. This polar head nature will result in either a mushroom or brush

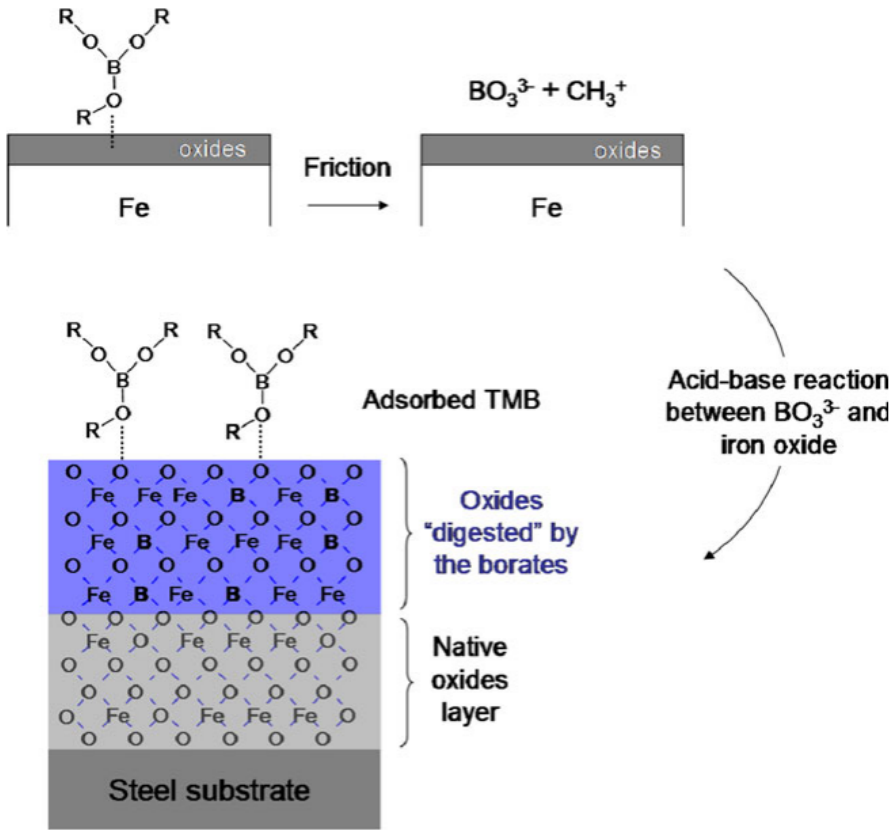

Figure 4.9: Formation of the boron glass tribofilm from borate ester.(Shah et al., 2013) Reprinted with permission, Copyright ©2013 Springer Science Business Media New York

Figure 4.10: Mechanism for adsorption of polymer friction modifiers.(Spikes, 2015) Reprinted with permission. Copyright ©2015, Springer Science Business Media New York

configuration of the polymer at the surface and, as a result, gives much higher coverage of the surfaces.

Work by Klein et al. was able to explain why these polymers act to reduce friction.

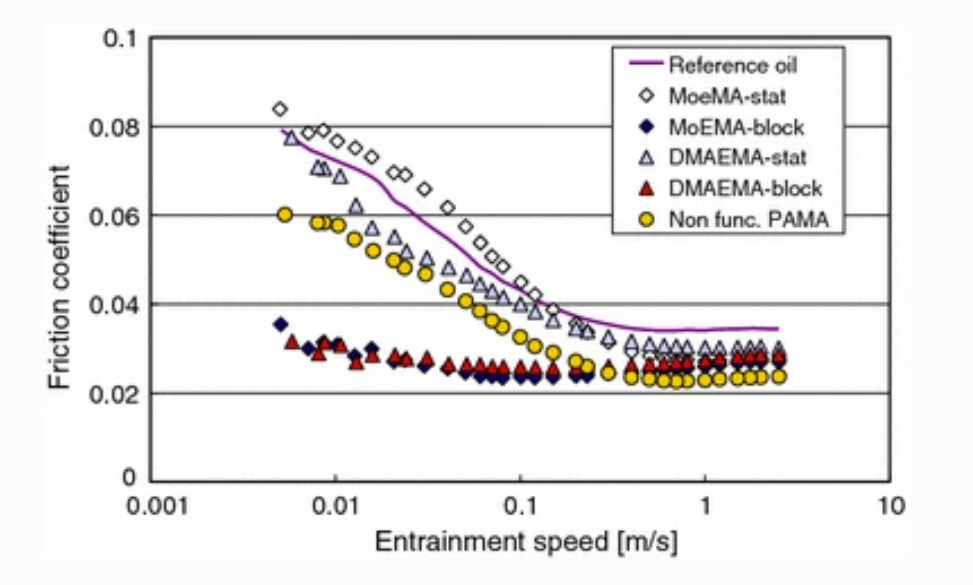

Figure 4.11: Friction versus entrainment speed for statistical and block copolymers.(Fan et al., 2007) Reprinted with permission. Copyright ©2007, Springer Science Business Media, LLC

When in a good solvent, a solvent where the polymer dissolves readily, molecular dynamics indicate little interaction between polymer chains on opposite sides of a contact. The osmotic pressure within the brushes acts to repel bushes on the opposite surface resulting, in the surfaces are held apart. Once sliding occurs, the chains all stretch with the sliding direction and as a result, the overlap of the opposite polymer chains is reduced further, resulting in very low friction.(Klein et al., 1994)

Cosimbescu et al. investigated star-shaped poly(alkylmethacrylates) PAMAs for use as both viscosity index improvers and friction modifiers. These stars had three arms and contained both polar and non-polar monomers in either a block or random configuration. They found that block copolymer stars effectively reduced friction in both the boundary and mixed lubrication regime, while when the polar content of the polymer went above 20%, the friction was reduced in both the block and statistical samples.(Cosimbescu et al., 2016) These polymers, however, were synthesised with relatively poor control meaning their dispersities are very significant. This high dispersity means that the size of the polymers varies quite greatly within test samples. Although this may not affect the friction performance of the polymers at all, this variation between samples may affect their

performance. Secondly, although many of the samples did produce friction reduction, this reduction was not particularly significant in the boundary regime. Also, comparisons with friction performance were only made to the base oil and a commercially available viscosity modifier, making it difficult to tell if this friction reduction was significant enough to allow these compounds to have commercial relevance as a friction modifier. Finally, the best performing polymer for friction reduction was the dodecyl methacrylate homopolymer that contains no polar content. This polymer will be the least likely to form a thin film, so the friction reduction was likely due to the viscosity thickening action of this compound, which means that any friction reduction by the other polymers could be due to this viscosity thickening mechanism. Without any surface analysis of the samples, it is impossible to say whether these polymers have formed a film like other friction modifiers or just acted to increase the oil's viscosity and allowed the oil to separate the contacting surfaces.

There have been multiple investigations into the effect of polyethylene (PE) as a polymeric friction modifier. Bercea et al. showed that low-density polyethylene chains formed suspensions of polymer coils within the oil when dissolved into oil at low concentrations (<2%). They found that these PE coils significantly reduced friction by up to 60% across a range of contact speeds. The PE also negated the effects of change in temperature of a contact on friction compared with pure base oil. It was theorised that it was due to these polymer coils adsorbing to the surface and friction is reduced.(Bercea and Bercea, 2009) Robinson et al. has also undertaken studies into highly branched PE with friction improvement occurring in the boundary and mixed regime.(Robinson et al., 2016b) Although Robinson et al. demonstrated that polar content improved friction performance, both papers show friction reduction with non-polar polymers. This friction reduction is somewhat unexpected due to the inability of these polymers to form a film, so we would expect the polymer to adsorb via a pancake configuration, if at all. Without any surface analysis of the contact, it is difficult to confirm this hypothesis. It could, in fact, just be because these polymer coils act to significantly increase the oil's viscosity across all the shear rates; this means the oil is more able to prevent surface contact. It is possible too that these coils may act to prevent surface contact themselves, effectively acting as soft ball bearings within the contact, but this is just a hypothesis that may be drawn from

these results.

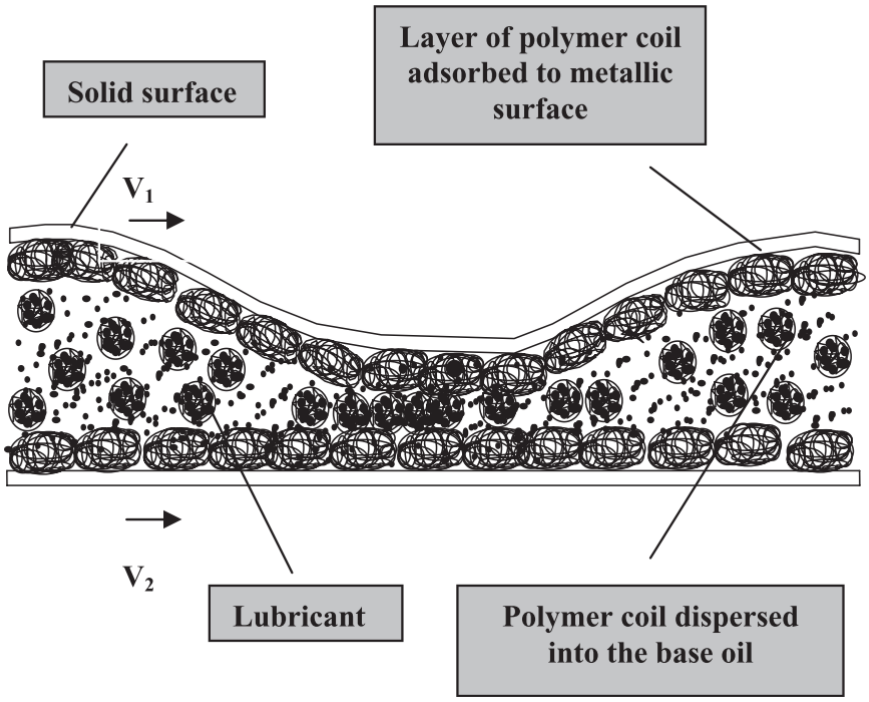

Figure 4.12: Proposed Schematic representation of the lubricant action in the prescence of polyethylene.(Bercea and Bercea, 2009) Reprinted with permission. Copyright ©2009, John Wiley & Sons, Ltd

Robinson et al. also investigated the use of aryl polyesters as viscosity and friction modifiers. They showed that these polymers could reduce friction in the boundary and mixed lubrication regimes and showed a similar friction reduction as a much more viscous oil and additive combination that was used as a benchmark.(Robinson et al., 2016a) These polymers are polar, and as such, it is reasonable to expect that they will form a thin film and, as a result, prevent contact and reduce the friction of the contact.

There are, however, some issues with polymeric friction modifiers. Firstly there is evidence to suggest that although these polymers are effective during continuous unidirectional movement, they may not be effective during more severe boundary conditions when a reciprocating contact is present.(Muller et al., 2008) There is also evidence to suggest that these polymers may not be effective in higher pressure or very low-speed contacts.(Klein et al., 1998). Suggesting that these polymer thin films are likely to break

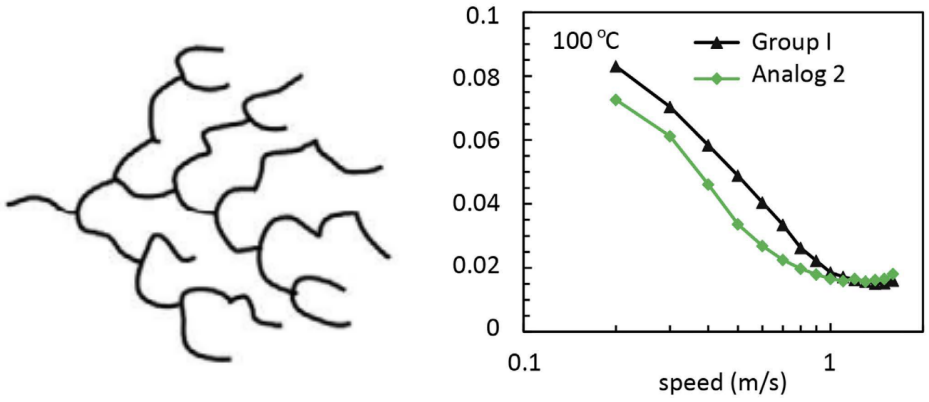

Figure 4.13: Left: example of hyperbranched polyester Right: friction performance of a hyperbranched polyester.(Robinson et al., 2016a) Adapted with permission. Copyright ©CC BY 4.0, https://creativecommons.org/licenses/by/4.0/legalcode

down in more extreme pressures and shears and cannot reduce friction. Also, these polymers are such large compounds that there will be a lot of steric hindrance between the chains. This steric hindrance means that close packing of the polymer film is unlikely to happen, and there may be limitations in their ability to reduce friction, or they may inhibit the formation of other additive films within the oil.

Ionic liquids are a more novel look at lubricants. These are charged liquids, made up of an anion and a cation, that have all the required properties of a lubricant. They are being viewed as a potential replacement to petroleum-based lubricants more typically used in engines due to their better wear, friction, anti-corrosion properties and potential to be biodegradable and non-toxic.(Ye et al., 2001; Stolte et al., 2012) This thesis will not focus on ionic liquids being used as a replacement for oil and will instead focus on research into their use as additives to existing lubricants. Examples of ionic liquids were shown in Figure 4.14.

Ionic liquids are charged carbon compounds and a large number of them are insoluble in carbon-based lubricants. Research into ionic liquids as additives began in earnest with the discovery of an oil-soluble ionic liquid in 2012 by Qu et al. They synthesised trihexyltetradecylphosphonium bis(2-ethylhexyl) phosphate that was fully soluble in a variety of carbon-based solutions, at 5 wt% this compound was able to effectively reduce wear and friction of a contact by up to 60%.(Qu et al., 2012) The difference between this compound

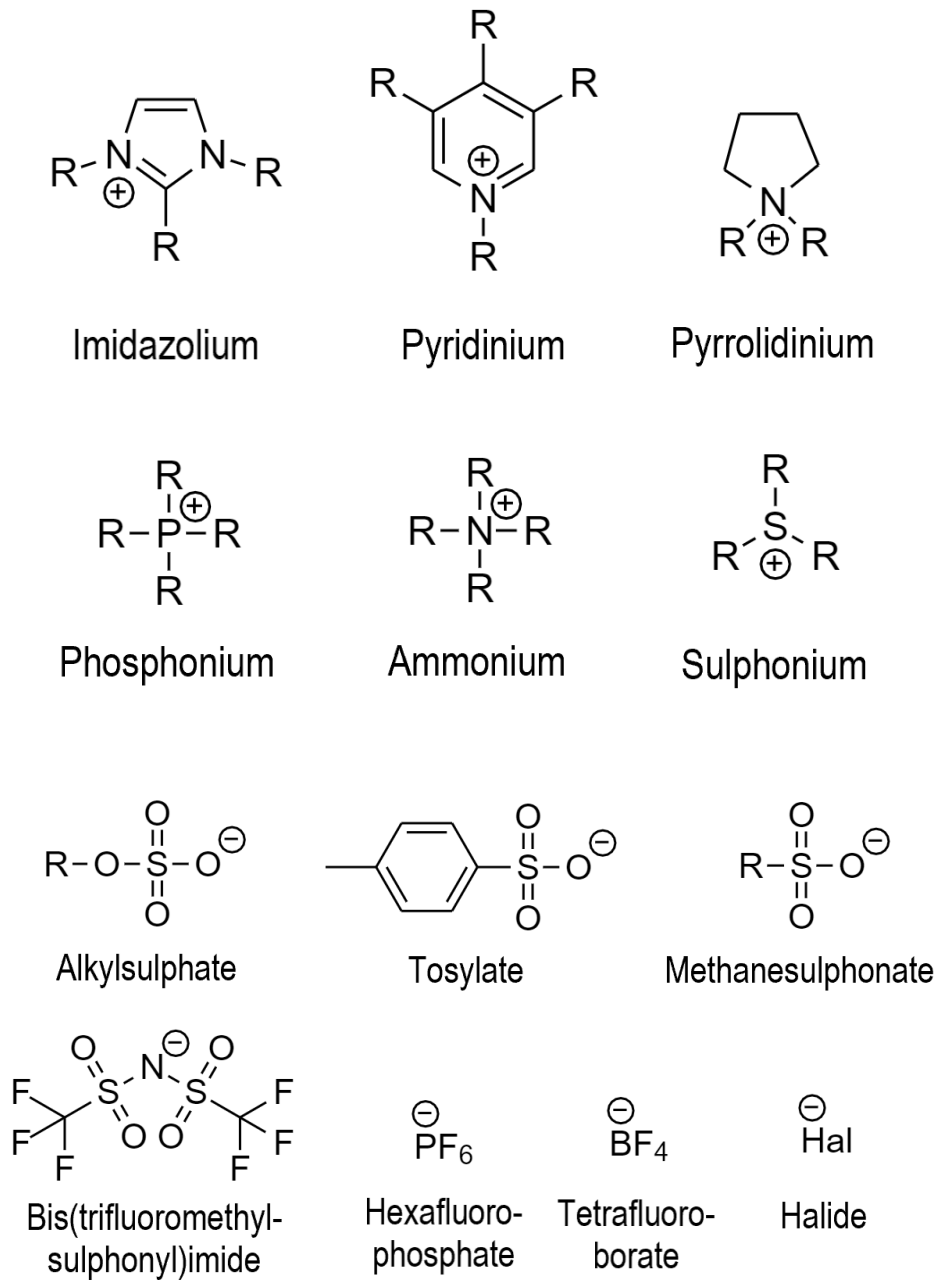

Figure 4.14: Examples of ionic liquids. Top: anions Bottom: cations

and previous ionic liquids was that both the anion and the cation had long carbon chains on them. These carbon chains act to reduce the charge density of the compounds and makes them soluble in oils. This ionic liquid was shown to form a thin film on the contact and can prevent surface contact.

Somers et al. further researched the solubility and performance of various ionic liquids in several oils. They found that most ionic liquids were soluble in polar oils so long as they had long carbon chains, whereas when a less polar oil was used, the bonding between the ions also had to be stronger. However, for ionic liquids to be effective within the oil, the ions have to be free of their opposing ion and any solvent interactions to adsorb to the contact and form a tribofilm. These factors explain why IL's were more effective at reducing friction in non-polar oils than more polar oils, both at lower concentrations and higher loads. With fewer ion to solvent interactions occurring in the non-polar solvent.(Somers et al., 2013)

Work by Huang et al. investigated the mechanism by which ionic liquids additives lubricate a contact. They did this by varying the anion of the liquid and using a variety of surface analysis techniques, and applying charges to the surfaces to effectively repel or attract the different charges of the ionic liquid. They found that at low loads, the ability of the ionic liquid to adsorb to the surface with the cation adsorption being of particular importance to the tribological performance. While at higher loads, the formation of a tribofilm by a chemical reaction of the ionic liquid to the surface becomes essential.(Huang et al., 2017) This means that for an ionic liquid to be effective in all conditions, it must be able to adsorb strongly to the surface, with the cation, in particular, having a long chain that can provide a dense packing at the surface; and then be able to undergo a breakdown reaction with the surface as loads increase. This paper does only investigate two ionic liquids that only vary due to their cation. These findings then may not be universal for all the different chemistries present within ionic liquids. This research also only investigates a steel-steel contact while other contacts may behave differently.

One of the most investigated ionic liquids are phosphonium cations, similar to those by Qu et al.(Qu et al., 2012) Barnhill et al. and Zhou et al. and have shown that phosphonium ionic liquids reduce friction.(Barnhill et al., 2014; Zhou et al., 2014) Barnhill et al. investigated the cation structure and found that smaller, more symmetrical cations show the greatest frictional performance due to their higher density and more thermally stable tribofilm. Unfortunately, larger carbon chains are required in order to be soluble in oil. Zhou et al., however, investigated the anions associated with the phosphonium

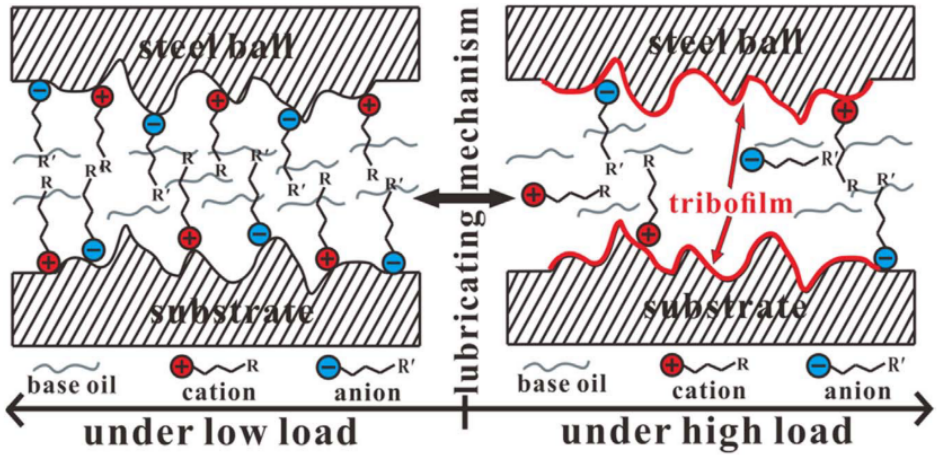

Figure 4.15: Proposed lubricating mechanism for Ionic liquids in a steel-steel contact.(Huang et al., 2017) Reprinted with Permission. Copyright ©2016 Elsevier Ltd

cation. They showed that molecule size alone determined oil solubility, and tribological performance showed the trend: organophosphate > carboxylate > sulphonate. Their results indicate that this anion primarily determines the formation of the tribofilm and reduce friction and wear.

Research into the use of ionic liquids with the common anti-wear additive ZDDP was undertaken by Qu et al. They found that ZDDP had a synergistic effect both in terms of friction and wear reduction with phosphonium-alkylphosphate ionic liquids; this effect is not present if either the chemistry of the anion or the cation is changed. They found that when the ZDDP and alkylphosphate, there was a significant increase in the oxygen, zinc, sulphur and phosphorous within the oil. These elements are the main components of the tribofilm, and their increased concentration would make the tribofilm formation more effective, resulting in friction and wear being substantially decreased. There is also a substantial change in the atomic ratio when compared with just a ZDDP additive; this is due to a chemical reaction between the ZDDP and the alkyl-phosphate anion due to the oxygen group forming a stronger bond to the zinc than the sulphur group, the reaction is shown in Figure 4.16. The tribofilm is generated with much higher zinc phosphate and iron phosphate than typical tribofilms and far fewer oxide groups and forms a tribofilm that has a lower hardness but due to the high concentrations of active elements can be replenished rapidly, leading to a sacrificial and self-healing tribofilm that maintains very low friction

and wear.(Qu et al., 2015) This work is very interesting and suggest synergism between different additives with inorganic liquids. There is no understanding exactly why this only occurs with the one group of inorganic liquids as it would be expected that another with the same alkylphosphate anion would exhibit the same phenomena, but this does not occur. Meaning that any synergistic effects of ionic liquids and other oil additives are likely to be very specific to that particular ionic liquid species, and more research should be undertaken in this area.

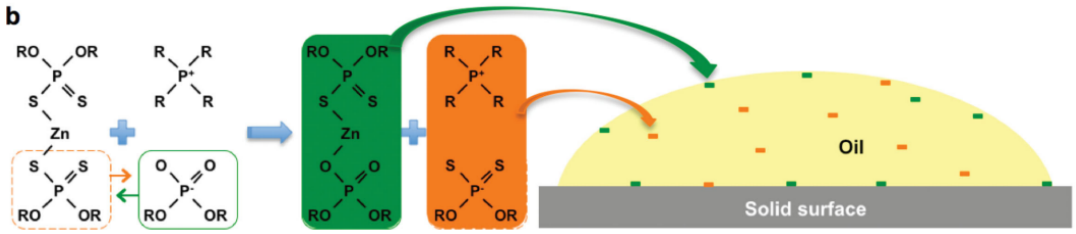

Figure 4.16: Formation of zinc alkylphosphate alkyldithiophosphate from the synergistic effect of ZDDP with phosphonium alkylphosphate anion.(Qu et al., 2015) Reprinted with permission, Copyright ©2015 Wiley-VCH Verlag GmbH & Co. KGaA, Weinheim

Other ionic liquids that have been investigated include methylimidazolium based ionic liquids. Battez et al. showed that these ionic liquids could reduce both friction and wear when added to mineral oils. These contained an anion that contained fluoride, and this resulted in the formation of a fluoride tribofilm.(Battez et al., 2009) These tests were performed in the mixed lubrication regime due to relatively low loads, meaning these experiments do not recreate the highest friction and wear conditions of a contact. Also, neither of the ionic liquids are readily soluble in the oil due to relatively small and highly polar anions. Fluoride tribofilms are also known to be unstable in the presence of water and can lead to a large amount of corrosion if it is present. As a result, these particular additives are not useful in an ICE but show methylimidazolium-based ionic liquids' potential.

Pyridinium based ionic liquids have also been investigated, such as work by Mahrova et al. on dicationic pyridinium ionic liquid. Here two pyridinium cations are bonded together with a polyethylene glycol chain connecting them. These displayed increased thermal stability than a monocationic pyridinium ionic liquid while also displaying significantly improved friction performance even at very low concentrations.(Mahrova et al., 2015)

One interesting area of research is the development of ionic liquids from natural sources,

such as amino or fatty acids. Work by Song et al. and Alves et al. found that these additives can be effective, but their experiments were either performed on pure ionic liquid or with another ionic liquid in solution.(Song et al., 2014; Domingos Alves et al., 2019) Work by Rivera et al., however, investigated fatty acid-based ionic liquids additives within a polyol ester motor oil. These oils showed friction improvement in a pure sliding contact at 25°C.(Rivera et al., 2019) These compounds, though do not show stability at temperatures that would be expected in an ICE due to these compounds not having high thermal stability. They also do not show effective friction reduction in situations where there is a sliding and rolling within the contact, meaning these compounds may not be effective for ICE conditions, but these early results suggest that there may be a potential for more environmentally friendly ionic liquid additives.

4.3 Inorganic Friction Modifiers

4.3.1 Mechanism of Inorganic Friction Modifiers

It has been known for some time that MoS_2 is capable of reducing friction within a contact.(Winer, 1967; Risdon and Gresty, 1975) This has been shown to occur across a variety of contact conditions, but MoS_2 itself is not soluble in motor oils, leading to the development of organomolybdenum compounds. These compounds make the molybdenum soluble within the oil and are then able to break down to form the MoS_2 film. The first of these organomolybdenum compounds was reported by Spengler et al. they found that when organomolybdenum compounds were added to mineral oils in the presence of sulphur, the compounds will thermally decompose to form MoS_2 that can then act to reduce friction.(Spengler and Weber, 1959)

Work by Graham et al. identified various ways that organomolybdenum compounds act to reduce friction within a contact. They showed that organomolybdenum compounds produced a rapid transition to low boundary friction, which was most effective at high additive concentrations and temperatures. This friction reduction was shown to occur only in reciprocating or high load rough surface continues contacts. They showed that this very low friction coefficient is due to the formation of nanocrystal MoS_2 upon the

asperity peaks. These flakes are shown to be very thin with only a few atoms thick and less than 30nm in diameter; the fact they only form on asperities indicates that surface contact is required for the formation of MoS_2. The lack of MoS_2 outside of the asperities indicates the mechanism for the formation of MoS_2 requires asperity contact and the high temperatures and exposure of an unreacted iron surface. Resulting in the iron being able to act as a catalyst to reduce the molybdenum to form the MoS_2 layers.(Graham et al., 2001)

Work by Groissiord et al. observed MoS_2 within the wear scars via XPS and used TEM to reveal individual sheets of MoS_2 that are a few atomic layers thick as shown in Figure 4.17 These sheets were only generated within the wear scar and the formation of these films requires surface contact to occur, again indicating a catalytic reaction with the surface.(Grossiord et al., 1998) A mechanism was presented, see Figure 4.18, but there is no evidence presented to confirm this mechanism and should be taken as a hypothesis. This method for the formation of MoS_2 is unlikely to occur via this manner. Firstly, it requires the breaking of very strong Mo=O bond while the much weaker Mo-S bond is retained; thermodynamically, this will not occur and in the event that the Mo=O bond breaks as would the Mo-S bond. It is possible that another additive or contact surface is acting in a synergistic or catalytic method for this reaction to occur. For example a lone pair on the oxygen could form a ligand bond to another metal within the contact, this would significantly weaken the Mo=O bond and may result in it breaking preferentially to the Mo-S bond. This, however, is not shown by Groissiord et al. and there is no evidence to prove this theory and as such can only be seem as a hypothesis for how a mechanism similar to that proposed in Figure 4.18 may occur.

Work by Topolovec Miklozic et al. confirmed the findings by Groissard et al. They used AFM and Raman to show that MoS_2 was formed when friction was reduced. These low lateral force areas were located only on rubbed surface high spots and were 10-40nm in diameter and 1-2nm thick.(Miklozic et al., 2001) This, combined with the previous work discussed, shows that these MoS_2 sheets form only upon surface asperities where the contact pressures are highest, this indicates a catalytic mechanism for their formation with the contact surfaces, but the exact reaction mechanism is still somewhat unverified.

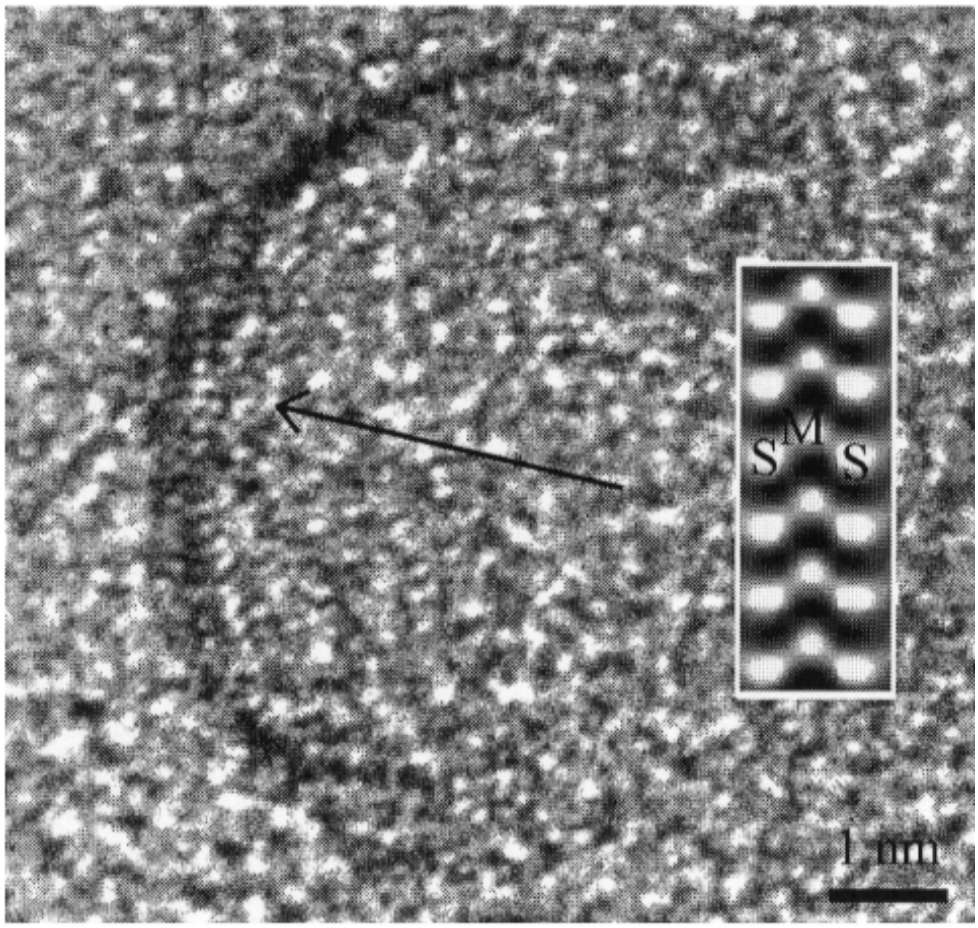

Figure 4.17: HRTEM image of wear debris revealing chevron-like structure of MoS_2 sheets.(Grossiord et al., 1998) Reprinted with permission, Copyright ©1999 Elsevier Science Ltd.

An alternative mechanism was suggested by Coffey et al. they suggested that the C-S bond was, in fact, cleaved and as such, the sulphurs remained attached to the molybdenum.(Coffey et al., 1996) This does not solve the issue of the stronger Mo=O bond breaking in preference to the Mo-S bond. These mechanisms also do not explain how organomolybdates that do not contain sulphur are still able to generate MoS_2 films on asperity contacts.(Yamamoto et al., 1987) This must be down to the transfer of sulphur from the oil or another additive present and has lead to the belief that organomolybdates have a synergistic relationship with the sulphur-containing anti-wear additive ZDDP.

Kasrai et al. investigated the effects of ZDDP addition on the performance of the organomolybdenum MoDTC; they found that friction and wear of a contact were reduced significantly by combining the two additives when compared with just one at a time.

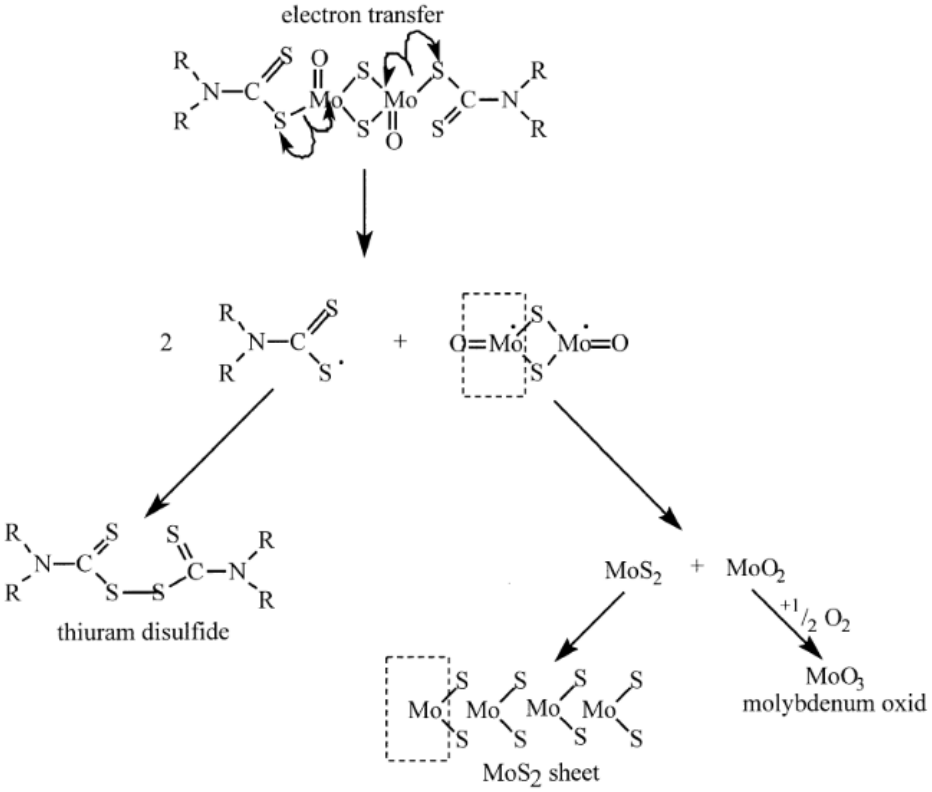

Figure 4.18: Proposed mechanism for the formation of MoS_2 sheets.(Grossiord et al., 1998) Reprinted with permission, Copyright ©1999 Elsevier Science Ltd.

They found that when just MoDTC was present, the MoS_2 film contained sulphates which were mainly on the surface. When ZDDP was added, these sulphate groups were not present. Meaning that ZDDP is sufficient enough to prevent the oxidation of the MoS_2, and so generates a better MoS_2 film; this suggests that these sulphates may lead to higher friction within the contact.(Kasrai et al., 1998)

Martin et al. suggested, however, that instead of promoting film production, the addition of ZDDP instead acted to remove the hard abrasive MoO_3 that can also act to oxidise and remove the MoS_2 film. This oxide removal involves the acid-base reaction between the MoO_3 and the Zinc polyphosphate glass and so this MoO_3 is removed.(Martin et al., 2000)

Morina et al. also reported that ZDDP increases the long term stability of the MoS_2 film. They found that when MoDTC was no longer present within the oil, meaning the MoS_2 film could not be replenished, the film broke down rapidly unless ZDDP was present.

This MoS_2 film protection is believed to be due to the high anti-wear of the ZDDP film that forms the base of the MoS_2 film.(Morina and Neville, 2007)

These results show a synergistic relationship between ZDDP and organomolybdenum friction modifiers; although this may not be additive synergistic, adding each improves the performance of the other at all concentrations.(Spikes, 1989) The exact mechanism by which this synergistic relationship occurs, however, is not fully understood, and the large number of different potential ways that have been reported suggest that the exact mechanism could be very complicated. With the increased push towards more environmentally friendly oil additives, there is also a push to remove sulfur-containing compounds from oils. This push would mean the removal of ZDDP and sulphur containing MoDTC groups from oils; this would lead to the inability to generate a MoS_2 film. Meaning the long term future of organomolybdenum friction modifiers is very much in question.

One of the negatives of using organomolybdenum compounds as friction modifiers is that if there is low sulphur or the system is oxidising, friction is not reduced. This lack of friction reduction has been observed by a variety of researchers and has been attributed to a variety of possible reasons: a ligand exchange between ZDDP and the organomolybdenum; oxidation of the MoS_2 to abrasive MoO_3; or that the organomolybdenums can even act as anti-oxidants themselves.(Johnson et al., 1997; Hoshino et al., 1998) No matter the explanation, this means that the performance of these compounds may be somewhat limited in some environments. Windom et al. performed Raman spectroscopy studies of MoS_2 films and showed that some oxidation of these films might even occur at ambient temperatures. This oxidation is minimal but becomes significant at around 375K, a lower temperature than a typical ICE would expect.(Windom et al., 2011) This research was performed in an oxygen atmosphere without any lubrication present and may not be representative of what we would expect in an engine but does suggest that breakdown of MoS_2 films to MoO_3 will occur at these temperatures, in particular if the films are exposed to some oxidising agents that are present within an engine such as nitrogen oxides.

4.3.2 Development of Inorganic Friction Modifiers

Research into organomolybdenum compounds has primarily centred around two main compounds MoDTCs, MoDDPs and organomolybdate, see Figure 4.19 for examples of each. All of these compounds work via the same mechanism as detailed above with the formation of MoS_2 film 4.18. As a result, there has been limited research into the effect of the rest of the compound on organomolybdenum compounds performance, with focus concentrated around the Mo and S within the compound. As a result, there is little consensus on the best design for organomolybdenum compounds like with OFM's.

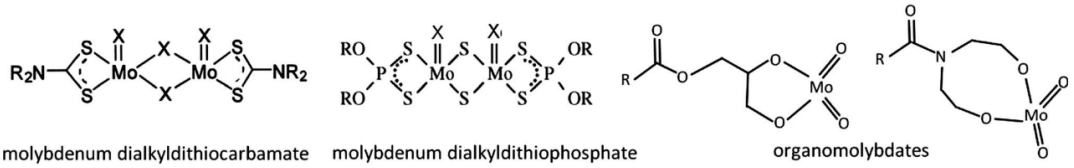

Figure 4.19: The three main organomolybdenum friction modifiers (Spikes, 2015) Reprinted with permission. Copyright ©2015, Springer Science Business Media New York

Some work has been undertaken to establish the best alkyl groups upon organomolybdenum groups. Sarin et al. shows that the alkyl group size has minimal effect on MoDDPs ability to reduce friction and wear within a contact.(Sarin et al., 1994) While two recent patents have suggested that having different alkyl groups result in MoDTC helps to lower friction with asymmetric amines being particularly effective.(Tanaka et al., 1997; Tynik et al., 2010) The reasoning for these observations, though, are unknown, and without more systematic investigations into the effect of alkyl groups on organomolybdenum compounds, it is not easy to understand their influence.

4.3.3 Modern Inorganic Friction Modifier Research

In recent years there has been limited research on improving organomolybdenum compounds for use on steel contacts; this is primarily due to understanding the mechanism by which this friction reduction occurs and the large number of known organomolybdenum compounds that can reduce friction in these conditions. Instead, work has predominantly focused on other types of contacts, in particular diamond-like carbon (DLC) based contacts.

Research by Barros et al. shows that the addition of MoDTC to a DLC contact can decrease the contact's friction and wear. XPS shows this is due to the formation of MoS_2 films within the contact area in a similar manner to steel contacts.(De Barros'bouchet et al., 2005) These results, as well as those shown on ZDDP films, indicate that organomolybdenum films can form on any contact regardless of the surface chemistry. This universal film formation mechanism indicates the reaction is not the result of catalysis by the surface and is an intramolecular reaction due to the stress and temperatures associated with the contact; this could indicate that organomolybdenum compounds may be universal friction modifiers for all contacts.

A large amount of research has suggested that the addition of organomolybdenum compounds to a DLC contact can increase the wear of the contact.(Vengudusamy et al., 2012; Yang et al., 2014; Haque et al., 2009) Work by Okubo et al. used Raman, XPS, ToF-Sims and nano-indentor to show that this increased wear due to MoDTC is due to the formation of hard and abrasive molybdenum carbide films. These molybdenum carbides result in increased wear only observed for DLC coatings where the hardness is less that of the molybdenum carbide film. They showed that adding ZDDP inhibits the formation of the molybdenum carbide and can therefore be used to limit wear within the contact.(Okubo et al., 2019) This again shows the synergy of organomolybdenum compounds with ZDDP but also shows that although organomolybdenum compounds may be universal friction modifiers, their effect on other aspects of the tribology may be unknown. With the move towards less ZDDP within the oil and more DLC being present within engines, organomolydenums may begin not to be as valuable as friction modifiers as in recent years.

4.4 Nanoparticle Friction Modifiers

One of the significant issues with the friction modifiers already discussed in this thesis is that they work by generating a film upon the surface of the contact. This film generation has many consequences, firstly these films often take some time to generate, and friction reduction is not achieved during the running-in period. These films can also be removed

from the surface and no longer act to reduce the friction of a contact. Finally, these films have to form upon the surface and often have to compete for contact space with other additives within the oil; this can reduce the effectiveness of the friction modifiers and the other additives.

Recent research has looked into nanoparticle-based friction modifiers; these are small enough to remain dispersed throughout the oil and fit through any filters and can reduce friction and often wear a contact.

4.4.1 Mechanism of Nanoparticle Friction Modifiers

Due to the wide variety of nanoparticles being investigated as friction modifiers and the early stage of the research, there have been various mechanisms theorised for how these nanoparticles can reduce friction. These mechanisms are shown in Figure 4.20. The rolling effect occurs when hard nanoparticles roll between the contacting surfaces, similar to what would occur with ball bearings. This rolling effect converts any sliding in the contact into sliding-rolling, resulting in substantially reduced friction and wear. The protective film is very similar to what has been observed with the previously discussed friction modifiers. Here the nanoparticles chemically or mechanically bond to the surface and prevent surface contact. The mending effect and the polishing effect act to reduce friction and wear by reducing the surface roughness of the contact, generating a smooth surface where less friction and wear can occur; this is known as surface enhancement effects. The mending effect occurs when nanoparticles deposit within any troughs, while the polishing effect removes the asperities from the surface. It is also possible that a combination of all these effects may occur.

Lee et al. investigated the role of nanoparticles in oil. They showed that nanoparticles within an oil acted to reduce the friction coefficient across all loads significantly. The increase in friction due to an increased load is also significantly reduced when compared with mineral oil. This friction reduction indicates that the nanoparticles are acting to prevent surface contact even at high loads, although they did not distinguish whether the rolling effect or a protective film was the cause for this. They then reused the previous surfaces without any nanoparticles present and found that the friction coefficient was re-

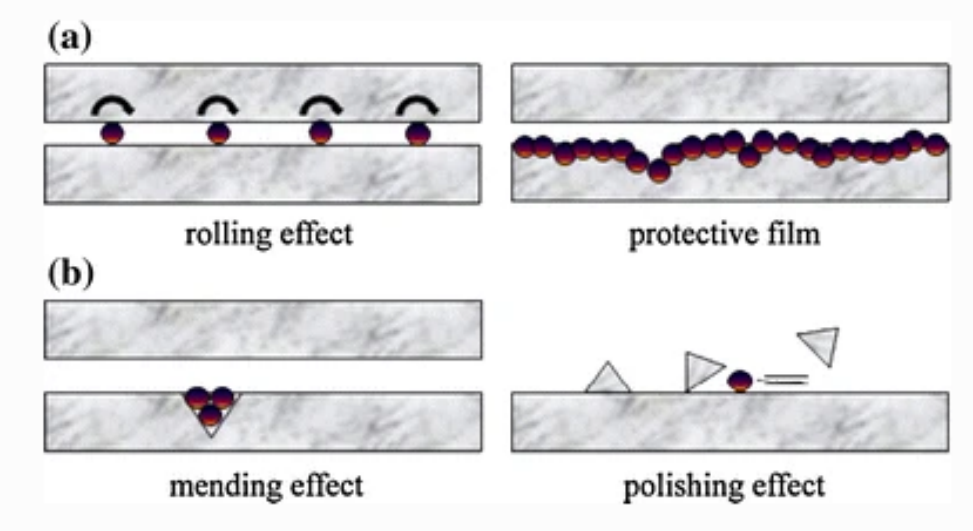

Figure 4.20: Possible lubricating mechanisms of nanoparticles within oil.(Lee et al., 2009) Reprinted with permission. Copyright ©2009, Springer Science Business Media, LLC

duced compared with those that had just been tested with mineral oil. The performance of these recycled surfaces suggests that some surface modification has occurred, and this was confirmed as surface roughness measurements of the surfaces showed that the nanoparticle surfaces were smoother than those immersed in mineral oil. Although again, they did not distinguish whether this was a polishing or mending effect.(Lee et al., 2009) These tests show that nanoparticles can interact with a contact in multiple ways to reduce friction effectively.

It is also possible that the mechanism by which nanoparticles reduce friction and wear depends upon the contact conditions. Work by Tevet et al. investigated the mechanisms that inorganic fullerene-like nanoparticles (IFs) can reduce friction and wear. Fullerenes are carbon compounds made up of rings of 5-7 carbons bonded together to form a mesh, examples of this are displayed in Figure 4.21. Inorganic fullerenes are similar to carbon fullerenes, but instead of carbon are made up of metal salts. They used in situ nanocompression, shear and scanning electron microscopy on a single nanoparticle to observe how these nanoparticles react to various contact environments. They showed that these IFs act to reduce friction by rolling within the contact at low loads, similarly to a ball bearing within the contact. A sliding mechanism occurs at slightly higher loads where the two surfaces are sufficiently close to prevent rolling. Here, the low surface energy of the various

planes of the IF allows it to shear while still maintaining its robust structure. These dual mechanisms prevent surface contact while also providing a low friction contact. At higher loads, an exfoliating mechanism occurs; here, the high stress on the nanoparticle causes it to break down to form a film upon the contacting surfaces, depositing on the asperities of the contact and lower friction of the contact. Examples of this are shown in Figure 4.22.(Tevet et al., 2011) This work displays that nanoparticles may act to reduce friction in a variety of different ways depending on the contact environments; as a result, their use as lubricant additives may be helpful across a wide range of applications. Work by Lahouji et al. using TEM-AFM on MoS_2 IFs rather than the WS_2 IFs discussed by Tevet et al. confirm the variety of mechanisms shown in Figure 4.22.(Lahouij et al., 2011) This suggests that these mechanisms may occur for a wide range of nanoparticle IFs.

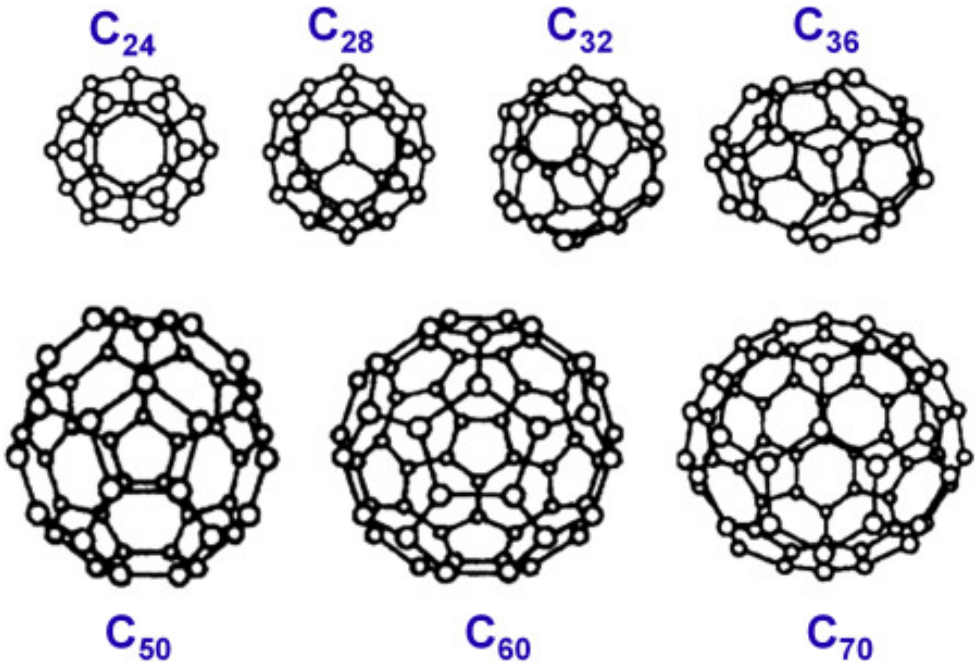

Figure 4.21: Examples of carbon fullerene compounds.(Malhotra and Ali, 2018) Reprinted with permission. Copyright ©2018 Elsevier Inc.

Further work by Lahouji et al. imaged and modelled the compression of a WS_2 IF. Here, nanoindenter-TEM was used to image the IF and record physical measurements of these IFs for use in modelling. They showed that upon compression, the hollow IFs compress; this compression continues until the space is no longer present and then the particles begin to tear and result in WS_2 nanosheets from the exfoliation. This exfoliation

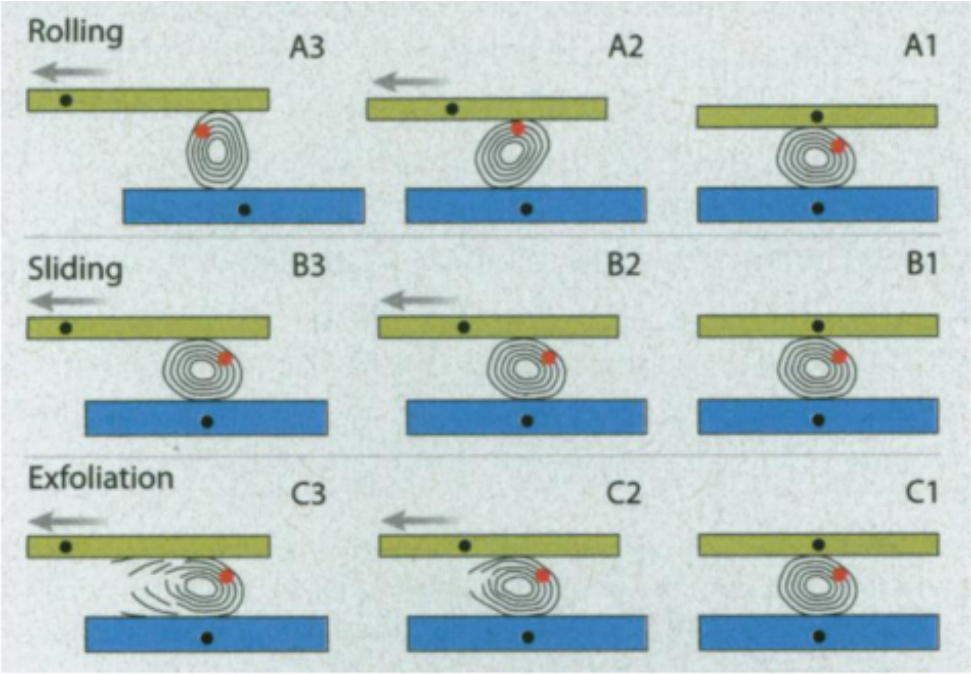

Figure 4.22: Mechanisms of multilayered IFs. The bottom surface is stationary as the upper surface moves left, similar to the AFM experiments undertaken (Tevet et al., 2011). Reprinted with Permission.

forms WS_2 layers upon the contact, which act to reduce the contact load. The fullerene particle is not reformed upon the decompression of this contact, and as such, this load reducing film is maintained and will result in lower friction and wear of the contact. This process is shown in Figure 4.23. Modelling this produces similar results as the experimental data and shows that the orientation of the fullerene with the contact also has a significant effect on how the fullerene responds to compression.(Lahouij et al., 2012) This work gives an idea of how inorganic fullerenes may interact within a contact and confirms the findings of previous work by Tevet et al. and Lahouji et al., and potentially provides a clear idea of the mechanism by which these nanoparticles lower friction. First by acting as bearings within the contact before significant pressure causes their exfoliation to generate low shear nanosheet films upon the contact surface.(Tevet et al., 2011; Lahouij et al., 2011) This work, however, does not take into account any shear that occurs within the contact and is, therefore, not fully representative of a contact.

Work by Joly-Pottuz et al. aimed to model how carbon-based "nano-onions" reduce friction within a contact. These nano-onions are spherical nested structures like fullerenes,

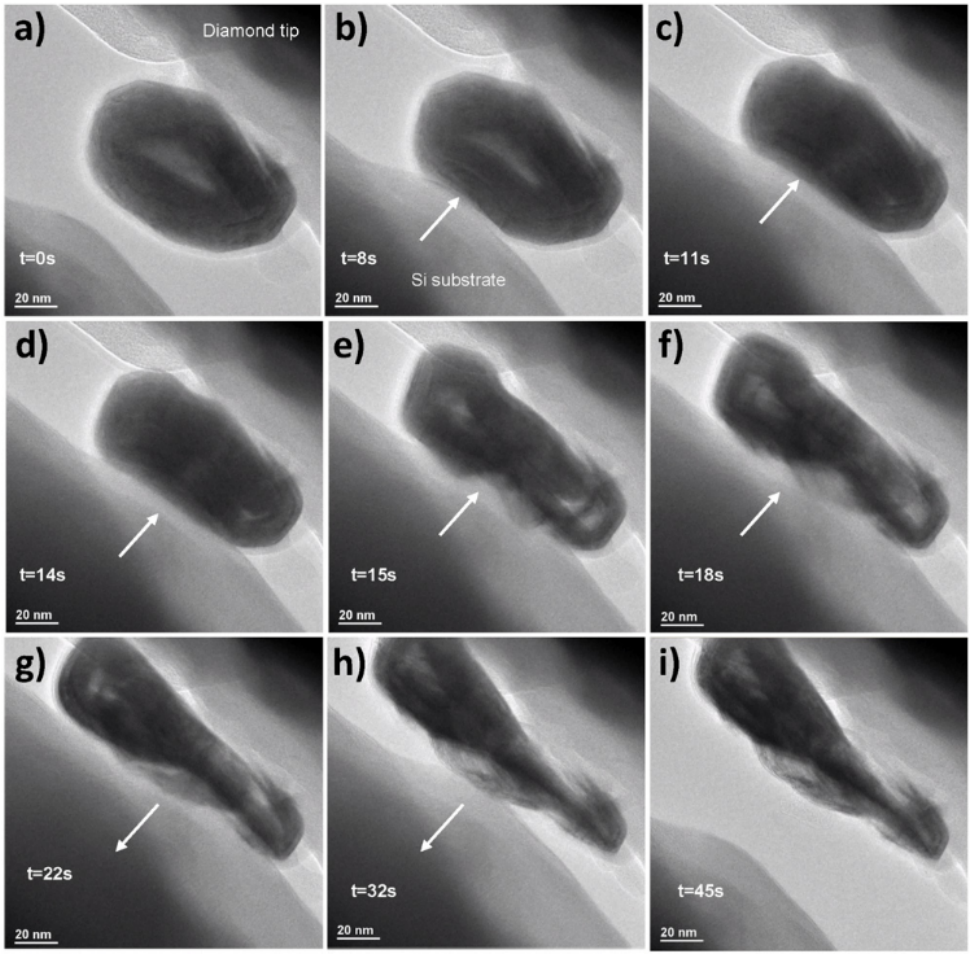

Figure 4.23: Images captured by nanoindentor-TEM of the compression of a WS_2 inorganic fullerene. (Lahouij et al., 2012) Reprinted with Permission. Copyright ©2012 IOP Publishing Ltd

and their lubricating mechanism is more complicated than IFs. Joly-Pottuz et al. used experimental data and molecular dynamics simulation to establish this mechanism. They found that carbon nano-onions without diamond cores were most effective at reducing friction and wear due to the abrasive nature of the diamond core. One interesting observation is that the addition of the nanoparticles encouraged the steel contacts to oxidise and form iron oxide with the magnetite crystal structure. This iron oxide is lubricious to the contact. They also found that instead of breaking down like IFs, these nano-onions remain intact and merely are compressed to form a tribofilm. These intact particles are then able to roll through the contact and, as a result, act via the rolling effect, see Figure 4.24.(Joly-Pottuz et al., 2010) One issue with this modelling is that it was undertaken on

a DLC contact. Here the interactions between the carbon nano-onions and the contact will be minimal, this may not be the case in a more traditional steel contact, which should be modelled too.

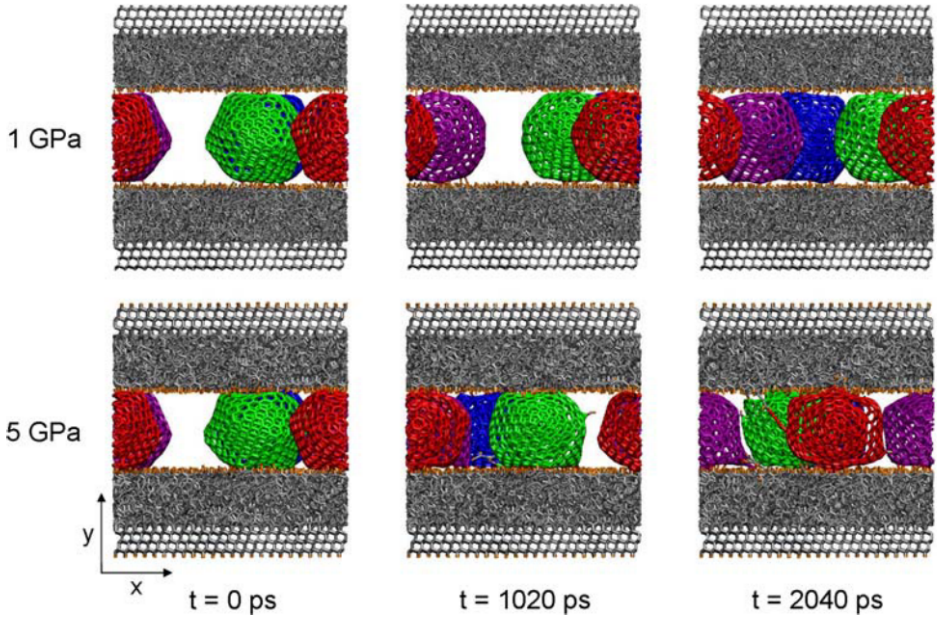

Figure 4.24: Visualisation of carbon nano-onion molecular dynamic simulations at 1 and 5 Gpa.(Joly-Pottuz et al., 2010) Reprinted with permission. Copyright ©2009, Springer Science Business Media, LLC

Ghaednia et al. investigated the effects of nanoparticles in elastohydrodynamic lubrication, showing that silver nanoparticles around 7nm could reduce friction in this lubrication regime. This effect was not due to any viscosity change or the formation of a silver film on the contacting surfaces. Molecular dynamics simulations of the system show that nanoparticles force lubricant molecules to flow with it, this artificially increases the velocity of the oil flow, and as such, there are fewer interactions between lubricant molecules resulting in reduced friction.(Ghaednia et al., 2013) These results show that nanoparticles within a contact may have more ways of decreasing the friction of a system than just those stated above. Further research in the area should also be undertaken to investigate how nanoparticles can decrease friction in other contacts. One potential flaw with this research is that the nanoparticles are not readily soluble within the solution; this means a polyvinylpyrrolidone coating agent was used to stabilise the nanoparticle.

Polyvinylpyrrolidone is a slightly polar polymer, and as previously stated in this review, polymers can act to reduce friction by generating a film and the resulting osmotic pressure and directional movement when sliding can help to reduce friction. This polarity means that any friction effect could have, at least in part, been because the nanoparticle just acted to improve the performance of the polyvinylpyrrolidone as a friction modifier and not due to the reasons detailed.

4.4.2 Nanoparticle Friction Modifier Research

Some of the earliest research into nanoparticles as friction modifiers involved research into fullerene molecules, particularly tungsten and molybdenum disulphides, with Tenne et al. and Feldman et al. first detailed how these nanoparticles could be synthesised via a relatively inexpensive process.(Tenne et al., 1992; Feldman et al., 1996) Rappaport et al. demonstrated that these nanoparticles could be effective solid-state lubricants and show greater tribological performance than the compounds out of nanoparticle form.(Rapoport et al., 1997) Rapoport et al. went on to investigate WS_2 as oil additives. They showed significantly reduce friction and wear of the contact at 5 wt%. Surface force apparatus analysis demonstrated that these nanoparticles could act via two mechanisms. At low loads, they act like ball bearings to convert sliding to rolling contact. At higher loads, these IFs gradually exfoliate to generate a WS_2 film which will reduce shear resistance and reduce friction and wear. SEM also showed these nanoparticles attract wear particles and prevent third body abrasive wear.(Rapoport et al., 2003) This shows the potential multi-mechanism method by which nanoparticles may be able to reduce friction within a contact.

Tannous et al. investigated fullerenes made of a blend of tungsten and molybdenum disulphides. While all nanoparticles were shown to reduce the friction within the contact, the most effective were those with the highest molybdenum content MoS_2 and $Mo_{0.8}W_{0.2}S_2$; while at higher pressure, the MoS_2 IF is the most effective at reducing friction and wear. These nanoparticles are small and have a lower crystallinity than larger IFs. This lack of crystallinity means that the bearing effect is unlikely to occur, and instead, an exfoliating mechanism is likely to occur. Although this mechanism is never confirmed, the least crys-

talline and highest defects IFs are also the ones that provide the lowest friction and wear in the experiment; as these particles would be the most likely to break down and exfoliate the surface, this does add some credence to the exfoliating surface hypothesis.(Tannous et al., 2010) These experiments were performed at ambient conditions, and these are unlikely to occur in an ICE.

Kogovesk et al. investigated MoS_2 nanotubes as oil additives in a PAO oil at 2 wt% MoS_2. They showed that these compounds reduced friction substantially in the boundary regime compared with the base oil, but perhaps the most interesting observation is that the addition of nanotubes results in the friction being the same for both a rough and smooth contact. This friction reduction can result from the formation of a thick, patchy boundary film due to compacting of the nanotubes or due to the nanotubes directly adhering to the surface.(Kogovšek et al., 2013) This work shows again that there are multiple methods by which nanoparticles can reduce that friction. Perhaps the biggest observation is the equal friction for both rough and smooth surfaces; this means the addition of nanoparticles may improve friction performance across a range of contacts equally, meaning these nanoparticles may reduce the need for fine surface finishing within the system.

As well as these sulphide based nanoparticles, a variety of other chemistry nanoparticles have been investigated; Li et al. investigated organic-inorganic nanoparticles that can be used as lubricant additives. These dialkyl dithiophosphate coated Cu, Ag, and LaF_3 nanoparticles are shown to be soluble in non-polar solvents and display a significant ability to increase wear and high-pressure protection of the contact in boundary lubrication conditions. Electrical contact resistance techniques show that these nanoparticles form a film on the surfaces, and SEM, EDS, and XPS techniques confirm that these films form and act to generate a smoother contact. They theorised that these nanoparticles could prevent surface contact, and at high shear, they decompose to generate a film that welds, attaches or reacts with the surface to form this protective layer. This welding effect acts not only to generate a protective film but also acts as a mending effect to smooth the surfaces, as shown in Figure 4.25.(Li et al., 2006) Although this research did not investigate the friction of the contact, it is reasonable to assume these nanoparticles would also reduce that

friction. One potential issue is the solubility of the nanoparticles and the longevity of these nanoparticles. They were only shown to remain soluble for "several months" at ambient temperature and 3 days at 140°c. It is not known if these nanoparticles would remain soluble across the full use of the oil, where temperature conditions can vary widely. Also, the long term performance of these films was not established. It is not known whether they remain on the surface or will break down over time. If they break down, it is not known if the film will be re-established, either by reforming the nanoparticles and allowing them to break down again or by the film chemicals that are released.

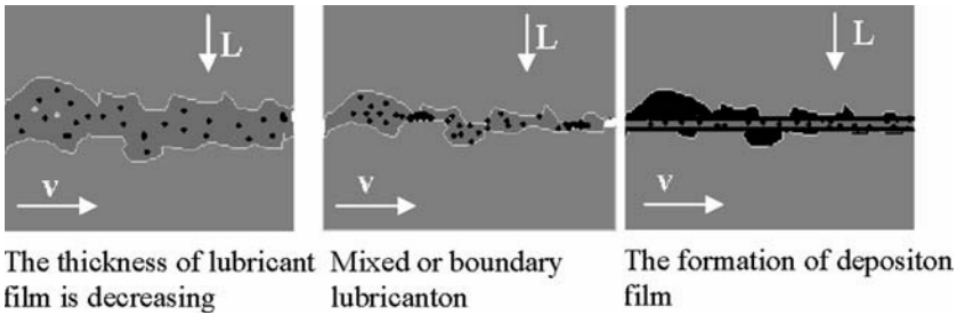

Figure 4.25: Scehmatic representation of the mechanism theorised by Li et al.(Li et al., 2006) Reprinted with permission. Copyright ©2006, Springer Science Business Media, Inc

Work by Zhang et al. on copper dialkyl dithiophosphate confirmed that these nanoparticles can indeed reduce the friction of the contact, and this friction decrease is maintained across a wide range of loading forces and that this friction reduction is maintained for 3 hours. They showed the same mechanism as Li et al. where a film of around 120nm was generated on the contact.(Zhang et al., 2009)

Metal oxide nanoparticles have been investigated as friction modifiers. A large number of oxides have been investigated, including Cu, Zn, Zr, Ti.

Ghaednia et al., and Yilmaz investigated copper-based nanoparticles(Ghaednia et al., 2015; Yilmaz, 2020) Ghaednia et al. investigated stable 9nm copper oxide nanoparticles and showed a decrease in friction of the contact. They proposed that the small nanoparticles effectively entered the contact, reduced the real area of the contact, and prevented surface contact.(Ghaednia et al., 2015) These nanoparticles, however, displayed an increase in wear which was likely due to abrasive wear of the small nanoparticles. This

wear, however, did decrease as nanoparticle concentration increased. Yilmaz, however, investigated copper, copper iron and copper-zinc oxide nanoparticles.(Yilmaz, 2020) They showed that the copper-zinc iron oxide was the most effective at reducing both the friction and wear of the contact. These nanoparticles also display higher viscosity and highest thermal stability and will be more able to support any load upon the surface and maintain this load support in a broader number of temperature environments; this explains the superior friction and wear performance. These results may indicate that increased stability of nanoparticles may improve their tribological performance. There was no post-experimental mechanistic analysis of the surfaces, though, meaning it is difficult to tell any difference in the mechanisms of these nanoparticles. However, these investigations involve nanoparticles that are not readily soluble in the oil, meaning that dispersants are added to the solution, sodium oleate for Ghaednia et al. and a glycol for Yilmaz. These dispersants have a structure similar to many organic friction modifiers and may reduce the friction of the contact themselves.

Battez et al. compared copper oxide nanoparticles to zirconium and zinc oxides in PAO. These nanoparticles all exhibit friction and wear reduction when compared to the base oil with ZnO and ZrO_2 at 0.5% displaying the best tribological behaviour. Elemental analysis and SEM images of the contact indicate that these nanoparticles act by tribosintering to the wear surface; this generates a tribofilm that prevents surface contact and supports the contact load, reducing both friction and wear.(Hernández Battez et al., 2008) These nanoparticles vary in size and display different wear responses as their concentration increases, with the larger CuO displaying a decrease in wear and the smaller ZnO and ZrO_2 showing an increase in wear. This could suggest a link between nanoparticle size and third body abrasive wear but could also be due to the chemical or physical nature of the nanoparticles. Further understanding of this may improve the design of friction modifier nanoparticles.

Another metal oxide additive that was investigated was a $ZnAl_2O_4$ nanoparticle by Song et al. These additives reduced the friction coefficient and wear of the contact by around 30% at a low 0.1 wt% concentration. This reduction was also significantly higher than both the ZnO and Al_2 O_3 additives separately, indicating a synergistic response

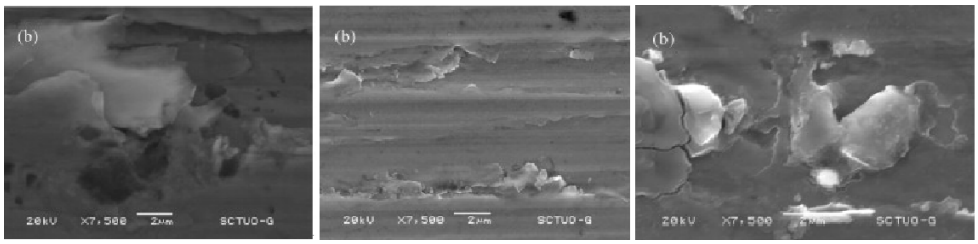

Figure 4.26: SEM Micrographs of nanoparticles in the wear scar Left: 0.5% ZnO Centre: 2% CuO Right: ZrO_2.(Hernández Battez et al., 2008) Reprinted with permission. Copyright ©2007 Elsevier B.V.

between the Zn and Al. The small nanoparticles deposit themselves within the micro-gaps and build a protective film as the nanoparticles are compacted into the surface and prevent surface contact.(Song et al., 2012) These nanoparticles are insoluble, and oleic acid is added as a surfactant. Oleic acid is a known friction modifier, and thus it is not known whether the friction reduction is due to the oleic acid or a synergistic relationship between the nanoparticle and oleic acid rather than the nanoparticle itself. The cyclohexanol solvent also has very different physical properties to most lubricants.

Titanium oxide nanoparticles have been researched by Wu et al. and Bogunovic et al. with both able to show that these nanoparticles can effectively reduce friction within the system.(Wu and Kao, 2011; Bogunovic et al., 2015) This is particularly important in the case of Wu et al., who conducted the research long term within a four-stroke single-cylinder ICE engine; this shows that these nanoparticles are effective within an engine rather than just the idealised conditions associated with the majority of lab tests. These nanoparticles, though, are not readily soluble within oils. With Wu et al. investigating larger nanoparticles (>59nm) and Bogunovic et al. adding organic friction modifiers like dispersants to the oil.

La_2O_3 nanoparticles have also been investigated as a friction modifier. Xu et al. studied the effects of these nanoparticles in a bio-oil, with good friction and wear reduction being observed.(Xu et al., 2015) These nanoparticles have a vast size range (20-1000nm), indicating that there is very little control over the synthesis of these nanoparticles. With the predominant mechanism being a bearing effect, the size of the nanoparticles likely affects their tribological performance, so a better understanding of the effect of size of the nanoparticles would be important. These nanoparticles were soluble in the oil for 7 days,

which is better than most previously reported nanoparticles, but their long term stability is unknown.

Research has also been undertaken to establish the ability of pure metal nanoparticles. Padgurskas et al. compared the effectiveness of iron, copper and cobalt nanoparticles and their combinations as lubricant additives. They found that all the nanoparticles reduced friction and wear within the contact with the copper nanoparticles, and a mixture of copper and one of the other nanoparticles being the most effective. Friction results are shown in Figure 4.27. Here copper displayed the ability to form a low-shear film while the other nanoparticles just acted by the mending effect.(Padgurskas et al., 2013) One drawback to these nanoparticles is that their formation requires the addition of water and other water-soluble chemicals to the oil. Water within the oil can lead to other negative consequences with other additives and can also negatively impact the physical properties of the oil itself.

The effect of silver nanoparticles around 5.6nm in polyethylene-glycol lubricants was also investigated by Ghaednia et al. These nanoparticles were shown to effectively reduce the friction and wear of the contact, with the friction coefficient being reduced across the entire Stribeck curve but in particular in the mixed regime. Surface analysis of the contact indicates that the particles do not interact with or alter the surface, and thus it is presumed they reduce friction via the bearing effect.(Ghaednia et al., 2016) These nanoparticles are not soluble themselves, and a polyvinylpyrrolidone (PVP) stabiliser group is added to the mixture, resulting in nanoparticles that are shown to be stable for 7 months. The silver nanoparticles may act to improve the potential performance of PVP as a friction modifier.

Modelling can allow for mathematical predictions as to the effects of nanoparticles within a contact. Ghaednia et al. were able to model the effects of nanoparticles on friction and wear using a rough surface model where nanometer-sized silica particles are investigated against micrometre sized rough surfaces. They showed that a high concentration of smaller particles with a narrow size distribution would reduce the friction coefficient of the contact. Though these particles can induce wear of the contact, this is minimised by using a narrow distribution of nanoparticles to decrease average pressure on the nanoparticles or larger particles.(Ghaednia and Jackson, 2013) This means the use of

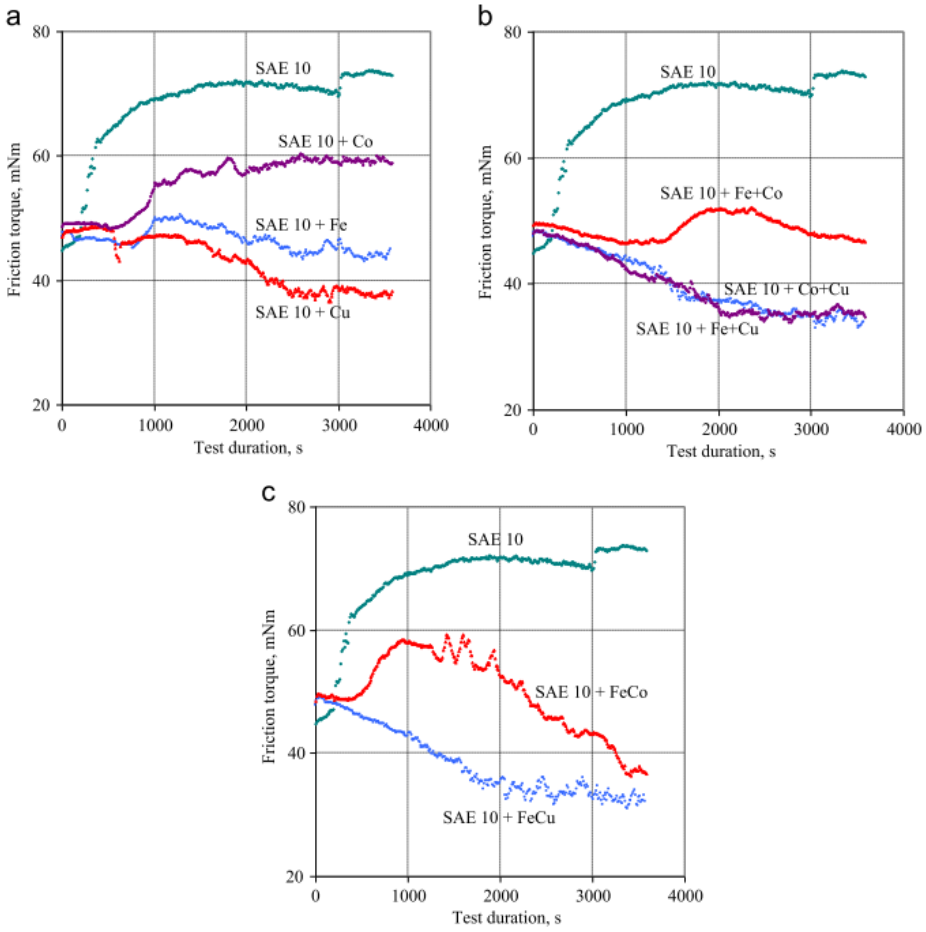

Figure 4.27: Friction torque graphs of SAE10 and oils with nanoparticles a) with metallic nanoparticles; b) with mixture of nanoparticles and c) with iron nanoparticles coated with Cu and Co.(Padgurskas et al., 2013) Reprinted with permission. Copyright ©Elsevier Ltd.

more consistently sized nanoparticles may be the most effective friction modifiers. This model, though, makes many assumptions that may not all be correct. It ignores the effect of fluid pressure on the particles and assumes the spheres can only compress by half before completely failing and effectively disappearing.

Hu et al. used molecular dynamics simulations of copper nanoparticles. The simulation showed that the copper nanoparticle would break down to form a copper film on the surface. This film prevents surface contact, and as such, there is no stick or friction at the contact; this is shown in Figure 4.28.(Hu et al., 2014) This is similar to previous results reported by Padgurskas et al. Both this model and the previously discussed one by Ghaednia et al. treat nanoparticles differently. Hu et al. consider nanoparticles weakly

bonded, and as such, they break down rapidly, while Ghaednia et al. treat them as very strongly bonded and are either in nanoparticle form or undergo catastrophic breakdown. The reality for most nanoparticles is likely between these two extremes, and a model that considers the strength of bonding of the nanoparticles both to chemical and physical strain would be beneficial to more accurately model the effects of nanoparticles within a contact.

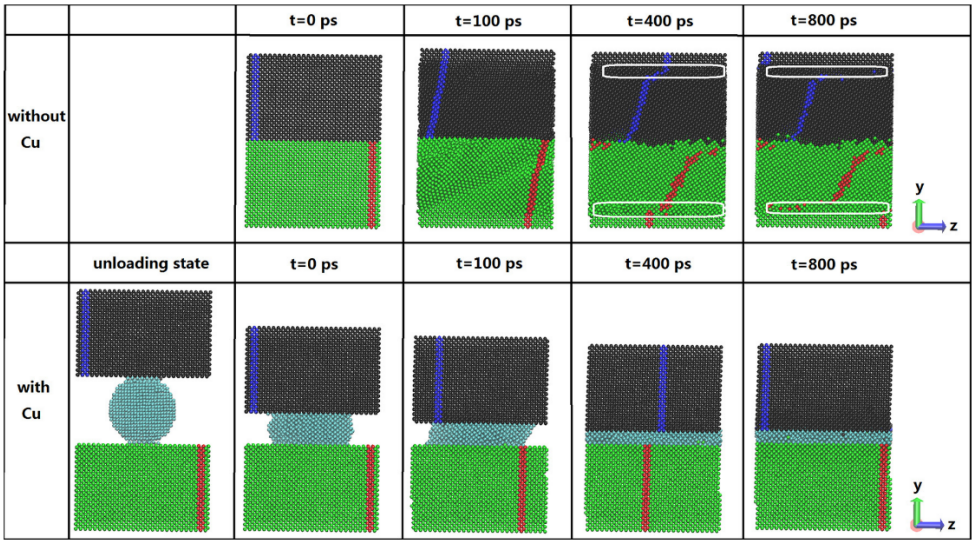

Figure 4.28: Still images at different sliding times. The blocks are coloured differently with the blue and red atoms used to visualise deformation. Contact is moving at 10 m/s with a load of 500 MPa.(Hu et al., 2014) Reprinted with permission. Copyright ©2014 Elsevier B.V.

As well as metal-based nanoparticles, there has been considerable research into carbon-based nanoparticles as friction modifier additives. Early work on graphite as a lubricant additive was undertaken by Lee et al. They showed that the contacts with the graphite had lower friction and wear. Surface analysis showed that the contacts with the graphite had a lower surface roughness than the surface before testing; this suggests that the graphite acts to polish the surface and remove asperities, resulting in lower friction and wear due to there being fewer asperity interactions between the two contacts.(Lee et al., 2009)

Jolly-Pottuz et al. investigated carbon nano-onions, TEM shown in Figure 4.29, as lubricant additives. They found that the non-diamond containing carbo-onions reduced friction and wear within the contact. The diamond containing compounds resulted in some abrasive wear, and their friction and wear reduction was less significant. Either these nanoparticles onions are exfoliated to generate graphene nanosheets upon the surface, or

that diamond-like carbon (a known low friction surface) tribofilms are generated.(Joly-Pottuz et al., 2008)

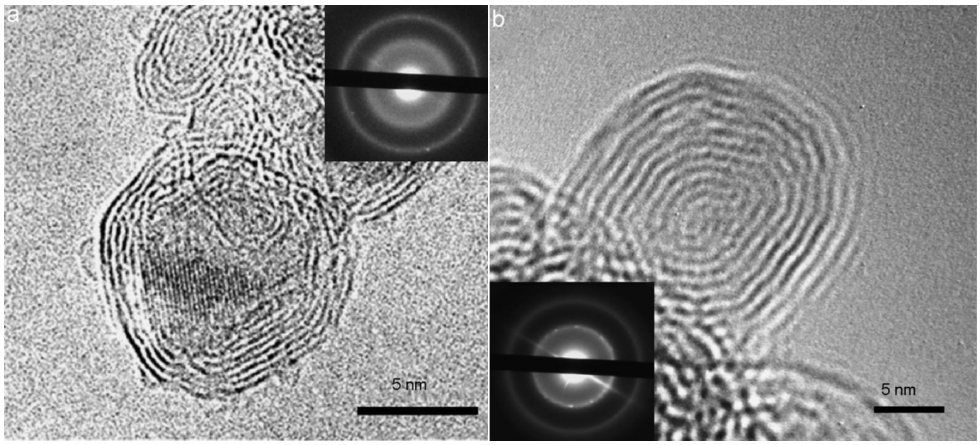

Figure 4.29: TEM images of carbon onions a) with diamond core b) completely graphitised.(Joly-Pottuz et al., 2008) Reprinted with permission. Copyright ©2007 Elsevier Ltd.

Lin et al. investigated modified graphene sheets as lubricant additives. They showed that these modified graphene platelets effectively reduced friction and wear at just 0.075 wt% as their small and thin laminated structure allowed them to enter the contact and prevent surface contact easily.(Lin et al., 2011) This work acted to improve the solubility of graphene by reacting it with stearic and oleic acid first. This reaction makes the usually insoluble graphene soluble in the lubricant and removes one of the most significant barriers for graphene as an oil additive. This stability is not constant though, with Lin et al. demonstrating that only 85% of the original graphene was dissolved within the solution after 3 hours after surface modification is undertaken. This poor solubility of the additive is still not sufficient for commercial use and must still be improved.

A significant amount of research has also focused on nanocomposite friction modifiers. These are nanoparticles that are made up of two or more different materials. These nanocomposites are made up of carbon and metal-based chemistry.

Zhang et al. investigated graphene oxide and copper nanocomposites. Here copper nanoparticles are present in graphene sheets of diameter 20nm. These nanocomposites showed greater friction and wear reduction than the graphene and copper nanoparticles alone. This improved tribological performance was shown to be due to the very thin

laminated structure of the graphene forms a tribofilm upon the metal while the copper nanoparticles can bear the load of the contact effectively. Figure 4.30 demonstrates this mechanism.(Zhang et al., 2013) The nanocomposites, however, are not soluble within the oil and a sorbitol monooleate dispersant was added. This polar dispersant could act to adsorb to the contact and lower the contact's friction; this cannot be disproved due to the dispersant not being present within the control experiment.

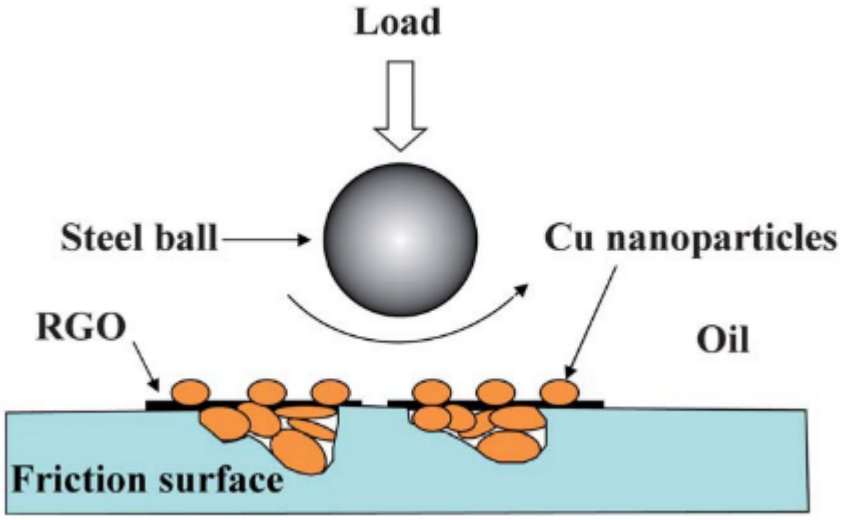

Figure 4.30: Mechanistic model of friction reduction of reduced graphene oxide and copper nanoparticle nanocomposites.(Zhang et al., 2013) Reprinted with permission. Copyright ©2011, Royal Society of Chemistry

Huang et al. investigated carbon quantum dot and copper sulphide nanocomposites for use as friction modifiers. These composites have a lot of the properties of graphite, while their surface functionalisation allows for the addition of copper sulphide to the surface. These nanoparticles were able to reduce the friction and wear of a contact effectively. The copper sulphide within the nanocomposites was shown to react with the iron in the oil. This reaction forms a copper iron sulphide alloy which can repair wear within the contact efficiently.(Huang et al., 2015) The long term performance and stability of these nanoparticles are unknown, but the quantum dots are known to be water-soluble, and so they are unlikely to be soluble in the oil long term.

Yang et al. also investigated copper nanoparticles on a graphitic based carbon. EDS

spectroscopy showed the presence of copper and nitrogen within the wear scar, indicating that both the copper nanoparticles and the graphitic carbon nitride can be transferred to the contact with the carbon nitride forming a low shear film and the copper nanoparticles being able to support any load.(Yang et al., 2015) Even with the addition of a sorbitane monooleate stabiliser, these nanocomposites were relatively insoluble, with precipitation being observed after 3 days of their addition.

As well as carbon and copper nanocomposites, Mo_2 can also be added carbon nanosheets. Song et al. demonstrated that these were able to effectively reduce the friction and wear of the contact at low concentrations with optimal performance being achieved at 0.02 wt%, with non-uniform MoS_2 dispersion (nanoflower) being particularly effective. XPS showed these nanoflowers form a unique microstructure upon the contact surface due to the synergistic effect of the graphene and the MoS_2. Here the nanoflowers deposit onto the contact area to form an adsorption film.(Song et al., 2019)

Nanoparticles have also been investigated as potential additives for more recently researched lubricants, ionic liquids. Kheireddin et al. showed that the addition of silica nanoparticles to a 1-butyl-3-methylimidazolium (trifluoromethysulfony)imide ionic liquid lubricant resulted in improved friction and wear performance when compared with the base lubricant. They showed that the optimum concentration of the 10-20nm particles was 0.05 wt% with an improvement of friction and wear performance being particularly large at higher loads; this was theorised to be due to the increased loading capacity with the nanoparticles and the formation of a particulate network that lead to higher fluidity of the nanoparticles under shear. This high fluidity allows the nanoparticles to more easily fill the valleys of the contact and improve lubrication; this is shown in Figure 4.31.(Kheireddin et al., 2013) One advantage of this research is that these silica nanoparticles are readily soluble within the ionic liquid; this is not the case with less polar solvents and sono stabilising compounds are required to be added. This work does not investigate their long-term stability and ability to reduce friction or reduce friction in the contact environments present within an ICE, as these experiments were undertaken in pure sliding contacts at room temperature.

The addition of graphene to ionic liquid lubricant has also been investigated by Khare

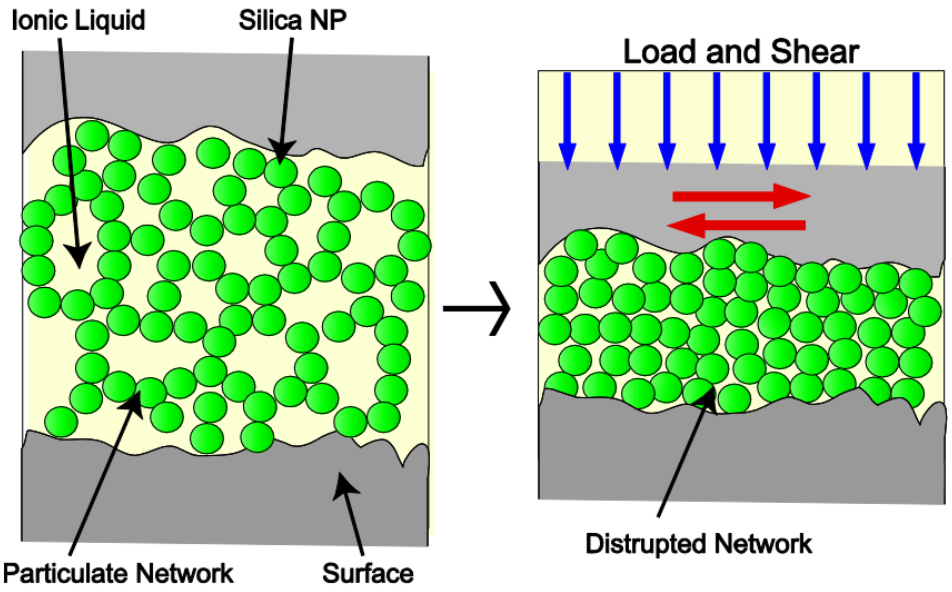

Figure 4.31: Schematic of the network of silica nanoparticles under loading and shearing.Kheireddin et al. (2013)

et al. They showed that both nanoparticles and nanosheets of graphene reduce the coefficient of friction and wear of a 1-butyl-3-methylimidazolium iodide ionic liquid. This friction and wear reduction was shown to be a three-way mechanism with the formation of an ionic liquid thin film, the graphene's bearing effect, and an exfoliating effect of the sheets.(Khare et al., 2013) This suggests that a vast number of nanoparticles may be effective friction modifiers within ionic liquids. This friction and wear reduction is not maintained long-term with an increase in friction and wear being observed after just 3 cycles of the testing. This increase is due to the abrasive nature of the wear particles and the agglomeration of the nanoparticles; this occurs relatively rapidly and indicates these are not effective as lubricant additives. TEM images of the nanoparticles show this agglomeration of nanoparticles even before testing, suggesting the long term stability of these additives even outside of the contact is not significant enough to be used as oil additives.

Work by Li et al. investigated MoS_2 nanoparticles as a dual additive with mercaptobenzothiazolate ionic liquids for use as friction modifiers in polyethylene glycol oils. They showed that the combination of additives effectively reduced the friction coefficient and wear protection of the contact at high temperatures compared to both the base oil and the

individual additives. This synergistic effect was activated at higher temperatures and was due to the mercaptobenzothiazolate anion of the ionic liquid with the cation having little effect. Here the ionic liquid promotes the formation of multiple layers of MoS_2 coating upon the surface of the metal. This film was not present without the ionic liquid, so it was theorised that the coating was due to the nanoparticles' reaction with the sulphur from the anions of the ionic liquid. This 50-90 nm tribofilm rich in MoS_2 is what acts to reduce friction and wear.(Li et al., 2018a)

All of the nanoparticles discussed above have some common issues. Firstly the synthesis of these nanoparticles requires large amounts of energy to synthesise; these high energy processes often increase the costs and difficulty of producing these nanoparticles for commercial purposes. Secondly, the solubility of these nanoparticles is often not high in motor oils; this means that often stabilisers are added to the solutions to improve the stability of these nanoparticle solutions. These stabilisers are long-chain polar compounds that adsorb to the surfaces of the nanoparticles and are often very similar to the chemistry of the organic friction modifiers discussed in this literature review. These stabilisers often increase the cost of these nanoparticles as friction modifiers, but also any friction reduction may be partly due to these stabilisers acting as organic friction modifiers. The long term stability of these nanoparticles is also unknown.

The potential use of polymerisation induced self-assembled nanoparticles would resolve both of these issues and were first investigated as friction modifiers by Zheng et al. They have reported using acrylic-based copolymer spheres synthesised via atom-transfer radical-polymerisation (ATRP). They found that these nanoparticles significantly reduced the friction coefficient of the base oil by >70% in the boundary lubrication regime and provided a more significant friction reduction than oils containing GMO at low entrainment speeds despite having only 0.5 wt% compared with GMO's 1 wt%. These nanospheres display different friction reduction properties compared with GMO. GMO reduces the friction coefficient at all entrainment speeds compared with base oil, and the friction coefficient decreases with increased entrainment speed. GMO is consistent with a typical Stribeck curve because as the entrainment speed increases, more oil will enter into the contact, and so the contact will move through the lubrication regimes, and as a result, there will

be less surface contact, thus reducing the friction coefficient. The nanospheres, however, show an increase in friction coefficient as entrainment speed increases to a peak before the friction coefficient decreases. This friction peak indicates that these nanospheres may be disrupting the flow of oil through a contact or that the number of nanospheres within the contact increases at higher entrainment speeds. Increasing the number of nanoparticles in the contact would increase the friction associated with their deformity by the metal surface, this trend, however, has only been observed with compounds containing poly(2-cinnamoyloxyethyl acrylate) cores that were used in this study, this means such a simple explanation may not be likely and could be due to a shear-thickening process. The coefficient of friction in the nanospheres, though never dramatically exceeds that of GMO at the same entrainment speeds, and so these nanospheres still provide a significant improvement in friction reduction when compared with GMO, as shown in Figure 4.32. It was also found that crosslinking these spheres improved their performance; this was because the crosslinking increased the mechanical stability of the spheres, and thus, they were less likely to break down. They also found that the addition of an amino acid capping agent improved their performance; this likely increased the attraction of the spheres to the surface of the metal as amino acids are polar, leading to an increase in the adsorption of the spheres and thus improves their lubricity performance.(Zheng et al., 2010)

It was proposed that this friction reduction was due to a particle entrapment mechanism where the spheres could deform and prevent steel-steel contacts. This deformity is similar to the bearing mechanism observed with other nanoparticles, and as a result, does not necessarily require the nanospheres to bond to the surface. This lack of bonding required means that these nanospheres could be used regardless of the material within the contact and could be "universal". This theorised mechanism is shown in Figure 4.33.

This work shows the potential of oil-soluble block copolymer nanospheres for use as friction modifiers, particularly in the high friction boundary regime. Their synthesis at 55°C and oil solubility mean they are readily dispersed within the oil solution, and their self-assembly nature means that these nanoparticles will be unlikely to degrade long term due to their much higher stability within the nanosphere than in solution. There are, however, many issues with this research. Firstly the ATRP polymerisation control ATRP

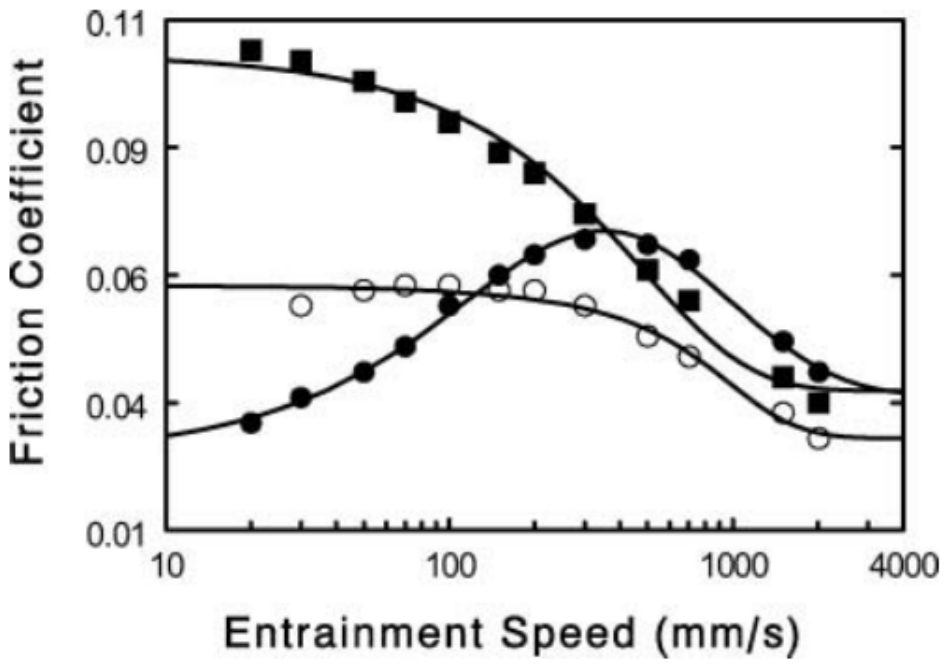

Figure 4.32: Stribeck curve for base oil (black squares); base oil with 1 wt% glycerol monooleate (clear circles) and 0.5 wt% PISA triblock copolymer nanospheres (black circles).(Zheng et al., 2010) Reprinted with permission.

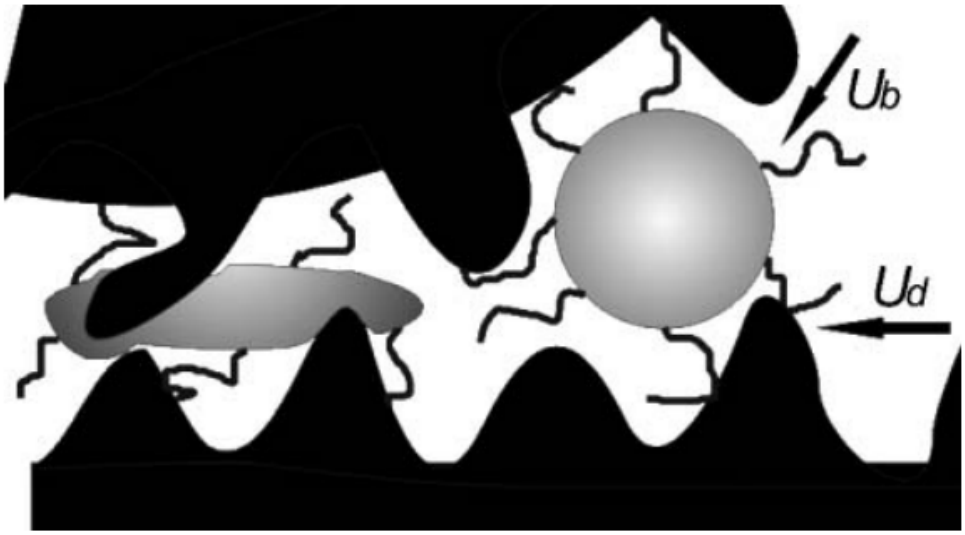

Figure 4.33: Proposed mechanism for the entrainment and deformation of nanospheres in a lubricated contact.(Zheng et al., 2010) Reprinted with permission.

involves the use of a copper-based catalyst to control the rate of polymerisation, which is difficult to remove from the motor oil once the polymerisation is complete. As a result, copper may be present within the oil in the internal combustion engine; this can lead to

large amounts of galvanic corrosion due to the transfer of electrons from the steel to the copper.(Khadom et al., 2015) This means that the use of ATRP is not advised for this application. The investigation also involved acrylate polymers; at high temperatures, these polymers are vulnerable to hydroxylation. Hydroxylation would result in the breakdown of the polymer to form a carboxylic acid; this results in the loss of the friction-reducing properties and could result in more corrosion of the contacting surfaces. The study also involves the use of protecting groups to stabilise the nanospheres; these protecting groups increase both the cost and the complexity of their formation and, as a result, makes them less industrially relevant. The crosslinking method used for the nanospheres was photocrosslinking, where UV light is used to initiate the crosslinking, and this results in a discolouration of the oil and, as a result, makes them less industrially relevant. The entrapment mechanism proposed by this research was also only a theorised mechanism with no evidence provided to show this is the case. As a result, any potential for the nanoparticles as "universal" friction modifiers is premature thinking.

Further work on block copolymers as potential oil additives was undertaken by Derry et al. They investigated poly(stearyl methacrylate)-poly(benzyl methacrylate)-poly(ethylene glycol dimethacrylate) triblock copolymer nanoparticles that were prepared via RAFT dispersion polymerisation. These nanoparticles were shown to be 48 nm in diameter and are $PSMA_{31}$-$BzMA_{200}$-$EGDMA_{20}$. These nanoparticles were shown to significantly reduce the friction of a contact in the boundary lubrication regime, even below the friction of glycerol monooleate, at 0.5 wt%; as shown in Figure 4.34. The theory was that these nanoparticles are drawn into the contact where they then undergo elastic deformation and prevent surface contact similarly to that theorised by Zheng et al.(Derry et al., 2019; Zheng et al., 2010). These nanoparticles were the first block copolymers for use as friction modifiers that were synthesised via a one-pot synthesis; meaning they are synthesised within the motor oil, reducing the number of steps and, therefore, the cost of their synthesis. The use of methacrylates and RAFT agents should also increase their long-term chemical stability within the solution and reduce any unwanted chemicals within the engine. These nanoparticles are similar to those investigated in this thesis and show their potential as friction modifiers. This research, however, only investigates one particular sized nanopar-

ticle in one type of contact. Here no attempt to investigate the effect of different sized nanoparticles or how they respond in different contacts, be it load differences or different chemistry contact surfaces. The research also does not further establish the mechanism by which these nanoparticles work either via surface analysis or in situ measurements and as such, the exact mechanism by which these nanoparticles, which are notably softer than most nanoparticles discussed above, can prevent surface contact and reduce the friction of the contact. Finally, only the friction of the contact was investigated; investigations into the effect of these nanoparticles on other tribological characteristics of the contact, such as wear or viscosity, would be prudent.

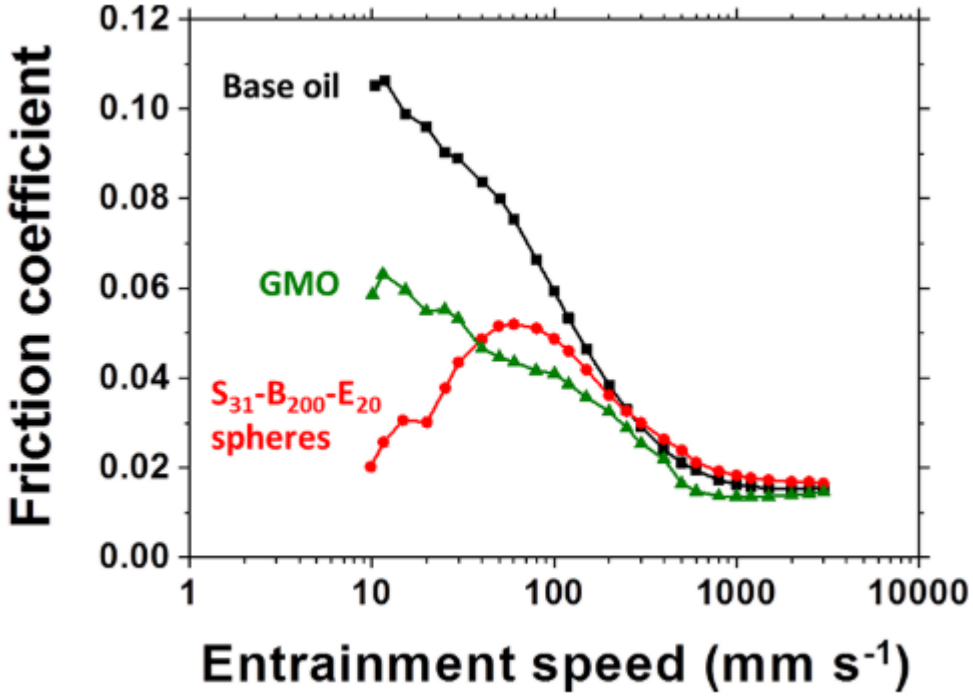

Figure 4.34: Stribeck curves showing the change in friction coefficient with entrainment speed for a lubricating base oil alone (black squares), for 0.5% w/w glyceryl monooleate (GMO, green triangles) in the same base oil, and for a 0.5% w/w dispersion of 48 nm diameter spheres dispersed in the same base oil (red circles). Data were recorded at a 20% slide-to-roll ratio (SRR) under an applied load of 35 N at 100 °C.(Derry et al., 2019) Reprinted with permission. Copyright ©CC-BY. https://creativecommons.org/licenses/by/2.0/legalcode

This may suggest multiple mechanisms by which the nanoparticles discussed in this thesis may act to reduce friction.

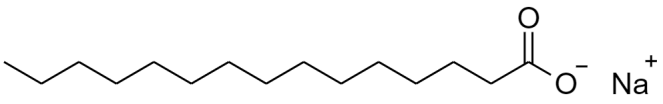

Figure 4.35: Structure of Soap

4.4.3 Soaps to reduce Friction

The nanoparticles investigated in this thesis, in particular those synthesised within water, behave similarly to soaps. Soaps are substances that dissolve in water in the form of an emulsion and are usually made up long chain fatty acids that are stabilised by the addition of an alkali to form a fatty acid salt. Here the hydrophilic charged acid group surrounds the hydrophobic carbon chain to form a micelle, this allows lipid soluble compounds to move into the centre of the micelle and results in the cleaning action of soap.

The micelle formation observed in soaps is similar to that discussed in this thesis for block copolymer nanoparticles and the ability of soaps to reduce friction has been observed too.

The most common form of soaps for use as lubricants are greases, these are emulsions of oils surrounded by a thickening agent that can be used as lubricants. These greases have very high viscosity and as such are able to maintain low friction in the boundary lubrication regime. As the shear of the contact increases these soaps display a shear thinning mechanism resulting in a lower viscosity to allow for flow of the grease within the contact. The reduction of friction by greases is believed to occur via a dual mechanism: firstly the shear of the grease leads to the breakdown of the emulsion resulting in the release or bleeding of the oil within the emulsion and the polar thickening agent that once surrounded the emulsion. This polar thickening agent is able to adsorb to the contact surface in a similar manner to that of organic friction modifiers, preventing surface contact and thus lowering friction. The oil that bleeds from the emulsion allows for the formation of a hydrodynamic lubricated contact.(Cann, 1996) This mechanism is shown in Figure 4.36. A large number of greases have been investigated with all these thickening agent and oil combinations displaying this same mechanism.(Rong-Hua, 1985; Cousseau et al., 2012; De Laurentis et al., 2017)

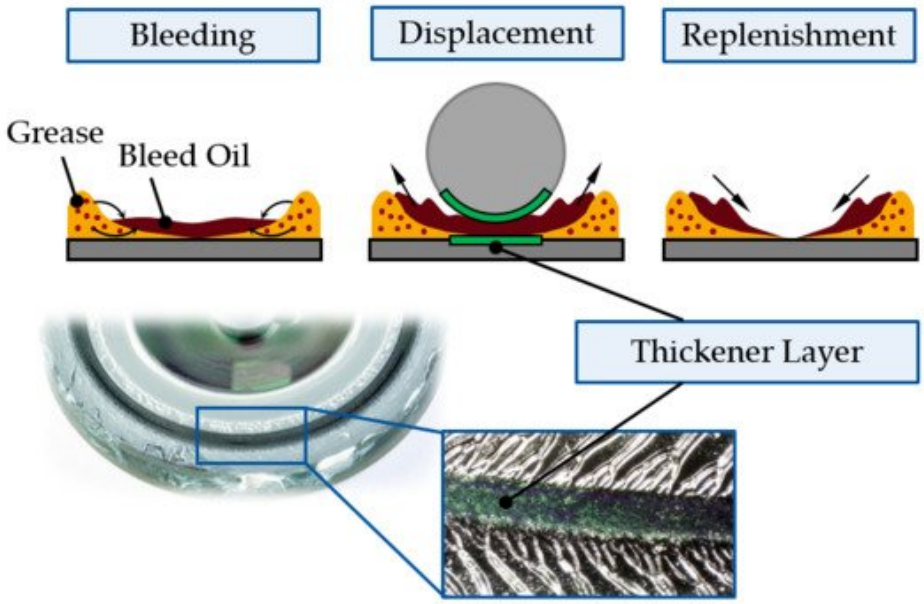

Figure 4.36: Mechanism for Grease as a lubricant.(Fischer et al., 2019) Reprinted With Permission. Copyright ©CC-BY 4.0. https://creativecommons.org/licenses/by/4.0/legalcode

These greases, however, are chemically dissimilar to those investigated in this thesis. While micelles are formed this does not occur within lubrication and as such there relevance for comparison is limited.

Multiple soap in water solutions have been shown to reduce liquid friction by reducing drag within a solution. These solutions appear to show a change in their properties as shear stress increases, this results in a large reduction in drag. This effect is reversible and so no degradation of the soap compound was observed.(Savins, 1967; Patterson L Zakin J M Rodriguez, 1969; Rodriguez, 1971) Multiple mechanisms have been suggested for this, either the breakdown of the soap micelle that leads to disentanglement occurring and as a result any visoelastic behaviour being disrupted.(Savins, 1967) Or that the soap may form polymers that result in friction reduction more similarly to the reorganisation of polymer chains that is observed in viscosity modifiers.(Rodriguez, 1971).

These papers, however, all involve the drag reducing properties of these soap solutions, this is only relevant in the hydrodynamic regime of a contact. Little more work has been undertaken to investigate the effect of traditional soaps in other lubrication regimes of

an engineering contact, with the majority of the focus being upon skin friction where lubrication regimes aren't observable.

Work undertaken by Sammy et al. investigated the effect of soap in water on the friction of rubber on ceramic contacts. They showed that the addition of soap significantly reduced the friction coefficient of the contact from around 0.3-0.5 to around 0.15.(Samy et al., 2007) This friction reduction was observed regardless of load and could indicate that soaps can be effective at reducing friction in a variety of lubrication regimes, however, without knowledge of the contact size and entrainment speed it is impossible to know this.

Work has also been undertaken on water based block copolymer nanoparticles for their use as friction modifiers by Li et al.(Li et al., 2018b) They investigated poly(3-sulfopropyl methacrylate potassium salt-co-styrene) nanoparticles as additives to water to improve the performance of Ti_6Al_4V alloys which are often used in artificial joints. They showed that these nanoparticles were able to effectively reduce friction and wear of the contact as shown in Figure 4.37. These nanoparticles were shown to be more effective at reducing friction and wear as the DP of the 3-sulfopropyl methacrylate potassium salt block (SPMA) increased from 1-3; concentration of the nanoparticle and load of the contact increased. This is due to the ability of the SPMA block to swell with the water solvent, allowing for elastic deformation of the nanoparticles within the contact, both decreasing the hertzian pressure of contact while the styrene core is able to act like a ball bearing within the contact. These nanoparticles accumulate and retain their shape within the contact and as such are able to form a tribofilm within the contact and as such friction and wear performance improves with time. While this experiment was undertaken in a sliding contact with relatively high loads and as such is likely to occur in the boundary regime, these nanoparticles have a hard core and as such are dissimilar to soaps or the soft nanoparticles studied in this thesis. They do, however, act as a comparison for similar PISA nanoparticles.

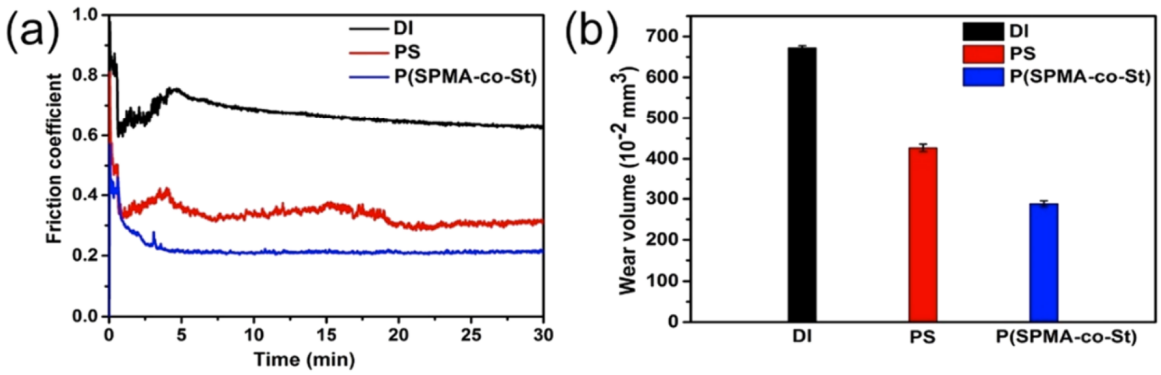

Figure 4.37: (A) Friction of Distilled water, Polystyrene nanoparticles and poly(3-sulfopropyl methacrylate potassium salt-co-styrene) nanoparticles on Ti_6Al_4V (B) Wear of Distilled water, Polystyrene nanoparticles and poly(3-sulfopropyl methacrylate potassium salt-co-styrene) nanoparticles on Ti_6Al_4V.(Li et al., 2018b) Reprinted with permission. Copyright ©2018 American Chemical Society

4.5 Conclusions

The literature discussed in this review shows the wide range of different friction modifiers that are commercially available or being researched, with different chemistries and mechanisms. These different additives have a variety of positive attributes negative effects.

Organic friction modifiers have been shown to reduce friction in a large variety of contacts effectively. However, these friction reductions are often relatively low and are not observed in high load or high sliding environments due to the relatively weak adsorption of the tribofilm. Inorganic friction modifiers are often more effective, particularly in high load and sliding environments; however, these often require high temperatures to activate, and their ability to reduce friction depletes as the oil ages. These consequences, combined with the environmental effects of increased sulphur content, toxic metals and higher ash content in the exhaust, has led to further investigation into other potential friction modifiers. Ionic liquids provide excellent wear and friction-reducing abilities but are costly to produce, often have low solubility in motor oils and provide potential corrosive effects to the engine. Polymeric friction modifiers provide quicker and more stable tribofilms than similar OFMs and result in hydrodynamic friction at lower sliding speeds. However, they can have a large number of antagonisms than single compound additives, e.g. viscosity increases, steric hindrance at contact surface, and are not as strong a tribofilm at lower sliding speeds.

This continued strive towards a superior friction modifier has led to investigations into various nanoparticle friction modifiers. While the exact mechanism for friction reduction is often unknown, they are often effective at reducing friction and/or wear in a contact. There are, however, several questions surrounding them. They are often costly and high energy to produce; they are insoluble in motor oils and can significantly affect other aspects of the contact, e.g. increasing third body abrasive wear. Their long term stability in the oil is also unknown and their effects on the exhaust gases of a vehicle.

The development of soft, low energy of production and readily soluble nanoparticle would resolve many of these issues, which has led to investigations into polymeric nanoparticles synthesised via polymerisation induced self-assembly. Investigations into these have been undertaken by Zheng et al. and Derry et al., but a thorough investigation into the development of a one-pot synthesised commercially viable nanoparticle and a thorough understanding of the mechanism by which they reduce friction has not been undertaken.(Zheng et al., 2010; Derry et al., 2019)

This thesis will continue to develop on work by Derry et al. investigating PSMA-PBzMA nanoparticles as friction modifiers in motor oils.(Derry et al., 2019) Testing their effectiveness in a wide variety of contact environments in order to establish which nanoparticles are the most effective friction modifiers and the mechanism by which they reduce friction.

Chapter 5

Synthesis and Chemical Analysis of Nanospheres

5.1 Introduction

This chapter will focus on the synthesis of a diblock copolymer of poly(benzyl methacrylate)-poly(stearyl methacrylate) (PBzMA-PSMA), where the stearyl methacrylate acts as the stabilising block, and the benzyl methacrylate acts as the core block. Both polymers were chosen due to their relatively quick polymerisation time and low cost. The BZMA is also one of few soluble compounds in the solution but becomes insoluble as the polymerisation occurs and can form a core block. While the SMA has a chain length of 18 and lines up well with the best chain lengths for OFM's as discussed in section 4.2.2. The SMA block was kept constant at a DP of 30; this was selected as previous work by Derry et al. showed that a PSMA block of 30 produces a nanosphere regardless of the size of the core block.(Derry et al., 2016b)

This synthesis will be undertaken via a one-pot protocol directly into the motor oil. This process was chosen due to the high industrial viability as it shortens the number of steps and time taken to produce the nanoparticles. This both reduces cost and time for effective polymerisation to be undertaken. It also means that the polymerisation could be undertaken directly into the oil, meaning that no solvent transfer had to be performed, and as such, no extra steps are required, or any contamination will occur.

5.2 Method

5.2.1 Kinetics

Stearyl methacrylate (SMA), cyano-4-(phenylcarbonothioylthio) pentanoic acid (PETTC; target degree of polymerisation = 30; 70.0% w/w in mineral oil) and T21s initiator (5% v/v in mineral oil) was dissolved in mineral oil. This solution was sealed in a 15ml vial and a nitrogen gas purge was undertaken for 30 min. The oxygen free solution was placed in a oil bath at 90 °C for 5 h with constant nitrogen purging. Every 15 minutes, a sample was withdrawn and analysed via nuclear magnetic resonance and gel permeation chromatography. Benzyl methacrylate (BzMA; target degree of polymerisation = 400; 20% w/w in mineral oil) and T21s initiator (5% v/v in mineral oil) was dissolved in mineral oil and a nitrogen gas purge was undertaken for 30 min. This mixture was transferred into the vial containing the poly(stearyl methacrylate) macro-CTA, and stirred at 90 °C for a further 5 h. Every 15 minutes, a sample was withdrawn and analysed via nuclear magnetic resonance, gel permeation chromatography and dynamic light scattering.

These experiments allow us to establish the time required for the synthesis of PSMA-PBzMA nanoparticles.

5.2.2 Synthesis and Cross-linking of PSMA-PBzMA polymers

Stearyl methacrylate (SMA), cyano-4-(phenylcarbonothioylthio) pentanoic acid (PETTC; target degree of polymerisation = 30; 70.0% w/w in mineral oil) and T21s initiator (5% v/v in mineral oil) was dissolved in mineral oil. The solution was sealed in a 25 ml round-bottomed flask and a nitrogen gas purge was undertaken for 30 min. The oxygen free solution was placed in a oil bath at 90 °C for 3 h. Benzyl methacrylate (BzMA; target degree of polymerisation = x; 20% w/w in mineral oil) and T21s initiator (5% v/v in mineral oil) was dissolved in mineral oil a nitrogen gas purge was undertaken for 30 min. This mixture was transferred into the round-bottom flask containing the poly(stearyl methacrylate) macro-CTA, and stirred at 90 °C for a further 3 h. This method is shown in Figure 5.1

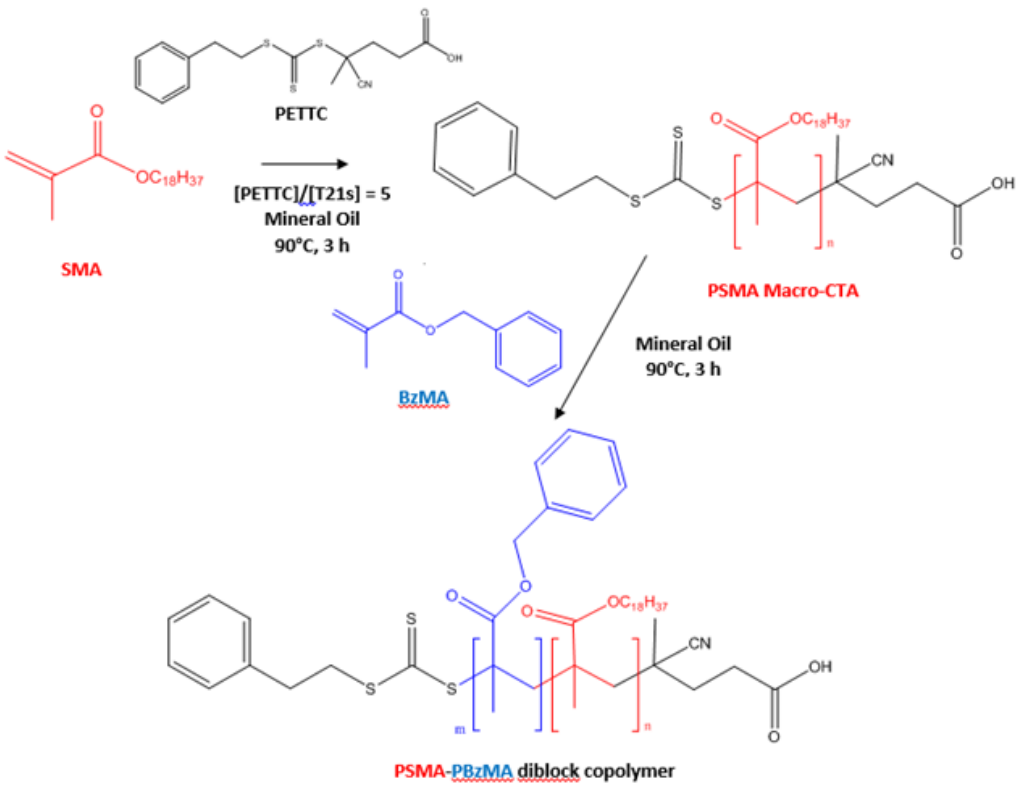

Figure 5.1: Synthesis of PSMA-PBzMA diblock copolymers

For crosslinked polymer spheres, ethylene glycol dimethacrylate (EGDMA; molar ratio of EGDMA:BzMA 1:10) was pre-purged with nitrogen gas for 30 min was added to the round bottom flask then heated in an oil bath at 90 °C for 2h. This crosslinking is shown in Figure 5.2

5.2.3 Nuclear Magnetic Resonance (NMR)

^{1}H NMR spectra was undertaken in $CDCl_3$ using a Bruker AV1-400 or AV1-250 MHz spectrometer. 64 scans were averaged per spectrum. Conversions are calculated by comparing the integration values (the area underneath a peak, which is proportional to the amount of hydrogen atoms associated with this peak) of the peaks associated with the polymer and those associated with the monomer.

^{1}H NMR detects the amount and location of hydrogen atoms within a compound, allowing for the calculation for the relative amounts of the monomer and the polymer within the oil.

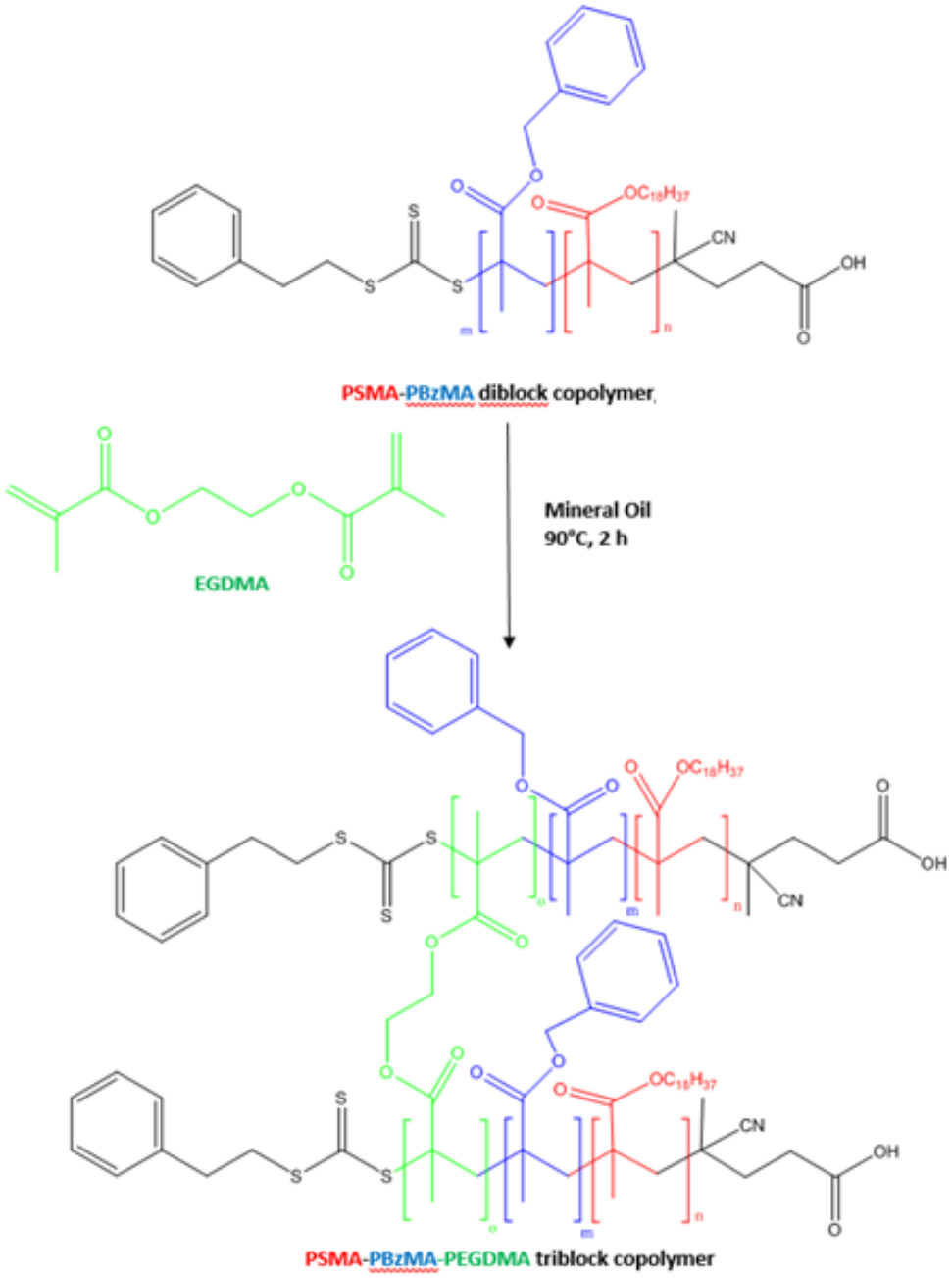

Figure 5.2: Synthesis of PSMA-PBzMA-PEGDMA triblock copolymer

5.2.4 Gel Permeation Chromatography (GPC)

The THF GPC set-up comprised an Agilent 1260 Infinity series degasser and pump, two Agilent PLgel 5 μm MIXED-C columns in series and a refractive index detector. THF eluent with triethylamine (2.0% w/w) and butylhydroxytoluene (0.05% w/v). This was operating at a flow rate of 1 mL/min and 30 °C. A series of twelve near-monodisperse

poly(methyl methacrylate) standards ranging from 800 g/mol to 2,200,000 g/mol was used for column calibration. Copolymer dispersions were filtered using a 0.2 μm syringe filter and diluted in THF eluent (0.10% w/w).

GPC is used to separate polymers based on their size and analyse the weight distribution of the polymers produced.

5.2.5 Dynamic Light Scattering (DLS)

DLS studies were performed using a Zetasizer NanoZS instrument (Malvern Instruments, UK) at a fixed scattering angle of 173°. Copolymers were diluted in n-dodecane or THF (0.10% w/w) before light scattering studies at 25 °C.

DLS is used to detect the size of nano-objects within a liquid by detecting changes in the scattering of light.

5.2.6 Transmission Electron Microscopy (TEM)

TEM was conducted using a Philips CM 100 instrument at 100kV with a Gatan 1k CCD camera. Diluted samples (0.1% w/w) were placed as droplets on carbon-coated copper grids, allowed to dry and then exposed to ruthenium (viii) oxide vapour for 7 min at 20°C before analysis. The heavy metal oxide acts as a positive stain for the PBzMA core block to improve electron contrast. Ruthenium(viii) oxide was prepared as follows. Ruthenium(iv) oxide (0.3g) was added to water (50g) to form a slurry; sodium periodate (2g) was added with stirring to produce a ruthenium(viii) oxide solution within 1 minute.(Trent, 1984) Images were taken by Dr. Matthew Derry, for which he is thanked. Images were analysed using ImageJ analysis software.

TEM uses electron scatter mapping to create 2D images on the nanometer scale.

5.2.7 Small Angle X-ray Scattering (SAXS)

SAXS data were collected using a laboratory SAXS/WAXS instrument (Xeuss 2.0, Xenocs, France) equipped with liquid gallium MetalJet X-ray source (Excillum, Sweden, wavelength λ=0.134 nm), a Dectris Pilatus 1M pixel SAXS detector (sample-to-detector dis-

tance 1.889 m) was used as a motorised scatterless slit for beam collimation. SAXS patterns were recorded over a range of $0.06nm^{-1}<q<5nm^{-1}$, where $q=(4\pi sin\Omega)/\lambda$ is the length of the scattering vector, and Ω is one half of the scattering angle. Glass capillaries of 2 mm diameter were used as a sample holder. The temperature was controlled using a heating/cooling capillary holding stage (Linkam Scientific Instruments Ltd., Tadworth, UK), with 5 min equilibration being allowed before data collection over 30 min. Data were reduced (normalisation and integration) using the Foxtrot software package supplied with the instrument and further analysed (background subtraction and data modelling) using Irena SAS macros for Igor Pro.(Derry et al., 2018; Ilavsky and Jemian, 2009) This was undertaken by Dr. Matthew Derry, for which he is thanked.

SAXS works to detect nanoscale differences in the density of a solution by detecting the scattering of x-rays, allowing for the imaging of nanoparticles.

5.3 Results

5.3.1 PSMA Block Kinetics

Kinetics analysis was undertaken to establish the length of time that the polymerisation reaction takes to occur. It also establishes the order of kinetics; this is the dependency of the reaction rate with the concentration of the reactants and is calculated by plotting the natural log of the initial monomer divided by the current monomer against time.

Figure 5.3 shows the kinetics for the PSMA block, targeting $PSMA_{30}$, here high conversions of around 75% were achieved within 100 minutes. As the reaction continues, the reaction rate is retarded as the amount of unreacted monomer within the solution decreases, with 95% conversion achieved after approximately 210 minutes. The high solid content mixture was still able to be efficiently stirred and, as a result, will be used for all synthesis.

The fact that the semi-logarithmic plot in Figure 5.3 is linear shows that the reaction is first-order kinetics, meaning that the rate of reaction is proportional to the concentration of the monomer within the solution.

Figure 5.4 shows the molar mass of the polymer block increases with increasing reaction

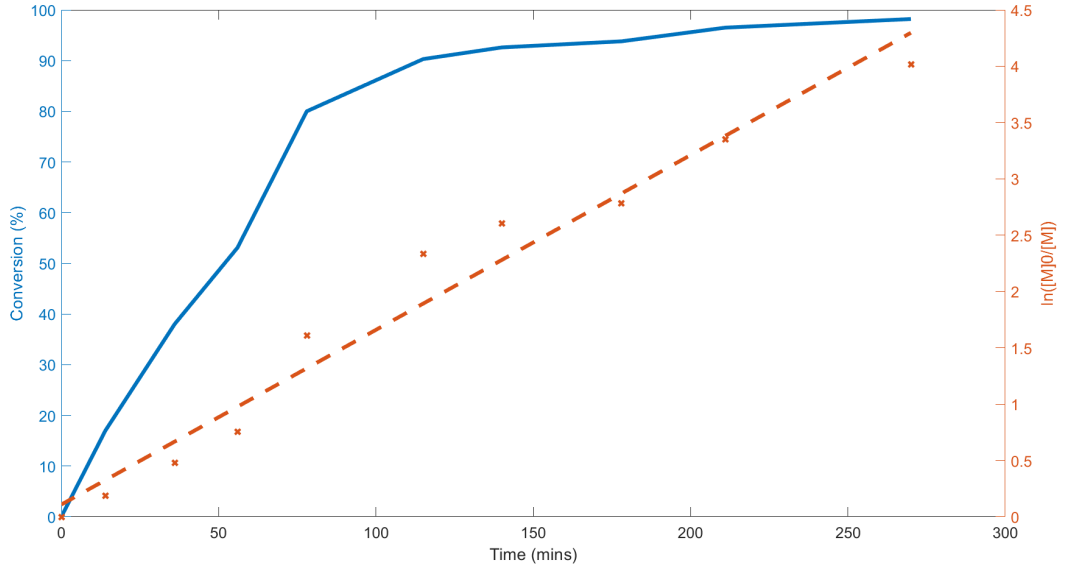

Figure 5.3: Kinetics of PSMA step at 70% solid, calculated from NMR

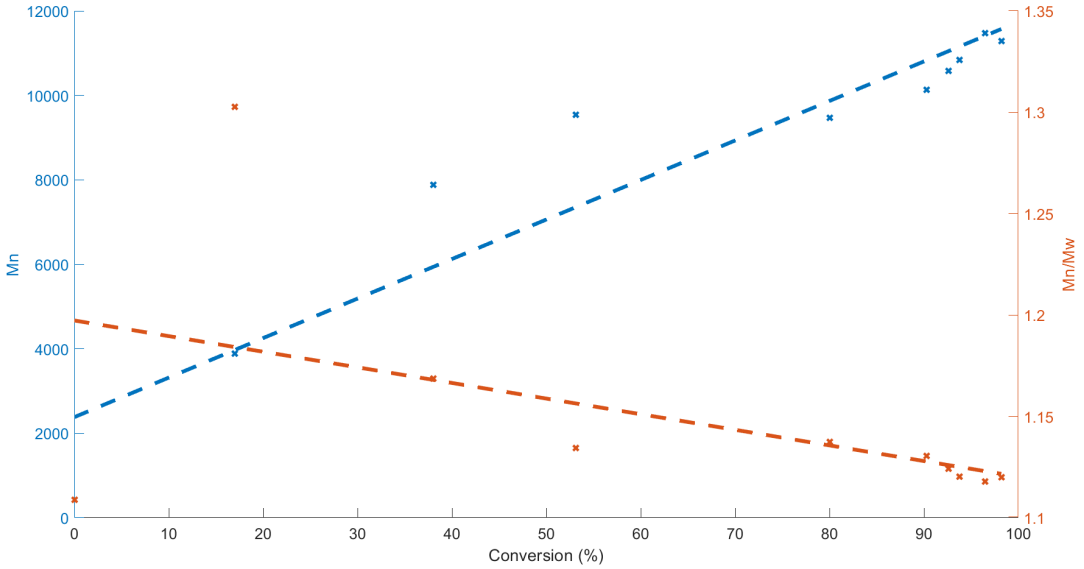

Figure 5.4: Mass dispersity of $PSMA_{30}$, obtained via GPC

conversion linearly. The dispersity of a polymer is also shown to be around 1.15 at high conversions, showing that excellent RAFT control has been achieved.

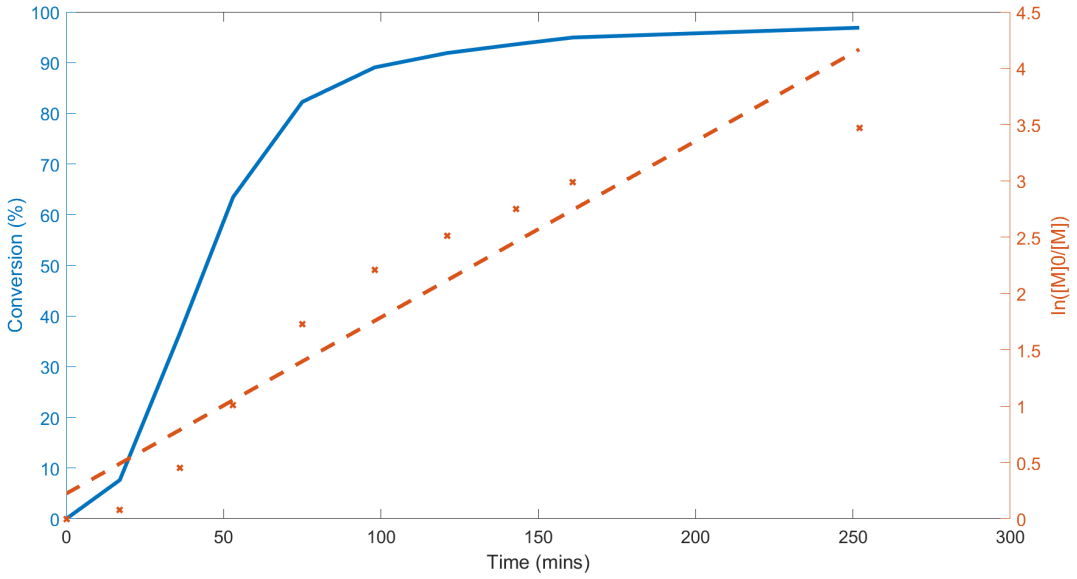

Figure 5.5: Kinetics of PBzMA step at 20% solid, calculated from NMR

5.3.2 PBzMA Block Kinetics

Figure 5.5 shows the kinetics of the spheres where $PBzMA_{400}$ is targeted. Here a very low rate of reaction is observed up until 20 minutes, after which the reaction occurs rapidly up to 80% conversion before the rate is retarded again. The reaction reaches 95% conversion after around 180 minutes.

The induction lag period is also shown in the semi-logarithmic plot, where a low gradient is observed. After this, the linear increase indicates first-order kinetics.

The early slow rate of reaction is due to the initial solubility of the PBzMA block; this means the polymerisation occurs in the solution where the concentration of monomer is relatively low. Once some polymerisation has occurred, the block copolymer will begin to form micelles as the PBzMA grows to a critical length and becomes insoluble within the oil. Any unreacted BzMA will then migrate into these cores and generate a locally high monomer concentration; this results in the reaction rate significantly increased. Similar observations has been demonstrated in previous papers by Derry et al. and Blanzas et al.(Derry et al., 2015; Blanazs et al., 2011)

GPC analysis of the BzMA dispersion polymerisation indicates an increase in molar mass with conversion as in Figure 5.6. The PD of the block is very large; this is because

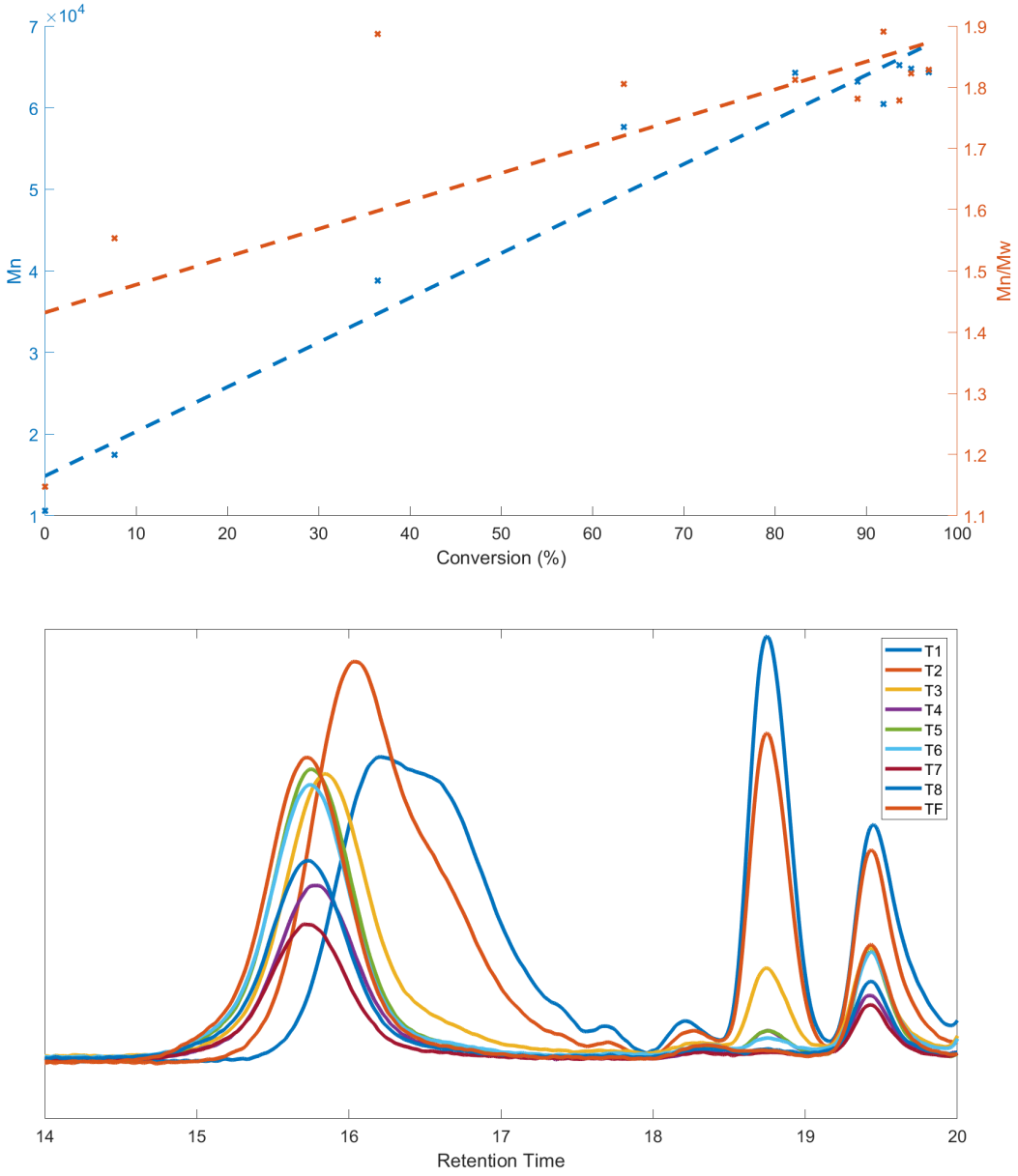

Figure 5.6: Mass Dispersity of $BzMA_{400}$ block, obtained via GPC Analysis

the PSMA block was left at high conversions for an extended period. Leaving RAFT polymerisations at high conversion reduces the concentration of active RAFT chain ends within the solution. These deactivated chains will not be able to polymerise to form the BzMA block. The GPC bell curves in Figure 5.6 as a second peak is present at a higher retention time; this indicates that a smaller deactivated chain is present within the vessel. These deactivated chains significantly increase the chain's PD and suggest there is poor

RAFT control that will likely not be observed when the initial PSMA block is not left for an extended period.

The kinetics and speed of reaction for the formation of these nanoparticles depends upon two factors: firstly the reactivity of the stearyl methacrylate, this determines the speed of the PSMA block where a more reactive monomer results in the formation of the block more rapidly. Stearyl methacrylate was chosen in part because there is a lack of significant stabilisation of the radical on the monomer and also the chain length does not significantly sterically hinder access to the reactive site. As such the reaction occurs rapidly with an increase in the concentration of the monomer being proportional to the rate of reaction. The second factor that influences the reactivity of the polymer is the rate at which the micelle formation begins. As shown in Figure 5.5 the rate of reaction significantly increases once the micelles begin to form and the polymerisation begins to occur in this emulsion. The formation of this emulsion is directly determined by the lipophobic nature of the BzMA block. Here a more lipophobic or polar block would form these micelles quicker, but if the monomer was too polar then the core monomer would be insoluble within the oil and as such would not interact with the dissolved PSMA block, resulting in no polymerisation occurring. As such a monomer with sufficient polarity or charge density to become insoluble rapidly once the formation of the core block begins would result in the quickest reaction rate.

5.3.3 Sphere Synthesis

In total, 19 different nanospheres were synthesised, with an SMA block with a DP 30 and a BzMA block DP of between 30 and 1000. 11 nanospheres are also crosslinked with the addition of EGDMA where the DP of the EGDMA block is 10% of the BzMA core block. This thesis will focus on the 11 nanospheres that also have corresponding crosslinked pairs. These were selected after initial trials indicated that the size range they occupy will be the most effective as friction modifiers and have BzMA block DP between 30 to 200.

Table 5.1 shows the all 19 non-cross-linked nanospheres that were synthesised. Up to a block size of 200 they were synthesised with good dispersity control. This PD shows a general trend to increase as the core block increases this is likely due to a similar

Core Polymer Targeted	Conversion	Actual BzMA Block Size	Dispersity	DLS Diameter (nm)	Dispersity
$PBzMA_{30}$	95%	$PBzMA_{29}$	1.12	24	0.256
$PBzMA_{40}$	94%	$PBzMA_{38}$	1.13	23	0.121
$PBzMA_{50}$	97%	$PBzMA_{48}$	1.13	27	0.059
$PBzMA_{62.5}$	96%	$PBzMA_{60}$	1.16	31	0.125
$PBzMA_{75}$	98%	$PBzMA_{74}$	1.15	40	0.115
$PBzMA_{87.5}$	97%	$PBzMA_{85}$	1.17	37	0.09
$PBzMA_{100}$	98%	$PBzMA_{98}$	1.18	34	0.055
$PBzMA_{125}$	98%	$PBzMA_{123}$	1.27	45	0.063
$PBzMA_{150}$	98%	$PBzMA_{147}$	1.23	39	0.031
$PBzMA_{175}$	98%	$PBzMA_{172}$	1.39	76	0.051
$PBzMA_{200}$	98%	$PBzMA_{196}$	1.31	49	0.02
$PBzMA_{225}$	98%	$PBzMA_{221}$	1.65	103	0.178
$PBzMA_{250}$	98%	$PBzMA_{245}$	1.74	125	0.04
$PBzMA_{300}$	98%	$PBzMA_{294}$	1.58	83	0.017
$PBzMA_{400}$	98%	$PBzMA_{392}$	2.02	120	0.005
$PBzMA_{500}$	98%	$PBzMA_{492}$	2.34	167	0.01
$PBzMA_{750}$	98%	$PBzMA_{737}$	2.84	293	0.121
$PBzMA_{1000}$	98%	$PBzMA_{979}$	3.47	318	0.056

Table 5.1: Synthesis of $PSMA_{30}PBzMA_X$ nanoparticles

phenomenon described in section 5.3.2 where leaving the PSMA block synthesis at high conversions leads to some of the RAFT agent breaking down leading to some dead chains that will affect the PD. These dead chains could be resolved by performing a purification step between both block polymerisations, but this would add time and cost to the synthesis, making it less industrially viable. The size of the nanospheres as calculated by DLS in general increases as the core block increases, although the results do not show a direct correlation as shown in Figure 5.7. The polymers with BZMA cores DP of 30, 50, 100, 150, 200, 300, 400, 500, 750 and 1000 were made using a pseudo-one-pot method, meaning that one block was formed and then the second was added later. Although theoretically identical, this requires a second initiation of the reaction and may not exactly replicate the conditions of a true one-pot synthesis. This difference results in a slight variation between the size of the nanospheres made by the one pot and the pseudo one-pot synthesis.

Previous research by Derry et al. on similar nanoparticles as those described in this thesis show the formation of smaller nanoparticles than observed here, in particular at higher DPs.(Derry et al., 2016a) For example for a BzMA core of 1000 Derry observed

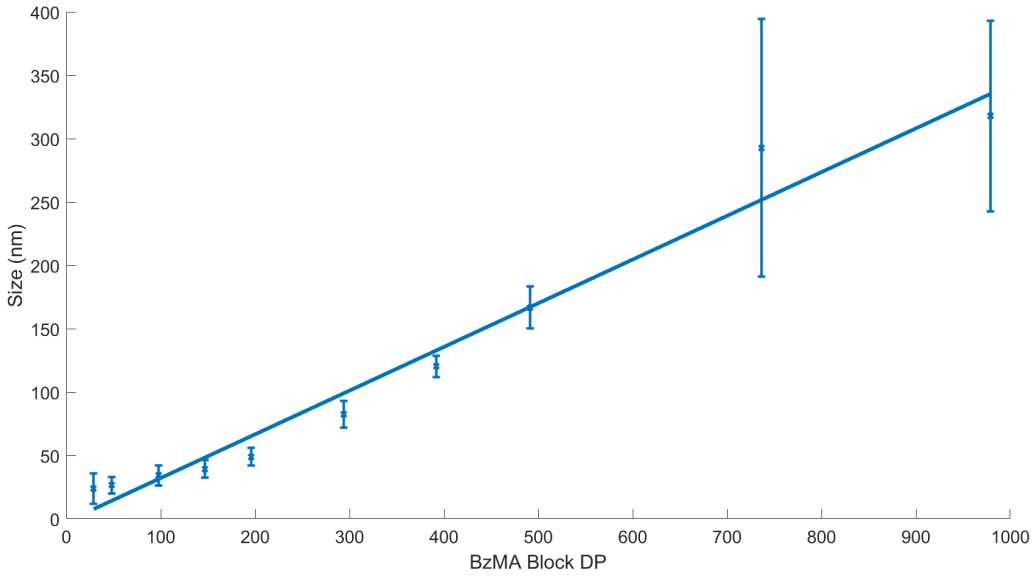

Figure 5.7: The effect of BzMA block size on the size of $PSMA_{30}PBzMA_X$ spheres

a nanoparticle size of 100nm rather than 318nm observed here. This difference is likely because the particles made by Derry et al. were not made via a one-pot protocol, and the formation of the PSMA block was terminated at around 75% conversions. This both allows for purification steps between the block synthesis and prevents any monomer starved conditions that can lead to the breakdown of the RAFT end-groups. The breakdown of any RAFT end groups would lead to the formation of larger spheres due to fewer active chains being able to react with the monomer; this results in larger chains and larger spheres. This will occur in more significant amounts in a one-pot synthesis as high conversions of the SMA monomer have to be achieved before the BzMA addition to limit any contamination of the BzMA block by the SMA. For the smaller spheres, up to a BzMA core DP of 200, the results described by Derry et al. are very similar to those observed in Figure 5.7. This is due to any decrease in active end-groups being less observable due to less BzMA monomer being present. This agreement with Derry et al. indicates that the one-pot synthesis is an effective method to synthesise PSMA-PBzMA nanospheres that are of use in an industry setting as friction modifiers.

Table 5.2 shows the crosslinked nanospheres that were synthesised. These nanospheres cannot be analysed via NMR or GPC as the crosslinking means that they are no longer

Core Polymer Targeted	DLS Diameter (nm)	Dispersity	DLS Diameter (THF) (nm)	Dispersity
$PBzMA_{30}$-$PEGDMA_3$	23	0.104	N/A	N/A
$PBzMA_{40}$-$PEGDMA_4$	28	0.119	29	0.132
$PBzMA_{50}$-$PEGDMA_5$	27	0.072	33	0.13
$PBzMA_{62.5}$-$PEGDMA_{6.25}$	31	0.106	43	0.15
$PBzMA_{75}$-$PEGDMA_{7.5}$	38	0.09	53	0.125
$PBzMA_{87.5}$-$PEGDMA_{8.75}$	40	0.053	58	0.129
$PBzMA_{100}$-$PEGDMA_{10}$	35	0.043	46	0.131
$PBzMA_{125}$-$PEGDMA_{12.5}$	46	0.056	73	0.148
$PBzMA_{150}$-$PEGDMA_{15}$	44	0.07	69	0.138
$PBzMA_{175}$-$PEGDMA_{17.5}$	73	0.071	138	0.122
$PBzMA_{200}$-$PEGDMA_{20}$	54	0.035	90	0.113

Table 5.2: Synthesis of $PSMA_{30}PBzMA_XEGDMA_{X/10}$ nanoparticles

soluble, and as such, these techniques cannot be used. To check that crosslinking has been succesful, DLS was undertaken in both dodecane and THF; this is because crosslinking the spheres prevents them from breaking down in THF as the BzMA block is soluble in the THF. If crosslinking occurred, we would expect the spheres to swell in THF but not break down. This swelling is observed in every nanosphere outside of the smallest $PBzMA_{30}$-$PEGDMA_3$, this is somewhat unsurprising as the amount of crosslinking in this sphere is very low, and it is, therefore, possible that the sphere would break down to some extent even if crosslinking was successful.

TEM images were taken of some of the nanospheres, as shown in Figure 5.8. These show that nanospheres were indeed synthesised, as shown by the circular stained black BzMA cores. Results for TEM sphere measurement are shown in Table 5.3. These are smaller than those measured via DLS because we can only stain the BzMA core and not the PSMA stabiliser block, and as such, the outside of our spheres is not visible. We can therefore assume that the $PSMA_{30}$ stabilising block adds approximately a further 15nm to the sphere size. The measured size for the $BzMA_{40}$ is significantly smaller than its crosslinked equivalent. These smaller nanoparticles are less stable when removed from the oil, as is done in TEM imaging; without the crosslinking present to maintain the stability of the spheres, these $BzMA_{40}$ nanoparticles are likely breaking down within the TEM, and this would explain the unexpected sphere diameters.

Core Polymer Targeted	TEM Diameter (nm)
$BzMA_{40}$	6.02±0.90
$BzMA_{40}$-$EGDMA_4$	12.87±1.78
$BzMA_{200}$	36.56±4.89
$BzMA_{200}$-$EGDMA_{20}$	34.11±4.89

Table 5.3: TEM analysis of block copolymer nanospheres

SAXS patterns were taken at 1% w/w of the same four nanospheres as TEM as shown in Figure 5.9. Here q is the length of the scattering vector, which is calculated in equation 5.1, where λ is the wavelength of the x-ray radiation and θ is half of the scattering angle.

$$q = 4\pi \sin\theta/\lambda \tag{5.1}$$

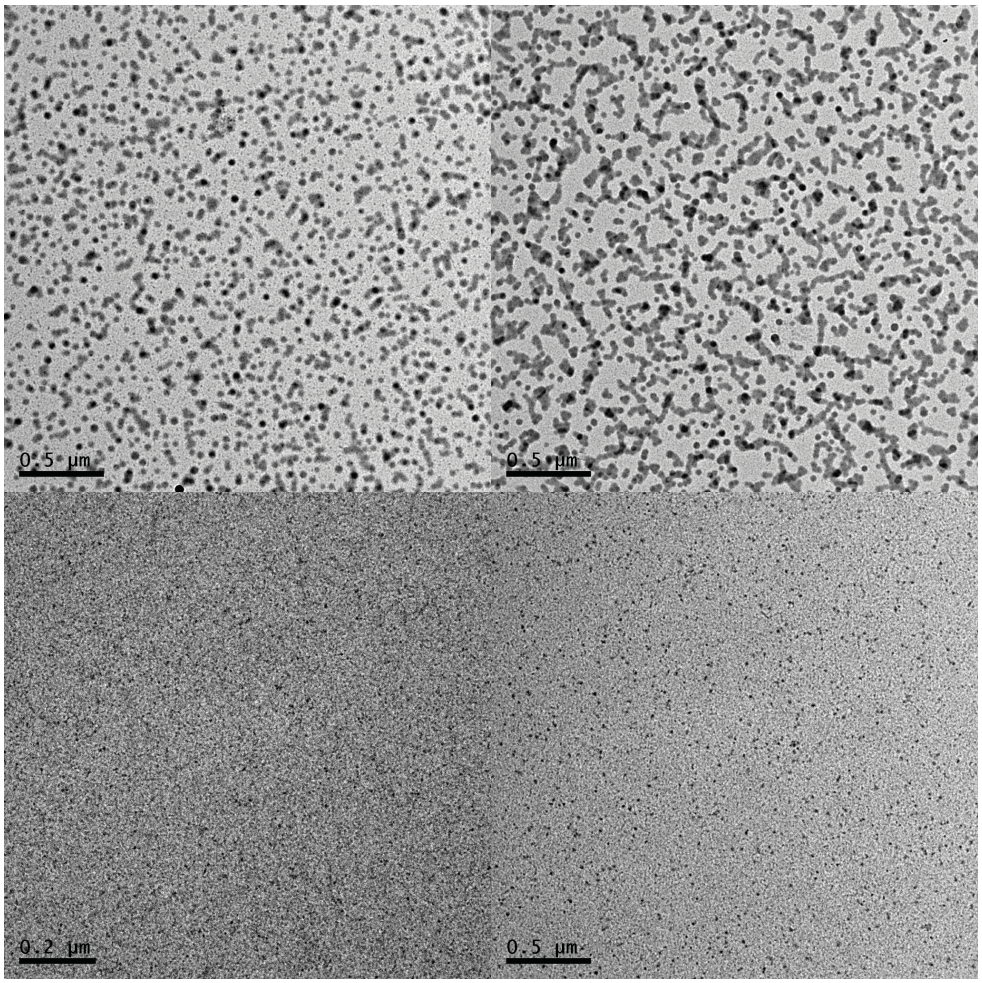

Figure 5.8: TEM images of nanospheres. Top Left: $PSMA_{30}PBzMA_{40}$ Top Right: $PSMA_{30}PBzMA_{40}$-$PEGDMA_4$ Bottom Left: $PSMA_{30}PBzMA_{200}$ Bottom Right: $PSMA_{30}PBzMA_{200}$-$PEGDMA_{20}$

Smaller values of q indicate that a larger structure is being observed. All of these plots show an approximately zero gradient at low values of q. This flat curve indicates that spherical micelles have been synthesised as the intensity measurements remain consistent in this narrow scattering region. Any slight gradient is likely due to any agglomeration of the nanospheres. The sudden increase in the gradient is shown to shift towards a lower q as the size of the BzMA block increases, indicating an increase in the sphere's dimensions and is consistent with the previous analysis. The modelled data display very high overlap with the raw SAXS data indicating that these molecules are micelles, as such the results taken from this data and shown in table 5.4 are valid.(Pedersen and Gerstenberg, 1996)

Table 5.4 shows the calculated data for these SAXS experiments. Here the size of the

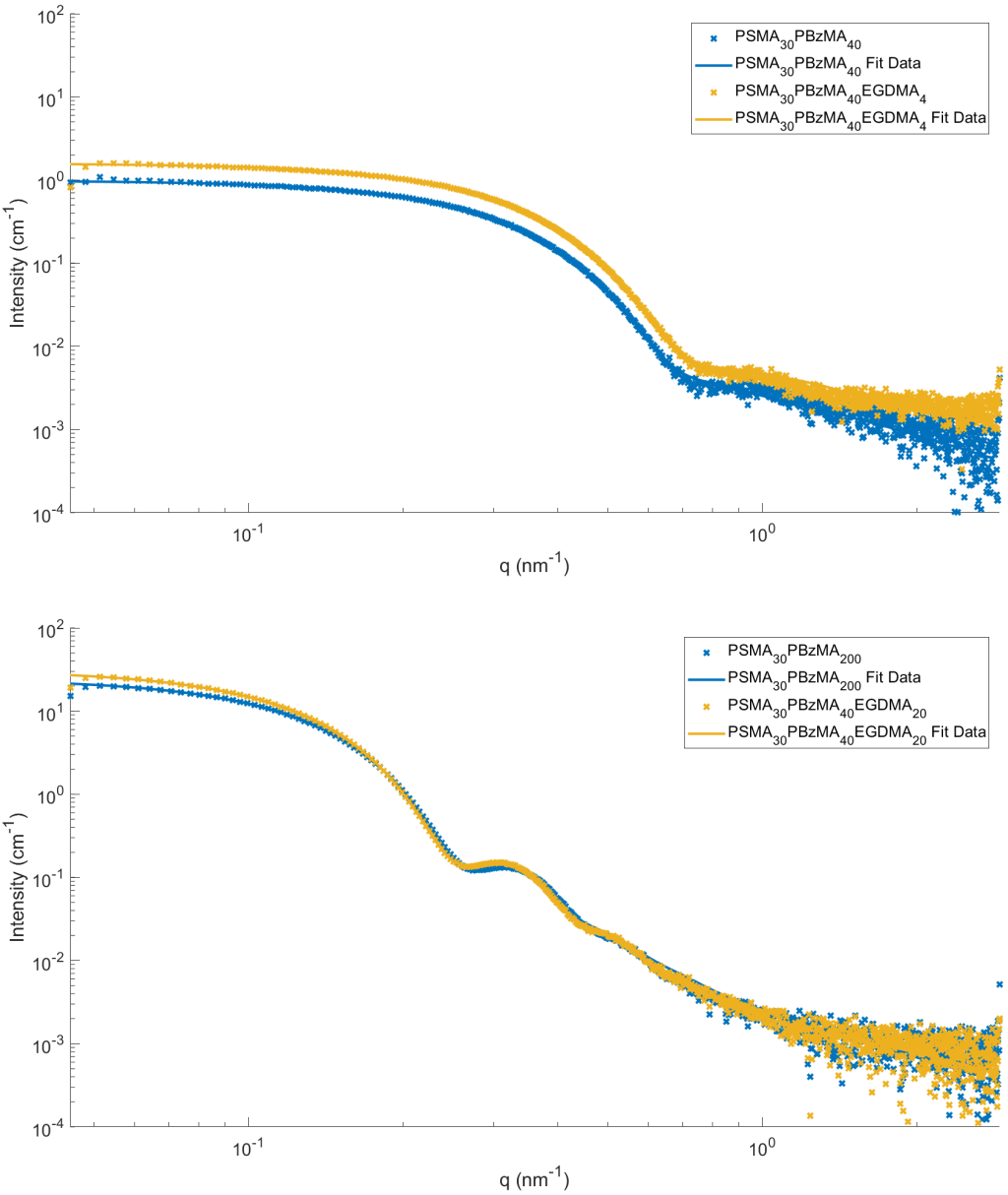

Figure 5.9: SAXS patterns for 1% w/w dispersions of block copolymer nanoparticles synthesised via RAFT dispersion polymerisation at 20% w/w solids in mineral oil. Top is for $PBzMA_{40}$ nanoparticles while bottom is $PBzMA_{200}$ nanoparticles. The data is fit to a spherical micelle model.(Pedersen and Gerstenberg, 1996)

spheres (D_s) is shown to be 16.5nm for the $PBzMA_{40}$ nanospheres and 37-38nm for the $PBzMA_{200}$ nanospheres. These are on a similar scale to that observed via DLS and would be expected to be lower due to SAXS measuring the volume-averaged diameter rather than the intensity averaged diameter in DLS (where we would expect larger spheres to

Core Chemistry	D_s (nm)	N_{agg}	S_{agg} (Å^{-2})	D_{int} (Å)
$PBzMA_{40}$	16.46±0.87	34.09	0.000999	32.64
$PBzMA_{40}$-$PEGDMA_4$	16.52±0.56	30.69	0.000964	32.2
$PBzMA_{200}$	37.09±3.13	361.82	0.00107	30.53
$PBzMA_{200}$-$PEGDMA_{20}$	38.05± 3.1	403.20	0.00111	29.98

Table 5.4: SAXS analysis of block copolymer nanospheres: spherical core diameter(D_s), mean aggregation number of a sphere (N_{agg}), number of copolymer chains per unit surface area (S_{agg}) and mean distance between adjacent chains at the core–shell interface (D_{int}) upon completion of the polymerisation.

have a greater impact on the average). Table 5.4 also shows that the mean aggregation number of the spheres, this is the average number of polymer chains within the sphere and shows that the smaller $PBzMA_{40}$ nanospheres have a much smaller number of polymer chains than the larger $PBzMA_{200}$ nanospheres. The average number of chains per unit area (S_{agg}) are shown to be larger for the $PBzMA_{200}$ nanospheres, while the distance between chains (D_{int}) is shown to be smaller. So the chains are more closely packed together within the larger core and could indicate an increased density of these spheres. However, these differences are minimal, and any difference in the mechanical properties of these spheres is likely to be small.

5.4 Conclusions

Eleven $PSMA_{30}$-$PBzMA_{30\text{-}200}$ block copolymer nanospheres were prepared via RAFT dispersion polymerisation with a further eleven having an EGDMA block added to crosslink the core. They were synthesised with good polymeric control and show a correlation between the DP of the BzMA core block and the DLS size of the nanosphere. DLS in THF also confirms that EGDMA crosslinking was successful. TEM and SAXS on two pairs of spheres show that well-ordered nanospheres were indeed formed and confirm the sizes observed via DLS.

Chapter 7 will investigate the effect of these PSMA-PBzMA nanoparticles on the tribological characteristics of contacts typical of those observed in an ICE

Chapter 6

Methodology for Tribological Testing

6.1 Sample Preparation

Samples for all tribological tests detailed below were prepared as follows: Hot water was run over glassware containing 20% w/w nanoparticle solution or GMO with manual agitation to generate a homogenous sample. The required amount of homogenous sample was diluted with NEXBASE 3043 group 3 oil which was provided by Witham group, for which they are thanked. This oil is a next generation oil designed for use in 5W and 10W engine oils with a viscosity of 5mPa.s at 100°C. This oil also complies closely with the base oil used by Derry et al.(Derry et al., 2019) allowing for comparison. Dilution was undertaken to generate a 0.5% w/w friction modifier solution for testing using a set of lab scales with accuracy allowable of up to 0.02g. This typically results in a maximum concentration error of ± 0.05%. This solution was manually agitated before addition to the testing apparatus.

6.2 Friction Testing

Mini Traction Machine Initial Profiles (MTM)

Initial tests were undertaken on the mini traction machine to establish an initial idea of the performance of the polymer nanoparticles as friction modifiers. Here a three-part test was

undertaken. The first step Stribeck curve of the nanoparticle oil, provides their frictional performance across the entire range of lubrication regimes from startup. The second step was one at 50 mms^{-1}, which provides the longer-term performance of the nanoparticles in the boundary lubrication regime. The final step is another Stribeck curve; this allows us to observe the long term performance of the nanoparticles and confirm that the nanoparticles do not break down or reduce in performance with time.

Stribeck curves were obtained using a PCS mini traction machine (PCS) consisting of 19.05mm diameter 52100 steel ball and 46mm diameter 52100 steel disc. The ball and disc are driven independently to create a sliding rolling ratio of 100%. Friction measurements were performed on mineral oil with and without 0.5% w/w additive at 100°C from 10-2500 mms^{-1} with a loading force of 35N. Two of these Stribeck curve runs were performed and separated by a 1 hour traction step at 50 mms^{-1}. Three repeats were undertaken with fresh samples used for each test.

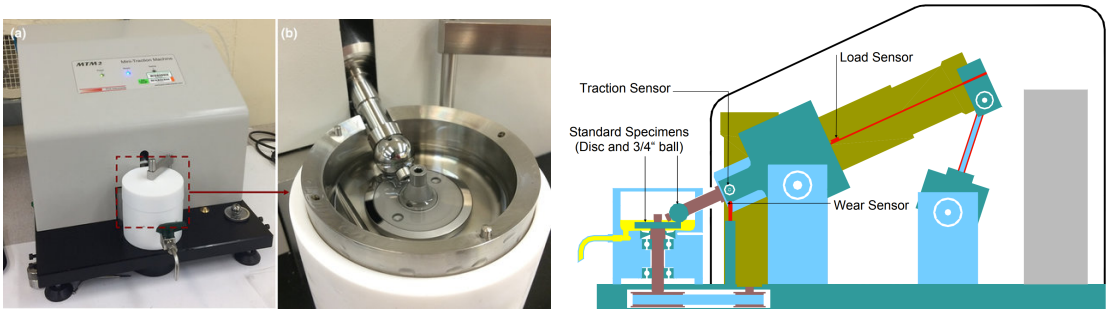

Figure 6.1: Images and Schematic of PCS Mini Traction Machine.(Gould et al., 2019; PCS Instruments, 2005) Reprinted with permission. Copyright ©2019 Springer Science & Business Media, LLC. Copyright ©2005 PCS Instruments

Temperatures of 100°C are comparable to temperatures within ICE and allow for an understanding of the performance of these nanoparticles in these conditions. Maximum contact pressure of 991.6 MPa were using hertzian contact equations where both the ball and disc have elastic modulus of 210 GPa and poissons ratio of 0.285. This pressure is in the upper range of what can be expected in an ICE. This combined with high sliding environments allow for the formation of an extended high friction boundary lubrication regime. These conditions also allow for direct comparison between the results of these nanoparticles and the nanoparticles produced by Zheng et al. and Derry et al.(Zheng

et al., 2010; Derry et al., 2019) with these contact pressures, temperature and SRR being the same as experiments described in these papers.

Glycerol Monooleate (GMO) was chosen to allow for a comparison to commercially available friction modifiers, due to high expense and ease of use a mixed oleate was used, containing 40-50% monooleate, 40-50% bisoleate and 5% trisoleate. This friction modifier was selected to allow for direct comparison with previous work undertaken by Zheng et al. and Derry et al.(Zheng et al., 2010; Derry et al., 2019)

Both ball and plate were polished to achieve $<0.02\mu$m average surface roughness. These highly polished surfaces are standard for MTM and mean that any effect of surface roughness on the friction results are minimised, meaning that any change in friction is to be the result of any additive within the oil rather than variance in the surface roughness of the samples.

Film thickness calculations were made using data provided by Witham group for NEXBASE 3043 and the lambda ratio was calculated. Composite surface roughness was calculated to be 11.31nm as both the surface contacts have a mean surface roughness of 8nm $\pm$ 2. Film thickness was calculated using an approximated pressure viscosity coefficient of 12 GPa^{-1}. This was approximated based off previous work undertaken by Masilela et al. for very similar group 3 oils as those used in this thesis.(Masilela and De Vaal, 2019). This allowed for film thickness calculation as described by Dowson and Hamrock as described in Chapter 2. The results for film thickness are shown in Figure 6.2.

This allowed for the calculation of lamda ratio to understand when the contact is in the boundary, mixed and hydrodynamic regime. Here the boundary regime (when film thickness is less than surface roughness) was shown to be below 280 mms^{-1}, mixed regime (when film thickness is up to three times the surface roughness) was shown to be between 280-1400 mms^{-1} and hydrodynamic regime above this speed.

Mini Traction Machine Sliding:Rolling Sweep (MTM SRR Sweep)

While the initial MTM tests suggest that PSMA-PBzMA nanoparticles may be effective friction modifiers in a linear contact, these tests were only undertaken at one sliding to rolling ratio of 100%. While a good initial test this does not provide information on the

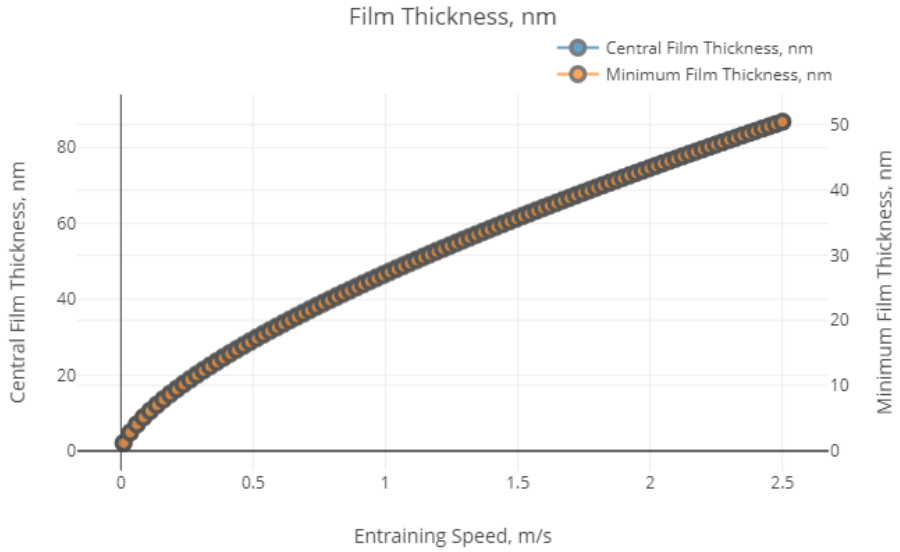

Figure 6.2: Central and Minimum Film thickness of MTM tests

wide number of linear contact conditions that a friction modifier may be exposed to in an internal combustion engine. These SRR sweep tests are undertaken using the MTM and produce Stribeck curves in contact conditions from a pure rolling contact, where friction should be zero, to a pure sliding contact, where friction should be highest.

Stribeck curves were obtained using a PCS mini traction machine (PCS) consisting of 19.05mm diameter 52100 steel ball and 46mm diameter 52100 steel disc. The ball and disc are driven independently to create a sliding rolling ratio. Friction measurements were performed on mineral oil with and without 0.5% w/w additive at 100°C from 10-2500 mms^{-1}, maximum speeds of 2000mms^{-1} were achieved at sliding:rolling ratio of 150% and 200%, with a loading force of 35N, 991.6 MPa. Stribeck curves were performed at SRR of 0%, 2%, 5%, 10%, 25%, 50%, 75%, 100%, 150%, 200%. Each SRR was undertaken sequentially on one set of samples with three repeats of the full SRR sweep being undertaken on fresh MTM samples.

The temperature and contact pressure of the experiments was kept consistent with previous MTM tests.

Glycerol Monooleate (GMO) was chosen to allow for a comparison to commercially available friction modifiers, due to high expense and ease of use a mixed oleate was used,

containing 40-50% monooleate, 40-50% bisoleate and 5% trisoleate. This friction modifier was selected to allow for direct comparison with previous work undertaken by Zheng et al. and Derry et al.(Zheng et al., 2010; Derry et al., 2019)

Both ball and plate were polished to achieve $<0.02\mu$m average surface roughness. These highly polished surfaces are standard for MTM and mean that any effect of surface roughness on the friction results are minimised, meaning that any change in friction is to be the result of any additive within the oil rather than variance in the surface roughness of the samples.

Film thickness calculations were made using data provided by Witham group for NEXBASE 3043. Composite surface roughness was calculated to be 11.31nm as both the surface contacts have a mean surface roughness of 8nm $\pm$ 2. Film thickness was calculated using an approximated pressure viscosity coefficient of 12 GPa^{-1}. This was approximated based off previous work undertaken by Masilela et al. for very similar group 3 oils as those used in this thesis.(Masilela and De Vaal, 2019). This allowed for film thickness calculation as described by Dowson and Hamrock as described in Chapter 2. The results for film thickness are shown in Figure 6.2.

This allowed for the calculation of lamda ratio to understand when the contact is in the boundary, mixed and hydrodynamic regime. Here the boundary regime (when film thickness is less than surface roughness) was shown to be below 280 mms^{-1}, mixed regime (when film thickness is up to three times the surface roughness) was shown to be between 280-1400 mms^{-1} and hydrodynamic regime above this speed.

While film thickness should be independent of SRR, and SRR is not involved in the calculation for film thickness. Work by Guegan et al. indicates that SRR can effect film thickness due to thermal effects on the contact. This is particularly the case at higher SRR where increased friction leads to elevated temperatures within the contact. They showed that this can have the effect of increasing the lambda ratio at which the EHD friction begins and as such an elevated entrainment speed is required to reach the elastrohydrodynamic regime at these higher SRRs.(Guegan et al., 2016)

TE54 Mini Traction Machine

TE54 is a continuous traction machine that involves two rollers driven independently. The TE54 is similar to the PCS MTM described above but instead removes the potential effects of spin to affect the results and allows for longer testing times in continuous contact.

Stribeck curves were obtained using a Phoenix Tribology Ltd TE54 mini traction machine consisting of 25mm diameter 52100 steel ball and 50mm diameter and 10mm width 52100 steel roller. The ball and roller are driven independently to create sliding rolling ratios. Friction measurements were performed on mineral oil with and without 0.5% w/w additive at 100°C at speeds of 0.01, 0.05, 0.1, 0.2, 0.4, 1, and 2.5 ms^{-1} for 1200s per speed to a load of 40.3N. Measurements were taken at sliding rolling ratios of 0%, 2%, 5%, 10%, 25%, 50%, 75%, 100%, 150% and 200%. Each SRR was undertaken sequentially on one set of samples with three repeats of the full SRR sweep being undertaken on fresh TE54 samples.

These temperatures and contact pressures were chosen to be consistent with those undertaken using the PCS MTM, with a maximum load of 1 GPa.

Speeds of the contact are shown in table 6.1.

Glycerol Monooleate (GMO) was chosen to allow for a comparison to commercially available friction modifiers, due to high expense and ease of use a mixed oleate was used, containing 40-50% monooleate, 40-50% bisoleate and 5% trisoleate. This friction modifier was selected to allow for direct comparison with previous MTM experiments.

Both ball and plate were polished to achieve $<0.02\mu$m average surface roughness. These highly polished surfaces mean that any effect of surface roughness on the friction results are minimised, meaning that any change in friction is to be the result of any additive within the oil rather than variance in the surface roughness of the samples.

Film thickness calculations were made using data provided by Witham group for NEXBASE 3043. Composite surface roughness was calculated to be 12.8 nm with the ball having a mean surface roughness of 8 ± 2nm and the roller having a mean surface roughness of 10 ± 1.5nm. Film thickness was calculated using an approximated pressure viscosity coefficient of 12 GPa^{-1}. This was approximated based off previous work undertaken by Masilela et al. for very similar group 3 oils as those used in this thesis.(Masilela

	Entrainment Speed (m/s)	**0.01**	**0.05**	**0.1**	**0.2**	**0.4**	**1**	**2.5**
2%	**Ball Speed (m/s)**	0.0101	0.0505	0.101	0.202	0.404	1.01	2.525
	Disc Speed (m/s)	0.0099	0.0495	0.099	0.198	0.396	0.99	2.475
5%	**Ball Speed (m/s)**	0.01025	0.05125	0.1025	0.205	0.41	1.025	2.5625
	Disc Speed (m/s)	0.00975	0.04875	0.0975	0.195	0.39	0.975	2.4375
10%	**Ball Speed (m/s)**	0.0105	0.0525	0.105	0.21	0.42	1.05	2.625
	Disc Speed (m/s)	0.0095	0.0475	0.095	0.19	0.38	0.95	2.375
25%	**Ball Speed (m/s)**	0.01125	0.05625	0.1125	0.225	0.45	1.125	2.8125
	Disc Speed (m/s)	0.00875	0.04375	0.0875	0.175	0.35	0.875	2.1875
50%	**Ball Speed (m/s)**	0.0125	0.0625	0.125	0.25	0.5	1.25	3.125
	Disc Speed (m/s)	0.0075	0.0375	0.075	0.15	0.3	0.75	1.875
75%	**Ball Speed (m/s)**	0.01375	0.06875	0.1375	0.275	0.55	1.375	3.4375
	Disc Speed (m/s)	0.00625	0.03125	0.0625	0.125	0.25	0.625	1.5625
100%	**Ball Speed (m/s)**	0.015	0.075	0.15	0.3	0.6	1.5	3.75
	Disc Speed (m/s)	0.005	0.025	0.05	0.1	0.2	0.5	1.25
150%	**Ball Speed (m/s)**	0.0175	0.0875	0.175	0.35	0.7	1.75	4.375
	Disc Speed (m/s)	0.0025	0.0125	0.025	0.05	0.1	0.25	0.625
200%	**Ball Speed (m/s)**	0.02	0.1	0.2	0.4	0.8	2	5
	Disc Speed (m/s)	0	0	0	0	0	0	0

Table 6.1: Speeds used for TE54 to achieve desired entrainment speed and SRR

and De Vaal, 2019). This allowed for film thickness calculation as described by Dowson and Hamrock as described in Chapter 2. The results for film thickness and the lambda ratio associated with this are shown in Table 6.2.

Entrainment Speed (ms^{-1})	Film Thickness (nm)	Lambda Ratio	Lubrication Regime
0.01	1.3	0.102	Boundary
0.05	3.89	0.304	Boundary
0.1	6.23	0.487	Boundary
0.2	9.98	0.78	Boundary
0.4	15.98	1.248	Mixed
1	29.81	2.329	Mixed
2.5	55.58	4.342	Hydrodynamic

Table 6.2: Film Thickness and Lambda ratio of samples throughout TE54 Testing

The use of TE54 is limited in tribological testing, and the calibration and preparation of samples were not fully understood before testing. The friction values are not what would be expected, particularly at low SRR ratios. Limitations in time and samples mean that a new round of testing is not possible, and as such, these results can only be viewed as comparative to the PCS MTM and observe changes in friction with the addition of the

nanoparticles over a long period of testing.

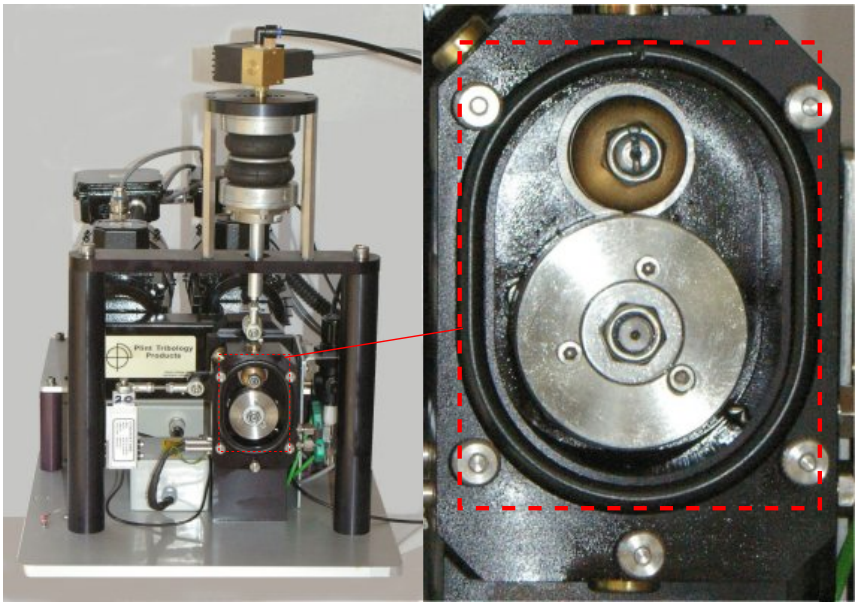

Figure 6.3: Image of TE54 test set up

Universal Mechanical Tester (UMT)

UMT testing results in a reciprocating pure sliding contact; this results in a very high friction environment due to the lack of contact rolling and the variation in the direction of the contact preventing a continuous suction of oil and any other additives into the contact area.

Friction results were obtained using a Bruker universal machine tribometer (UMT) consisting of a 6.35mm diameter 52100 steel ball and 70mm 52100 steel plate. Friction measurements were performed on mineral oil with and without 0.5% w/w additive at 10mm/s at a load of 30N for a stroke length of 50mm to a total sliding distance of 400m. This method is in keeping with ASTM G133: Standard Test Method for Linearly Reciprocating Ball-on-Flat Sliding Wear. Three repeats were undertaken with fresh UMT samples for each repeat.

ASTM G133: Standard Test Method for Linearly Reciprocating Ball-on-Flat Sliding Wear defines that experiments should be undertaken at maximum contact pressure 2 GPa, this is achieved through use of 30N load. It is not possible, however, with a UMT to heat

Figure 6.4: Image and Schematic for Universal Machine Tribometer

the lubricant and as such all experiments were undertaken at room temperature. While not an ideal representation of a ICE this does allow for observation of friction effects at "start up" of an engine and will act comparatively to mineral oil and GMO controls that were undertaken in the same conditions.

Glycerol Monooleate (GMO) was chosen to allow for a comparison to commercially available friction modifiers, due to high expense and ease of use a mixed oleate was used, containing 40-50% monooleate, 40-50% bisoleate and 5% trisoleate. This friction modifier was selected to allow for direct comparison with previous MTM experiments.

Both ball and plate were polished to achieve $<0.02\mu$m average surface roughness. These highly polished surfaces mean that any effect of surface roughness on the friction results are minimised, meaning that any change in friction is to be the result of any additive within the oil rather than variance in the surface roughness of the samples.

Film thickness calculations were made using data provided by Witham group for NEXBASE 3043. Composite surface roughness was calculated to be 12.8 nm with the ball having a mean surface roughness of 8 $\pm$ 2nm and the roller having a mean surface roughness of 10 $\pm$ 1.5nm. Film thickness was calculated using an approximated pressure viscosity coefficient of 12 GPa^{-1}. This was approximated based off previous work undertaken by Masilela et al. for very similar group 3 oils as those used in this thesis.(Masilela and De Vaal, 2019). This allowed for film thickness calculation as described by Dowson and Hamrock as described in Chapter 2 with a minimum film thickness of 2.89nm and a lambda ratio of 0.226, meaning this experiemnt is undertaken within the boundary regime.

6.3 Wear Testing

Upon completion of friction testing detailed above, the wear of the contact surface was measured; this allows for the observation of any potential effect of the polymer nanoparticles on contact wear. These measurements were performed by optical 3D measurement and by profilometry.

6.3.1 Sample Preparation

Upon completion of friction tests the samples were cleaned via a three step process: first they were wiped with blue roll to remove any excess oil, they were then rinsed with acetone and heptane and wiped with blue roll, finally they were ultrasonicated in acetone for 10 minutes in order to remove any remaining oil from the surface. Prior to wear measurement these steps were repeated in order to ensure the samples were adequately cleaned, before being allowed to dry thoroughly before measurement.

6.3.2 Optical 3D measurements

Optical 3D measurements were undertaken using an Alicona InfiniteFocusSL. Optical images are taken at various heights above the sample and are combined to form a 3D representation of the surface. This 3D image allows for the measurement of the wear scar depth. Measurements were undertaken at 10x magnification with profiles generated based on the average of 1000 lines across the wear scar.

Three methods were used to define the wear: 1. The maximum difference between the highest and lowest point on the surface (peak to trough). This is most susceptible to error caused by surface roughness. 2. A visual assessment (eyeball) of where the wear scar occurs and is distinct for the surface roughness. Visually fitting a mean line through the wear surface and the original surface. 3. A Fourier curve fits the surface and uses the difference between the highest and lowest points on the fitted curve.

An example of this is demonstrated in Figure 6.5.

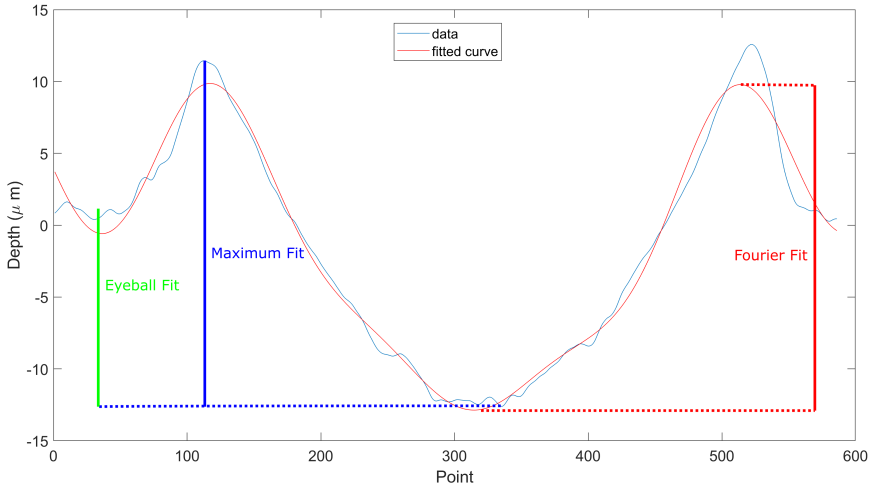

Figure 6.5: Example profile from a wear scar from Optical 3D measurements to demonstrate the three measurement methodologies

6.3.3 Profilometry

Linear Profilometry was undertaken using a Mitutoyo Surftest SJ-500. Measurements of 5mm in length were undertaken at speeds of 0.2 mm/s with a tip of 5 μm in radius.

Three methods were used to define the wear of these samples as described above for the Optical 3D measurements and displayed in Figure 6.5.

Only UMT samples were measured via profilometry as the tip radius is too large to enter and measure the MTM wear scars.

6.4 Viscosity and Stability Testing

6.4.1 Viscosity Measurements

Viscosity measurements were undertaken using a TA instruments Discovery HR10 rheometer using a 40.0mm 1.99944°cone plate. Three temperature sweeps were undertaken at 25, 40 and 80 °c at a shear rate of 10-1500s^{-1}.

These experiments to observe any potential effect of nanoparticle addition on the viscosity of the oil both pre and post testing. This test was undertaken at multiple shears and temperatures to ensure a thorough understanding of these nanoparticle effects either

due to a potential non-newtonian effect or an effect on oil viscosity with temperature. This will allow for an understanding and confirmation of friction effects of the nanoparticles and allow for a discussion on the hypothesis that any friction effects are the result of a change in oil viscosity which is the case for some of the friction modifiers in the literature. stability testing upon completion of tribological experiments will confirm the long term stability of these nanoparticles within a contact.

6.4.2 Gel Permeation Chromatography (GPC)

The THF GPC set-up comprised an Agilent 1260 Infinity series degasser and pump, two Agilent PLgel 5 μm MIXED-C columns in series and a refractive index detector. THF eluent contained triethylamine (2.0% w/w) and butylhydroxytoluene (0.05% w/v). This set-up was operating at a flow rate of 1 mL/min and 30 °C. A series of twelve near-monodisperse poly(methyl methacrylate) standards ranging from 800 g/mol to 2,200,000 g/mol was used for column calibration. Copolymer dispersions were filtered using a 0.2 μm syringe filter and diluted in THF eluent (0.10% w/w).

This will allow for an observation of polymer chain length upon completion of experiments and as such will allow for observation of any potential polymer breakdown that occurs in tribological testing.

6.4.3 Dynamic Light Scattering (DLS)

DLS studies were performed using a Zetasizer NanoZS instrument (Malvern Instruments, UK) at a fixed scattering angle of 173°. Copolymer dispersions were filtered using a 0.2 μm syringe filter and diluted in n-dodecane (0.10% w/w) before light scattering studies at 25 °C.

This will allow for observation of nanoparticle size upon completion of tribological testing. This will be compared to previously measured nanoparticles pre-testing and display any change in the nanoparticles as a result of being exposed to a tribological contact.

6.5 Adsorption Testing

6.5.1 Mini Traction Machine Spacial Layer Imaging (MTM-SLIM)

MTM-SLIM is a method for measuring additive films during a tribological test, often described as in situ. Here white light is shined onto a silica/chromium glass with the MTM ball loaded upon it. Some light is reflected by the chromium within the glass, while some passes through the additive film and are reflected by the MTM ball. These light reflections are recombined to form an interference image by a high-resolution RGB camera. This RGB image can then be analysed in order to determine the film thickness of the contact.

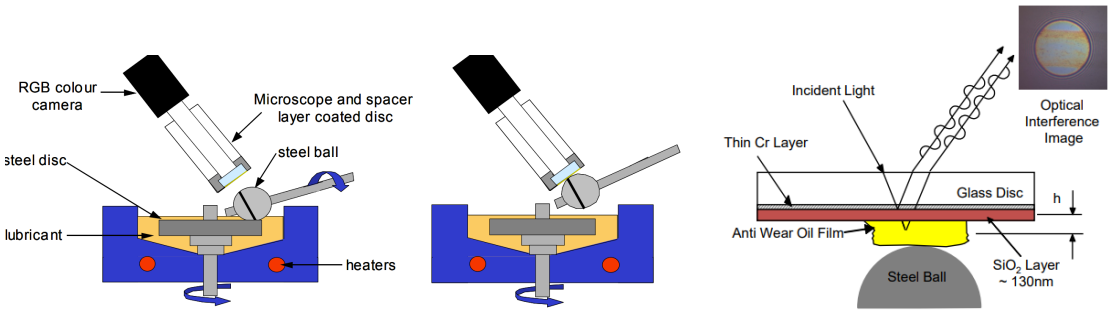

Figure 6.6: Schematic for Measurement of thin films by MTM-SLIM.(PCS Instruments, 2005) Reprinted with permission. Copyright ©2005 PCS Instruments

Friction and Film measurements were obtained using a PCS mini traction machine (PCS) consisting of 19.05mm diameter 52100 steel ball and 46mm diameter 52100 steel disc. The ball and disc are driven independently to create a sliding rolling ratio of 5%. Friction measurements were performed on mineral oil with and without 0.5% w/w additive at 35mms^{-1}, 100°C with a loading force of 35N, 991.6 MPa, for 4 hours. Spacial layer images were undertaken before testing, then after 30, 60, 90, 120, and 180 minutes and upon completion of testing. The 52100 steel ball was loaded upon a 100 nm spacial layer film to 20N.

These contact conditions were chosen as they are similar to those undertaken during the tribological testing of these nanoparticles with the low entrainment speed meaning that the experiment is undertaken in the boundary regime where friction is highest and this thesis is most interesting in any effect of the nanoparticles. This allows for an understanding of the

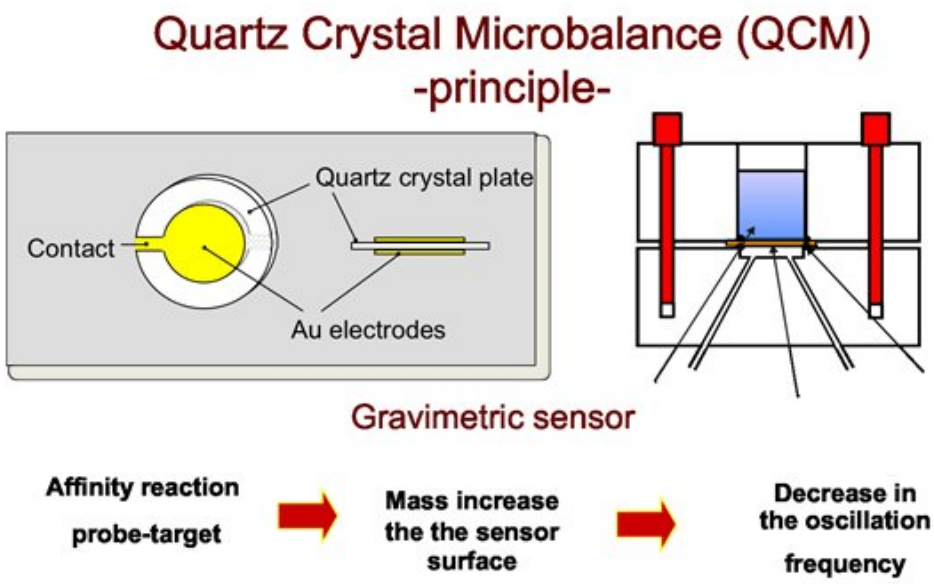

Figure 6.7: Schematic of Quartz Crystal Microbalance.(Scarano et al., 2016) Reprinted with permission. Copyright ©2016 CC-BY-3, https://creativecommons.org/licenses/by/3.0/legalcode

film formation that would occur in the boundary regime of contacts studied previously in this thesis. The low SRR of 5% was chosen to be in a similar range with previous film thickness studies that were undertaken using MTM-SLIM.(Zhang and Spikes, 2016; Parsaeian et al., 2017)

6.5.2 Quartz Crystal Microbalance (QCM)

Quartz crystal microbalance (QCM) measures the thickness of a film formed upon the surface by measuring changes in the frequency of the sound waves generated by a quartz crystal resonator, allowing for the measurement of the films generated by the polymer nanoparticles. A schematic of QCM is shown in Figure 6.7

Before testing, Gold QCM sensors were ultrasonicated in 99% ethanol for 30 minutes, then rinsed in milliQ water and gently dried under a nitrogen flow. These sensors were set in the QCM flow cell modules to 55°C. Once the temperature had stabilised, oils were then introduced. Mineral oil was pumped through the system at a 0.25 ml/min rate with a peristaltic pump, and baseline readings were taken when equilibrium was reached. Growth oils were then introduced to the flow cell, and growth was permitted for approx.

60 minutes. Afterwards, the mineral oil was reintroduced.

This experiment was undertaken upon gold surfaces rather than the steel surfaces used throughout the rest of this thesis. Gold is the standard surface for QCM due to its inert nature meaning that any changes in the mass measured is the result of any adsorbed film rather than any potential chemistry on the surface. While ideally these experiments would have been undertaken upon steel, gold is an adequate substitute with similar polar attraction to steel and also prevents the need for a deeper understanding of effects of steel on QCM that are outside the framework of this thesis. As such the standard of gold was chosen instead.

Film thickness is calculated by measurement of the change in resonance of the crystal and the decay of this resonance with time. This allows for measurement of the mass and density of the film and as such a film thickness can be inferred.

6.6 Mechanical Testing of Nanoparticles

Nanoindentor SEM studies were undertaken; these allow for imaging of PSMA-PBzMA nanoparticles as they are indented, allowing for an understanding of how they may interact within a contact.

Samples were dissolved to 0.1% w/w in heptane and deposited on a silicon wafer slice, and let to rest for 24 hours.

An alemnis In-Situ SEM indenter was used with an Synton MDP pure diamond conical tip with a tip radius of 0.71 microns. The cone angle for the tip was 60°. The tip was lowered into a safe contact speed to bring it towards the surface of the sample. A displacement control was then set at 500nM, and loading and unloading curves were taken from the sample.

During each test, a Nova 450 SEM from FEI was utilised for image capture. An ETD detector with an imaging voltage of 5Kv with a spot size of 3.5 was utilised; the magnification utilised ranged from 5000-10,000 X for live imaging.

Chapter 7

Tribological Testing of Nanospheres

7.1 Introduction

This chapter will investigate the effects of PSMA-PBzMA nanoparticles on the tribology of a variety of different contacts. It will focus on three main areas: friction of a variety of contacts; the wear associated with these contacts, and the oil's viscosity. It will also investigate the long term stability of these nanoparticles.

7.2 Friction

7.2.1 Mini Traction Machine Initial Profiles (MTM)

Figure 7.1 displays the initial Stribeck curves for both the standard and crosslinked nanoparticles.

Figure 7.1 shows that the baseline mineral oil and also the commercially available glycerol monooleate displays a traditional Stribeck curve shape. High friction is observed at low speeds due to high metal to metal contact in the boundary regime, with friction-reducing as the speed of the contact increases. By comparison, it is shown that all the nanoparticles have a significant effect on the friction of the contact. All the nanoparticles result in a reduction of the coefficient of friction in the boundary lubrication regime; this will be studied further in figure 7.3, but the nanoparticles behave differently outside of the

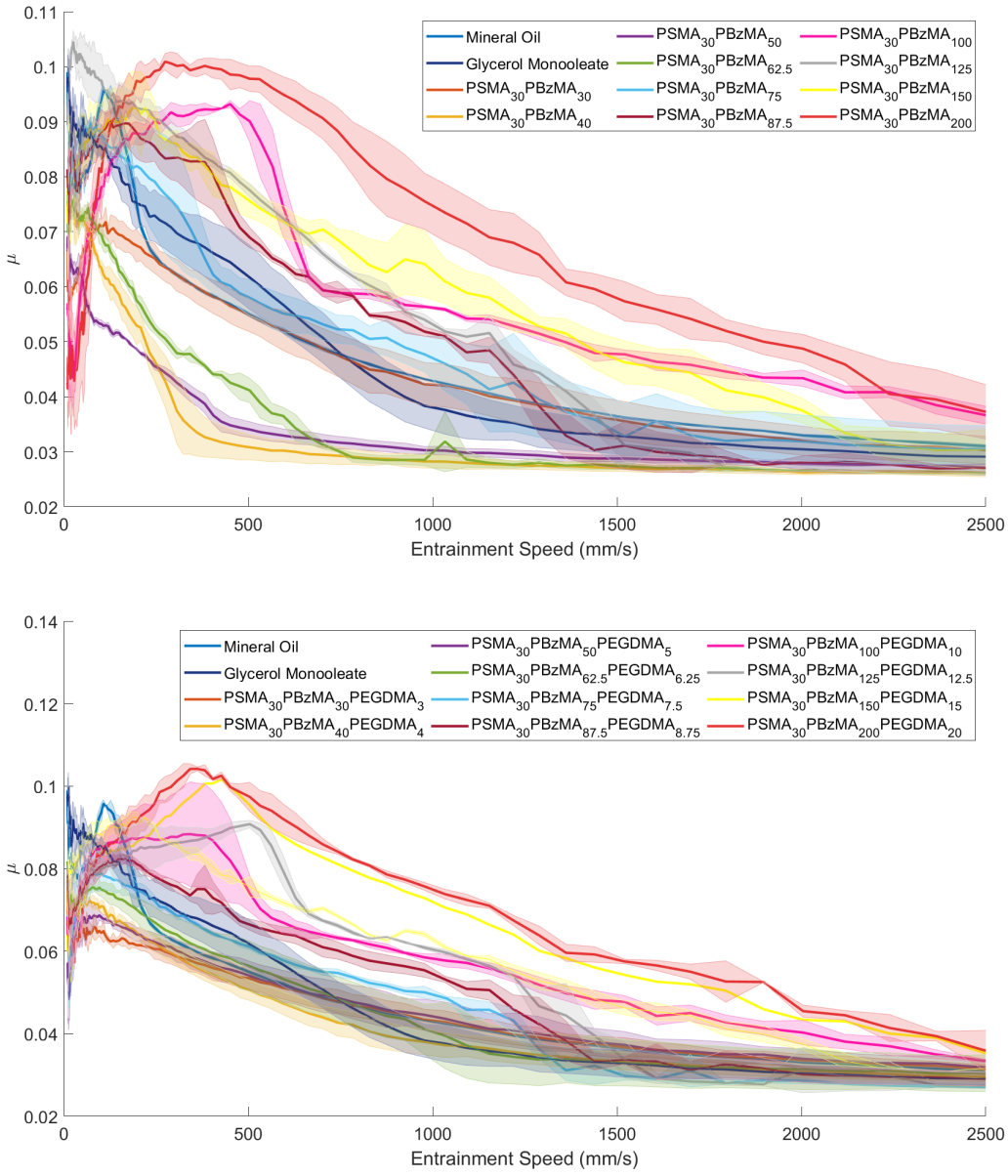

Figure 7.1: Top: Initial Stribeck curves for 0.5 wt% $PSMA_{30}PBzMA_X$ nanoparticles, error bars are standard deviations of 3 tests on fresh MTM samples Bottom: Initial Stribeck curves for 0.5 wt% $PSMA_{30}PBzMA_XPEGDMA_{(X/10)}$ nanoparticles, error bars are standard deviations of 3 tests on fresh MTM samples

boundary regime. The smaller nanoparticles, up to the $BzMA_{75}$ cores behave similarly to the mineral oil, with friction continuing to reduce as the speed of the contact increases. The smallest nanoparticles maintain reduced or equal friction across all the lubrication regimes, with a particular reduction being observed in the non-cross-linked $PBzMA_{40}$,

$PBzMA_{50}$ and $PBzMA_{62.5}$. These nanoparticles may be effective friction modifiers across a range of contact environments and suggest there is a strong correlation between the size of the nanoparticles and their ability to reduce friction outside of the boundary lubrication regime. The greater ability of the non-crosslinked nanoparticles to reduce the friction may indicate that the increased mechanical stability of the crosslinking may hinder the friction modifier capabilities of the nanoparticles. This better performance of non-crosslinked nanoparticles suggests that the deformation and potentially partial breakdown of the nanoparticles may be required for the nanoparticles to most effectively reduce the friction of the contact outside of the boundary lubrication regime, this may provide some evidence for the deformation theory put forward by Zheng et al.(Zheng et al., 2012) but other theories may also be possible. The larger nanoparticles, however, display a very different Stribeck curve. These display the same low friction in the boundary lubrication regime before seeing a significant increase in friction in the mixed and hydrodynamic regimes. One possible explanation for this friction increase is that there is an increase in surface contact with speed, likely because these larger nanoparticles are likely preventing the oil from entering the contact; this phenomenon is displayed in Figure 7.2. The crosslinked nanoparticles display a greater peak friction coefficient in the mixed lubrication regime, again indicating that their higher structural stability may hinder this initial friction-reducing capability. Another possibility for this increase in friction in the upper boundary and mixed lubrication regime could be the result of these nanoparticles elongating the boundary lubrication regime of the contact. This could be due to the generation of a film within the contact, this film may act to disrupt the flow of oil or result in a lower viscosity film within the contact. This would result in less separation of the two contacts and as a result would result in higher friction. Also this film may actually be very high viscosity, this would result in large amounts of liquid-liquid friction within the contact which may be the cause of this spike in friction. Insight into the possible mechanism will be discussed further with the wear results.

These initial friction results indicate that smaller, non-crosslinked nanoparticles may be the most effective friction modifiers due to their ability to deform and within the contact more, and their small size does not prevent oil flow in the mixed or boundary lubrication

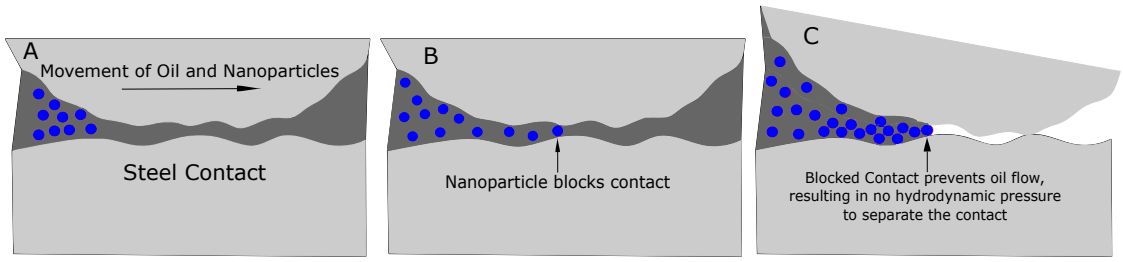

Figure 7.2: Schematic of oil starvation of contact by larger nanoparticles

regime.

Friction modifier performance is most important in the boundary lubrication regime. Here the surface contact is at its highest in typical lubrication, and reducing this, using friction modifiers, is very important. Figure 7.3 displays the initial friction performance in the boundary lubrication regime, which for this contact was calculated to be at speeds below 280mm^{-1}. Here the majority of nanoparticles are all shown to reduce the friction of the contact in boundary conditions, with all crosslinked nanoparticles displaying friction reduction up to 280 mms^{-1}. The least effective nanoparticles in the boundary regime appear to be the middle-sized polymer cores. These sized nanoparticles result in the smallest friction reduction and are the quickest to result in friction that exceeds that in the mineral oil samples. The smaller nanoparticles result in the most consistent friction reduction with all the nanoparticles lower than $BzMA_{62.5}$ resulting in consistent friction reduction across all contact speeds within the boundary lubrication regime. The nanoparticles that result in the most significant friction reduction are the $BzMA_{200}$ core nanoparticles, with low friction of 0.0415. This friction is significantly lower than the crosslinked nanoparticles and again suggests that the increased mechanical stability from the crosslinking results in worse friction performance in the boundary lubrication regime at startup; this does not appear to be the case with smaller nanoparticles where the majority display lower friction in the crosslinked nanoparticles.

These initial stribeck curve results for the larger crosslinked nanoparticles are very similar to those previously reported by Zheng et al. and Derry et al. with low friction in the boundary lubrication regime followed by a spike in friction in the upper boundary and mixed lubrication regime before a decrease into the hydrodynamic regime.(Zheng et al., 2010; Derry et al., 2019) The results for $PSMA_{30}PBzMA_{200}PEGDMA_{20}$ are almost

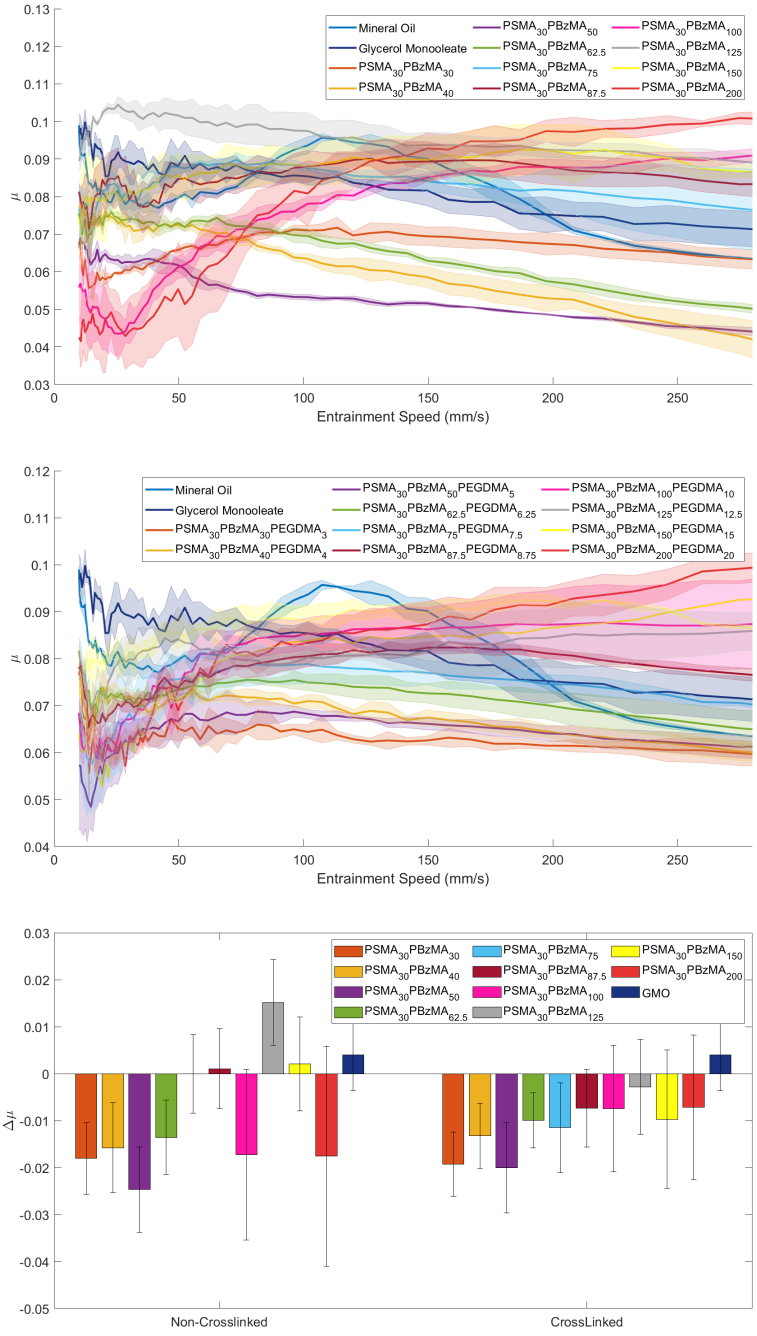

Figure 7.3: Top: Friction of $PSMA_{30}PBzMA_X$ nanoparticles in the boundary lubrication regime, speeds below 280mm^{-1}, error bars are standard deviations of 3 tests on fresh MTM samples Centre: Friction of $PSMA_{30}PBzMA_XPEGDMA_{(X/10)}$ nanoparticles in the boundary lubrication regime speeds below 280mm^{-1}, error bars are standard deviations of 3 tests on fresh MTM samples Bottom: Initial mean boundary lubrication area of the Stribeck curves for 0.5 wt% $PSMA_{30}PBzMA_X$ and $PSMA_{30}PBzMA_XPEGDMA_{(X/10)}$, error bars are standard deviations of 3 tests on fresh MTM samples nanoparticles

identical to those reported by Zheng et al. while also showing very similar nanoparticle diameter under TEM, 34nm for $PSMA_{30}PBzMA_{200}PEGDMA_{20}$ and 35nm for those reported by Zheng et al. Both Zheng et al. and Derry et al. display much lower peak friction coefficients than those reported in this thesis, 0.05 by Derry et al. and 0.07 for Zheng et al. compared to 0.105 for $PSMA_{30}PBzMA_{200}PEGDMA_{20}$ nanoparticles reported in this thesis. This is despite larger nanoparticles being studied by Derry et al. at 48nm under TEM. This indicates that there are multiple factors that affect the ability of these nanoparticles to reduce friction across all the lubrication regimes.

To the authors knowledge the shape of the larger nanoparticles, where the friction coefficient increases with entrainment speed to a maximum value before decreasing again, has only been observed by Zheng et al., Derry et al. and the results within this thesis as well as with Gold colloidal nanoparticles reported by Chinas et al. as shown in Figure 7.4.(Zheng et al., 2010; Derry et al., 2019; Chinas et al., 2003) The fact that this trend is not observed in any other nanoparticle based friction modifiers indicates that there is a universal mechanism within these nanoparticles that is resulting in this increase in friction. One possibility is that all these nanoparticles are much softer than those investigated elsewhere, this may result in a compression of the nanoparticles at higher shear rates that results in an increase in friction. This may result in the oil starvation or high viscosity film mechanism that can reduce friction. This effect is reduced when the entrainment speed is further increased resulting in a larger film thickness, resulting in lower loads upon the nanoparticles or the nanoparticles being able to flow around the area of highest contact pressure. This theory is further supported by the fact that the nanoparticle that displays the smallest increase in friction is the gold nanoparticles investigated by Chinas et al.(Chinas et al., 2003) These nanoparticles, while malleable will have a much high hardness than the polymer nanoparticles investigated in this thesis and previous literature,(Zheng et al., 2010; Derry et al., 2019) resulting in a smaller compression effect. This effect will be much smaller for the smaller nanoparticles discussed in this thesis and their smaller size means that the film thickness will be sufficient to remove any load upon the nanoparticles at a lower entrainment speed. This means that the compressive effect that is resulting in any friction increase with the polymer nanoparticles will be much

smaller with the smaller sized polymer nanoparticles and will also occur over a much smaller entrainment speed range, hence why it does not appear to have any effect on the friction coefficient in these tests.

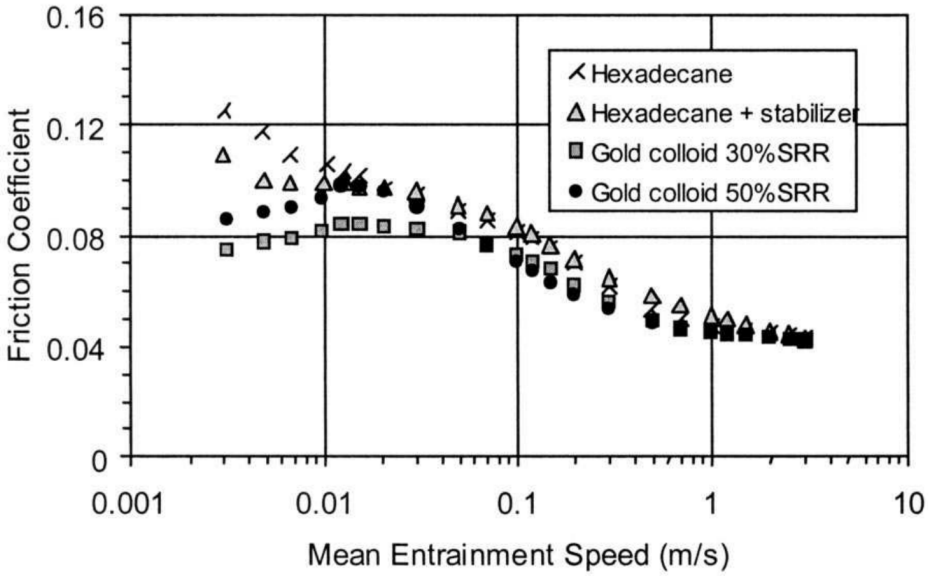

Figure 7.4: Stribeck Curves for Oleate capped gold colloidal nanoparticles in n-hexadecane.(Chinas et al., 2003) Reprinted with permission. Copyright ©2003 by ASME

Upon completion of the initial Stribeck curve, an hour-long traction step was undertaken within the boundary lubrication regime; this should allow for observation of the long term friction reduction performance of these nanoparticles. These results are shown in Figure 7.5 and 7.6.

These long term traction results show that there is a great difference between the non-crosslinked and crosslinked nanoparticles. The non-crosslinked nanoparticles with a core of $BzMA_{75}$ and smaller display a consistent friction performance throughout the traction step. This friction is below that of the mineral oil, and only the $BzMA_{75}$ displaying friction higher than the lowest level of the GMO. The lowest friction for these small nanoparticles was observed with $BzMA_{50}$ (0.077) < $BzMA_{62.5}$ (0.087) < $BzMA_{30} \approx BzMA_{40}$ (0.091) < $BzMA_{75}$ (0.094).

However, the larger non-crosslinked nanoparticles display a large variance in their friction performance with time, with a large increase in friction coefficient with time being observed. This increase could be due to a variety of reasons, such as the break down of

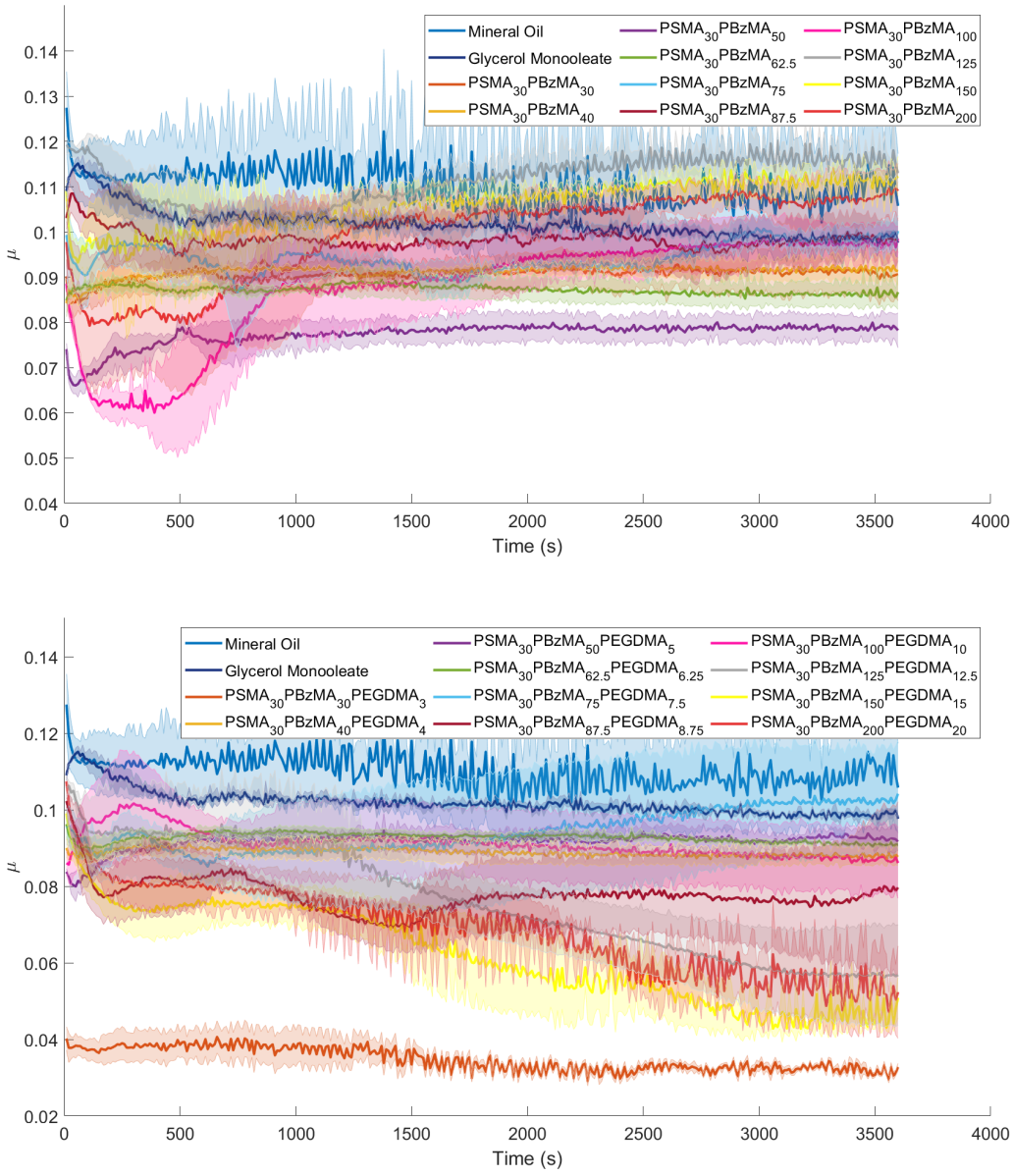

Figure 7.5: Top: Boundary lubrication traction step for 0.5 wt% $PSMA_{30}PBzMA_X$ nanoparticles, error bars are standard deviations of 3 tests on fresh MTM samples Bottom: Boundary lubrication traction step for 0.5 wt% $PSMA_{30}PBzMA_XPEGDMA_{(X/10)}$ nanoparticles, error bars are standard deviations of 3 tests on fresh MTM samples

these larger nanoparticles or that their large size may result in the prevention of oil from entering the contact in a similar way to that theorised in the initial Stribeck curves, see Figure 7.2, or the alteration of the viscosity of the oil in a similar way to that theorised in the initial Stribeck curves. This process, though, is much slower to occur than in the

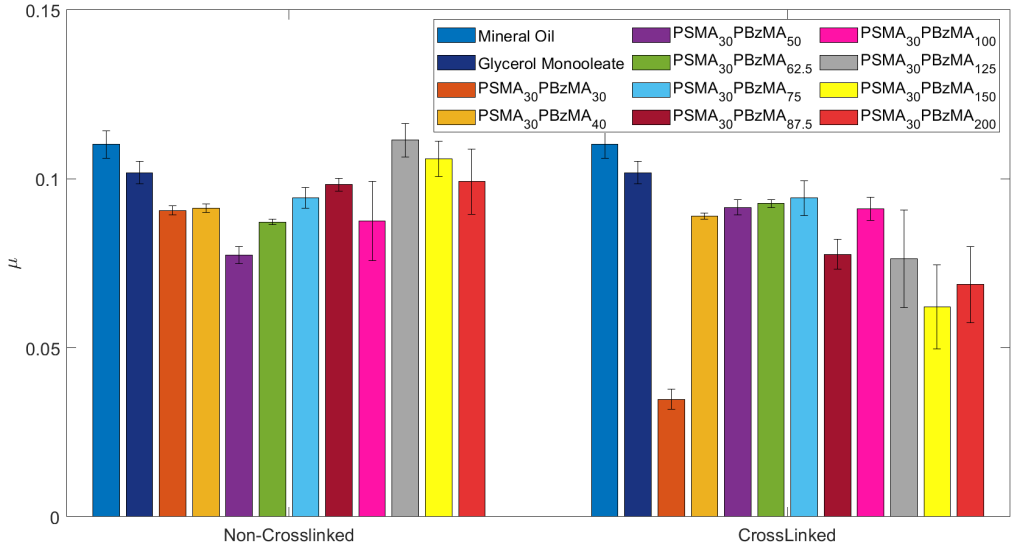

Figure 7.6: Mean boundary lubrication traction step for 0.5 wt% $PSMA_{30}PBzMA_X$ and $PSMA_{30}PBzMA_XPEGDMA_{(X/10)}$ nanoparticles

initial Stribeck step due to the contact's slow speed.

The crosslinked nanoparticles display improved friction performance when compared with both the mineral oil and glycerol monooleate, with the only exception being the $BzMA_{75}PEGDMA_{7.5}$ core nanoparticles whose peak friction exceeds that of the GMO. The smaller nanoparticles display consistent friction performance, similarly to the non-crosslinked equivalents. This friction reduction is approximately equal to the non-crosslinked nanoparticles, and for these smaller nanoparticles, it appears that the crosslinking has little effect on the boundary regime reduction of friction over some time. This is not the case with the $BzMA_{30}PEGDMA_3$ nanoparticles, where the friction coefficient is significantly reduced with crosslinking. The reasoning for this is unknown as there appears to be no similar reduction in similar sized nanoparticles. Nanoparticles with larger than 125 BzMA cores display a reduction in friction with time, with the lowest friction of all the nanoparticles of 0.05-0.06 observed by the end of the traction step. This trend is the opposite of the non-crosslinked friction nanoparticles, where the friction increases. This difference indicates that the increased mechanical stability of the crosslinked nanoparticles, rather than the size of the nanoparticles, is responsible for their improved friction performance. It is

also possible that these crosslinked nanoparticles form a stable tribofilm upon the surface contact over time. Here their increased mechanical stability may result in them generating a more stable tribofilm which acts to reduce friction. The build up of this tribofilm will occur with time and may explain the improvement of the cross-linked nanoparticles friction reduction with time. Non-crosslinked nanoparticles, however, may not have sufficient mechanical stability and break down with time in the boundary lubrication regime, or the mechanical instability may cause large deformation to block and prevent oil from entering the contact or generate film of different viscosity to the bulk solution as discussed above. This means that these larger non-crosslinked nanoparticles may not be effective friction modifiers over a prolonged time. Further work should be undertaken to confirm this theory.

Upon completion of the traction step of the experiment, a second Stribeck curve was run allowing for a comparison of the friction-reducing capabilities of the nanoparticles over a prolonged period. These results are shown in Figure 7.7.

The final Stribeck results show similar trends to the initial Stribeck's for both the crosslinked and non-crosslinked nanoparticles, as shown in Figure 7.1. Here the smaller nanoparticles show lower friction across all lubrication regimes, while larger nanoparticles increase friction with speed; this was theorised to be the result of these nanoparticles starving the contact of oil by preventing oil flow into the contact in the mixed boundary lubrication regime or the result of a change in viscosity of the oil within the contact due to the formation of a film within the contact.

Figure 7.8 shows the performance of these nanoparticles in the boundary regime during the final stribeck curve test. These results display the importance of crosslinking on long term friction reduction in the boundary regime. Here the smaller nanoparticles display low friction in the boundary regime that is approximately equivalent to their friction in the initial stribeck curve. The larger non crosslinked nanoparticles, however, no longer result in the significant friction reduction that is shown in the initial stribeck results while this significant friction reduction is still observed with the crosslinked nanoparticles. This shows that the increased structural stability of the crosslinked nanoparticles is important for boundary friction reduction for the large nanoparticles. Interestingly the amount that

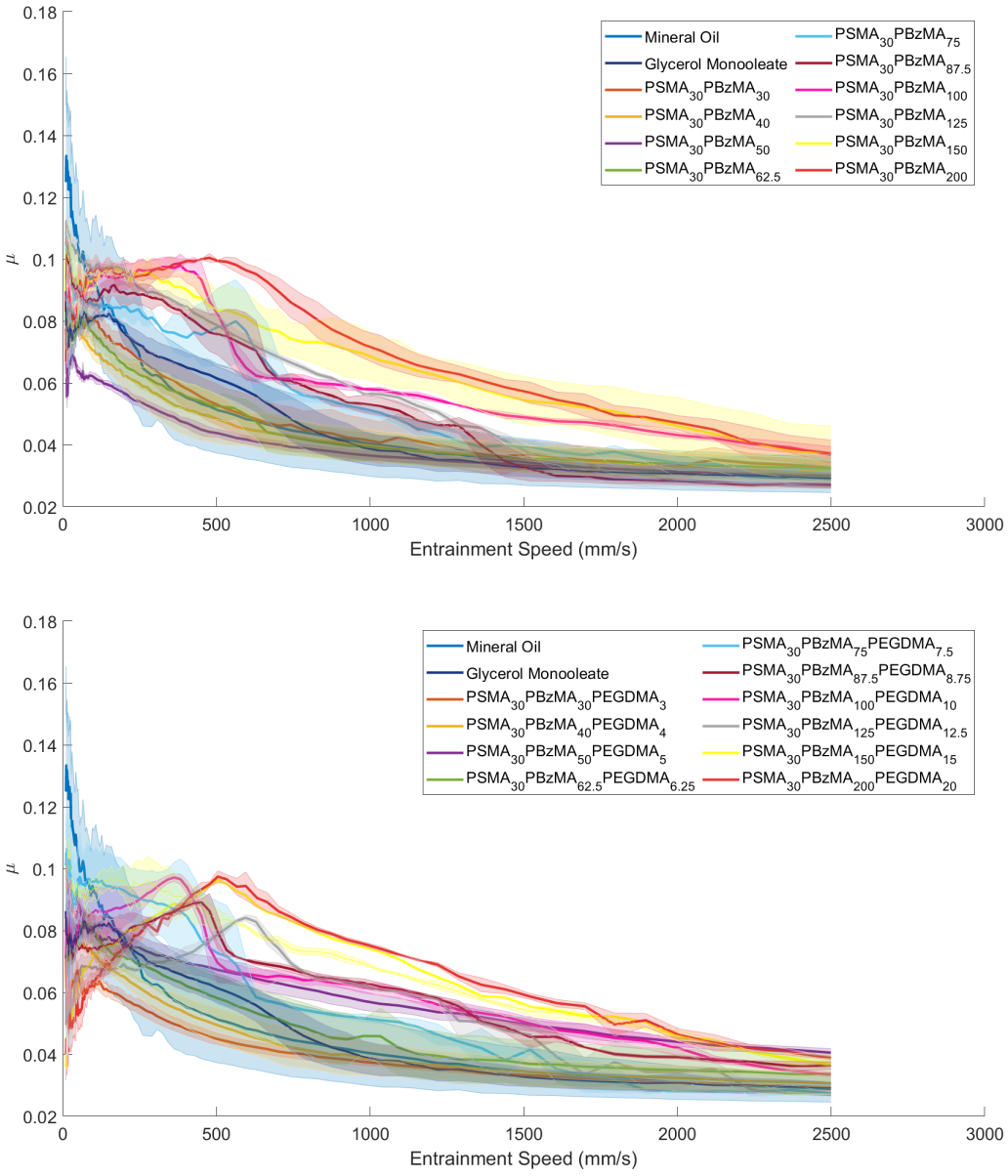

Figure 7.7: Top: Final Stribeck for 0.5 wt% $PSMA_{30}PBzMA_X$ nanoparticles, error bars are standard deviations of 3 tests on fresh MTM samples Bottom: Final Stribeck for 0.5 wt% $PSMA_{30}PBzMA_XPEGDMA_{(X/10)}$ nanoparticles, error bars are standard deviations of 3 tests on fresh MTM samples

friction is reduced in the boundary regime is in general greater than that observed with the initial stribeck curves. This indicates that these nanoparticles may form a film over time that helps to reduce the friction of the contact as is observed with the significant increase in friction reduction that is observed with GMO.

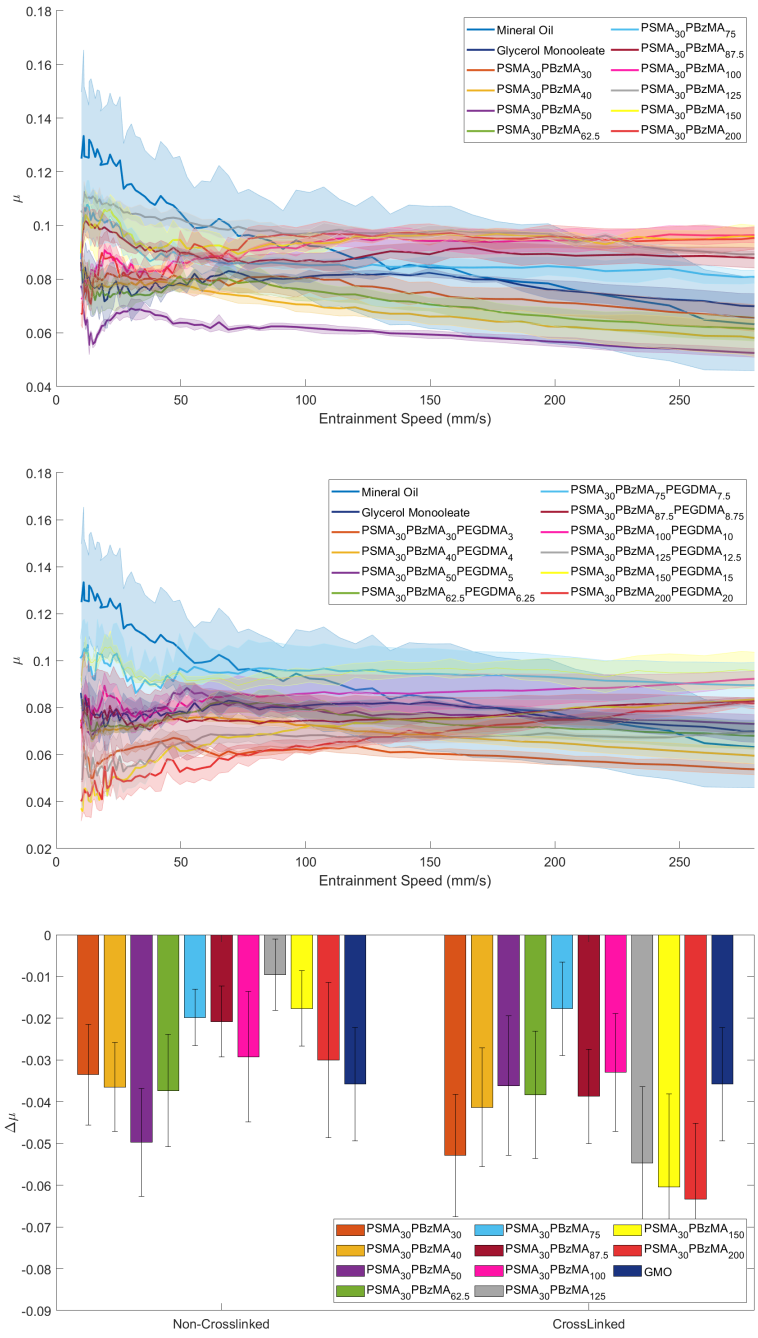

Figure 7.8: Top: Final Friction of $PSMA_{30}PBzMA_X$ nanoparticles in the boundary lubrication regime, speeds below 280mm^{-1}, error bars are standard deviations of 3 tests on fresh MTM samples Centre: Final Friction of $PSMA_{30}PBzMA_XPEGDMA_{(X/10)}$ nanoparticles in the boundary lubrication regime speeds below 280mm^{-1}, error bars are standard deviations of 3 tests on fresh MTM samples Bottom: Final mean boundary lubrication area of the Stribeck curves for 0.5 wt% $PSMA_{30}PBzMA_X$ and $PSMA_{30}PBzMA_XPEGDMA_{(X/10)}$, error bars are standard deviations of 3 tests on fresh MTM samples nanoparticles

Figure 7.9 displays the mean friction reduction of these PSMA-PBzMA based nanoparticles compared with mineral oil in the boundary lubrication regime (< 100 mm/s). This figure confirms the results discussed, with initial frictions show that friction reduction is most effective with the small and largest non-cross-linked, with an increase in friction observed between 37-45nm. Interestingly this trend is less noticeable with the crosslinked nanoparticles, where friction reduction appears to be approximately constant regardless of nanoparticle size, with only 23-27nm nanoparticles showing slightly lower friction results. Interestingly the final post traction step results show a much larger friction reduction of all the nanoparticles compared to the mineral oil. This reduction is particularly the case with the smaller non-crosslinked nanoparticles (23-31nm) and all the crosslinked nanoparticles. This increased friction reduction could result from the nanoparticles friction reducing ability approving with time or that these nanoparticles result in very similar friction coefficients, and the mineral oil shows an increase in friction. The latter is likely to be accurate as there is a difference of 0.0315 between the initial mineral oil friction and the final post traction step friction.

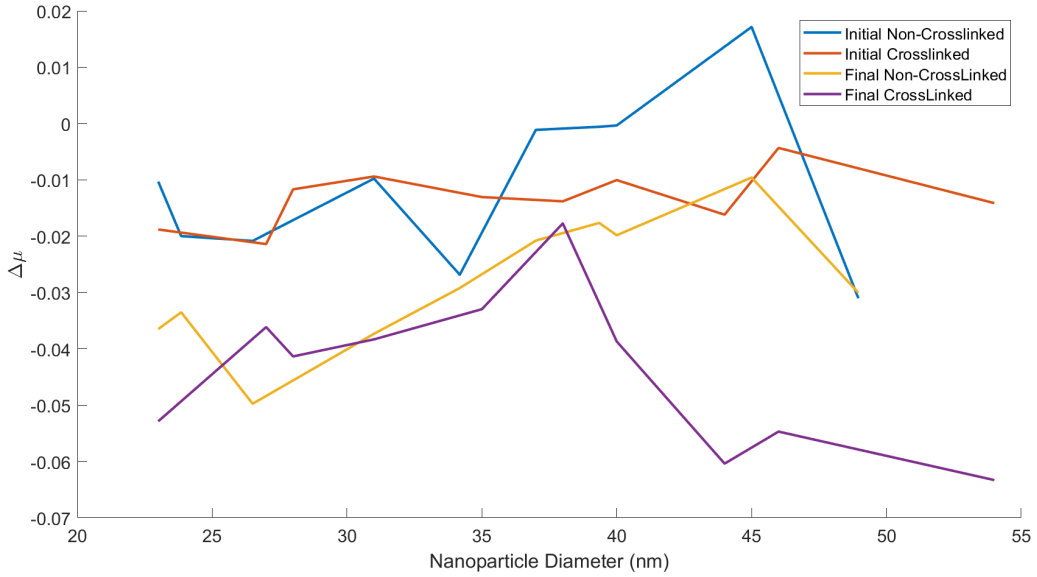

Figure 7.9: Effect of size of $PSMA_{30}PBzMA_X$ based nanoparticles on their ability to reduce friction in the boundary lubrication regime

For a clearer view of how the traction step affected the friction performance of the

nanoparticles in all lubricant conditions, the change in friction between the initial and final Stribeck curves was calculated. These results for the boundary lubrication regime are shown in Figure 7.10.

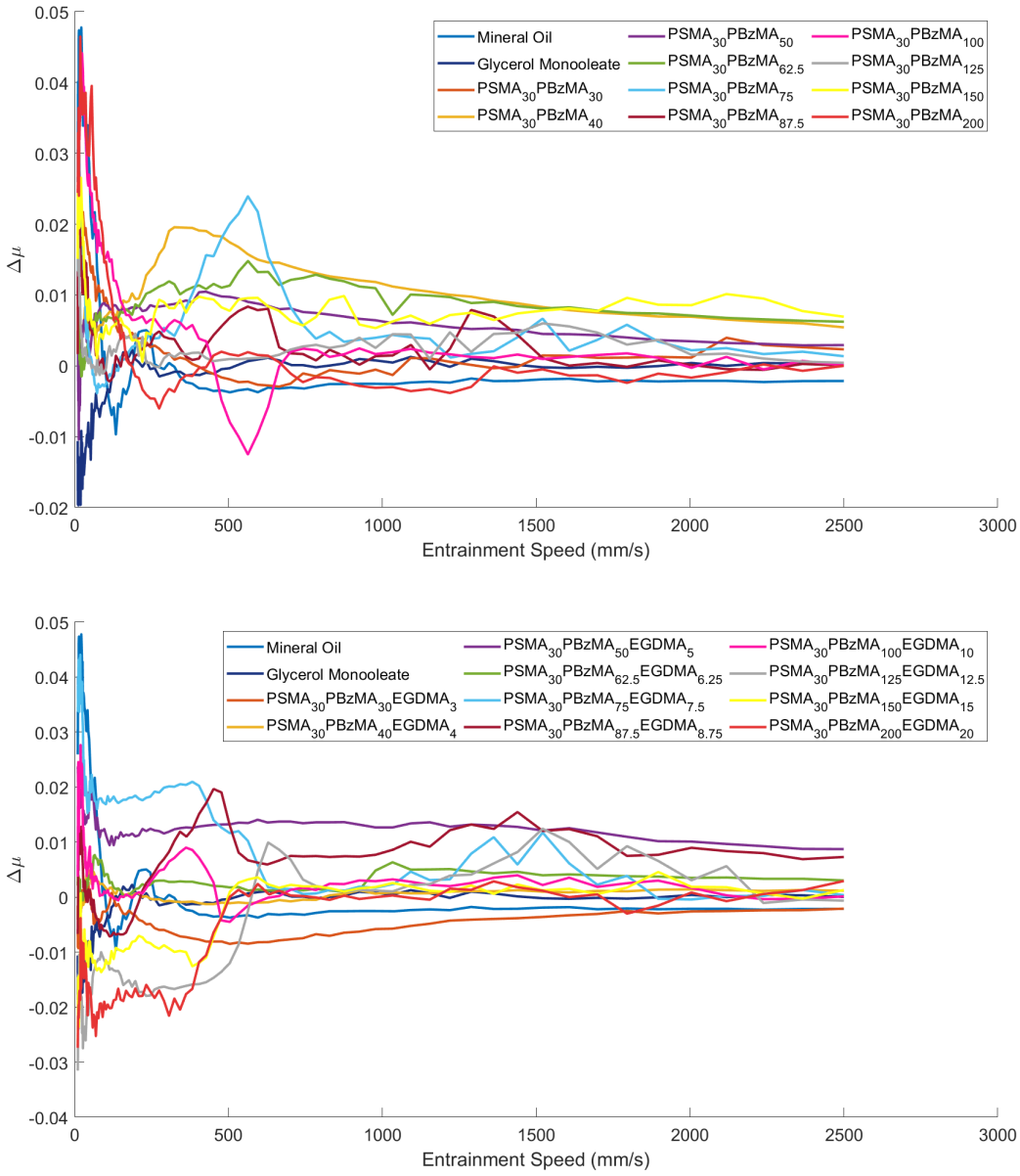

Figure 7.10: Top: Change in friction on initial and final Stribeck curves for 0.5 wt% $PSMA_{30}PBzMA_X$ nanoparticles Bottom: Change in friction on initial and final Stribeck curves for 0.5 wt% $PSMA_{30}PBzMA_XPEGDMA_{(X/10)}$ nanoparticles

This comparison allows us to see that the change in friction between the Stribeck curves varies across the lubrication regimes; while the friction is shown to change by up to

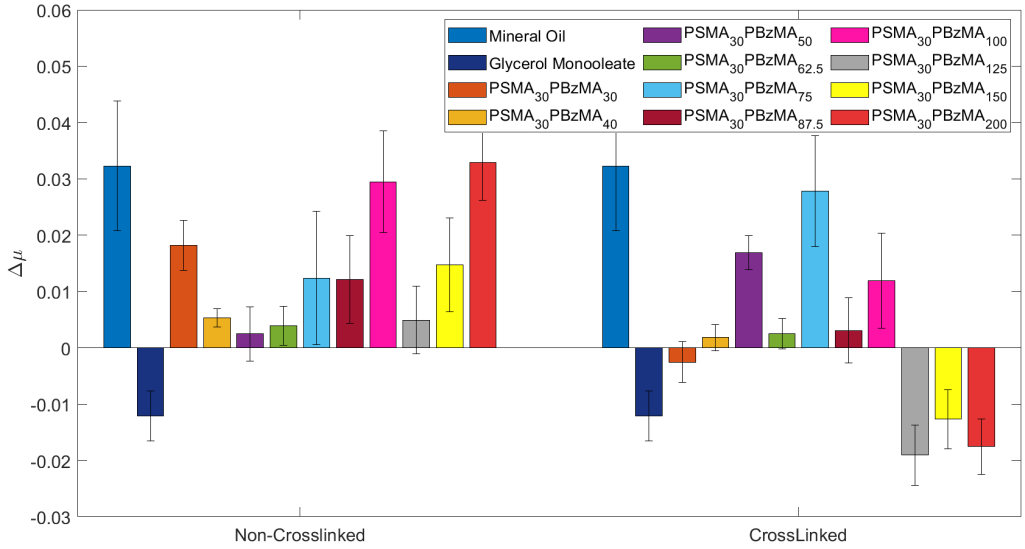

Figure 7.11: Mean friction change in friction on initial and final Stribeck curves for 0.5 wt% $PSMA_{30}PBzMA_X$ and $PSMA_{30}PBzMA_XPEGDMA_{(X/10)}$ nanoparticles in the boundary lubrication regime, error bars are standard deviations of 3 tests on fresh MTM samples

0.05 in the boundary lubrication regime, this friction change decreases as speed increases. The majority of the nanoparticles display an increase in friction across all speeds, with the only exceptions being larger crosslinked nanoparticles (>125 BzMA) in the boundary and mixed lubrication regime. This increase in friction with time spent in the contact and may indicate that these nanoparticles may break down within the contact. Studies into the stability of these nanoparticles after long term experiments were undertaken in section 7.4. It is unclear whether this decrease in friction-reducing capabilities would be present if the experiment was paused and the nanoparticles were allowed to re-assemble within the static lubricant. The increase in friction with these nanoparticles in the boundary lubrication regime after the traction step is relatively small with smaller nanoparticles displaying an increase of less than 0.02 though this number does increase up to 0.035 for larger non crosslinked nanoparticles, as shown in Figure 7.11. These nanoparticles, however, still display lower friction than the mineral oil, and a large number display lower friction than the GMO, and as such, they are still effective friction modifiers within the contact . More extended experiments and used oil testing will allow us to observe their long term performance and stability.

Initial MTM results demonstrate these PSMA-PBzMA nanoparticles are able to effectively reduce the friction of the contact in the boundary lubrication regime; this reduction was maintained throughout the traction step and shows these nanoparticles provide effective long term friction reduction in this regime. Smaller nanoparticles ($\leq$ 28nm) display reduced friction across all contact speeds, with crosslinking of these nanoparticles displaying little effect in the friction-reducing capabilities of these nanoparticles. Larger nanoparticles, however, display low friction in the boundary regime before showing a significant increase in friction as the contact speed increases, likely due to these nanoparticles preventing the flow of oil into the contact and starving the contact of oil, crosslinking these larger nanoparticles results in a slight reduction in friction across all contact speeds. Crosslinking of all size nanoparticles also appears to increases the long term stability of their friction-reducing capabilities. As a result of these initial profiles, two size nanoparticles were selected for all future testing. $BzMA_{200}$ core nanoparticles, and its crosslinked alternative, was selected due to it having the largest friction reduction in the boundary lubrication regime; these nanoparticles also display a large difference between the crosslinked and non-crosslinked nanoparticles allowing for further insight into the potential instability of the polymer nanoparticles. The other nanoparticle selected was the $BzMA_{40}$ nanoparticles and its crosslinked alternative. These nanoparticles display the most consistently low friction across all lubrication regimes, and this friction reduction appears to be maintained with longer testing times, suggesting that these nanoparticles may be the most effective as friction modifiers. Figures 7.12-7.14 display the results of the nanoparticles that will be discussed further in this thesis. These results clearly show the trend that is observed with all the nanoparticles. With the smaller $BzMA_{40}$ nanoparticles displaying lower friction than the mineral across all entrainment speeds and with this friction reduction being maintained throughout the traction step and the final stribeck curve. While the larger $BzMA_{200}$ core nanoparticles initially reducing friction by the greatest amount in the boundary lubrication regime, particularly the cross-linked nanoparticles, before increasing in friction through the higher speed boundary regime, the mixed and hydrodynamic regime. This friction reduction is affected by time in the traction step. With the non crosslinked nanoparticles displaying an increase in friction with time, while

the reverse is the case for the crosslinked nanoparticles.

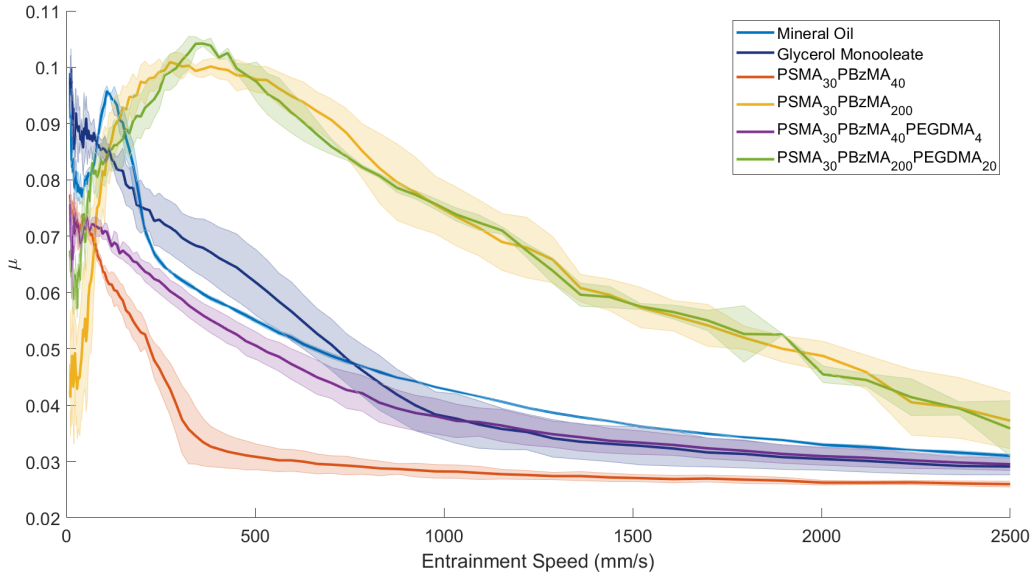

Figure 7.12: Top: Initial Stribeck for 0.5% $PSMA_{30}PBzMA_X$ and $PSMA_{30}PBzMA_XPEGDMA_{(X/10)}$, error bars are standard deviations of 3 tests on fresh MTM samples

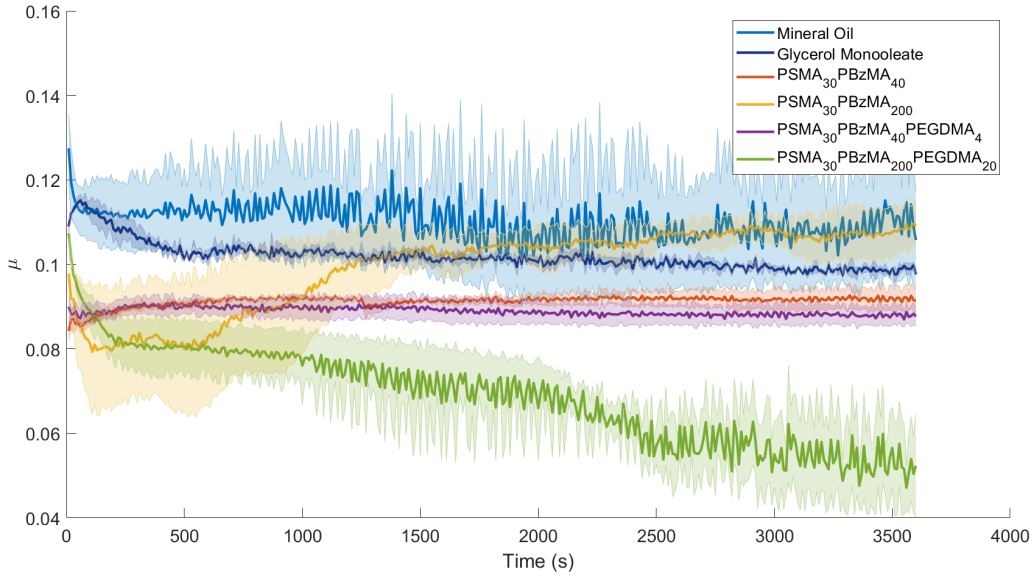

Figure 7.13: Boundary lubrication traction step for 0.5 wt% $PSMA_{30}PBzMA_X$ and $PSMA_{30}PBzMA_XPEGDMA_{(X/10)}$, error bars are standard deviations of 3 tests on fresh MTM samples

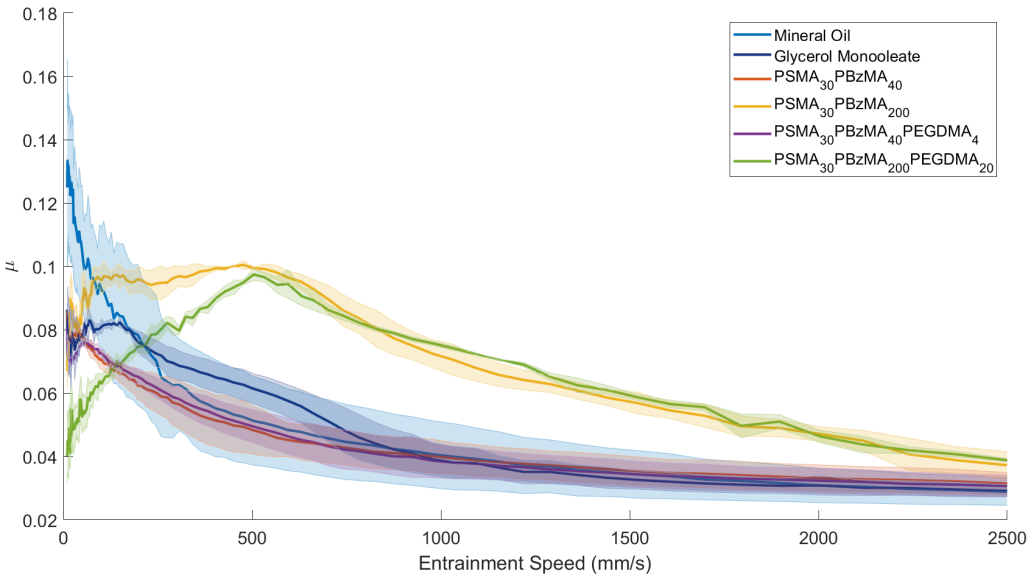

Figure 7.14: Final Stribeck for 0.5% $PSMA_{30}PBzMA_X$ and $PSMA_{30}PBzMA_XPEGDMA_{(X/10)}$, error bars are standard deviations of 3 tests on fresh MTM samples

7.2.2 Mini Traction Machine SRR Sweep (MTM SRR Sweep)

Stribeck curves for MTM testing of the nanoparticles at SRR of 0%, pure rolling, are shown in Figure 7.15.

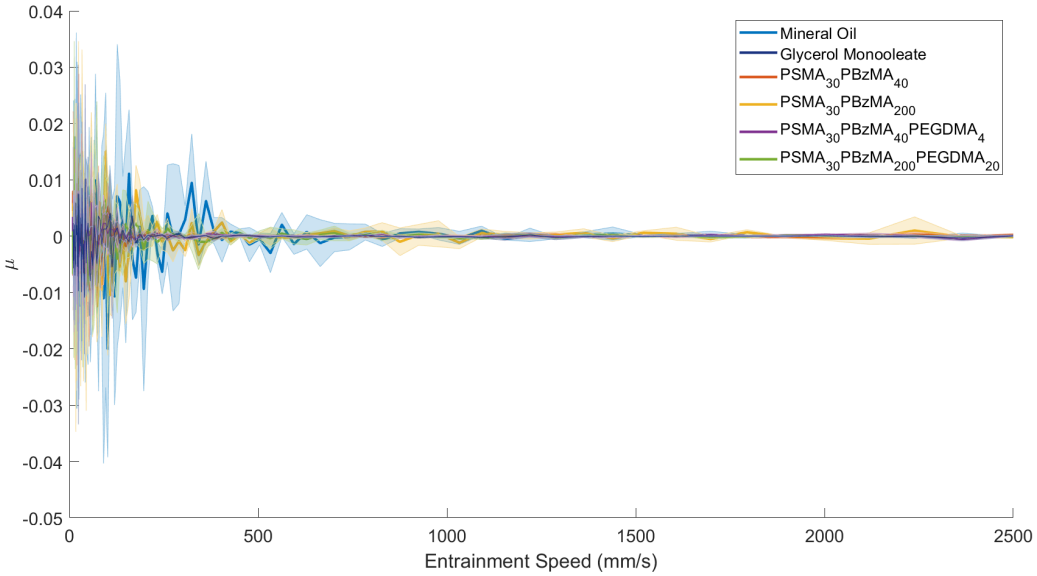

Figure 7.15: Stribeck curve for 0.5% PSMA-PBzMA nanoparticles at SRR of 0% as measured using a PCS MTM, error bars are standard deviations of 3 tests on fresh MTM samples

Figure 7.15 is important as it demonstrates the approximate accuracy of the MTM at generating the correct SRR ratio. At 0% the contact should be pure rolling; this means that both the ball and plate should be running at the same speed, and as such, no friction should occur. Figure 7.15 shows that at low contact speeds, the friction does vary somewhat with a median of 0. this demonstrates that while remaining close to the correct SRR, at low speeds, the MTM is not precise enough to maintain the correct SRR. This lack of precision at low speeds means that although results at these low speeds will be undertaken at very close to the correct SRR, there will be some inaccuracies in the results. As the speed of the contact increases, however, the friction moves towards zero, demonstrating that at higher contact speeds, the SRR is accurate. While there is some variance in SRR at low speeds, this is far more accurate than other machines available for testing and will produce the most accurate friction results.

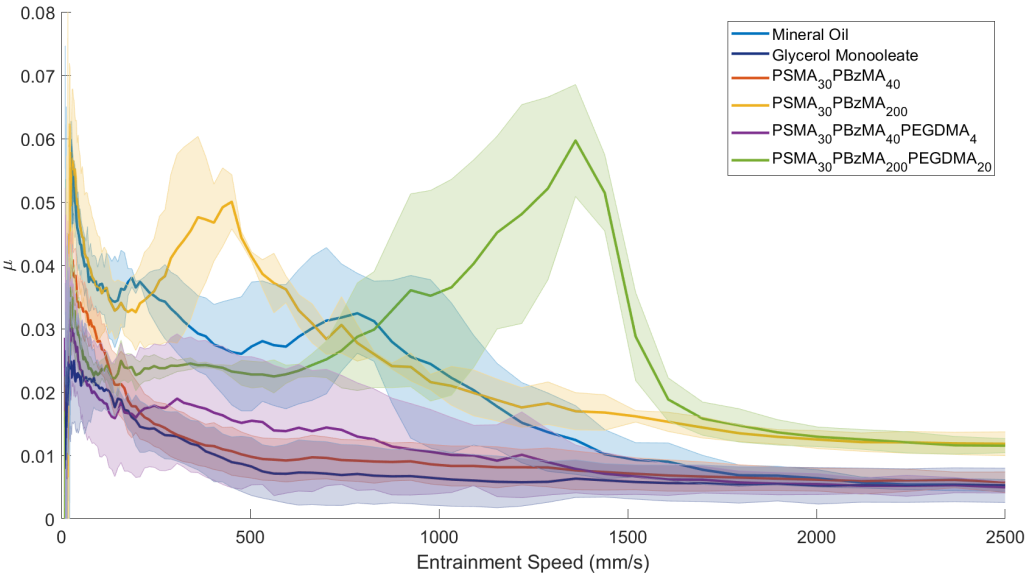

Figure 7.16: Stribeck curve for 0.5% PSMA-PBzMA nanoparticles at SRR of 2% as measured using a PCS MTM, error bars are standard deviations of 3 tests on fresh MTM samples

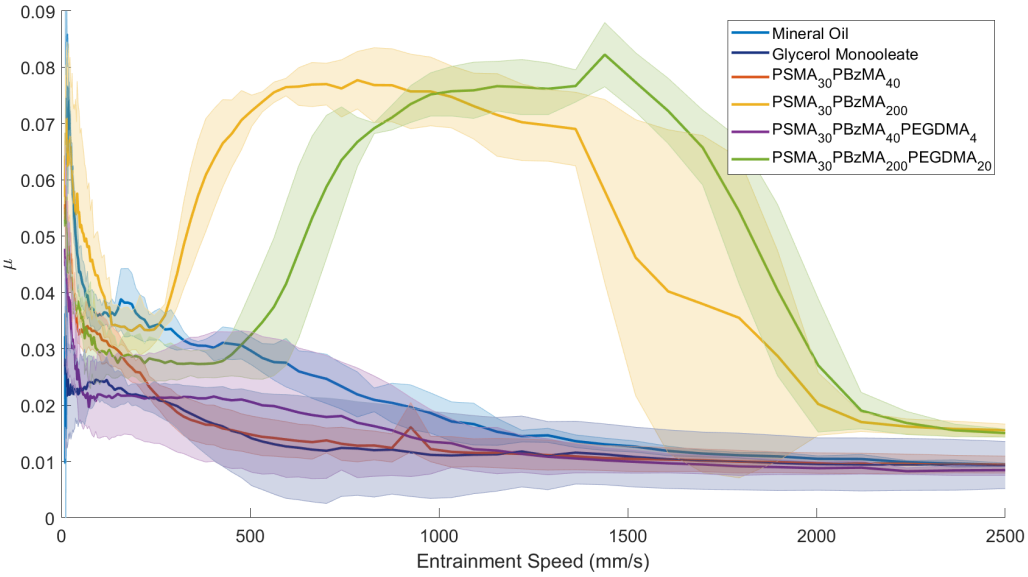

Figure 7.17: Stribeck curve for 0.5% PSMA-PBzMA nanoparticles at SRR of 5% as measured using a PCS MTM, error bars are standard deviations of 3 tests on fresh MTM samples

Figure 7.16-7.18 demonstrates the performance of PSMA-PBzMA nanoparticles at low SRR ratios. At these SRR ratios, the applied load will mostly be upon the lubrication

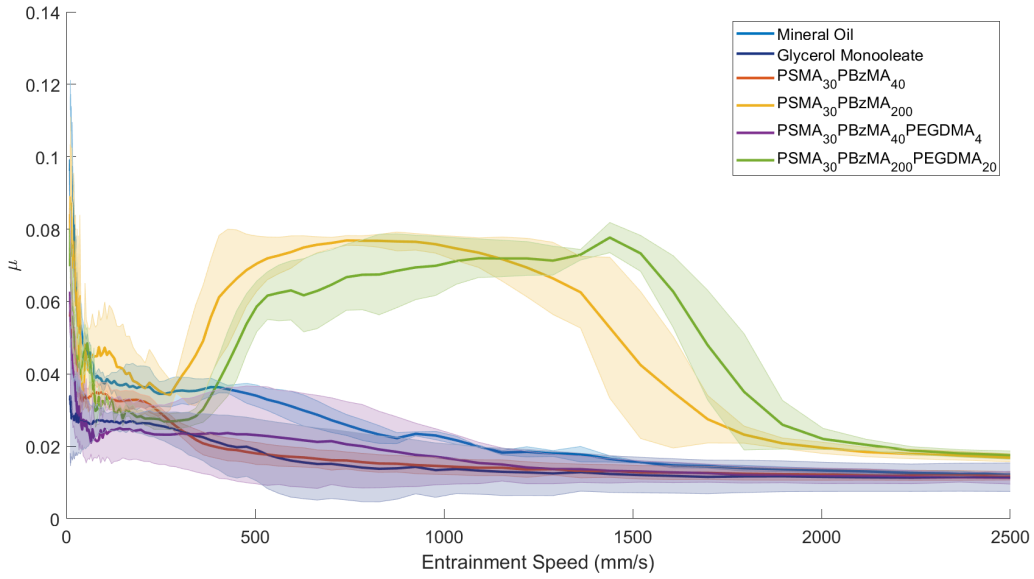

Figure 7.18: Stribeck curve for 0.5% PSMA-PBzMA nanoparticles at SRR of 7.5% as measured using a PCS MTM, error bars are standard deviations of 3 tests on fresh MTM samples

friction, here there will be a large amount of movement of oil into the contact, so there will be less asperity contact at equivalent speeds. As a result, the boundary lubrication regime will only be present at low contact speeds. All three SRR show the same trend. At low entrainment speeds, all of the nanoparticles but the uncrosslinked $PSMA_{30}PBzMA_{200}$ nanoparticles reduce the coefficient of friction when compared with mineral oil, as shown in greater detail in Figures 7.19-7.21. The larger nanoparticles then display an increase in friction as the speed of the contact increases, whereas the smaller nanoparticles maintain low friction across all contact speeds by approximately the same amount as glycerol monooleate. Interestingly unlike much at the higher SRR studied in Section 7.2.1, these nanoparticles display higher friction in the at very low entrainment speeds than GMO. This indicates that these nanoparticles, while still very effective friction modifiers, are not as effective as commercially available products at these low SRR ratios and very low entrainment speeds. However, the smaller crosslinked $PSMA_{30}PBzMA_{40}PEGDMA_4$ nanoparticles does at least match GMO's friction reducing capabilities at speeds greater than 50 mm/s.

These results indicate that the larger $PSMA_{30}PBzMA_{200}$ based nanoparticles are less

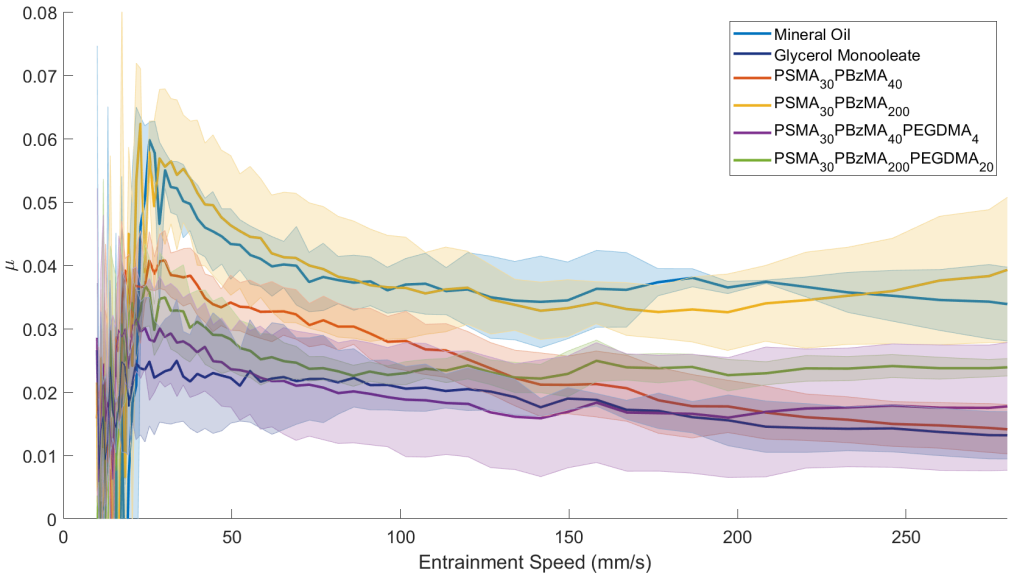

Figure 7.19: Boundary regime friction at entrainment speeds less than 280 mm/s for 0.5% PSMA-PBzMA nanoparticles at SRR of 2% as measured using a PCS MTM, error bars are standard deviations of 3 tests on fresh MTM samples

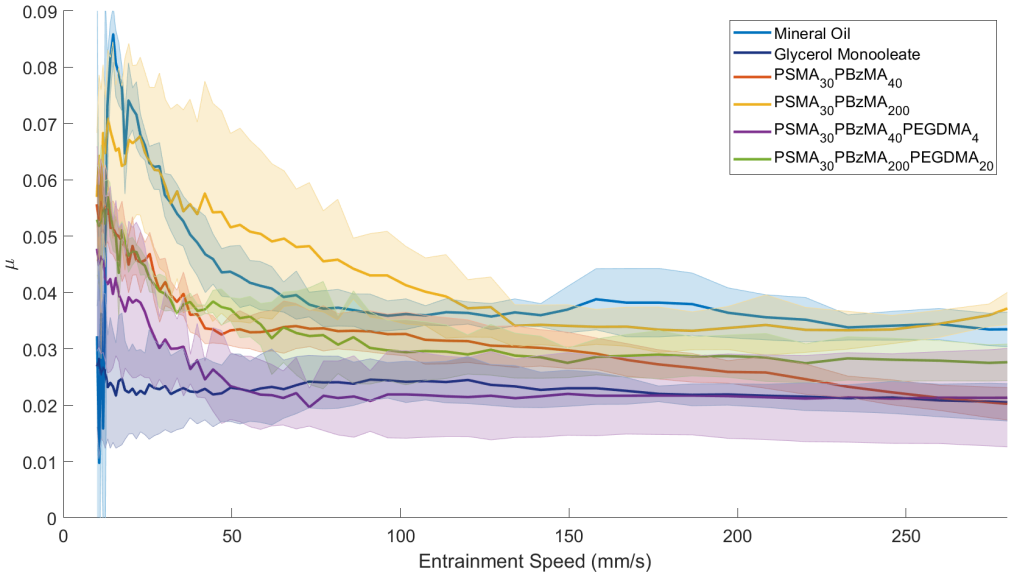

Figure 7.20: Boundary regime friction at entrainment speeds less than 280 mm/s for 0.5% PSMA-PBzMA nanoparticles at SRR of 5% as measured using a PCS MTM, error bars are standard deviations of 3 tests on fresh MTM samples

able to enter the contact at these low SRR ratios, resulting in limited or no friction reduction. The fact that the uncrosslinked $PSMA_{30}PBzMA_{200}$ do not reduce the friction

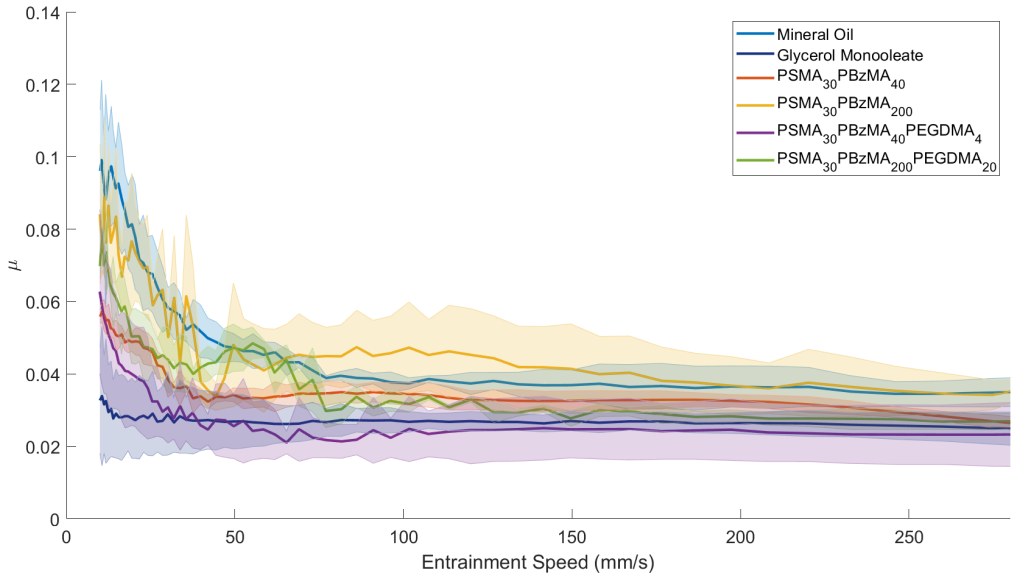

Figure 7.21: Boundary regime friction at entrainment speeds less than 280 mm/s for 0.5% PSMA-PBzMA nanoparticles at SRR of 7.5% as measured using a PCS MTM, error bars are standard deviations of 3 tests on fresh MTM samples

of the contact at all indicates that either their lower structural stability results in either them being unable to enter the contact or that they break down within the contact, a diagram of this effect is shown in Figures 7.22 and 7.23. This lower stability results in the nanoparticle being unable to form a film or be compressed within the contact resulting in no friction reduction. As the speed increases, larger nanoparticles act to increase friction by either preventing the flow of oil into the contact or by formation of a viscosity altering film due to their ability to be compressed.

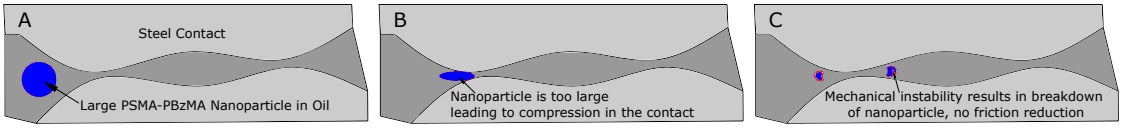

Figure 7.22: Drawing of compressive breakdown of $PSMA_{30}PBzMA_{200}$ nanoparticles within a contact

The smaller $PSMA_{30}PBzMA_{40}$ based nanoparticles are small enough to enter the contact and, as a result, produces a decrease approximately equal to the thin-film friction reduction of GMO. While the crosslinked nanoparticles display lower friction than their non-crosslinked equivalent at low contact speeds, indicating higher structural stability is

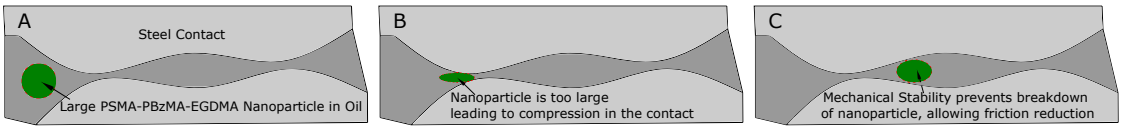

Figure 7.23: Drawing of compressive stability of $PSMA_{30}PBzMA_{200}EGDMA_{20}$ nanoparticles within a contact

vital for boundary lubrication friction reduction, the non-crosslinked $PSMA_{30}PBzMA_{40}$ nanoparticles result in lower friction than their crosslinked counterparts at higher contact speeds. This friction reduction suggests that at higher contact speeds, the ability of the small non-crosslinked nanoparticles to deform within the contact may be essential to reducing friction in the hydrodynamic lubrication regime, this may be a result of their deformation allowing for easier flow of oil into the contact, they are able to breakdown within the contact to allow for easy oil flow or generate a highly lipid friendly film to allow for easy oil flow or possibly through the generation of a high viscosity film within the contact that is able to effectively prevent any surface contact at much lower speeds than other friction modifiers. This means that the optimal type of nanoparticle added to the oil may differ depending on the lubrication regime in which the engine or motor is typically running.

Figures 7.24-7.28 displays the Stribeck curves as the sliding nature of the contact increases towards sliding and rolling speed are equal. Here the total speed of the contact increases even though the entrainment speed, and as such the film thickness remain constant. As such while film thickness remains constant at an equivalent entrainment speed the number of times that asperities of the contact will interact increases at equivalent entrainment speeds. This should lead to an increase in friction of the contact even though the film thickness does not change. This is displayed with friction coefficients for mineral oil in the boundary regime increasing significantly from around 0.05 at SRR 2 to 0.1 at SRR 100, this trend is also shown with the polymer nanoparticles although the size and chemistry of the nanoparticles have an effect of how this change in SRR affects the friction reduction.

These results display the importance of crosslinking to the nanoparticles, as both the crosslinked nanoparticles display a significant friction reduction in the boundary regime

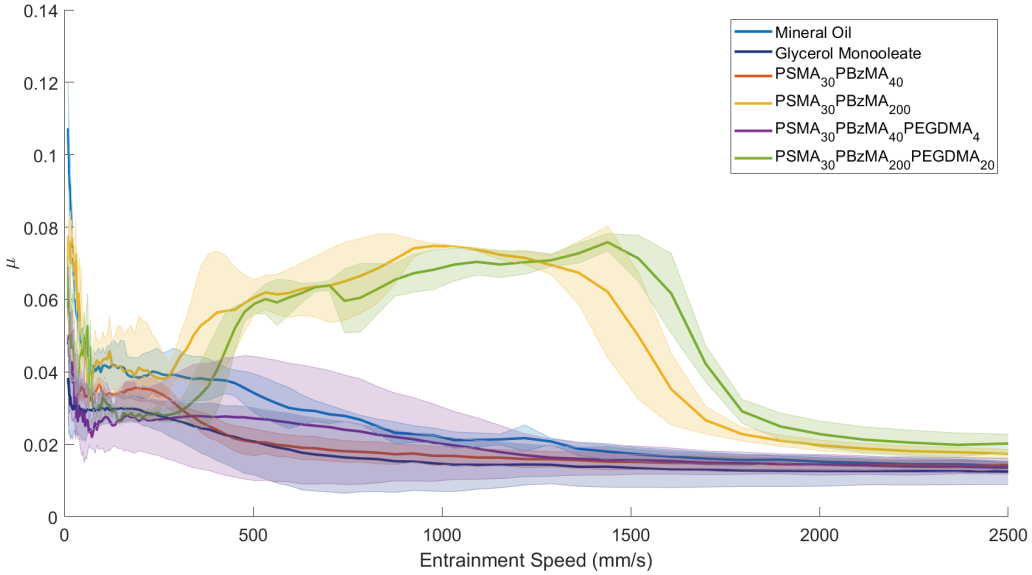

Figure 7.24: Stribeck curve for 0.5% PSMA-PBzMA nanoparticles at SRR of 10% as measured using a PCS MTM, error bars are standard deviations of 3 tests on fresh MTM samples

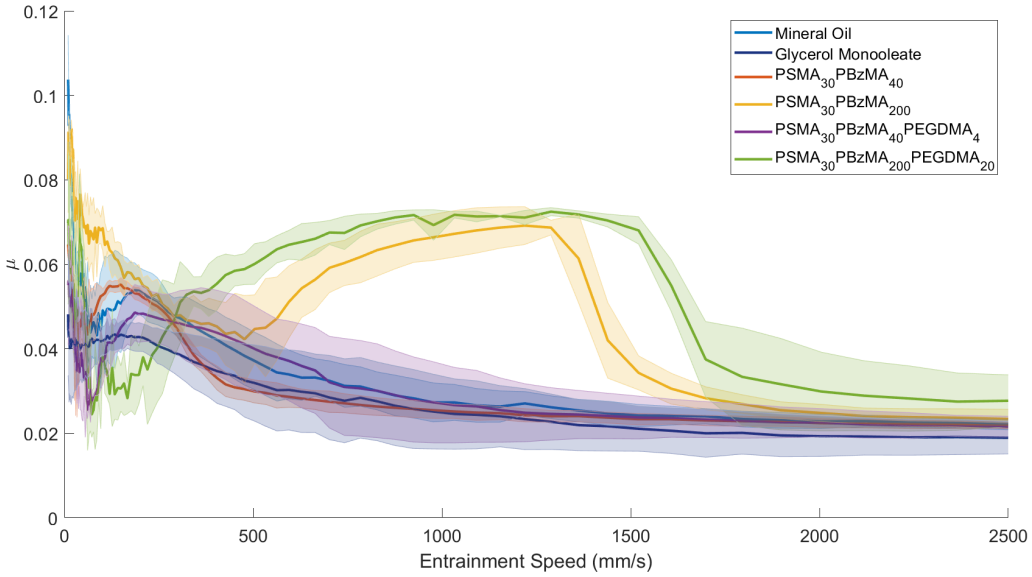

Figure 7.25: Stribeck curve for 0.5% PSMA-PBzMA nanoparticles at SRR of 25% as measured using a PCS MTM, error bars are standard deviations of 3 tests on fresh MTM samples

compared to both the mineral oil and their non crosslinked equivalent, this is shown in greater detail in Figures 7.29-7.33. The improved stability that results from the crosslink-

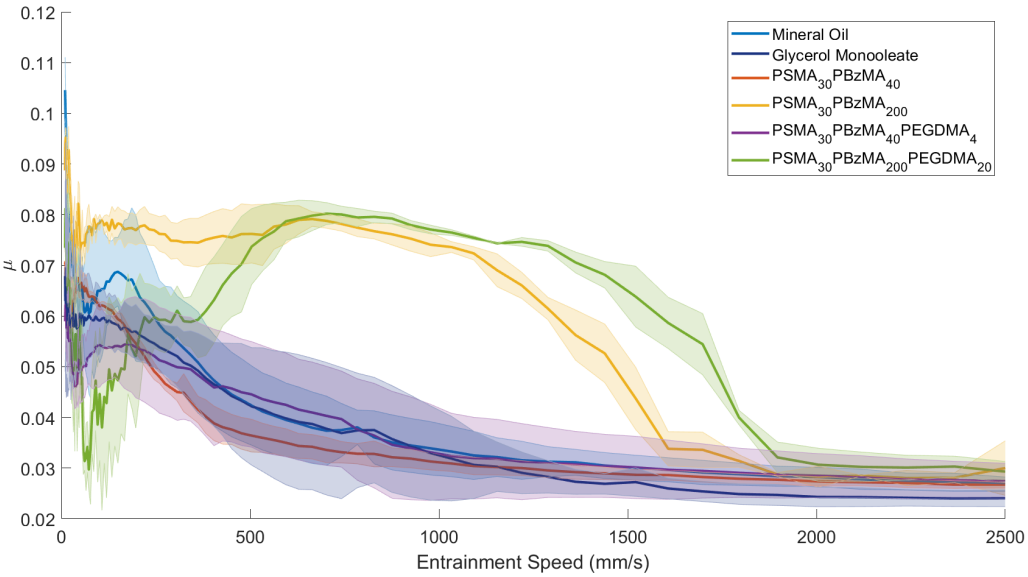

Figure 7.26: Stribeck curve for 0.5% PSMA-PBzMA nanoparticles at SRR of 50% as measured using a PCS MTM, error bars are standard deviations of 3 tests on fresh MTM samples

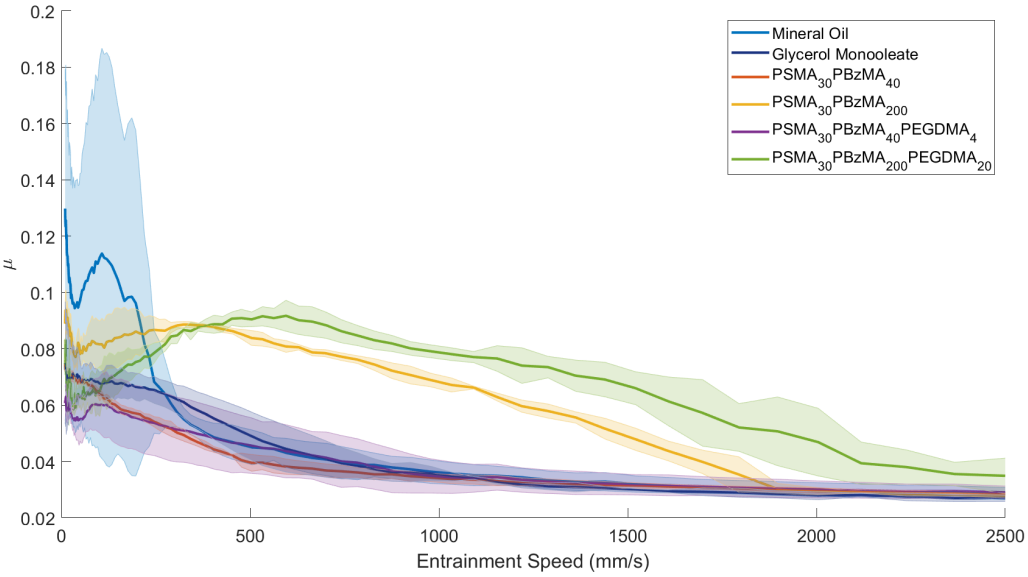

Figure 7.27: Stribeck curve for 0.5% PSMA-PBzMA nanoparticles at SRR of 75% as measured using a PCS MTM, error bars are standard deviations of 3 tests on fresh MTM samples

ing means these nanoparticles will likely maintain their size and shape within the contact and prevent surface contact. The smaller $PSMA_{30}PBzMA_{40}PEGDMA_4$ nanoparticle

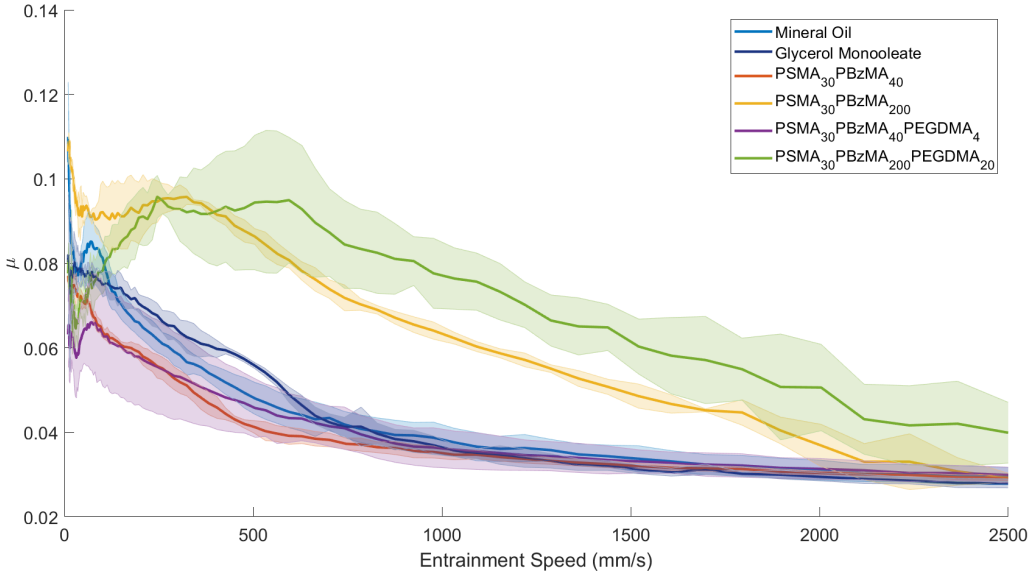

Figure 7.28: Stribeck curve for 0.5% PSMA-PBzMA nanoparticles at SRR of 100% as measured using a PCS MTM, error bars are standard deviations of 3 tests on fresh MTM samples

maintains lower or equal friction to mineral oil at all contact speeds while the larger $PSMA_{30}PBzMA_{200}PEGDMA_{20}$ nanoparticles demonstrate a significant increase in friction as the contact speed increases, likely due to them forcing starvation of oil to the contact. The $PSMA_{30}PBzMA_{200}$ nanoparticles display higher friction than the mineral oil across all contact speeds with only the SRR 75%, where it only displays lower friction in the boundary regime. The smaller $PSMA_{30}PBzMA_{40}$ nanoparticles do not show the lowest level of friction in the boundary regime, but they do display a friction reduction compared with mineral oil. However, they display the lowest friction in the mixed and hydrodynamic regimes, indicating that a degree of instability of these small nanoparticles may reduce friction in the mixed and hydrodynamic regimes by the greatest amount.

Figures 7.29-7.33 also display a clear trend with the larger $PSMA_{30}PBzMA_{200}$ based nanoparticles, with the entrainment speed at which the friction of these nanoparticles begins to increase becoming lower as SRR increases. This is displayed as in Figure 7.29 the friction coefficient of these nanoparticles remains at a steady state throughout the boundary regime while at higher SRR the friction is shown to increase steadily at subsequently lower entrainment speeds. With an increase in friction being observed with

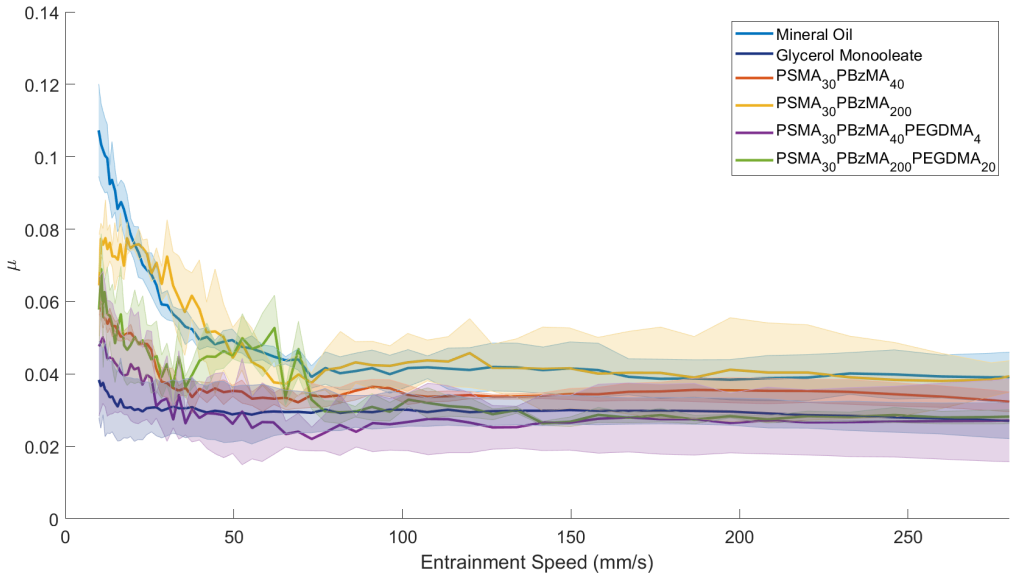

Figure 7.29: Boundary regime friction at entrainment speeds less than 280 mm/s for 0.5% PSMA-PBzMA nanoparticles at SRR of 10% as measured using a PCS MTM, error bars are standard deviations of 3 tests on fresh MTM samples

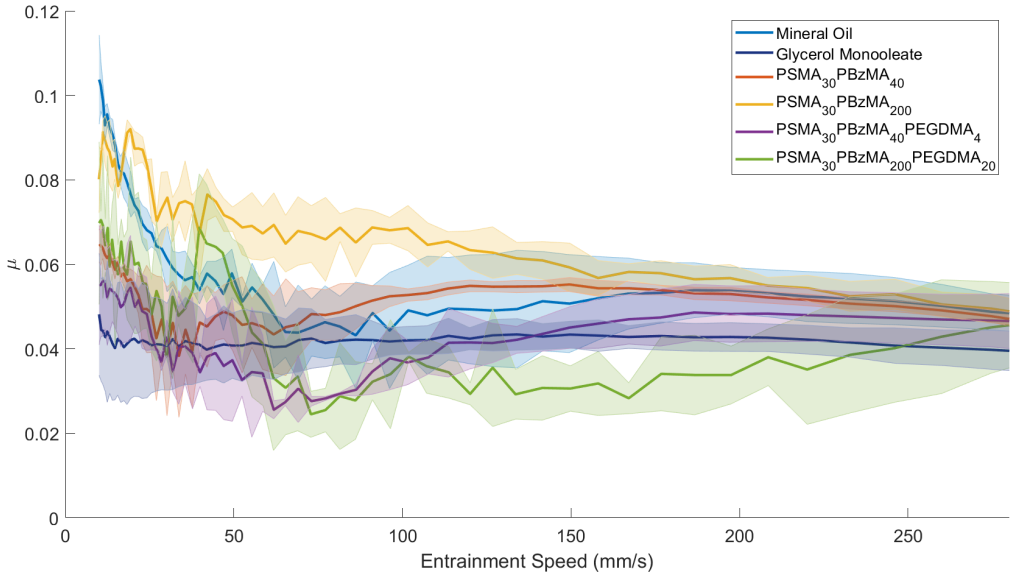

Figure 7.30: Boundary regime friction at entrainment speeds less than 280 mm/s for 0.5% PSMA-PBzMA nanoparticles at SRR of 25% as measured using a PCS MTM, error bars are standard deviations of 3 tests on fresh MTM samples

$PSMA_{30}PBzMA_{200}PEGDMA_{20}$ nanoparticles at speeds greater than 50 mm/s at SRR 100, as shown in Figure 7.33. This indicates that the oil starvation or formation of a

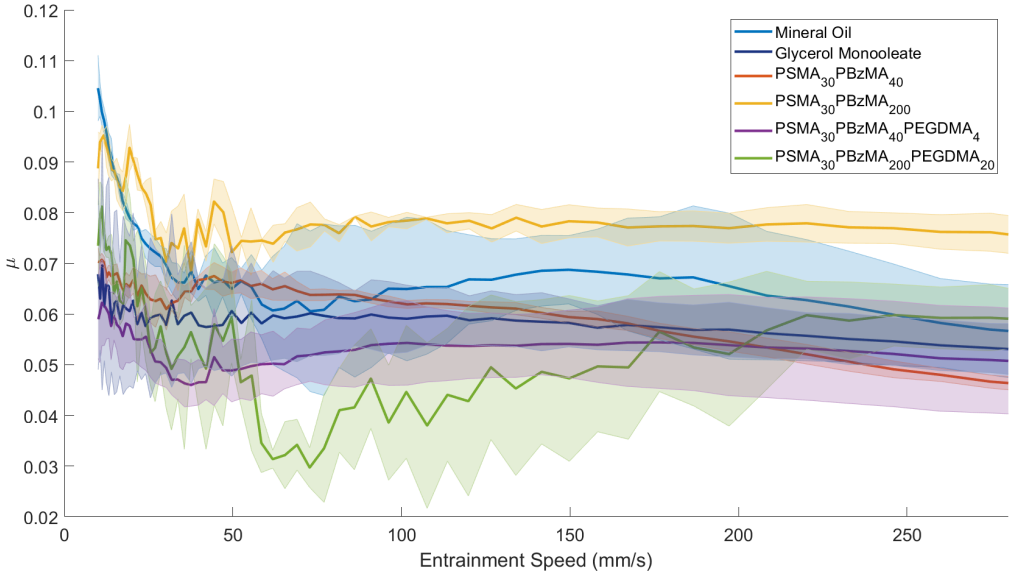

Figure 7.31: Boundary regime friction at entrainment speeds less than 280 mm/s for 0.5% PSMA-PBzMA nanoparticles at SRR of 50% as measured using a PCS MTM, error bars are standard deviations of 3 tests on fresh MTM samples

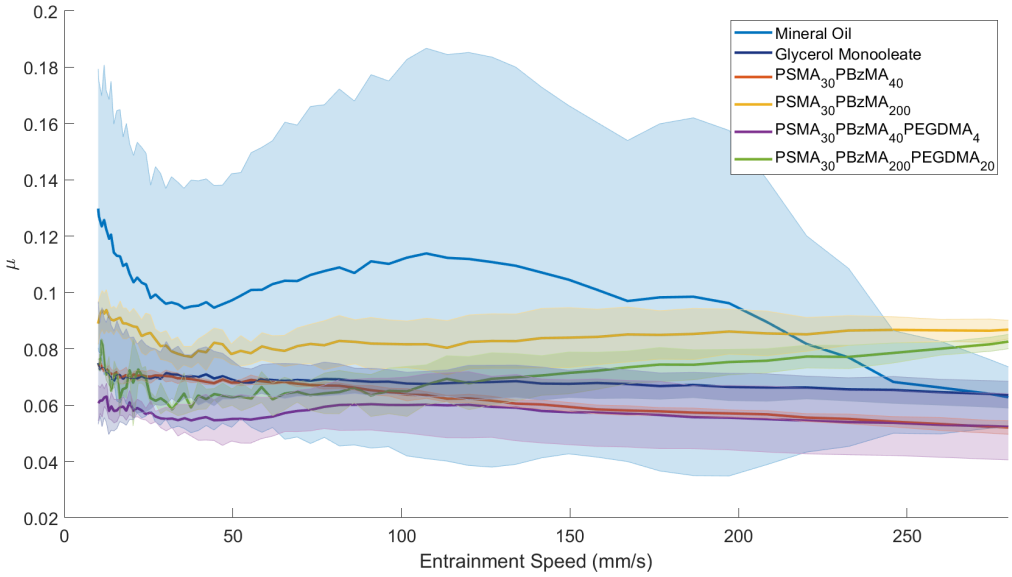

Figure 7.32: Boundary regime friction at entrainment speeds less than 280 mm/s for 0.5% PSMA-PBzMA nanoparticles at SRR of 75% as measured using a PCS MTM, error bars are standard deviations of 3 tests on fresh MTM samples

higher viscosity film to increase friction of the contact occurs at lower entrainment speeds as SRR increases. This is likely the result of greater shear forces being associated with

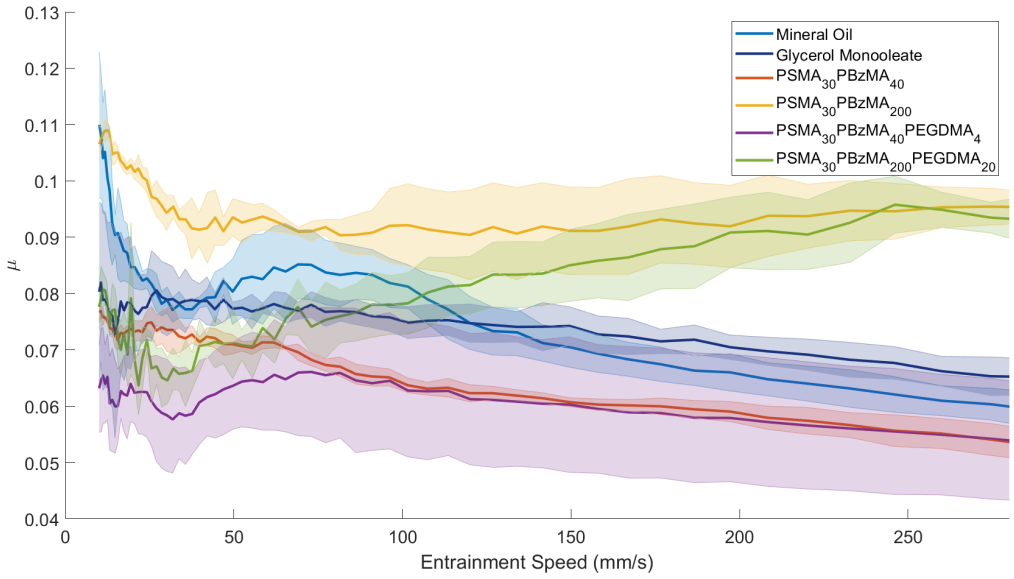

Figure 7.33: Boundary regime friction at entrainment speeds less than 280 mm/s for 0.5% PSMA-PBzMA nanoparticles at SRR of 100% as measured using a PCS MTM, error bars are standard deviations of 3 tests on fresh MTM samples

these nanoparticles as SRR increases. This means that an equivalent compressive action upon the nanoparticles happens at lower entrainment speeds resulting in the friction increasing mechanism.

A different trend is also observable with the $PSMA_{30}PBzMA_{40}PEGDMA_4$ at very low entrainment as SRR increases. At lower SRR ratios the the friction coefficient decreases initially in the extreme boundary lubrication regime, as shown in Figure 7.29-7.31 where the $PSMA_{30}PBzMA_{40}PEGDMA_4$ nanoparticles friction coefficient decreases by as much as 0.02 at speeds below 50 mm/s, however at higher SRR ratios, see Figures 7.32-7.33, this trend is not observed with these nanoparticles displaying low friction, significantly below that observed with GMO, observed immediately. This could be due to the generation of a tribofilm of these nanoparticles within the contact over time as the SRR ratios are tested sequentially or indicate that the higher shears at these higher SRRs actually improve the friction performance of these smaller nanoparticles in the extreme boundary lubrication regime.

Figure 7.34-7.35 displays the Stribeck curves as the sliding speed becomes greater than the rolling speed for a SRR 200% resulting in a pure sliding contact. At these higher

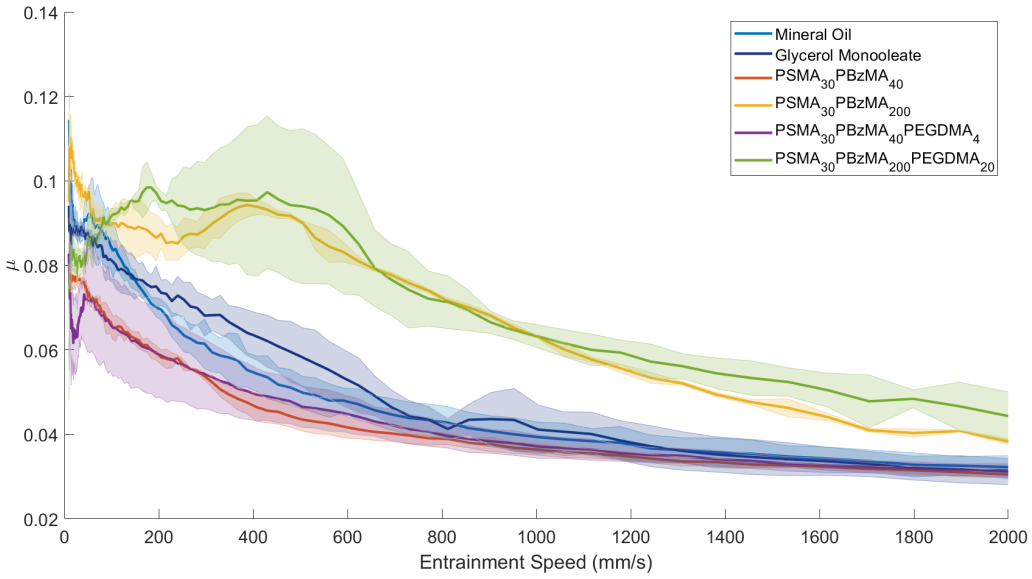

Figure 7.34: Stribeck curve for 0.5% PSMA-PBzMA nanoparticles at SRR of 150% as measured using a PCS MTM, error bars are standard deviations of 3 tests on fresh MTM samples

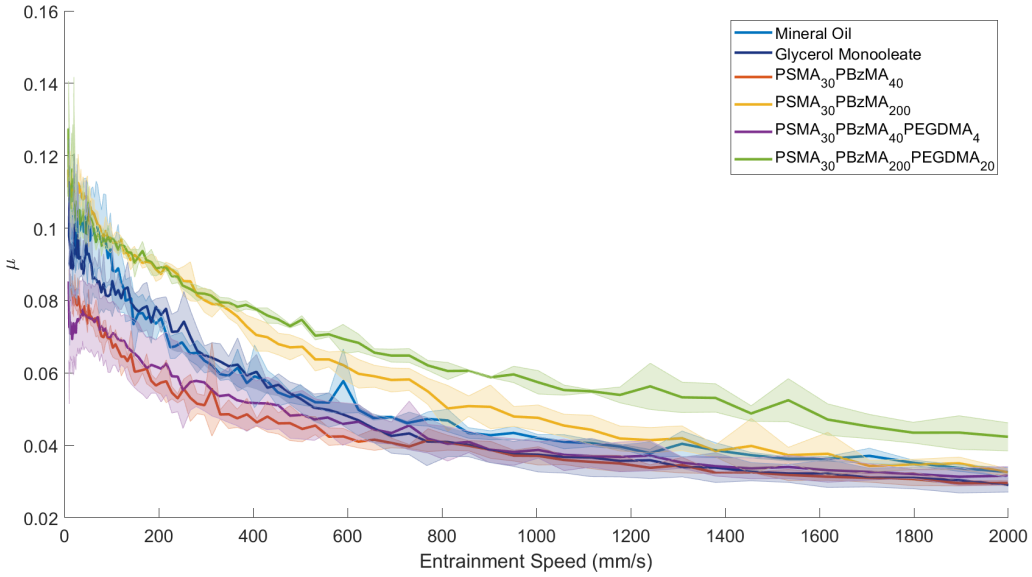

Figure 7.35: Stribeck curve for 0.5% PSMA-PBzMA nanoparticles at SRR of 200% as measured using a PCS MTM, error bars are standard deviations of 3 tests on fresh MTM samples

sliding speeds the larger $PSMA_{30}PBzMA_{200}$ nanoparticles display much higher friction than the smaller $PSMA_{30}PBzMA_{40}$ nanoparticles. The larger non-crosslinked displaying

higher friction at all speeds compared to mineral oil, while the larger crosslinked nanoparticles only displaying lower friction in the boundary regime of the SRR of 150%. These nanoparticles are likely too large to enter and separate the contacting surfaces in a contact with more sliding characteristics. The higher friction indicates that these nanoparticles prevent the oil from entering the contact across all speeds in these contact environments. It is also possible that the high shear forces associated with these contacts can lead to severe deformation of the nanoparticles, resulting in the formation of a high viscosity film around the contact, leading to an increase in friction. In the pure sliding contact, the large $PSMA_{30}PBzMA_{200}$ nanoparticles do not display the increase in friction with entrainment speed that is observed at most other SRR ratios, with a more traditional Stribeck curve being observed. At high sliding the high shear in the contact will lead to large amounts of deformation at lower entrainment speeds, resulting in any effect of the oil deprivation or high viscosity film being observed at much lower entrainment speeds and as such the increase in friction with speed is not observed. It is also possible that few of these larger nanoparticles can enter the contact, instead flowing around the contact point, thus meaning any effect of the oil depravation or high viscosity film are far reduced. The smaller $PSMA_{30}PBzMA_{40}$ nanoparticles display lower friction than mineral oil and GMO across all contact speeds in these high sliding environments, with a negligible difference being observed between the friction reduction of the crosslinked and non crosslinked nanoparticles. These small nanoparticles can still enter to contact and prevent surface contact and reduce the friction of the contact with the stability of the nanoparticle not affecting this ability to prevent surface contact.

Figures 7.36-7.37 demonstrate the continued trend of the larger $PSMA_{30}PBzMA_{200}$ based nanoparticles displaying peak boundary regime friction at lower entrainment speeds as SRR increases, indicating that these nanoparticles are not useful as friction modifiers in high SRR environments. Interestingly at these very high SRRs, the non-crosslinked $PSMA30PBzMA_{40}$ nanoparticles begin to show low friction at very low entrainment speed with no significant drop in friction observable at speeds below 50 mm/s. This may indicate that these non crosslinked nanoparticles simply take longer to form an effective tribofilm at these low entrainment speeds, or that that greater shears are required for these less

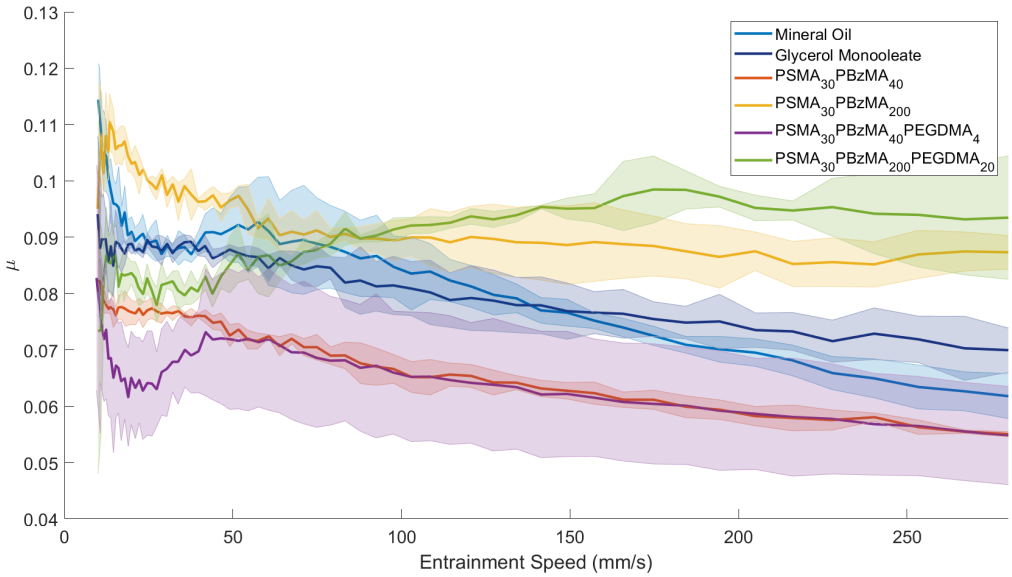

Figure 7.36: Boundary regime friction at entrainment speeds less than 280 mm/s for 0.5% PSMA-PBzMA nanoparticles at SRR of 150% as measured using a PCS MTM, error bars are standard deviations of 3 tests on fresh MTM samples

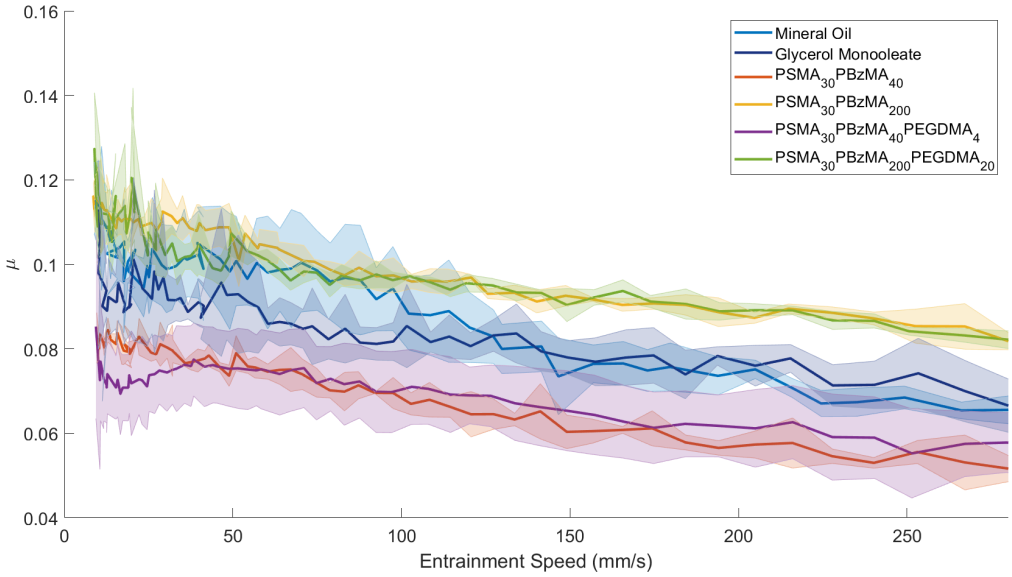

Figure 7.37: Boundary regime friction at entrainment speeds less than 280 mm/s for 0.5% PSMA-PBzMA nanoparticles at SRR of 200% as measured using a PCS MTM, error bars are standard deviations of 3 tests on fresh MTM samples

structurally stable nanoparticles to reach maximum friction reducing capabilities at these low speeds.

These MTM SRR sweep tests demonstrate that the $PSMA_{30}PBzMA_{40}$ nanoparticles display friction reduction across all SRR and speeds, except approximately equal friction in the uncrosslinked nanoparticles in the boundary regime of SRR of 25% and 50%. The larger non-crosslinked $PSMA_{30}PBzMA_{200}$ display higher friction than mineral oil in most contact environments and speeds, while the crosslinked equivalents display lower friction than mineral oil in the boundary regime in all but the pure sliding contact, with very low frictions being observed in mid-range SRR (44% reduction at 25% and 50% reduction at 50%). At higher contact speeds, however, the friction of these nanoparticles increases; this is likely the result of oil starvation or formation of a high viscosity contact that disrupts oil flow

7.2.3 TE54 Mini Traction Machine

As TE54 experiments are relatively under reported a calibration was not undertaken prior to these experiments. Due to the cost and lengthy nature of the experiments it was not possible to repeat them but they are useful as comparison to the PCS MTM as they provide a different contact size to be investigated. As a result of the poor calibration, however, the friction coefficient or the y axis of all these results can only be taken as a relative number and cannot be compared to either previous experiments or even other TE54 SRR's.

Figures 7.38-7.40 demonstrate the performance of the nanoparticles at low SRR and also best shows the limitation of the TE54. The lack of calibration of the ball size results in an unexpected Stribeck shape, friction increasing with speed at low speeds rather than decreasing. These results show that the crosslinked nanoparticles effectively reduce the friction of the contact in the boundary regime, with the smaller crosslinked $PSMA_{30}PBzMA_{40}EGDMA_4$ nanoparticle reducing friction across all speeds. These results confirm the observations previously seen in the MTM SRR sweep tests. The $PSMA_{30}PBzMA_{200}$ nanoparticles also show the same trend as observed in the MTM SRR sweep tests, with friction approximately equal to mineral oil at low contact speeds but higher friction at higher contact speeds. Interestingly though, the $PSMA_{30}PBzMA_{40}$ nanoparticles do not show the same result as the MTM SRR sweep experiments. While the friction in the

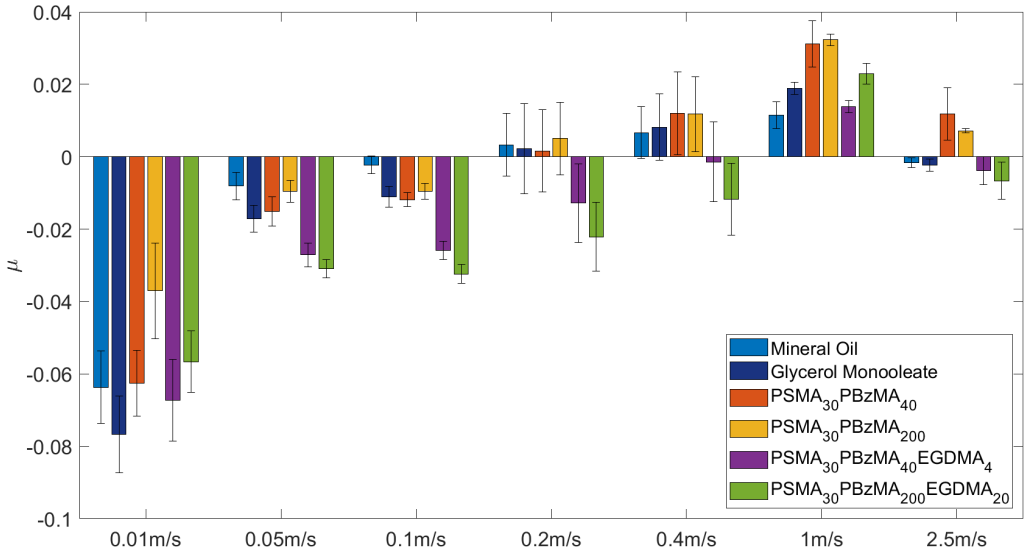

Figure 7.38: Friction of 0.5% PSMA-PBzMA nanoparticles at SRR of 2% as measured using a TE54 MTM, error bars are standard deviations of 3 tests on fresh TE54 samples

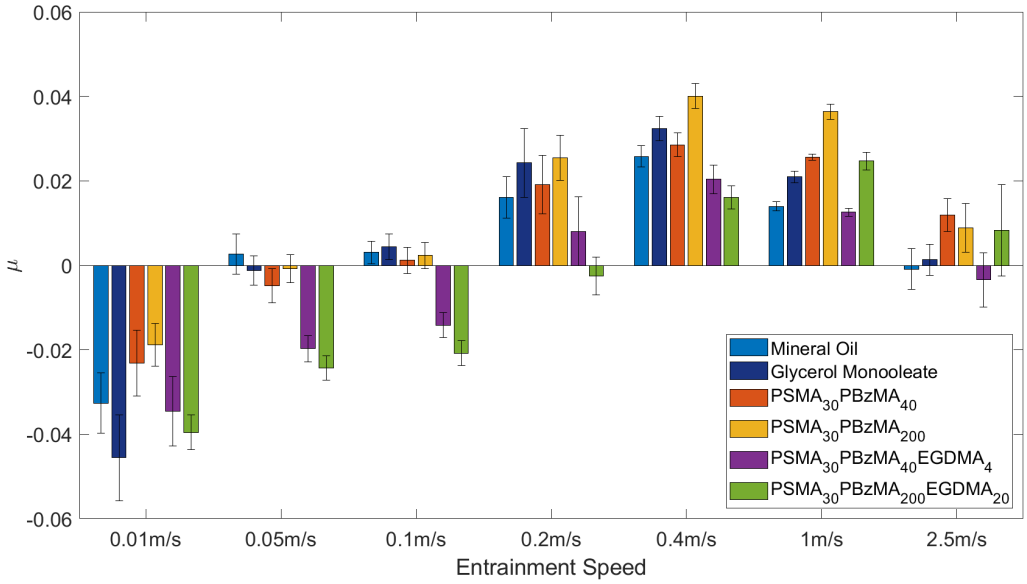

Figure 7.39: Friction of 0.5% PSMA-PBzMA nanoparticles at SRR of 5% as measured using a TE54 MTM, error bars are standard deviations of 3 tests on fresh TE54 samples

boundary regime is lower in the SRR of 10%, it is equal to mineral oil in the other SRR and the friction at higher speeds is higher than that of the mineral oil. This increased friction is contradictory to the MTM SRR sweep where the friction of the $PSMA_{30}PBzMA_{40}$

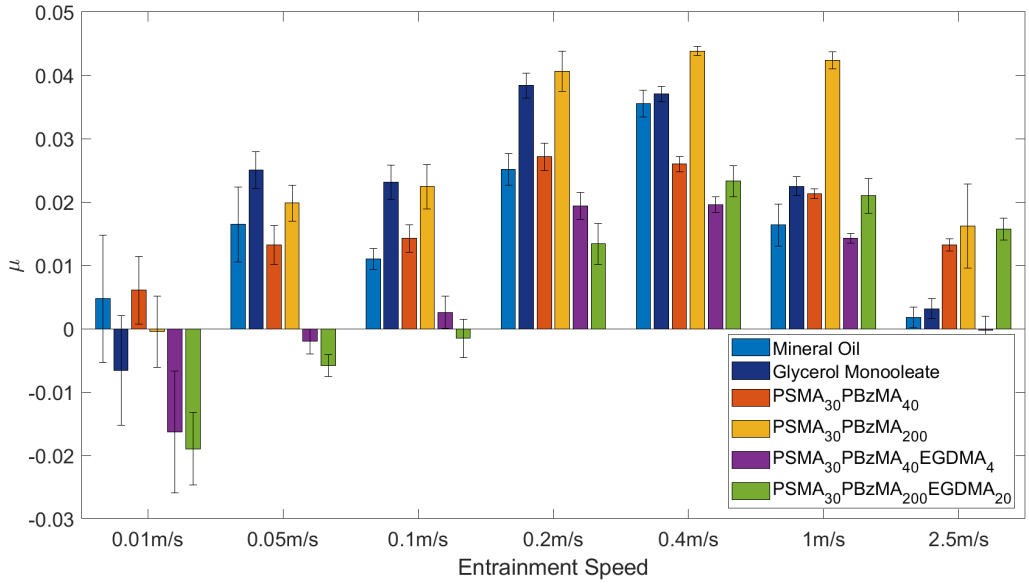

Figure 7.40: Friction of 0.5% PSMA-PBzMA nanoparticles at SRR of 10% as measured using a TE54 MTM, error bars are standard deviations of 3 tests on fresh TE54 samples

nanoparticles is lower across all contact speeds.

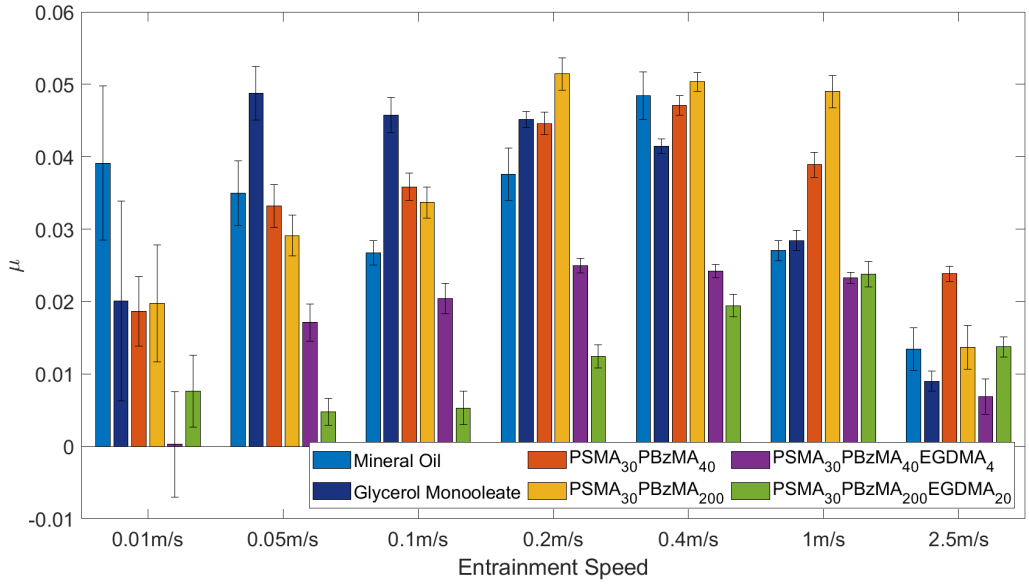

Figure 7.41: Friction of 0.5% PSMA-PBzMA nanoparticles at SRR of 25% as measured using a TE54 MTM, error bars are standard deviations of 3 tests on fresh TE54 samples

Figure 7.41-7.43 show an increase in sliding speed, and as a result, we would expect an increase in friction of the contact. Again the nanoparticles perform identically to

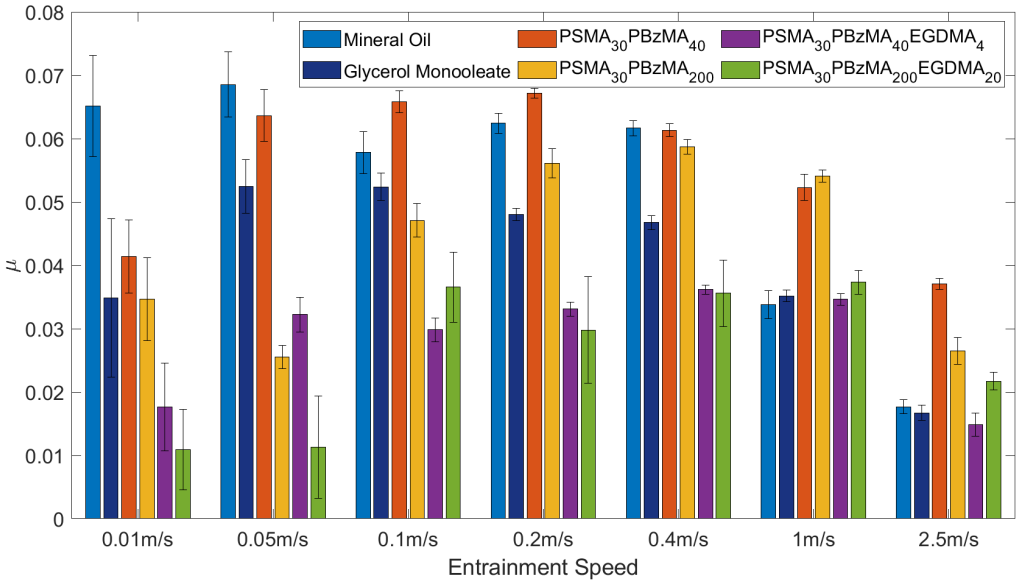

Figure 7.42: Friction of 0.5% PSMA-PBzMA nanoparticles at SRR of 50% as measured using a TE54 MTM, error bars are standard deviations of 3 tests on fresh TE54 samples

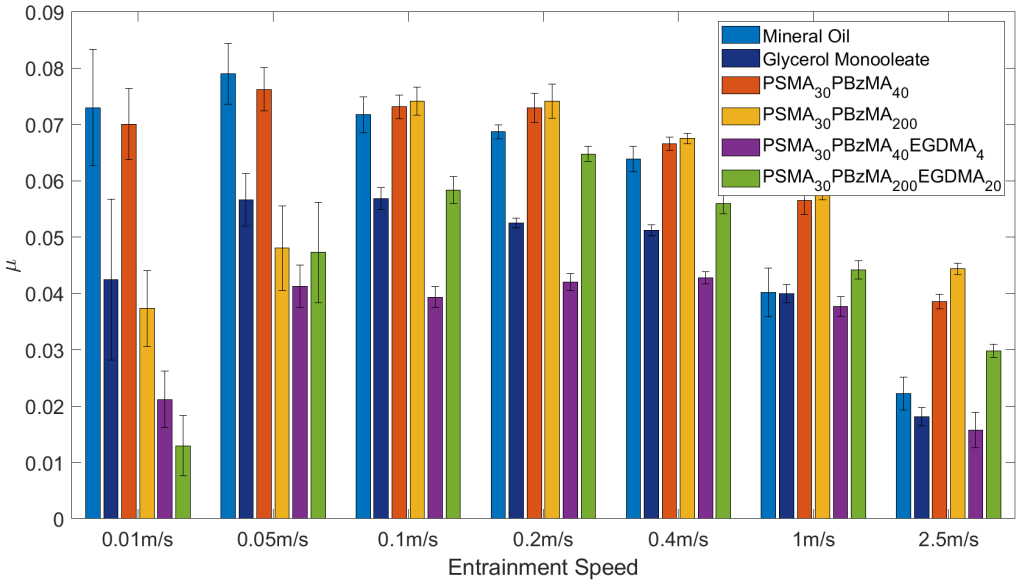

Figure 7.43: Friction of 0.5% PSMA-PBzMA nanoparticles at SRR of 75% as measured using a TE54 MTM, error bars are standard deviations of 3 tests on fresh TE54 samples

that observed at lower SRR ratios. The crosslinked nanoparticles are effective friction modifiers in the boundary regime, with the $PSMA_{30}PBzMA_{40}PEGDMA_4$ nanoparticles reducing friction across all speeds. The $PSMA_{30}PBzMA_{200}$ based nanoparticles act to

reduce friction in the boundary regime before showing an increase in friction, to above the level of the pure oil, at higher speeds. The $PSMA_{30}PBzMA_{40}$ nanoparticles, however, show relatively small friction reduction in the boundary regime, with no consistent friction reduction observable at SRR of 75% and also show significantly higher friction than mineral oil at higher contact speeds.

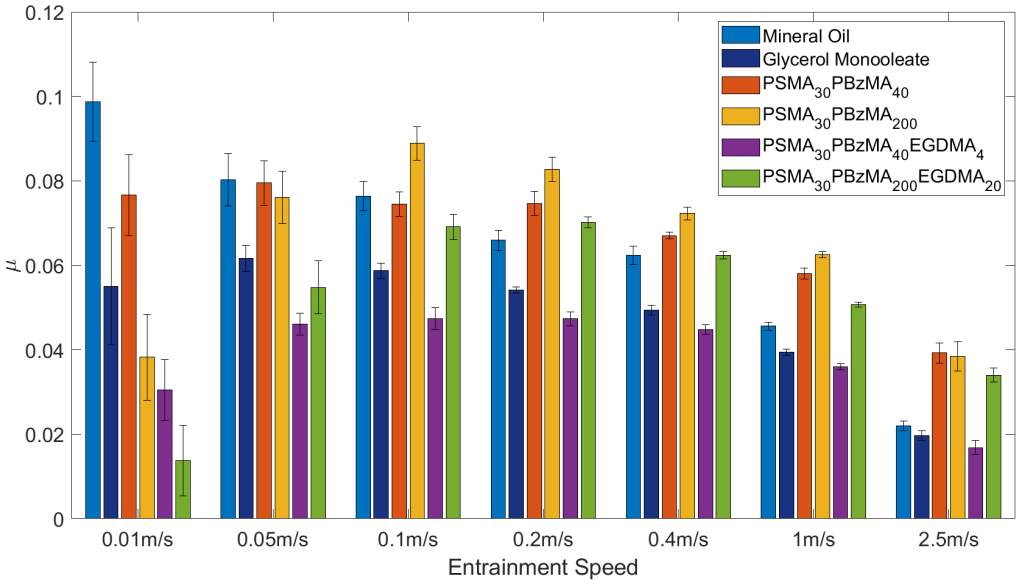

Figure 7.44: Friction of 0.5% PSMA-PBzMA nanoparticles at SRR of 100% as measured using a TE54 MTM, error bars are standard deviations of 3 tests on fresh TE54 samples

Figures 7.44-7.46 show how the nanoparticles affect a contact with a high sliding nature. At these high SRR ratios, the smallest crosslinked $PSMA_{30}PBzMA_{40}PEGDMA_4$ nanoparticles maintain significantly lower friction in the boundary regime and also maintain lower friction than the mineral oil across all speeds. While the $PSMA_{30}PBzMA_{200}PEGDMA_{20}$ nanoparticles show large reductions in friction in the boundary regime, at SRR 100% and 150%, at 200% this friction reduction is no longer present. These nanoparticles are likely not entering the contact in sufficient numbers to reduce the friction of the contact. At high speeds and SRR (>150%), however, the $PSMA_{30}PBzMA_{200}PEGDMA_{20}$ nanoparticles do act to reduce friction compared with the mineral oil. This lower friction is surprising given that this has not been observed at lower SRR speeds or in the PCS MTM SRR sweep experiments, and the reasoning for this discrepancy is not known. At higher SRR ratios,

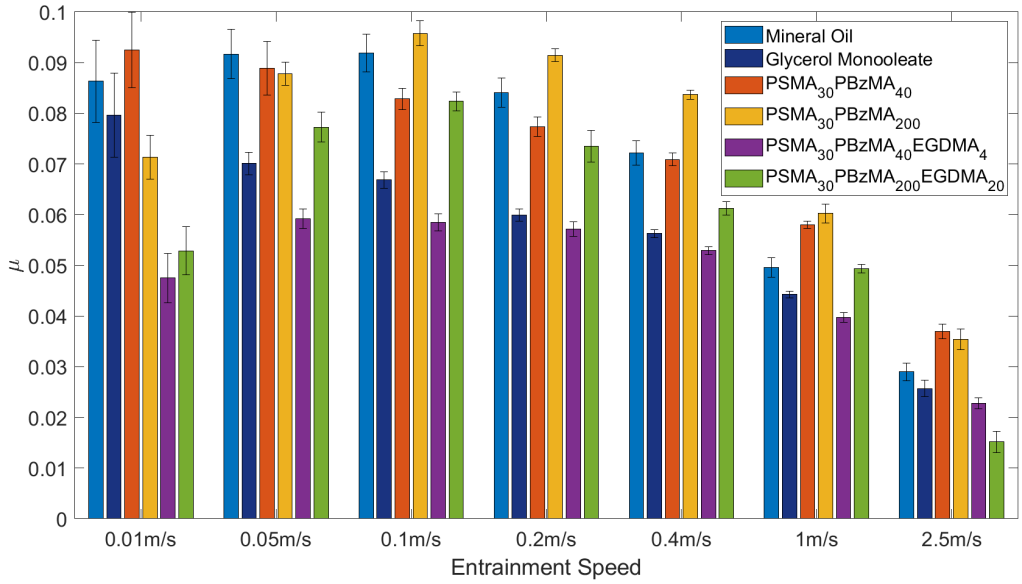

Figure 7.45: Friction of 0.5% PSMA-PBzMA nanoparticles at SRR of 150% as measured using a TE54 MTM, error bars are standard deviations of 3 tests on fresh TE54 samples

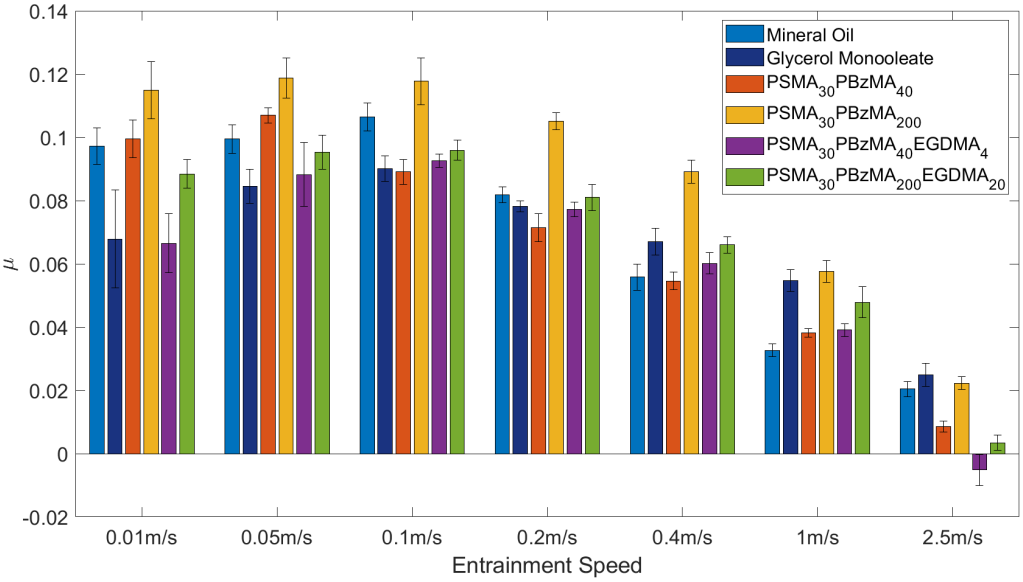

Figure 7.46: Friction of 0.5% PSMA-PBzMA nanoparticles at SRR of 200% as measured using a TE54 MTM, error bars are standard deviations of 3 tests on fresh TE54 samples

non-crosslinked nanoparticles are less effective friction modifiers, with friction increasing within a pure sliding content.

These TE54 results confirm the findings of the previous MTM SRR sweep results. The

exceptions to this being the $PSMA_{30}PBzMA_{40}$ nanoparticles. These do not reduce friction, outside of in the boundary regime of some SRR ratios. The contact area in the TE54 is greater than that in the MTM. As a result, the smaller nanoparticle may not be able to effectively prevent surface contact of this larger contact, while the more structurally stable crosslinked $PSMA_{30}PBzMA_{40}PEGDMA_4$ are likely not as compressed. As a result, each nanoparticle's steric and physical hindrance will be reduced, allowing more nanoparticles to enter the contact and prevent surface contact and lower friction. The calibration issue of these tests, however, could also be to blame for this difference in result.

7.2.4 Universal Machine Tribometer (UMT)

Figure 7.47 shows the mean friction coefficient results using the UMT, while Figure 7.48 displays the development of friction through time.

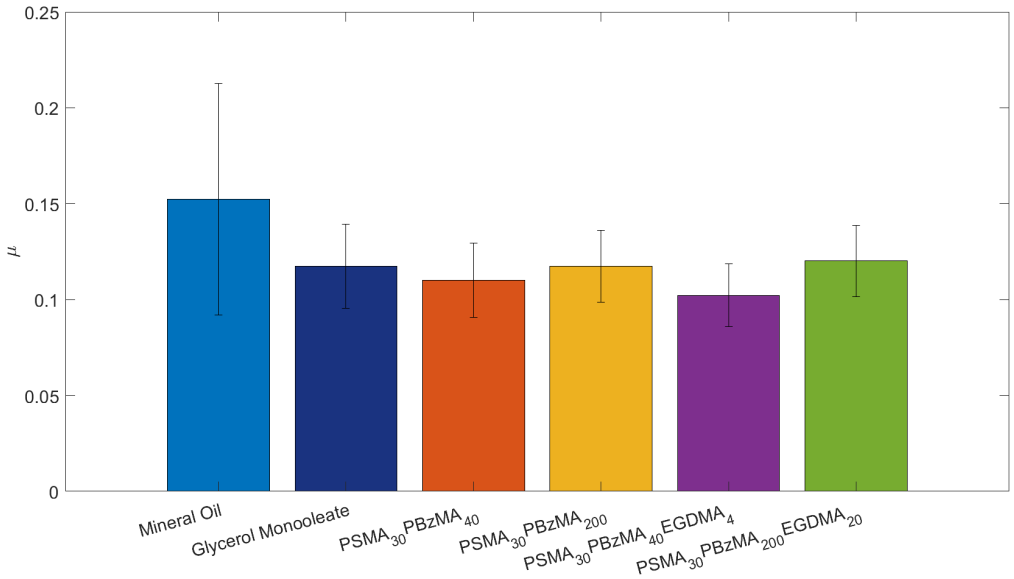

Figure 7.47: Friction of a reciprocating contact with 0.5% PSMA-PBzMA nanoparticles using a universal machine tribometer, error bars are standard deviations of 3 tests on fresh UMT samples

The mean friction results from the UMT, as shown in Figure 7.47, are significantly higher than those for the continuous contacts previously discussed. This higher friction is expected as friction is highest in a sliding contact, and the reciprocating nature of the

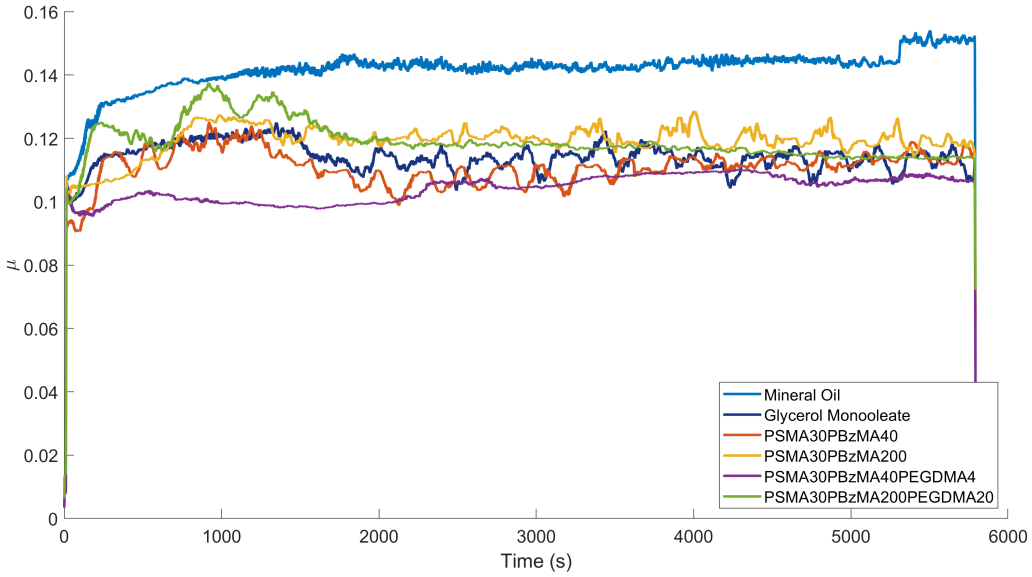

Figure 7.48: Friction of a reciprocating contact with 0.5% PSMA-PBzMA nanoparticles using a universal machine tribometer

contact results in reduced lubricant replenishment in the contact. The mineral oil tests display friction that would be expected for an unlubricated steel contact, indicating that the mineral oil does not reduce friction. Figure 7.48 shows that this friction reduction occurs almost immediately and is maintained at a approximately equal level throughout testing. This indicates that the mechanism by which this friction reduction occurs is immediate and is either the result of an entrapment mechanism or that any film generated is formed rapidly upon exposure to the contact. The only nanoparticle that does appear to change with time is the $PSMA_{30}PBzMA_{200}PEGDMA_{20}$ nanoparticles. These decrease in friction with time in a similar manner to the MTM traction step results observed earlier in this thesis. This indicates that these nanoparticles are generating a film that is more able to adequately prevent surface contact and as a result reduce friction.

The addition of all of the additives significantly reduced the friction of the contact. The most significant friction reduction appears to be in the small $PSMA_{30}BzMA_{40}$ based nanoparticles, in particular the crosslinked nanoparticles. Interestingly the larger $PSMA_{30}BzMA_{200}$, in particular the non crosslinked nanoparticles, display higher friction than GMO.

The better friction reduction of the smaller nanoparticles indicates that these nanoparticles more readily enter the reciprocating contact; this may be due to them being more readily pulled into the contact. The improved performance of the crosslinked nanoparticles indicates that their improved stability improves friction performance; this may be due to the non-crosslinked nanoparticles breaking down within the contactor that the crosslinked nanoparticles better maintain their shape in the more variable reciprocating contact.

7.3 Wear as Surface Damage

7.3.1 Wear Scars

Figure 7.49 show an example of the wear scars generated upon completion of tribological testing. These wear scars show clear scratch marks where the ball has passed over the contact surface, indicating that abrasive wear is present within the contact. There does not appear to be any transfer particles from the ball within the wear scar. However, some large wear spots are present in the wear scars, particularly in contacts where sliding has occurred, indicating that some adhesive wear has occurred from the contact surface to the balls. There are no signs of erosive, fatigue or other types of wear upon the contact. As a result, these contacts have primarily been worn by abrasive wear, with some adhesive wear.

7.3.2 Optical 3D measurements

Figure 7.50 displays the wear scars upon completion of the PCS MTM SRR sweep; the different measurement methods display the same trend with Maximum > Fourier fit > visual assessment. These MTM SRR sweep display very little change in the wear of the contacts across all measurement methods, with a large overlap observed with the standard deviations and no observable trend with the addition of nanoparticles.

TE54 wear scars, as shown in Figure 7.51, appear to show that the larger $PSMA_{30}PBzMA_{200}$ nanoparticles display lower wear than the $PSMA_{30}PBzMA_{40}$ nanoparticles. With the crosslinked $PSMA_{30}PBzMA_{200}PEGDMA_{20}$ showing lower mean wear than the base min-

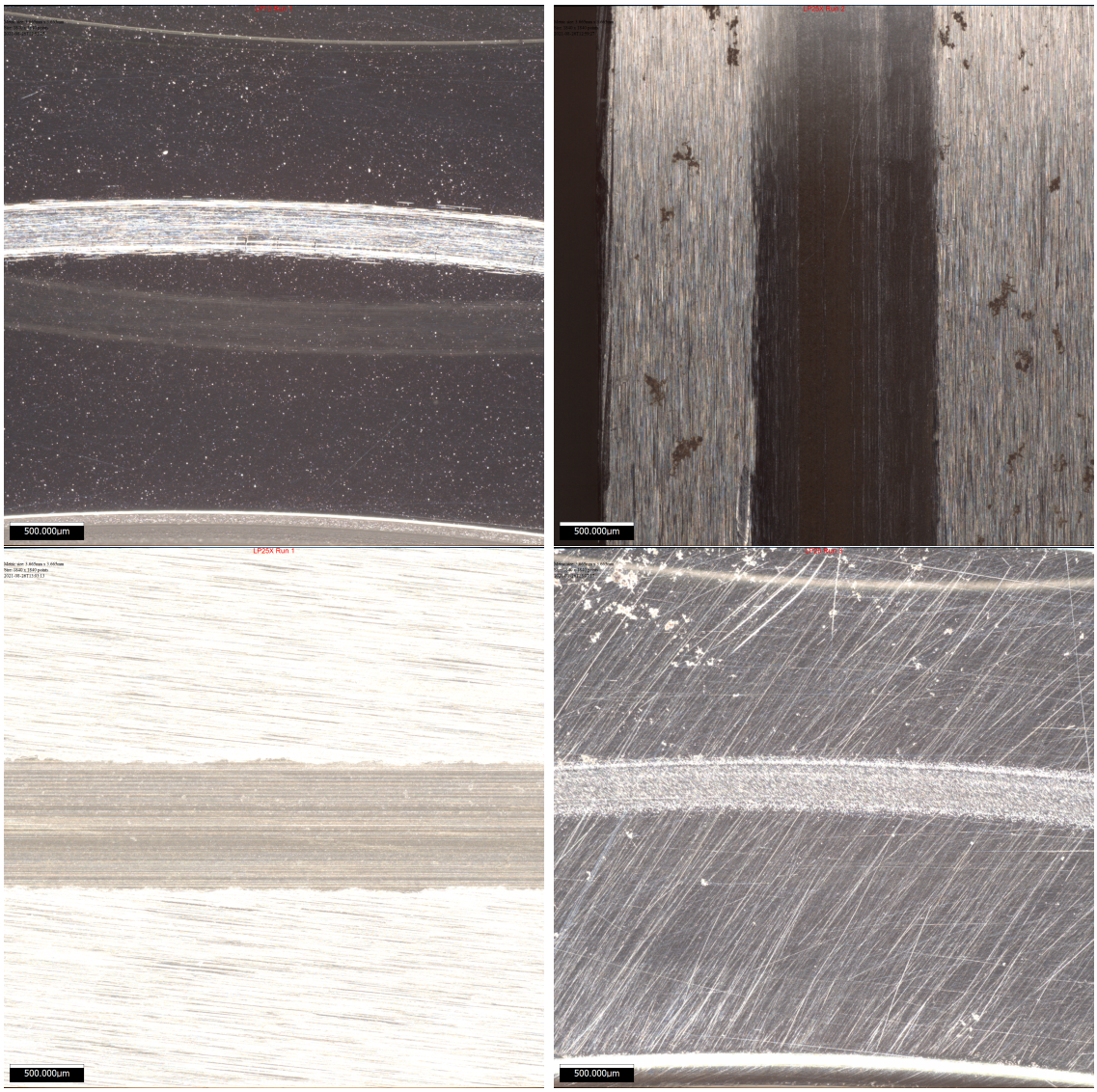

Figure 7.49: Examples of wear scars generated after tribological testing. From left to right: SR Sweep, TE54, TE54, MTM-Film

eral oil, while the rest show higher wear than the mineral oil. However, these results may not be significant as there is overlap between the mineral oil and the nanoparticles standard deviations. Meaning any effect of wear by the nanoparticles may be minimal.

Wear in the UMT reciprocating testing is significantly higher than the other tests, as shown in Figure 7.52. This higher wear is expected as the sliding, reciprocating nature of the contact results in much higher wear than a continuous contact with more of a rolling nature. These results show that the larger $PSMA_{30}PBzMA_{200}$ based nanoparticles show slightly lower wear than the smaller $PSMA_{30}PBzMA_{40}$, and lower than the mineral oil.

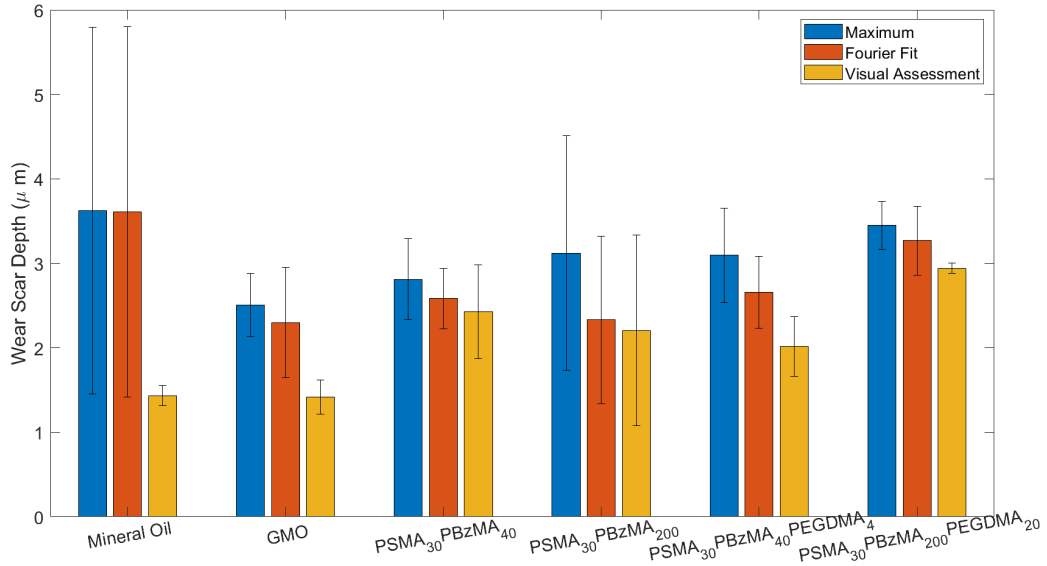

Figure 7.50: Optical 3D measurements of MTM SRR Sweep wear scars

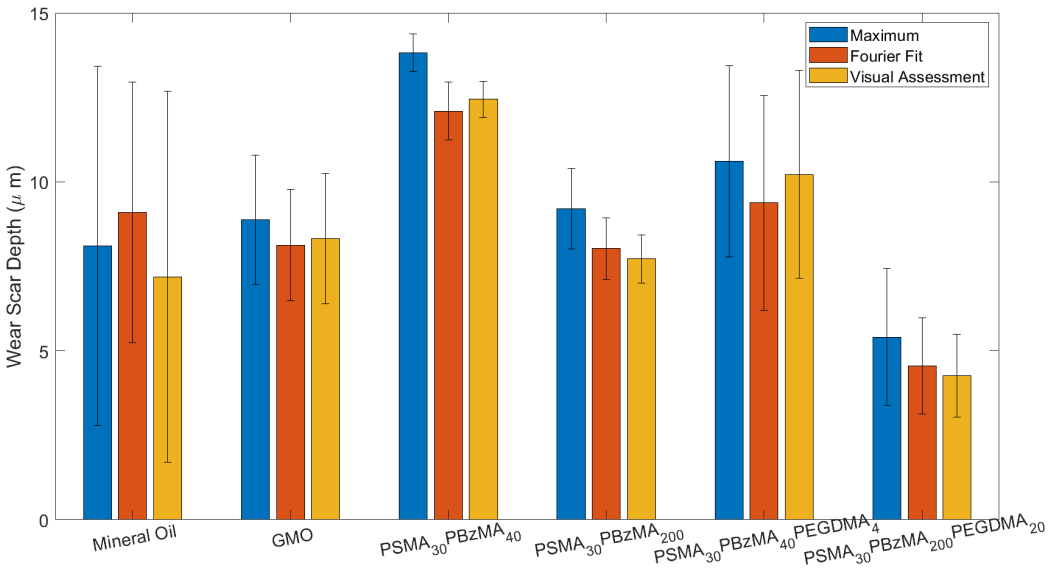

Figure 7.51: Optical 3D measurements of TE54 wear scars, error bars are standard deviations of 3 tests on fresh TE54 samples

However, this difference is relatively small and has overlap with the standard deviations of mineral oil, indicating that any change in wear is likely relatively small.

The MTM film generation experiment is performed at low SRR ratios, and so the amount of wear is meagre; this is shown in Figure 7.53. Here the $PSMA_{30}PBzMA_{40}PEGDMA_4$

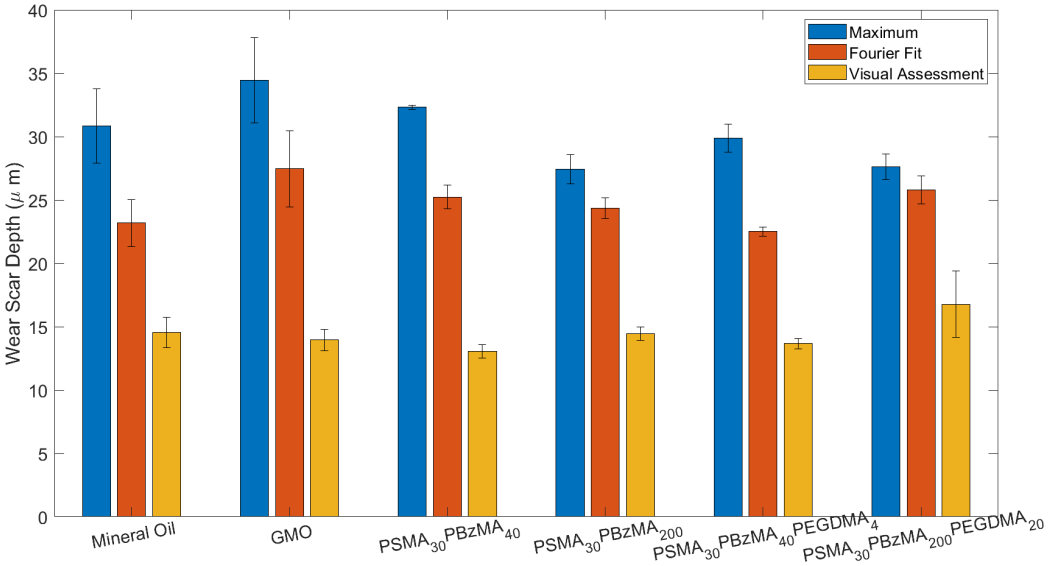

Figure 7.52: Optical 3D measurements of UMT wear scars, error bars are standard deviations of 3 tests on fresh UMT samples

displays the lowest wear of all samples, with the other nanoparticles showing wear equal to or higher than the mineral oil. Again though, the standard deviations of these samples overlap, indicating that any change in wear is insignificant.

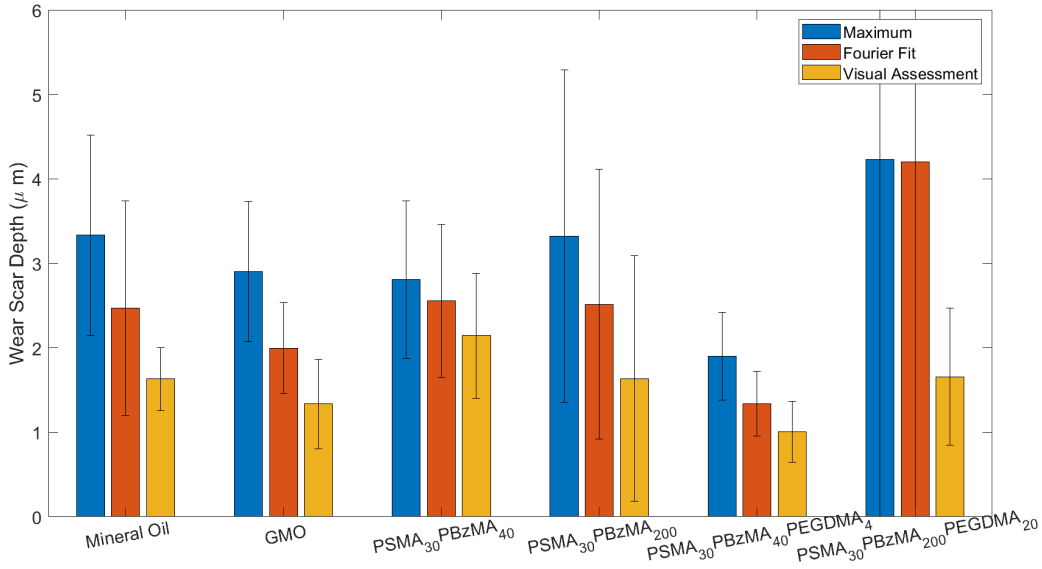

Figure 7.53: Optical 3D measurements of MTM film generation wear scars, error bars are standard deviations of 3 tests on fresh MTM samples

7.3.3 Profilometry

Profilometry of the UMT samples shows similar wear scar depths as those observed in the optical measurements, as shown in Figure 7.54. However, these results show far smaller standard deviations than the Alicona, indicating that the profilometry measurements are more consistent.

These show that all the nanoparticles reduce the wear of the contact when compared with the mineral oil samples. With larger wear reduction being observed by the larger $PSMA_{30}PBzMA_{200}$ nanoparticles and crosslinking. This indicates that larger and more physically stable nanoparticles may reduce wear of the contact; this wear reduction is small.

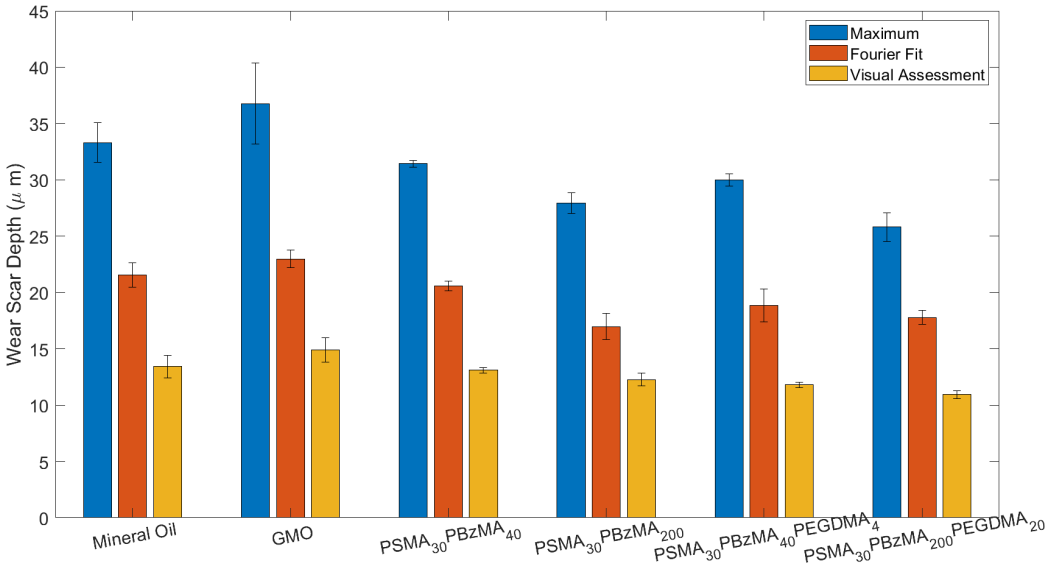

Figure 7.54: Profilometry of UMT wear scars, error bars are standard deviations of 3 tests on fresh UMT samples

Both the optical and profilometry results demonstrate that these polymer nanoparticles display very little effect on wear of the contact with a possible slight reduction in wear compared with the base mineral oil, this is not universal with all the results though and is often within the standard deviations. This lack of change in wear between different nanoparticles could indicate that the oil starvation theory for the increase in friction observed with the larger nanoparticles may not be correct. This is because this oil starvation

would lead to an increase in surface contact and as a result would be expected to see an increase in wear. This adds some validity to the idea of a viscous film being the reason for this increase in friction. It is also possible that any increase in wear due to oil starvation is negated by a decreased surface contact in the boundary regime cause by these larger nanoparticles.

This is often not the case with other nanoparticles, which can be effective as both friction modifiers and for wear reduction, as discussed in Chapter 4. This is interesting as often the only nanoparticles that reduce wear in a contact are those that either break down and exfoliate within a contact such as inorganic fullerenes studied by Rapoport et al. and others.(Rapoport et al., 1997, 2003; Joly-Pottuz et al., 2010; Tevet et al., 2011) Or those that are able to form films upon the contact surface to prevent wear such as metal nanoparticles investigated by Li et al. and others.(Li et al., 2006; Hernández Battez et al., 2008; Song et al., 2012) Alternatively nanoparticles have been shown to result in a large increase in wear through abrasion. This is often the case with hard metal nanoparticles that do not break down within the contact, such as those investigated by Ghaednia et al. and others.(Ghaednia et al., 2015; Khare et al., 2013) To the authors knowledge, no nanoparticles like those discussed in this thesis have been researched before that appear to have a minimal affect on wear. This difference is likely due to the soft nature of the polymer nanoparticles compared with previously researched nanoparticles. These soft nanoparticles can be crushed under load and cannot support as high pressures as harder nanoparticles. However, the soft nature of these nanoparticles does mean that they do not encourage any abrasive wear within the contact, and the addition of currently available anti-wear additives to the oil would likely result in the wear of the system being reduced enough for a commercially viable oil in and ICE.

7.4 Viscosity

7.4.1 Results

Measurements of the effects of nanoparticle addition to the mineral oil on viscosity are shown in Figure 7.55. These show that the addition of PSMA-PBzMA nanoparticles

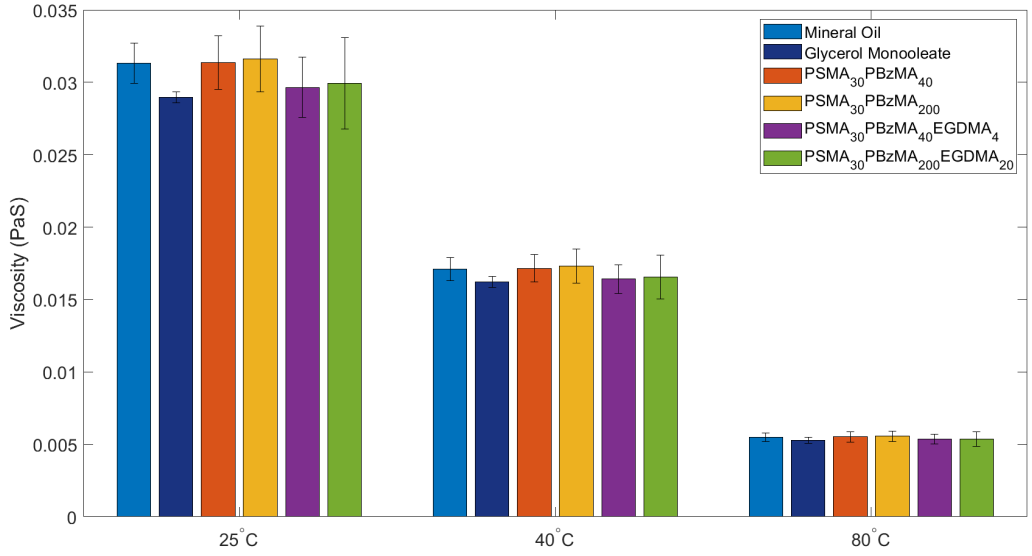

Figure 7.55: Viscosity Measurements of 0.5% PSMA-PBzMA nanoparticles, error bars are standard deviations of 3 tests on fresh samples

has little to no effect on the oil's viscosity across all the temperatures measured. These nanoparticles are in isolated nanospheres that interact relatively little and do not change the flow of the liquid. This lack of change in viscosity means that the friction results are due to the potential mechanisms associated with the nanoparticles within the contact rather than just as a result of a potentially more viscous oil that can separate the contact surface. These samples show no change in viscosity with shear rate, indicating that these are Newtonian.

7.5 Stability of Nanoparticles

Upon completion of tribological testing of the mineral oils containing nanoparticles, several tests were undertaken to establish if the nanoparticles are still present and stable. These tests demonstrate the long term stability of the nanoparticles within a tribological environment such as an ICE. Three tests were undertaken to establish this: GPC to ensure the size and dispersity of the polymers remains consistent; DLS to ensure the size of the nanoparticles remains consistent; viscosity as any change in the polymer chain would result in a change in the viscosity of the solution.

7.5.1 Viscosity

One way to measure the stability of the nanoparticles within the contact is to compare the viscosity of the oil both prior to and after tribological experiments were undertaken. In its nanosphere state, the polymers will entangle relatively little and not affect the liquid's viscosity. If these nanospheres break down, however, the polymers will interact and entangle with each other, increasing the oil's viscosity. Previous work by Hamley et al. has demonstrated that under high shears, these block copolymer nanoparticles may break down; a schematic of this is shown in Figure 7.56.(Hamley et al., 1998; Pople et al., 1998; Hamley, 2000, 2001) This would result in the breakdown of the nanoparticles and would increase the viscosity of the oil. Figures 7.57-7.62 demonstrate the viscosity of the tested oils.

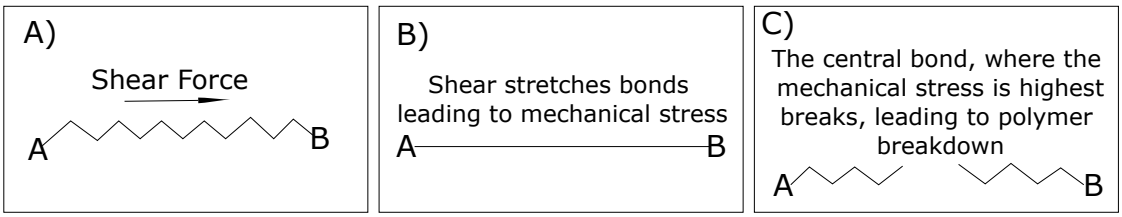

Figure 7.56: Schematic for breakdown of polymer chains under shear forces

These figures demonstrate that there is little to no change in viscosity, with any change resulting in a decrease of viscosity of the nanoparticles after testing. This slight decrease in viscosity would not occur if the nanoparticles were breaking down, and as a result, the polymer chains were able to entangle, increasing their viscosity. This viscosity change indicates there is unlikely to be any breakdown of the nanoparticles within the contact, and as a result, they are likely stable within an ICE. It is also possible that the method by which these tests were undertaken may result in any nanoparticle breakdown not being observed. These testing methods involve using an oil reservoir; this means that the majority of the tested oil will be within this reservoir rather than within the contact. This reservoir testing method could result in very few nanoparticles entering the contact and being exposed to potential breakdown, while the vast majority remains in the reservoir being exposed to very little physical strain.Resulting in any nanoparticles that break down in the contact not being observable compared to the bulk oil. Tests were planned that would be performed

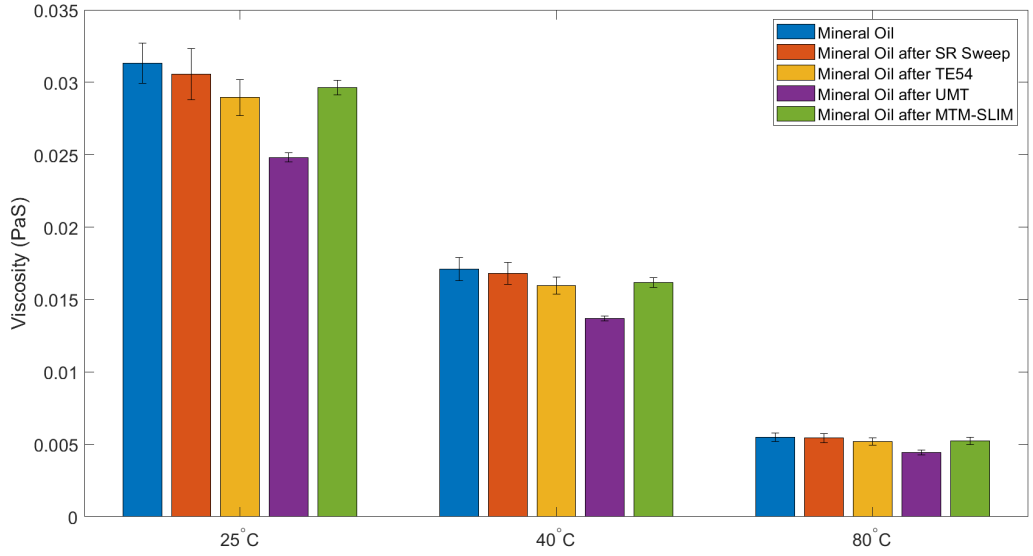

Figure 7.57: Viscosity of Mineral Oil samples after Tribological Testing, error bars are standard deviations of 3 tests on fresh samples

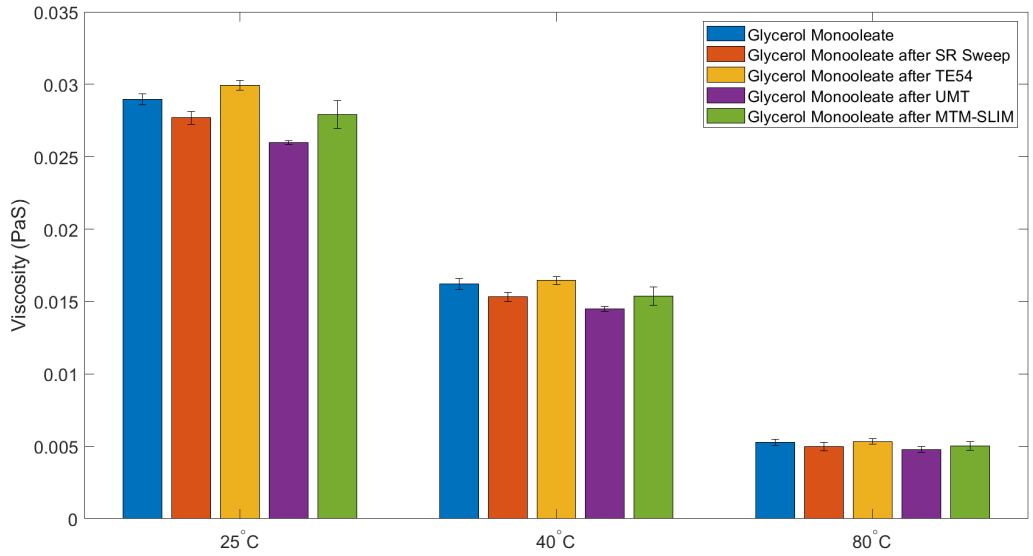

Figure 7.58: Viscosity of Glycerol Monooleate samples after Tribological Testing, error bars are standard deviations of 3 tests on fresh samples

via an alternative oil addition mechanism, e.g. drip-feeding. This would have resulted in all the nanoparticles entering the contact, and any nanoparticle breakdown would be observed upon test completion.

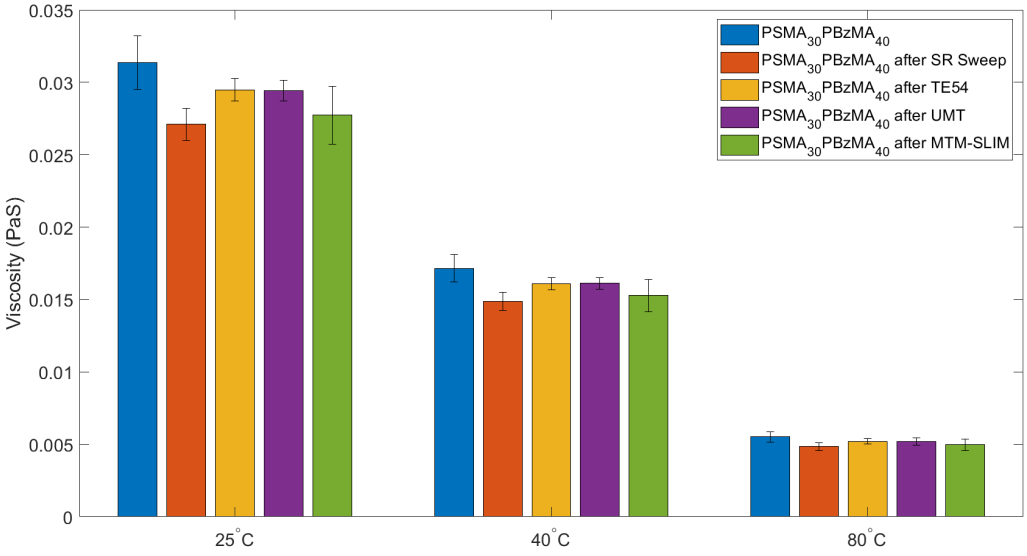

Figure 7.59: Viscosity of $PSMA_{30}PBzMA_{40}$ samples after Tribological Testing, error bars are standard deviations of 3 tests on fresh samples

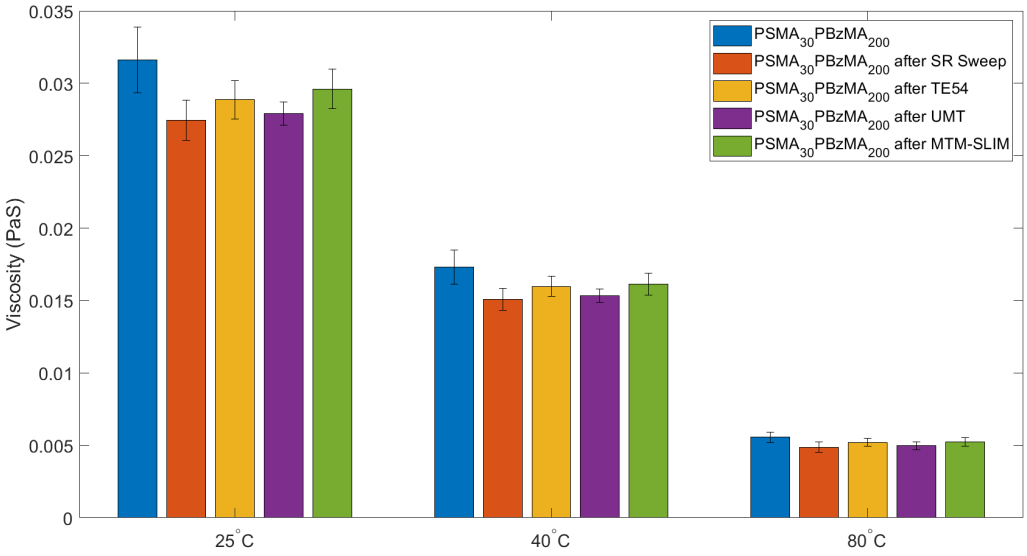

Figure 7.60: Viscosity of $PSMA_{30}PBzMA_{200}$ samples after Tribological Testing, error bars are standard deviations of 3 tests on fresh samples

7.5.2 Gel Permeation Chromatography (GPC)

GPC measurements of the nanoparticles upon completion of testing are displayed in Table 7.1, measurements of crosslinked nanoparticles are not possible as these nanoparticles will

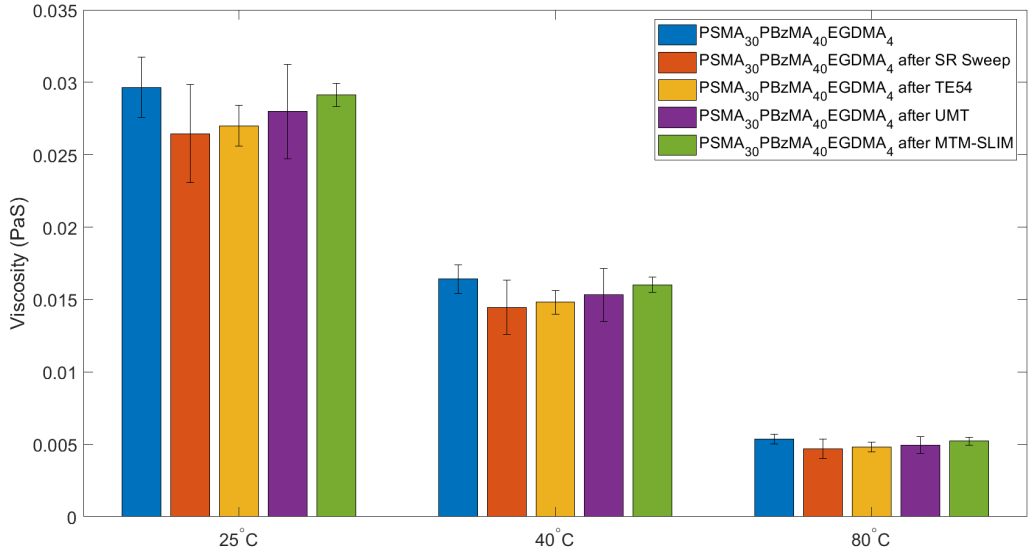

Figure 7.61: Viscosity of $PSMA_{30}PBzMA_{40}PEGDMA_4$ samples after Tribological Testing, error bars are standard deviations of 3 tests on fresh samples

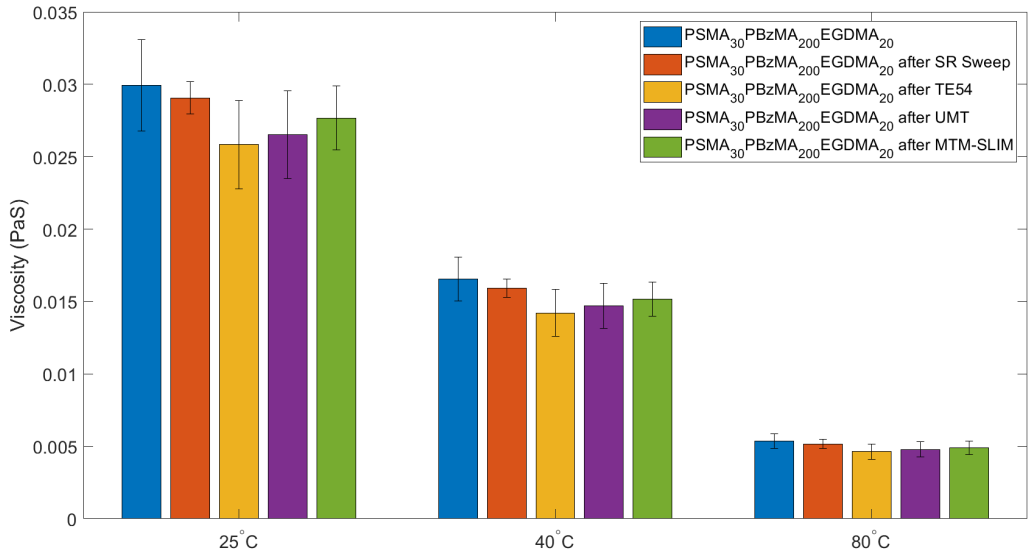

Figure 7.62: Viscosity of $PSMA_{30}PBzMA_{200}PEGDMA_{20}$ samples after Tribological Testing, error bars are standard deviations of 3 tests on fresh samples

not dissolve into the solution due to the crosslinked nature. Due to the calibration alteration from GPC to GPC, these results cannot be quoted as accurate weights. It can be used comparatively with these results. Table 7.1 shows that both size nanoparticles display

very similar molecular masses both before and after tribological testing, with dispersities remaining low for the smaller nanoparticles and decreasing with the larger nanoparticles. This lack of mass change indicates that these polymer chain lengths remain stable after tribological testing, and we would expect that the nanoparticles remain stable. The decrease in dispersity for the larger nanoparticles could indicate that some of the larger chains within the solution are breaking down, which would result in the decrease in M_w observed in these results. This effect, though, is likely to be negligible on nanoparticle stability as the M_n of the polymers appear to remain approximately stable, and the nanoparticles will still be present.

	Initial		SRR Sweep		TE54		UMT		MTM Film	
Sample	Mn (g mol^{-1})	PD	Mn (g mol^{-1})	PD	Mn (g mol^{-1})	PD	Mn (g mol^{-1})	PD	Mn (g mol^{-1})	PD
$PSMA_{30}PBzMA_{40}$	14607	1.13	15139	1.08	12539	1.10	15318	1.08	15751	1.08
$PSMA_{30}PBzMA_{200}$	43670	1.31	46972	1.14	48585	1.12	45059	1.16	47782	1.13

Table 7.1: Gas Permeantation Chromatography of PSMA-PBzMA nanoparticles upon completion of tribological testing

	Initial		SRR Sweep		TE54		UMT		MTM Film	
Sample	Size (nm)	PDI	Size (nm)	PDI	Size (nm)	PDI	Size (nm)	PDI	Size (nm)	PDI
$PSMA_{30}PBzMA_{40}$	23	0.12	37	0.317	105	0.42	24	0.29	25	0.48
$PSMA_{30}PBzMA_{200}$	49	0.02	59	0.04	97	0.2	56	0.03	58	0.04
$PSMA_{30}PBzMA_{40}EGDMA_4$	28	0.12	29	0.21	110	0.3	25	0.21	26	0.22
$PSMA_{30}PBzMA_{200}EGDMA_{20}$	54	0.04	61	0.05	73	0.11	59	0.04	63	0.1

Table 7.2: Dynamic Light Scattering of PSMA-PBzMA nanoparticles upon completion of tribological testing

7.5.3 Dynamic Light Scattering (DLS)

Table 7.2 shows the DLS results upon completion of tribological testing. The majority of the nanoparticles display a slight increase in their z-average diameter, with an increase in PDI often being observed. While the nanoparticles are still stable, there is a process resulting in their size being altered. This size alteration is surprising because if the polymer chains were breaking down due to shear forces, then chains have been shown to break bonds in the centre of the polymer chain, resulting in significantly smaller nanoparticles or complete breakdown of the nanoparticles, rather than the increase in size observed. This change in size is also contrary to the maintenance of polymer chain size observed via GPC. One potential explanation for the increase in nanoparticles is the presence of wear particles within the solution. If these were not filtered out using the pipette filters, these would scatter light and affect the DLS results; this would explain the increase in z-average as these wear particles would likely be larger than the polymer nanoparticles. Another possible explanation would be that these nanoparticles may be able to act as vesicles for wear particles. This would occur if the wear particle were more stable within the BzMA core than within the mineral oil solution, increasing the size of the polymer nanoparticles. While this mechanism has not been reported in oil-soluble nanoparticles, it has been observed in water-soluble nanoparticles as a method of removing toxins and bacteria from solution, and an oil-based mechanism is likely possible.(Donnell et al., 2016; Li et al., 2019) The presence of wear particles, within or outside the nanoparticles, affecting the DLS result is most likely due to the much larger increase in TE54 DLS. These TE54 experiments were undertaken over 24 hours, with a much larger contact area, and the amount of wear particles within the solution is visually much greater than the other solutions.

7.6 Conclusions

These results demonstrate that PSMA-PBzMA nanoparticles can effectively reduce the friction of a contact in the boundary lubrication regime. This friction reduction is shown to occur in a variety of contact environments, including across all SRR in a continuous

contact and a reciprocating contact. Meaning that these nanoparticles can be effective friction modifiers in motor oils. The most effective friction modifiers across all contact environments and speeds appear to be the smaller nanoparticles, with $PSMA_{30}PBzMA_{40}$ based nanoparticles being focused on in particular in this thesis. The only exception to this is the $PSMA_{30}PBzMA_{40}$ nanoparticles in the TE54 testing where little to no friction reduction is observed, the exact reason for this discrepancy is unknown, and the question of the calibration issue with the TE54 could be to blame for these results. Larger nanoparticles, with $PSMA_{30}PBzMA_{200}$ being focused on in this thesis, appear to display friction reduction in the boundary regime in a large number of contact conditions. This friction reduction is not universal in all contact environments, in particular at higher SRR and these larger nanoparticles also display a significant increase in friction in the mixed and hydrodynamic regime, likely due to them preventing the flow of oil into the contact, and as such, they are unlikely to be commercially viable friction modifiers. Crosslinking of nanoparticles appears to improve the friction-reducing ability of these nanoparticles in the boundary regime, with this effect being larger in larger nanoparticles. Cross-linking also improves the nanoparticles long term stability of the friction performance, with a smaller increase in friction coefficient being observed after prolonged testing times. These results mean that the use of small (20-30nm) $PSMA_{30}PBzMA_{X}PEGDMA_{X/10}$ nanoparticles produce stable long term friction reduction in all contact environments and speeds, with non-crosslinked similarly sized nanoparticles displaying slightly less effective but similar results. These smaller nanoparticles have shown they can be effective friction modifiers in an internal combustion engine, although more testing is required to confirm this hypothesis, such as longer-term and ICE component testing. Larger $PSMA_{30}PBzMA_{X}EGDMA_{X/10}$ nanoparticles (>35nm) can effectively reduce friction in the boundary regime but show a large increase in friction at higher contact speeds, with the non-crosslinked similarly sized nanoparticles displaying the same trend but with smaller friction reduction in the boundary regime. Due to the oil starvation at higher speeds, these larger nanoparticles are unlikely to be commercially viable friction modifiers. However, the large boundary lubrication friction reduction of these in some conditions could be viable in some niche applications.

These nanoparticles appear to have little influence on the wear and viscosity of the mineral oil and are stable after prolonged periods of testing. These results all suggest that the small $PSMA_{30}PBzMA_{40}$ nanoparticles may be effective friction modifiers in motor oils.

Though we know that these nanoparticles do act to reduce friction, we do not know how they act to reduce this friction, they have shown not to increase the oil's viscosity, and a different mechanism must be occurring. Chapter 8 will investigate the mechanism by which these nanoparticles can reduce the friction of a contact.

Chapter 8

Mechanistic Analysis

8.1 Introduction

This chapter will focus on understanding the mechanisms by which these PSMA-PBzMA nanoparticles reduce friction. This understanding helps understand the processes that can affect their friction performance and can help design and develop similar friction modifiers. Allowing for understanding the factors that influence friction reduction and optimises these factors in future iterations of these friction modifiers as the most commercially viable product is developed.

8.2 Spacial Layer imaging of MTM (MTM-SLIM)

8.2.1 Results

Friction

Figure 8.1 displays the friction results for the PSMA-PBzMA nanoparticles during the film measurement testing.

These friction results, performed at a low sliding:rolling, demonstrate that the friction of the contact remains constant throughout the entire 4 hour test. At these low SRR and speeds the nanoparticles are stable and result in a prolonged reduction in friction compared to mineral oil. The larger nanoparticles, both crosslinked and non-crosslinked, display the

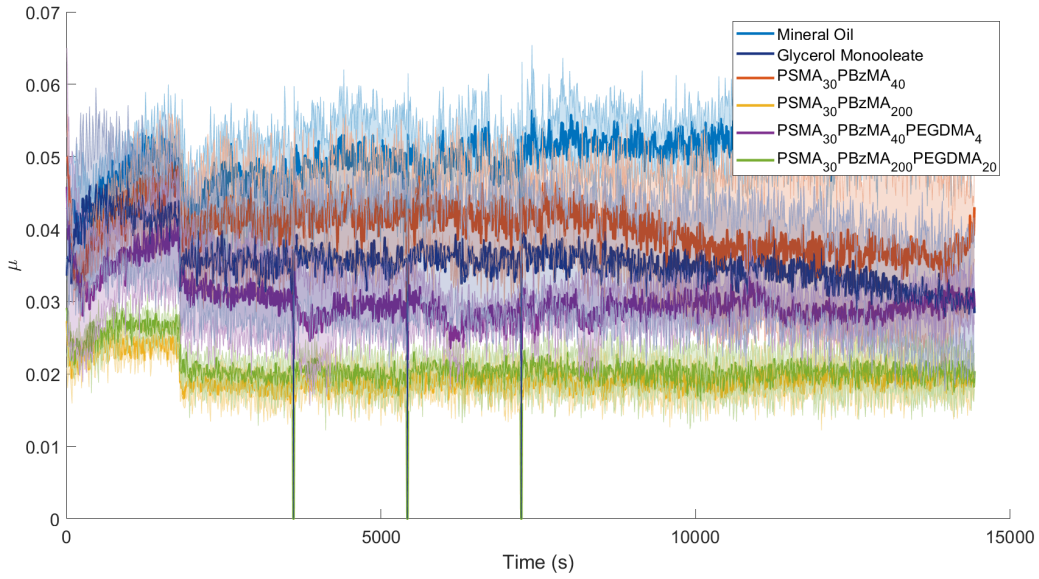

Figure 8.1: Friction of 0.5% PSMA-PBzMA nanoparticles in mineral oil during spacial layer image testing

lowest frictions of around 0.02, a friction reduction of around 60% when compared with base mineral oil. However, the smaller nanoparticles display a different friction coefficient between crosslinked and non-crosslinked, with the crosslinked having a friction coefficient of around 0.03, a 40% decrease compared with mineral oil, and the non crosslinked having a friction coefficient of 0.04, a 20% reduction compared with mineral oil. These results appear to contradict the previous results in Chapter 7 which demonstrated that the smaller nanoparticles were more effective at reducing friction in the boundary regime across all SRR ratios; this may indicate that these larger nanoparticles are only effective in a consistent contact where speed and SRR remain constant throughout testing. With consistent suction of these larger nanoparticles into the contact. In contrast, this is not the case with a Stribeck curve measurement using the MTM, where each friction measurement is recorded separately, with the motor momentarily pausing between measurements.

Film Thickness

Throughout the MTM-SLIM testing, spacial layer images were taken before testing and then at regular intervals throughout the testing. Example images are shown in Figures

8.2-8.7. Tribofilm thickness measurements from these images are shown in Figures 8.8.

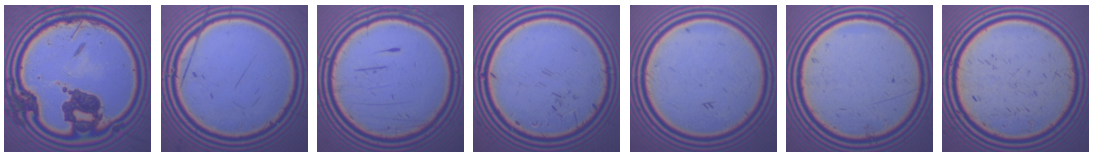

Figure 8.2: Spacial Layer Images of Mineral Oil. From left to right: Initial film, 30 minute film, 60 minute film, 90 minute film, 120 minute film, 180 minute film, Final film

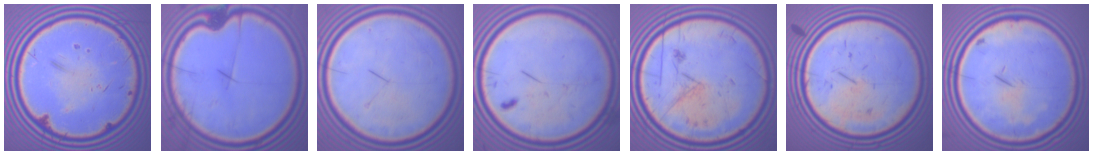

Figure 8.3: Spacial Layer Images of 0.5% Glycerol Monooleate. From left to right: Initial film, 30 minute film, 60 minute film, 90 minute film, 120 minute film, 180 minute film, Final film

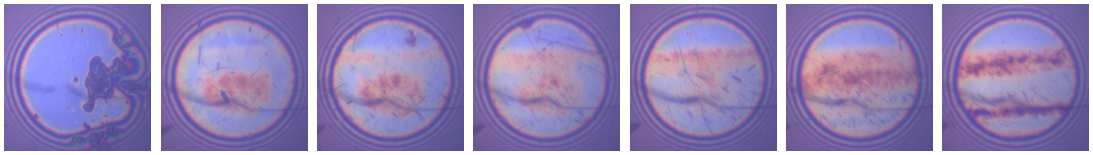

Figure 8.4: Spacial Layer Images of 0.5% $PSMA_{30}PBzMA_{40}$ in mineral oil. From left to right: Initial film, 30 minute film, 60 minute film, 90 minute film, 120 minute film, 180 minute film, Final film

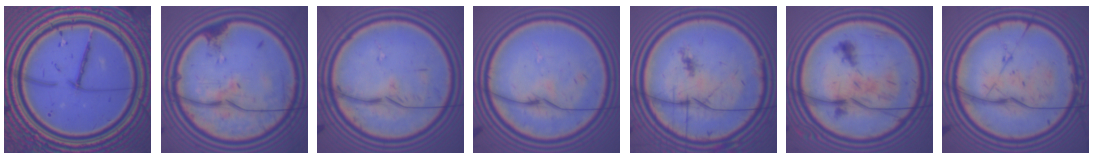

Figure 8.5: Spacial Layer Images of 0.5% $PSMA_{30}PBzMA_{40}EGDMA_4$ in mineral oil. From left to right: Initial film, 30 minute film, 60 minute film, 90 minute film, 120 minute film, 180 minute film, Final film

These spacial layer images show that both pure mineral oil and 0.5% glycerol monooleate do not form a tribofilm within the contactor that any film is negligible. The fact that GMO does not display a film is somewhat surprising as this is an organic friction modifier, and as such, we would expect a thin film to form. It is difficult to understand the validity of this result as there appears to be limited literature on the use of spacial layer imaging on

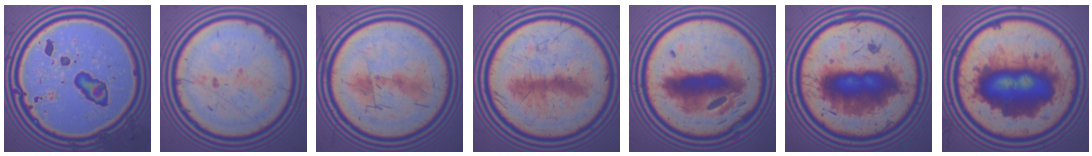

Figure 8.6: Spacial Layer Images of 0.5% $PSMA_{30}PBzMA_{200}$ in mineral oil. From left to right: Initial film, 30 minute film, 60 minute film, 90 minute film, 120 minute film, 180 minute film, Final film

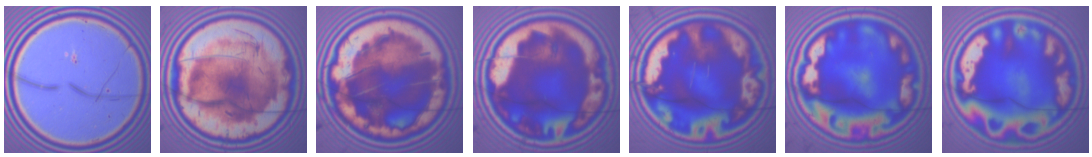

Figure 8.7: Spacial Layer Images of 0.5% $PSMA_{30}PBzMA_{200}EGDMA_{20}$ in mineral oil. From left to right: Initial film, 30 minute film, 60 minute film, 90 minute film, 120 minute film, 180 minute film, Final film

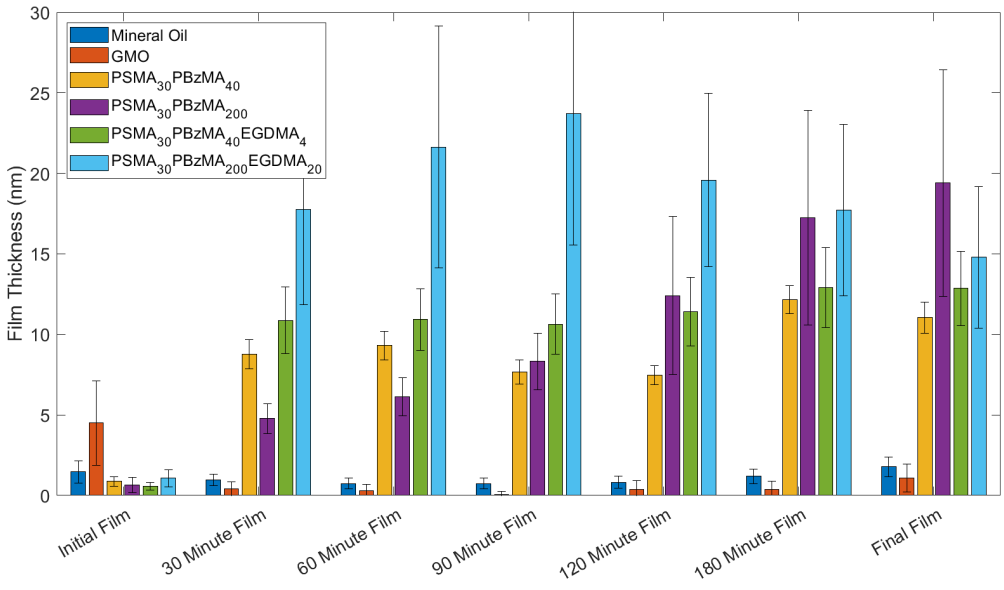

Figure 8.8: Tribofilm thickness of 0.5% $PSMA_{30}PBzMA_X$ nanoparticles in mineral oil as measured by spacial layer imaging

OFMs, with the majority using quartz crystal microscopy, which is discussed in section 8.3. The reasoning for this is unknown but could be because it is difficult to image these OFMS by this method, and the lack of film being observed is not an issue.

Figure 8.8 demonstrates that PSMA-PBzMA nanoparticles form a tribofilm within a contact. This tribofilm formation appears to be immediate, with approximately full

depth films formed by the 30 minute image. This full-film is not present, however, for the large non crosslinked $PSMA_{30}PBzMA_{200}$ nanoparticles. This nanoparticles appears to grow with time within the contact from 4 nm after 30 minutes up to 19 nm after 240 minutes. This difference in film formation is surprising as these nanoparticles still produce immediate friction reduction; this means that it is likely that these PSMA-PBzMA nanoparticles reduce friction by an alternative or synergistic mechanism than just pure tribofilm formation.

Tribofilm thickness appears to follow the trend that the larger $PSMA_{30}PBzMA_{200}$ based nanoparticles form larger tribofilms than the smaller $PSMA_{30}PBzMA_{40}$ nanoparticles; this is likely due to the larger diameter of these nanoparticles. It also appears that crosslinked nanoparticles form larger films than non-crosslinked; this is likely due to the higher physical stability of the nanoparticles meaning that any film formed is more stable.

The average film thickness for all these nanoparticles is lower than the average diameter of the respective nanoparticle. As a result, these nanoparticles are not achieving true monolayer coverage, which is likely in part due to steric hindrance of nanoparticles preventing adsorption of another nanoparticle to the contact nearby. By dividing the film thickness of each nanoparticle by the diameter of said nanoparticle, it is possible to approximate the percentage coverage of each film. These percentage coverages show that the smaller $PSMA_{30}PBzMA_{40}$ based nanoparticles display slightly higher coverage than the larger nanoparticles (49% and 44% compared with 38% and 42%). These percentage coverages indicate that these smaller nanoparticles can more tightly pack into the contact and provide more uniform coverage; the much narrower standard deviations confirm this for the $PSMA_{30}PBzMA_{40}$ based nanoparticles and the much lower maximum film thickness of these nanoparticles, as shown in table 8.1. These more uniform tribofilms likely have a part to play in the greater friction reduction of these nanoparticles across all contact speeds with films able to separate the contact without preventing oil flow into the contact. Except for the $PSMA_{30}PBzMA_{40}$ nanoparticles, these nanoparticles display a maximum film thickness that is greater than the nanoparticle diameter, indicating that these nanoparticles are stacking and tangling to form larger films than just monolayer coverage, a schematic of this is shown in Figure 8.9. These maximum films are particularly large in

Sample	Maximum Film Thickness (nm)
Mineral Oil	14.5
GMO	53.5
$PSMA_{30}PBzMA_{40}$	19.1
$PSMA_{30}PBzMA_{40}EGDMA_4$	66.4
$PSMA_{30}PBzMA_{200}$	136.3
$PSMA_{30}PBzMA_{200}EGDMA_{20}$	157.9

Table 8.1: Maximum Tribofilm Thickness by Spacial Layer imaging

the $PSMA_{30}PBzMA_{200}$ based nanoparticles and may explain the oil starvation or highly viscous film within the contact in the mixed regime, resulting in greater friction. The slightly larger maximum film may also explain why the non crosslinked $PSMA_{30}PBzMA_{40}$ nanoparticles often display slightly lower friction in the mixed lubrication regime than their crosslinked equivalent, which is most noticeable in the MTM SRR Sweep testing, see section 7.2.2.

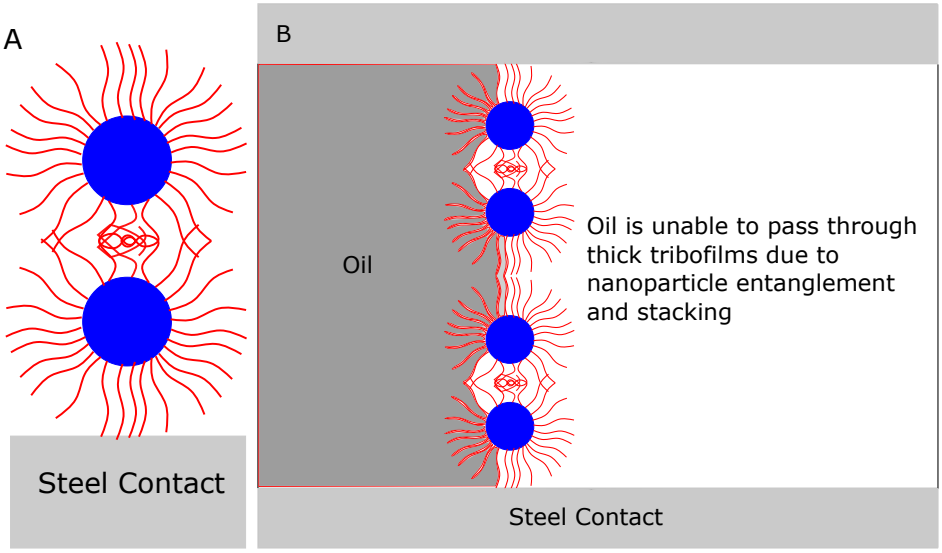

Figure 8.9: A: Schematic of tangling of Stearyl Methacrylate chains to generate a thick tribofilm. B: How tangling of stearyl methacrylate chains can result in oil starvation of a contact

Sample	Film depth (nm)	Film depth after removal of sample (nm)
Glycerol Monooleate	12.774	0.749
$PSMA_{30}PBzMA_{40}$	8.53	6.468
$PSMA_{30}PBzMA_{40}PEGDMA_4$	20.288	4.353
$PSMA_{30}PBzMA_{200}$	29.112	27.823
$PSMA_{30}PBzMA_{200}PEGDMA_{20}$	30.581	32.108

Table 8.2: Measurement of tribofilm using quartz crystal microbalance

8.3 Quartz Crystal Microbalance

8.3.1 Results

QCM measurements of $PBzMA_{40}$, $PBzMA_{200}$, their respective crosslinked nanoparticles were undertaken with GMO also being measured to compare these nanoparticles to more traditional friction modifiers. Averages for these measurements are displayed in Table 8.2 with graphs to display film growth with time shown in Figures 8.10-8.14. These graphs are split into 3 sections: The initial zero calibration using the mineral oil, shown in red, the film growth once the sample is added and finally, the pure mineral oil reintroduction as shown in green.

These results display the film formation of the friction modifiers and their long term stability. Here the glycerol monooleate shows that a 12.8nm film is formed but is not stable once the pure mineral oil is reintroduced. Here GMO forms a film is weakly bonding to the gold sensor and that this bonding is weak enough to be removed and replenished. This replenishment of the film is not possible once the mineral oil is reintroduced, and therefore the film is removed. Interestingly, despite having similar surface chemistry, the PSMA-PBzMA based nanoparticles display quite different film-forming properties. All the nanoparticles are shown to form a film upon the surface. This average surface film depth is smaller than the diameter of the nanoparticles, with the $PSMA_{30}PBzMA_{40}$ being much smaller than the nanoparticle diameter. Meaning that although there is significant surface coverage of these nanoparticles, there is not the formation of a monolayer. The lack of monolayer is the same as is observed in MTM-SLIM and may be due to steric hindrance preventing close packing of the nanoparticles. The lower film depth of the $PSMA_{30}PBzMA_{40}$ nanoparticles may indicate that the bonding of these is reduced when

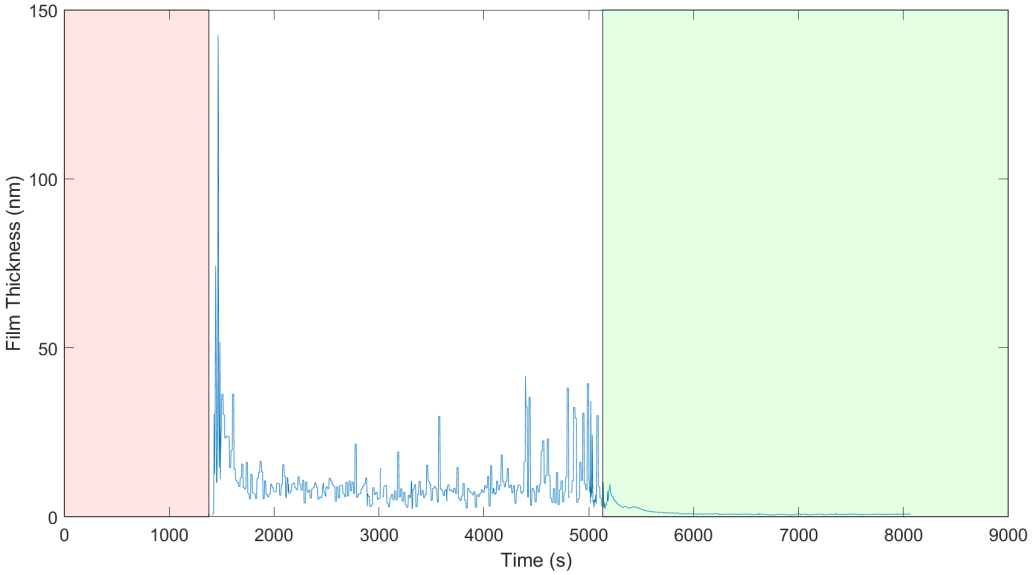

Figure 8.10: Film growth of 0.5 wt% GMO in mineral oil by quartz crystal microbalance, the red section represents the film during the control stage where no GMO is present in the mineral oil, white is after the addition of GMO to the oil and green is once the pure oil is added again

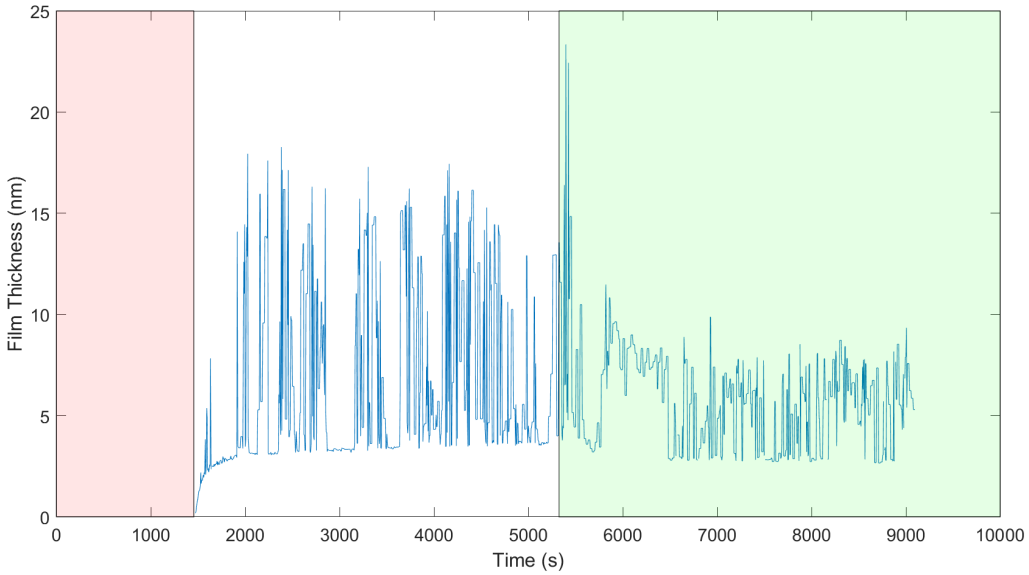

Figure 8.11: Film growth of 0.5 wt% $PSMA_{30}PBzMA_{40}$ in mineral oil by quartz crystal microbalance, the red section represents the film during the control stage where no nanoparticle is present in the mineral oil, white is after the addition of nanoparticle to the oil and green is once the pure oil is added again

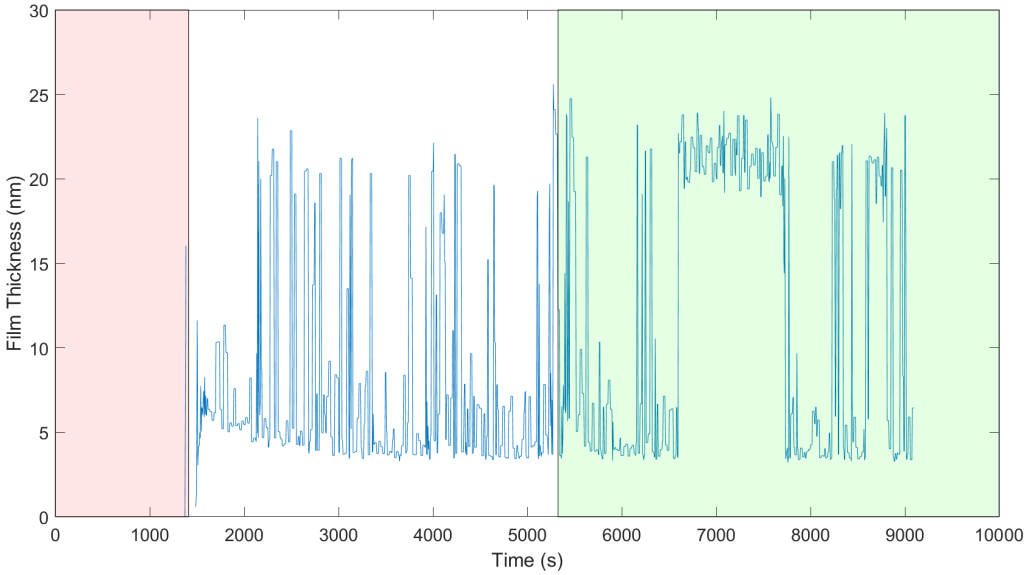

Figure 8.12: Film growth of 0.5 wt% $PSMA_{30}PBzMA_{40}PEGDMA_4$ in mineral oil by quartz crystal microbalance, the red section represents the film during the control stage where no nanoparticle is present in the mineral oil, white is after the addition of nanoparticle to the oil and green is once the pure oil is added again

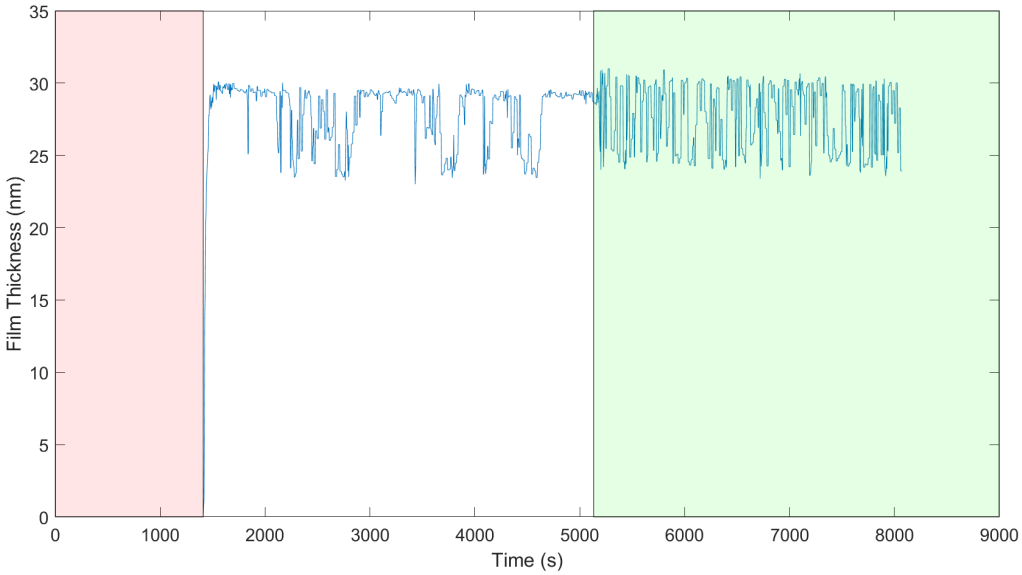

Figure 8.13: Film growth of 0.5 wt% $PSMA_{30}PBzMA_{200}$ in mineral oil by quartz crystal microbalance, the red section represents the film during the control stage where no nanoparticle is present in the mineral oil, white is after the addition of nanoparticle to the oil and green is once the pure oil is added again

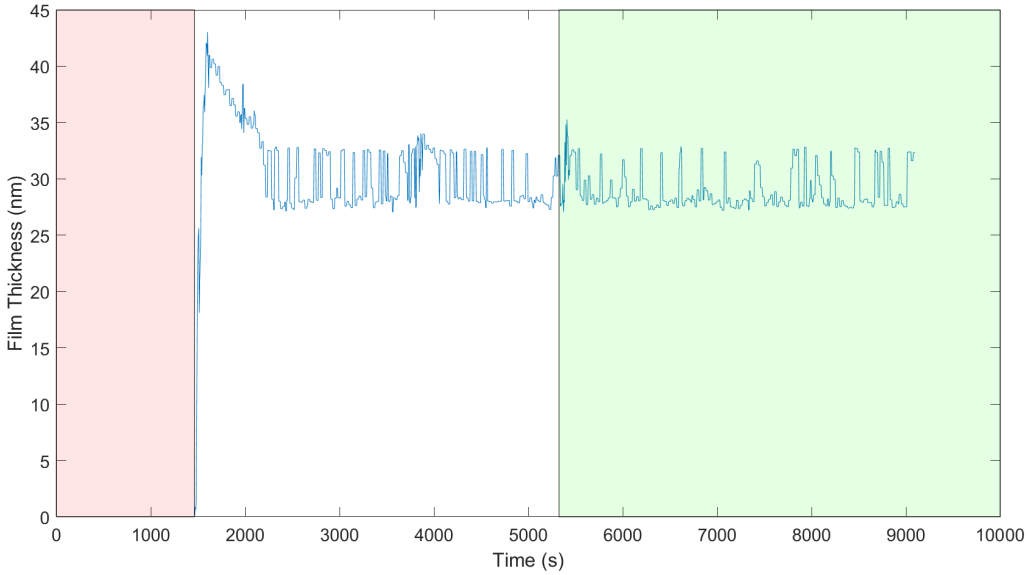

Figure 8.14: Film growth of 0.5 wt% $PSMA_{30}PBzMA_{200}PEGDMA_{20}$ in mineral oil by quartz crystal microbalance, the red section represents the film during the control stage where no nanoparticle is present in the mineral oil, white is after the addition of nanoparticle to the oil and green is once the pure oil is added again

compared to the other nanoparticles. This smaller film is surprising as the surface chemistry of the spheres is the same and may instead be a result of reduced stability of these nanoparticles as spheres resulting in greater steric hindrance or the formation of a different structure at the surface, such as a worm-like structure or a more typical friction modifier film. This would explain why the crosslinked, and as a result, more stable in their sphere structure, $PSMA_{30}PBzMA_{40}PEGDMA_4$ form a much larger surface film as they maintain their spherical structure.

Upon reintroduction of the pure mineral oil, the smaller nanoparticles with the $PBzMA_{40}$ cores show a reduction in the film size, indicating that, like the glycerol monooleate, these nanoparticles are weakly bonded to the surface, and so, they are removed from the surface. The larger $BzMA_{200}$ nanoparticles, however, maintain their film during this reintroduction period. This difference in film stability is unexpected due to the similar surface chemistry of the nanoparticles. It could be due to the larger surface area of each nanoparticle exposed to the surface, resulting in a larger number of the acid capping groups in contact with the surface, leading to a stronger bonding of the nanoparticles.

However, these film results do not appear to give a complete picture of these nanoparticles' friction reduction mechanism. If film formation were the only method of friction reduction, then we would expect these larger nanoparticles to reduce friction by the greatest amount due to their thicker and more stable tribofilm. This, however, is often not the case, indicating that a synergistic mechanism may be in place. Section 8.4 will investigate other potential synergistic mechanisms that may reduce the friction of the contact.

8.4 Physical Measurements

Nanoindentor SEM studies were undertaken; these allow for imaging of PSMA-PBzMA nanoparticles as they are indented, allowing for an understanding of how they may interact within a contact.

Figure 8.15 demonstrates the indentation of a cluster of $PSMA_{30}PBzMA_{1000}$. These large nanoparticles (318 nm) were chosen as the tip of the nanoindenter, and the SEM can only study relatively large nanoparticles. While not ideal, the physical characteristics of this nanoparticle should be very similar to the smaller nanoparticles studied earlier in this thesis, providing a good comparison.

Figure 8.15 goes from before indentation in image 1 through to indentation has been completed in picture 7. Observing the images makes it possible to visualise the effect of a contact upon the PSMA-PBzMA nanoparticles. Images 2 and 3 demonstrate the compression of the nanoparticle; here as the indentor moves down into the nanoparticles, the nanoparticle is compressed with relatively low resistance. This compression results in the spreading of the nanoparticle around the contact and would result in the soft nanoparticle preventing contact of the hard surfaces. Image 4 displays the full compression of the nanoparticle to their "fracture point", here the nanoparticle has reached a significant enough level of compression has reached a critical point where the amount of load to increase compression further is lower than what was required to reach its current level of compression. This is typically the point at which a nanoparticle fractures and is no longer useful as a friction modifier. In this case, however, the nanoparticle is still in place and can prevent surface contact by surrounding the contact tip. This stability of the

nanoparticle is shown in images 5-7. Here the compression of the nanoparticle decreases as the indentor begins to lift. Here the nanoparticle appears to display an elastic property with the nanoparticle surface rebounding to reform its original shape. This reformed shape shows no signs of cracking and would likely be able to support the contact again.

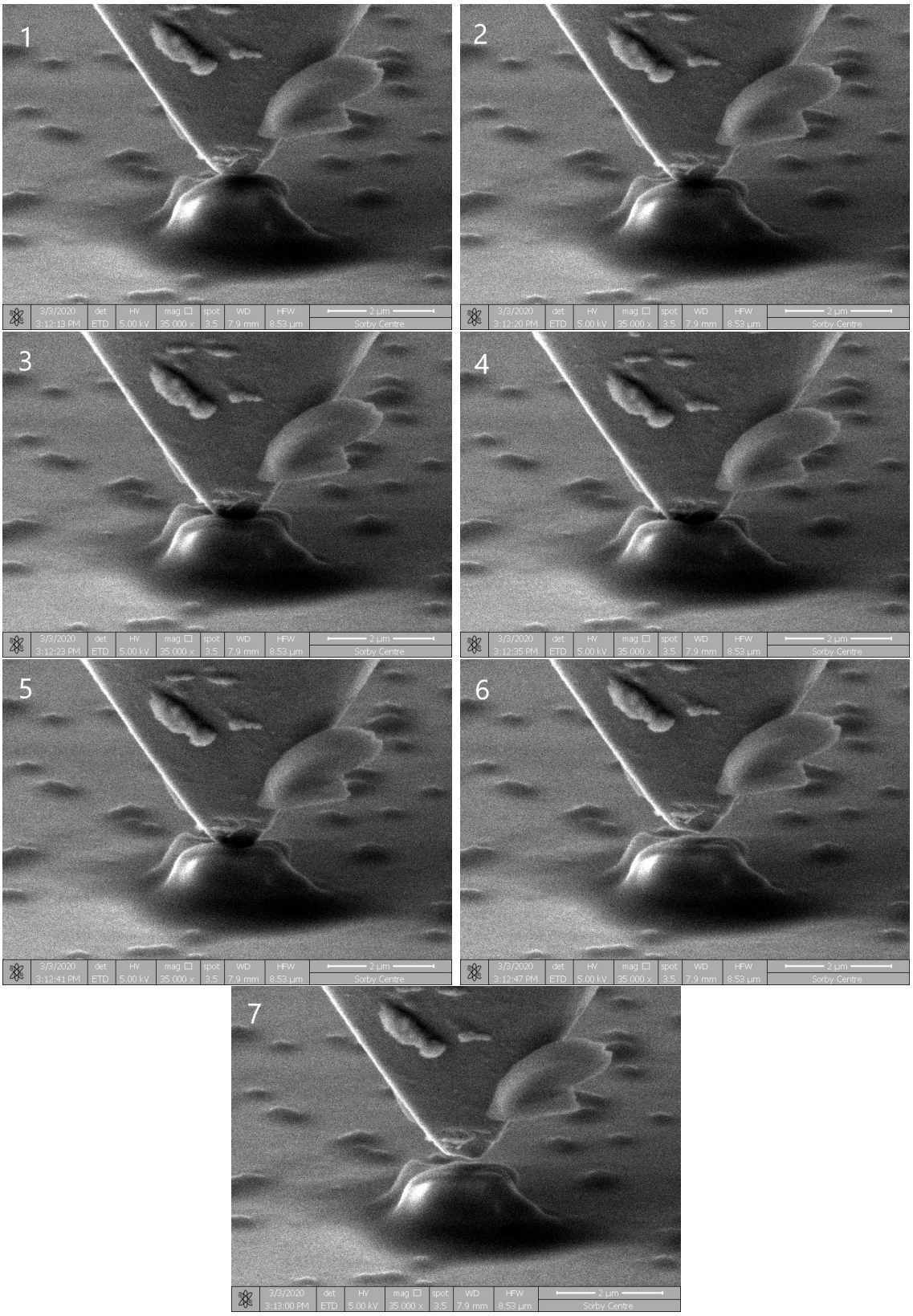

Figure 8.15: Nanoindentor SEM images of $PSMA_{30}PBzMA_{1000}$ nanoparticles

These images show that the nanoparticle can deform and spread to prevent surface contact and is then able to reform once not exposed to a load. These nanoparticles can be recycled through the contact and explain both the short term and long term friction reducing ability of the nanoparticles. Because these experiments have to be undertaken in a vacuum there is no oil present. This lack of oil means that the stability of the nanoparticle is compromised as the difference in solubility between the two blocks is no longer acting to maintain the nanoparticle shape. It would be expected that the nanoparticles could break down to their polymer chains or cluster to form amorphous areas of polymer. The fact that these nanoparticles were able to remain stable and behave to deform, reform and prevent surface contact in this environment means that this is more likely to happen within the oil where their inherent solvent stability is in effect. In solution, these nanoparticles will likely undergo compression and reformation, spreading them across the contact area and preventing surface contact. The improved performance of crosslinked nanoparticles, as shown in section 7.2 is likely the result of these nanoparticles having greater structural integrity and, as a result, will be less likely to break down fully and will more readily reform within the contact.

The physical properties of these nanoparticles are shown in Figure 8.16; these values are calculated based on the "fracture point" of the nanoparticle or the point at which further compression by the nanoindenter becomes significantly easier. These results show that the plastic depth of these nanoparticles is significant, with plastic nature being observed for a depth of 362.2nm, this is significantly less than the full compression applied of 500nm, yet we still observe at intact nanoparticle rebounding. This means that while easier to compress beyond 362.2nm, the nanoparticle is still capable of elastic nature to prevent surface contact beyond this point, meaning that these nanoparticles can be significantly compressed while maintaining an ability to alter their shape and form a protective surface on the contact. This value is greater than the diameter of a single nanoparticle, indicating that these compression tests were undertaken on a cluster of nanoparticles. This may be the case within a real-life contact, or the contact may be supported upon a single nanoparticle. However, the depth of deformity means that even in individual nanoparticles, we can expect a large degree of plastic compression upon entrapment and prevent surface

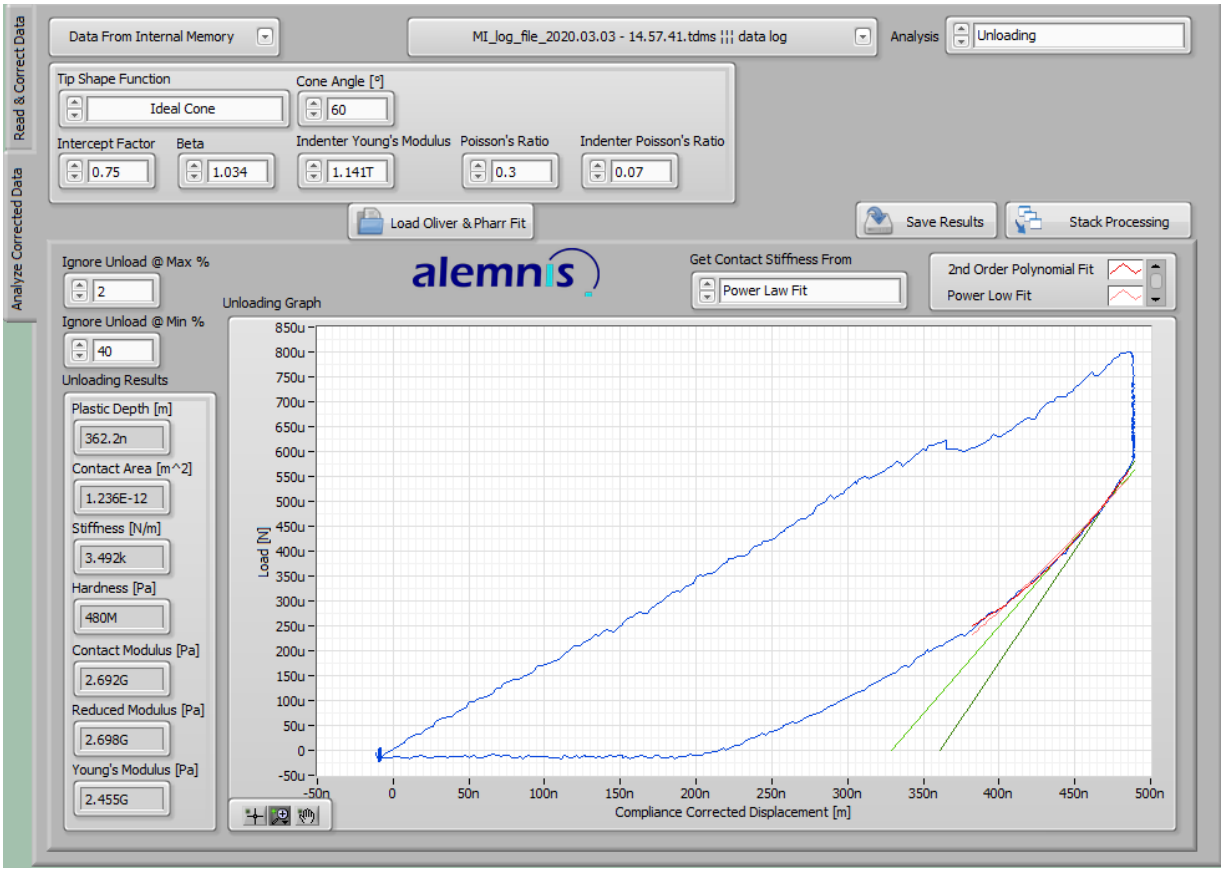

Figure 8.16: Physical properties of $PSMA_{30}PBzMA_{1000}$ nanoparticles using nanoindentor

contact to large compressions. These nanoparticles also display a low Young's modulus of 2.46 GPa. This means the nanoparticles are not stiff when stressed and, as a result, can compress easily in the contact. These nanoparticles result in a soft surface at the contact that can deform readily and, as a result, greatly reduced friction compared with the stiff steel surfaces (Young's modulus of 190-215 GPa).

8.5 Conclusions

PSMA-PBzMA nanoparticles were investigated to establish the mechanism by which they reduce friction within a contact. Film analysis was undertaken by spacial layer imaging and quartz crystal microscopy to investigate the most common mechanism in organic friction modifiers where a tribofilm forms and prevents surface contact. These show that all the PSMA-PBzMA nanoparticles form a tribofilm immediately after exposure to the contact,

with only $PSMA_{30}PBzMA_{200}$ nanoparticles not forming a full tribofilm in SLIM testing. These maximum tribofilms are greater when the PSMA nanoparticle is larger, or there is crosslinking present, and these larger nanoparticles also form more stable tribofilms. Spacial layer imaging of both crosslinked nanoparticles and the larger non-crosslinked nanoparticles shows maximum film thicknesses significantly larger than the nanoparticle diameter, suggesting that these nanoparticles appear to stack onto each other in some form. This may explain why these nanoparticles display an increase in friction in the mixed and hydrodynamic regime, as these thicker films may starve the contact of oil. The fact that the larger and more stable nanoparticles do not result in the largest increase in friction in the boundary regime suggests a different or synergistic mechanism is present, and this was investigated using nanoindenter SEM. Nanoindentor SEM was undertaken on $PSMA_{30}PBzMA_{1000}$ nanoparticles. These tests show these nanoparticles are compressed within the contact, preventing surface contact by spreading around the contact point. Upon removal of the compressive force, the nanoparticles elastically rebound and reform without any visible damage. This rebounding means this compression can be undertaken again within the contact resulting in long term effects. The physical properties of the nanoparticles display that they maintain their elastic properties to a deep compression and have a low Young's modulus, indicating that these nanoparticles can be readily compressed while maintaining soft and malleable properties. These nanoparticles can be highly compressed within a contact while being soft and easily sheared, resulting in a very low friction contact by preventing contact of the hard steel surfaces. This provides provide evidence for the entrapment mechanism that was theorised by Zheng et al. in their work discussed in chapter 4.(Zheng et al., 2010)

These results display a potential dual mechanism to decrease friction within the contact, forming a tribofilm and compressing a soft and malleable sphere to prevent contact. This dual mechanism shows why these nanoparticles can rapidly reduce friction and maintain this friction reduction across a variety of contact environments where a single mechanism may not be effective alone; a schematic of this dual mechanism is displayed in Figure 8.17.

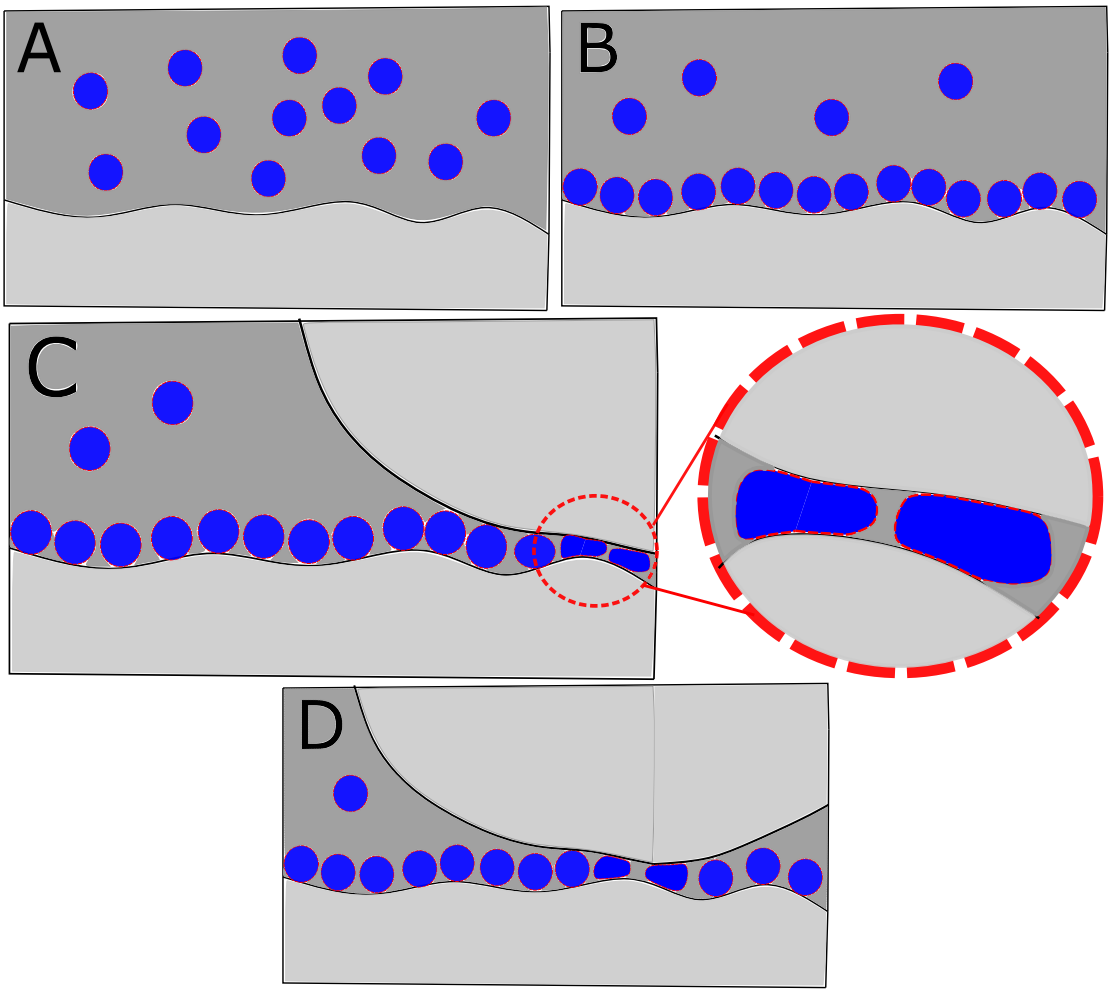

Figure 8.17: Dual mechanism for the reduction of friction by PSMA-PBzMA nanoparticles. A) PSMA-PBzMA nanoparticles enter the contact. B) The nanoparticles readily adsorb to the steel surface to form a tribofilm. C) The nanoparticles enter the contact and are compressed, preventing surface contact and forming a soft malleable counterface with significantly reduced friction. D) As the contact continues to move the nanoparticles elastically rebound to their original shape to allow for future friction reduction

Chapter 9 will investigate the ability of different chemistry nanoparticles and lubrication to reduce the friction of a contact. These experiments allow for confirmation of the findings of this chapter as the presence of a dual mechanism to reduce friction means that we would expect these very different nanoparticles also to display a friction-reducing capability

Chapter 9

Water Soluble Nanoparticles

9.1 Introduction

Thus far, all experiments have been undertaken on PSMA-PBzMA nanoparticles within mineral oil. These experiments have not yet shown whether the tribological improvements displayed above result from the nanoparticles within the contact or the specific chemical and physical interactions of the PSMA-PBzMA nanoparticles. This chapter charts experiments undertaken on nanoparticles in distilled water; these conditions are the exact opposite chemically to the previously studied nanoparticles. Here a non-polar polymer is stabilised by a polar polymer in a polar solvent, meaning that any tribological effects of these nanoparticles are unlikely to be due to the same chemical properties as the PSMA-PBzMA nanoparticles and may show that any tribological effect is the result of generic soft polymer nanoparticles being present within the contact. These experiments will be undertaken on two different sized nanoparticles, with and without crosslinking.

9.2 Method

9.2.1 Synthesis of Poly(N,N-dimethylacrylamide) (PDMAC) precursor via RAFT Solution Polymerization

A $PDMAC_{77}$ macro-CTA was synthesised via RAFT solution polymerisation of N,N-dimethylacrylamide (DMAC) in dioxane at 70 °C using a 2- (Dodecylthiocarbonothioylthio)-2-methylpropionic acid (DDMAT) RAFT agent, as previously described.(Byard et al., 2017) The purified $PDMAC_{77}$ precursor was obtained as a yellow solid. End-group analysis using UV spectroscopy indicated a mean degree of polymerisation of 77, and the Mn and Mw/Mn were 6900 g mol^{-1} and 1.24, respectively, as judged by DMF GPC.

9.2.2 Synthesis of $PDMAC_{77}PDAAM_X$ Diblock Copolymer Spheres by RAFT Aqueous Dispersion Polymerization

The typical protocol for the synthesis of $PDMAC_{77}PDAAM_{40}$ spheres was as follows. $PDMAC_{77}$ precursor (1.49 g, 0.022 mmol), ACVA (5.2 mg, 0.019 mmol, CTA/ACVA molar ratio = 10), and DAAM monomer (1.261 g, 7.5 mmol; target DP = 40) were weighed into a 50 ml round bottom flask. Deionised water adjusted to pH 2.5 with 1M HCl (24.76 mL) was added to give a 10% w/w aqueous solution, a nitrogen gas purge was undertaken for 30 min before addition to an oil bath at 70 °C. This solution was stirred for 4 h and then exposed to air to quench the reaction. The DAAM monomer conversion was greater than 99% according to 1H NMR spectroscopy, while the Mn and Mw/Mn were 9400 g mol^{-1} and 1.35, respectively, according to DMF GPC.

9.2.3 Post-polymerization Cross-Linking Using ADH

A typical protocol for cross-linking $PDMAC_{77}PDAAM_{40}$ spheres is as follows. A 10% w/w aqueous dispersion of $PDMAC_{77}PDAAM_{40}$ spheres (12.0 g) prepared using the previously stated methodology and adipic acid dihydrazide (ADH; 0.054 g, 0.37 mmol, DAAM/ADH molar ratio = 10.0) were added to a 20 ml vial. The solution was stirred at 25 °C for 6 h

9.2.4 1H NMR Spectroscopy

All NMR spectra were recorded using a 400 MHz Bruker Avance III HD 400 spectrometer in deuterated methanol at 25 °C.

Gel Permeation Chromatography (GPC)

Setup was comprised of two Agilent PL gel 5 μm Mixed-C columns and a guard column connected in series to an Agilent 1260 Infinity GPC system equipped with both refractive index and UV-vis detectors (only the refractive index detector used) at 60 °C. The GPC eluent was HPLC-grade DMF containing 10 mM LiBr at a flow rate of 1.0 ml min^{-1} . DMSO was used as a flow-rate marker. Calibration was achieved using a series of ten near-monodisperse poly(methyl methacrylate) standards (ranging in Mp from 625 to 618 000 g mol^{-1}). Results were analysed using Agilent GPC/SEC software.

9.2.5 Dynamic Light Scattering (DLS)

DLS was undertaken at 25 °C using a Malvern Zetasizer NanoZS instrument using the Stokes-Einstein equation, which assumes perfectly monodisperse, non-interacting spheres. Measurements were made on 0.1% w/w copolymer dispersions in deionised water or methanol using disposable plastic cuvettes. Data was averaged over three consecutive runs.

9.2.6 Mini-traction Machine

Stribeck curves were obtained using a PCS mini traction machine (PCS) consisting of 19.05mm diameter 52100 steel ball and 46mm diameter 52100 steel disc. The ball and disc are driven independently to create a SRR of 100%. Friction measurements were performed on mineral oil with and without 0.5% w/w additive at 25°C from 10-2500 mms^{-1} with a loading force of 35N. Two of these Stribeck curve runs were performed and separated by a 1 hour traction step at 50 mms^{-1}.

9.3 Results

9.3.1 Synthesis of PDMAC-PDAAM nanoparticles in Distilled Water

Table 9.1 shows the physical attributes of the nanoparticles synthesised. These nanoparticles were synthesised to high conversions (>99%) with good control of polymer chain length and form stable nanoparticles. The DLS results show a low dispersity index resulting in consistent sizes, and this should improve their friction reducing performance as more consistent film coverage should be achieved.

	GPC		DLS	
Sample	Mn (g mol^{-1})	PD	Size (nm)	PDI
$PDMAC_{77}PDAAM_{40}$	9361	1.35	23	0.09
$PDMAC_{77}PDAAM_{150}$	13530	1.36	44	0.05
$PDMAC_{77}PDAAM_{40}ADH_4$	N/A	N/A	28	0.05
$PDMAC_{77}PDAAM_{150}ADH_{15}$	N/A	N/A	41	0.09

Table 9.1: Synthesis of $PDMAC_{77}PDAAM_X$ nanoparticles

9.3.2 Friction of PDMAC-PDAAM nanoparticles in Distilled water

These experiments were identical to those undertaken on the PSMA-PBzMA nanoparticles for their initial friction profiles, as discussed in section 7.2.1, the only difference being that these experiments were performed at a lower temperature. The initial Stribeck curves for the water-based nanoparticles are shown in Figure 9.1.

These water-based nanoparticles all show a similar trend to the larger PSMA-PBzMA nanoparticles. Here friction below that observed with pure distilled water is present in the boundary lubrication regime, with low friction coefficients of around 0.03 compared to around 0.07 for the distilled water, before increasing as the speed of the contact increases. This lower friction indicates that these water-based nanoparticles prevent surface contact in the boundary regime before preventing the replenishment of lubricant or forming high viscosity films that disrupt water flow into the contact at higher speeds. The very high

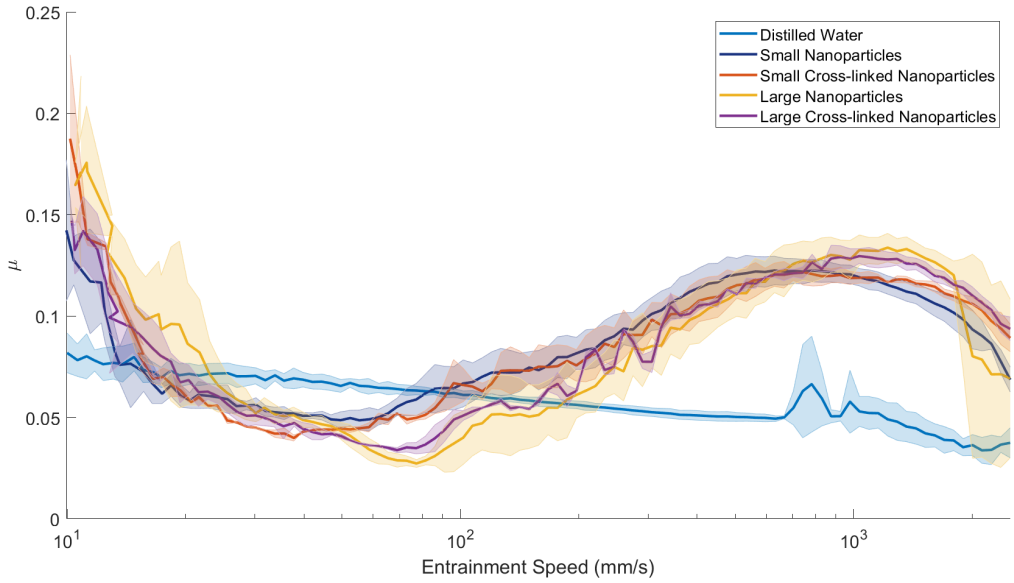

Figure 9.1: Initial Stribeck Curve for 0.5 wt% $PDMAC_{77}PDAAM_X$ nanoparticles

frictions at ultra-low speeds that are observed in the nanoparticle-containing liquids are somewhat strange. The friction coefficient observed here is often higher than that we would expect to observe for a pure steel-steel contact, 0.12. This means that these friction results are likely the result of inaccuracy in the force transducer at these very low speeds. This inaccuracy appears not to be the case once speeds greater than 20 mm/s are observed.

The boundary regime traction step results, shown in Figure 9.2, show that the larger water nanoparticles and the more stable crosslinked small nanoparticles display significantly lower friction in the boundary lubrication regime for a prolonged period. Here an approximate 50% reduction of friction is observed from 0.1 for water and 0.05 for the larger nanoparticles and 0.08 for the small crosslinked nanoparticles. The smaller non crosslinked nanoparticles, however, display a higher friction than the distilled water.

Upon completion of the traction step, a second Stribeck curve was undertaken, shown in Figure 9.3 Three of the nanoparticles display lower friction coefficients than the distilled water in the boundary lubrication regimes, with friction coefficients of around 0.05-0.08 compared with 0.1 for distilled water. The friction coefficient of these nanoparticles increases as the contact's speed increases, similarly to that observed in the initial Stribecks; this is likely due to the starvation of lubricant from the contact. However, the small non-

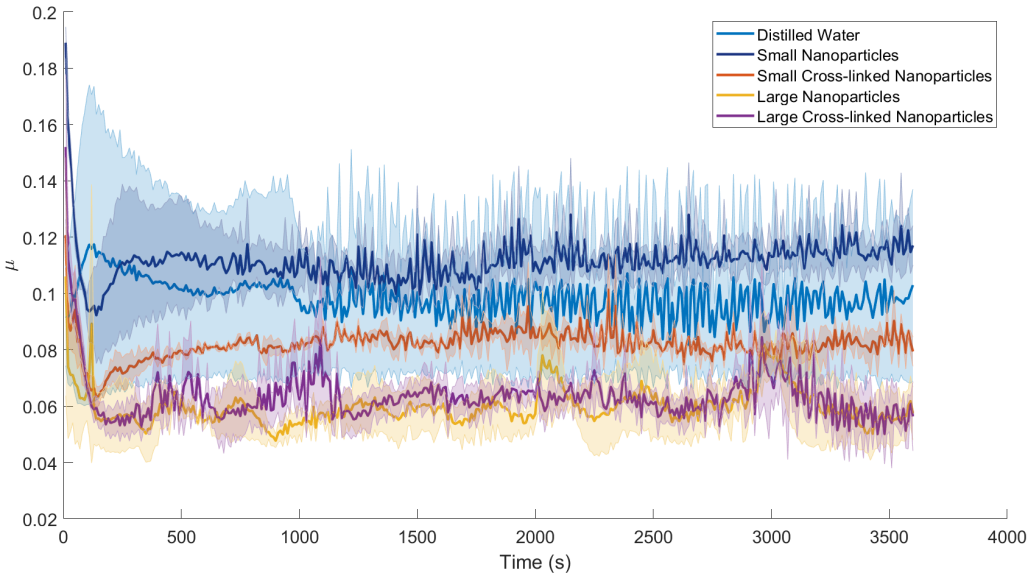

Figure 9.2: Boundary lubrication traction step for 0.5 wt% $PDMAC_{77}PDAAM_X$ nanoparticles

crosslinked nanoparticles display an equal to or higher friction coefficient than the distilled water across all contact speeds. This may be due to the breakdown of the nanoparticles throughout the test that results in the nanoparticles not being able to prevent surface contact; the higher friction at higher speeds, however, indicates that these nanoparticles do still result in the starvation of lubricant from the contact. In these tests, the maximum friction observed is around 0.16, significantly higher than that observed in a steel-steel contact of 0.12. This high friction is likely the result of rusting of the contact, which is observable on the balls and plates upon the completion of testing. These results show that the majority of these water-based nanoparticles reduce the coefficient of friction of the contact in the boundary lubrication regime and maintain this friction reduction throughout the testing, indicating a maintained stable low friction resulting from the water-based nanoparticles.

These reduced boundary lubrication frictions indicate that one of the mechanisms by which these PISA nanoparticles reduce friction is independent of the chemistry of the nanoparticles. As such, PISA nanoparticles' reduction of friction in the boundary lubrication regime may occur on all different chemistry nanoparticles. This means that

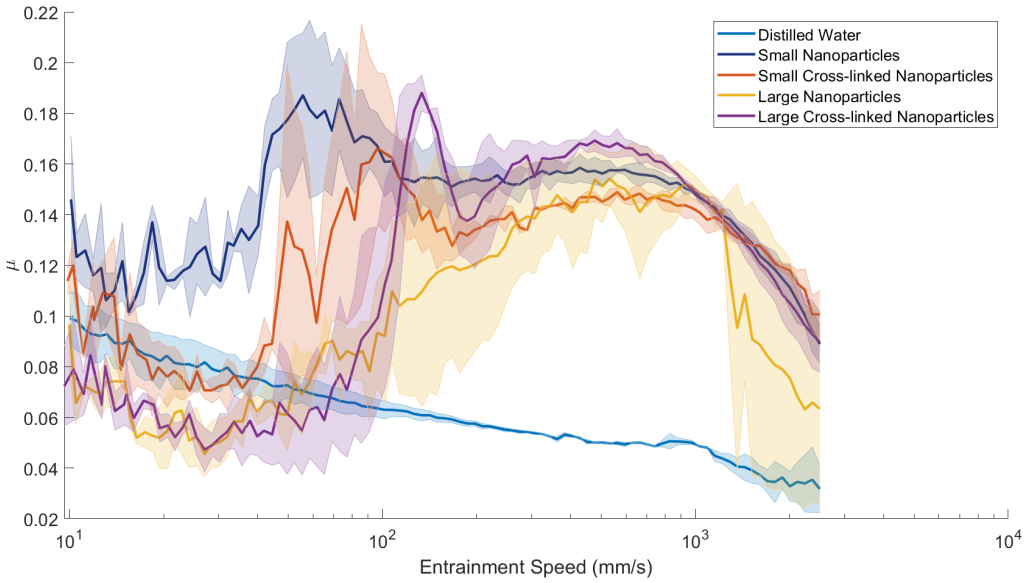

Figure 9.3: Final Stribeck curves for 0.5 wt% $PDMAC_{77}PDAAM_X$ nanoparticles

polymeric nanoparticle friction nanoparticles may be designed to be commercially viable based on a wide range of factors, e.g. cost of monomer, cost of synthesis, polymer stability etc. Rather than being designed purely based on their optimum chemistry to reduce friction.

These polymer nanoparticles display very different trends to many other soap systems previously investigated in the literature. While they display similar initial boundary regime performance to the P(SPMA-co-St) nanoparticles investigated by Li et al.(Li et al., 2018a) This effect is not maintained throughout the test with all the nanoparticles in this thesis displaying an increase in friction with time in the boundary regime unlike the development of a tribofilm to reduce friction that that is observed in P(SPMA-co-St) nanoparticles. This is likely the result of the nanoparticles reported by Li et al. both being significantly larger than those reported in this thesis at around 150-300nm, having a much harder core and also having a far more polar charged outer layer. This means they are much more able form a larger and more stable tribofilm upon the surface that can undertake large deformation and as such can maintain long term friction reduction. The smaller and more less mechanically stable nature of these nanoparticles means an effective tribofilm is less likely to form. These nanoparticles also do not act to reduce drag at higher speeds that is reported with

soaps in previous literature, with higher friction than water observed at higher contact speeds.(Savins, 1967; Patterson L Zakin J M Rodriguez, 1969; Rodriguez, 1971) This indicates that these nanoparticles are neither breaking down or forming polymers like traditional soaps and instead are likely forming a viscous film that is acting to disrupt flow of the oil leading to an increase in drag like the PSMA-PBzMA block nanoparticles discussed in this thesis.

These experiments were undertaken in distilled water at a pH of 5; previous work has shown that the PDMAC-PDAAM nanoparticles will have an anionic surface charge due to the ionisation of the terminal carboxylic acid group. This negatively charged surface will result in an attraction to the steel contact and, as a result, may improve their friction performance. It has been shown that by decreasing the pH of the solution, the carboxylic acid groups will be capped, resulting in a neutral surface charge. The following experiments were undertaken at pH 2; this allows us to compare the effect of the surface charge on frictional performance on otherwise identical nanoparticles.

9.4 Friction of PDMAC-PDAAM nanoparticles at pH 2

The neutralisation of the PDMAC-PDAAM nanoparticles results in a significant change in their friction performance, as shown in Figure 9.4. Here the neutralisation of the nanoparticle appears to result in a significant increase in friction of the contact, with friction significantly above that of the distilled water and peak frictions that are approximately equal to unlubricated steel contact. Here removal of the surface charge of the contact removes the friction-reducing properties of the nanoparticles and reduces the ability of the water to lubricate the contact. This finding is surprising as previous work by Zheng et al. demonstrated that neutral nanoparticles can still act as friction modifiers.(Zheng et al., 2010) There is also no apparent reason why these neutral nanoparticles actively hindered the friction performance of the water; this is because the lowest friction in the pH 2 nanoparticles is in the larger nanoparticles. This means that lubricant starvation or formation of highly viscous film to disrupt water flow is unlikely to be the source of the

issue as we would expect the larger nanoparticle to cause this more readily.

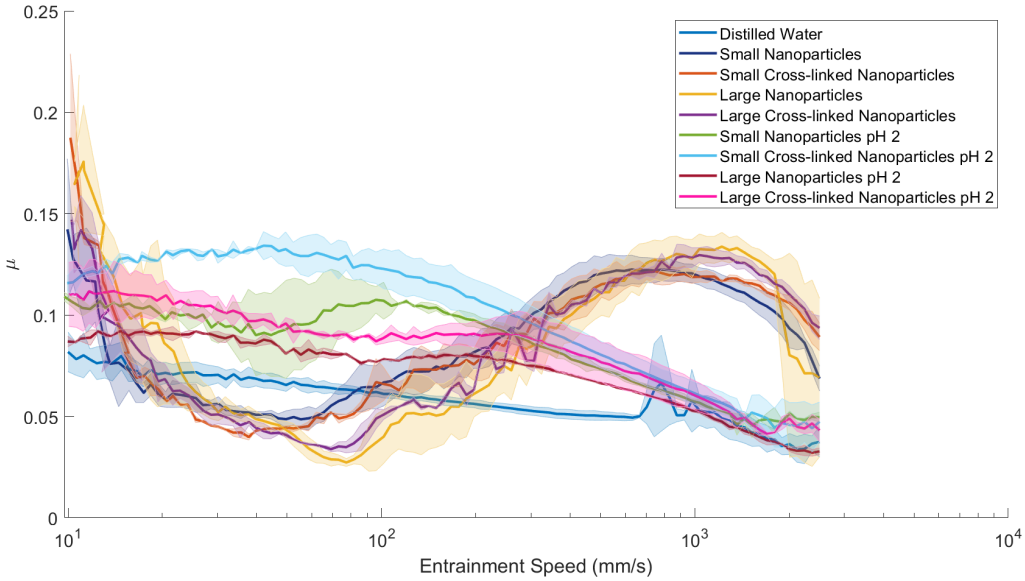

Figure 9.4: Initial Stribeck Curve for 0.5 wt% $PDMAC_{77}PDAAM_X$ nanoparticles at pH 2

The long term boundary traction step, shown in Figure 9.5, displays a similar trend to the initial Stribeck curve. Here the pH 2 samples display high friction equal to the friction of an unlubricated steel contact. However, the large crosslinked nanoparticles display slightly lower friction than the other nanoparticles, again indicating that the nanoparticles do not result in lubricant starvation.

The Stribeck curve upon completion of the traction step, Figure 9.6, show almost identical results to the initial Stribeck; this indicates that the friction increasing effect of the neutral nanoparticles is stable long term.

9.5 Conclusions

Two different sized PDMAC-PDAAM water-soluble nanoparticles, 23nm and 44nm, and their crosslinked equivalents were synthesised with good control. These nanoparticles are physically similar to the PSMA-PBzMA mineral oil soluble nanoparticles, discussed earlier in this thesis, and allow us to investigate whether the effect of self-assembled polymer nanoparticles as friction modifiers is universal or is chemistry specific. These nanoparticles

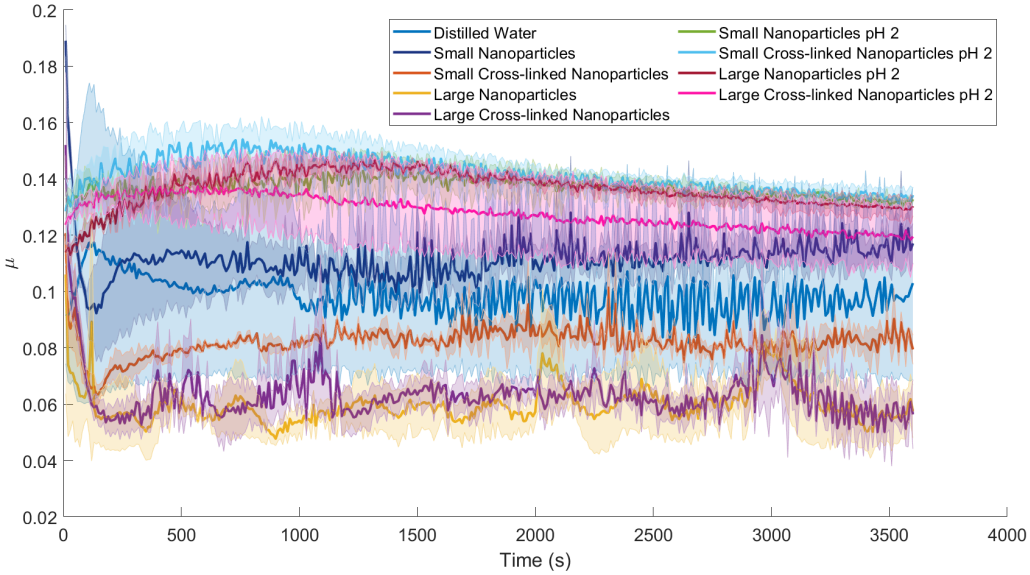

Figure 9.5: Boundary lubrication traction step for 0.5 wt% $PDMAC_{77}PDAAM_X$ nanoparticles at pH 2

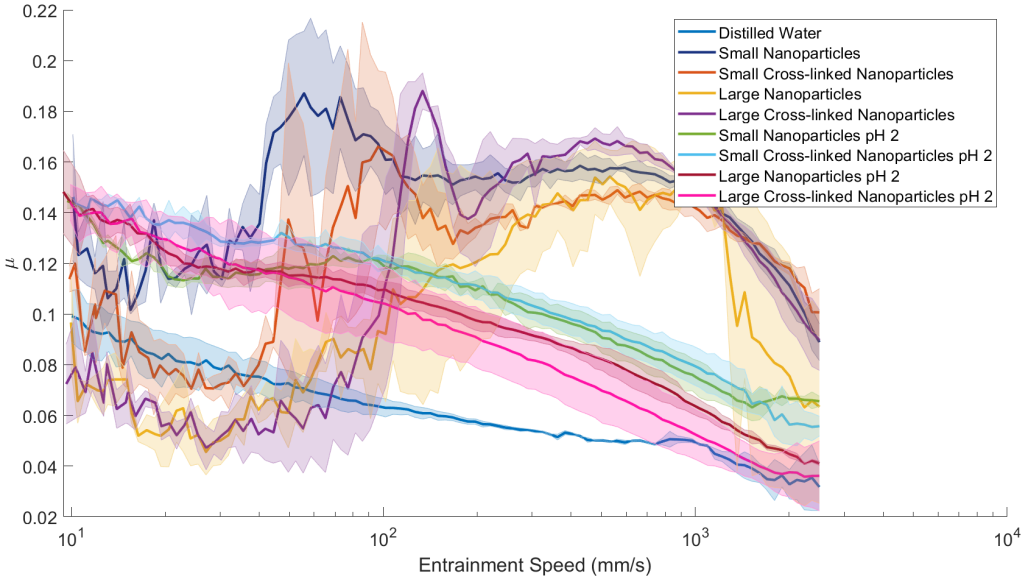

Figure 9.6: Final Stribeck Curve for 0.5 wt% $PDMAC_{77}PDAAM_X$ nanoparticles at pH 2

display sustained friction reduction in the boundary lubrication regime, with the larger 44nm nanoparticles displaying particularly low frictions. This friction reduction indicates that polymerisation self-assembled nanospheres are likely to be able to reduce the friction of the contact regardless of the specific chemistry of the block copolymers. Experiments at

pH 2 where the surface of the polymer will be neutral, however, show a significant increase in friction compared with distilled water. This indicates that a surface charge, and as a result, attraction to the contacting surfaces will at least improve, and maybe necessary, for these polymer nanoparticles to reduce friction within a contact. These results are contrary to previous work by Zheng et al., who showed that uncharged polymer nanoparticles in mineral oil could reduce friction within the contact.(Zheng et al., 2010) This means that the increase in friction may be specific to the water solvent or be the result of an unexpected effect of the higher pH liquid e.g. increased rusting of the contact.

However, these results demonstrate that a block copolymer nanoparticle that can adsorb to the contacting surface will act to reduce friction in the boundary lubrication regime of the contact and can be useful as friction modifiers. This means that a commercially viable polymeric nanoparticle friction modifier can be designed to consider multiple factors of design (e.g. cost, ease of synthesis, performance) rather than being limited to select polymer chemistries.

Chapter 10

Conclusions and Future Work

10.1 Conclusions

The development of friction modifiers is of utmost importance for the continued move towards more environmentally friendly engines and machines by reducing frictional losses. Although many friction modifiers are known, they often have negatives, and continued research into new products is critical.

Work undertaken by Zheng et al. and Derry et al. displayed the potential effectiveness of block copolymer nanospheres as friction modifiers, but these studies were limited. They did not give a complete understanding of these nanoparticles across multiple contact types and an understanding of how they reduce friction.

- Eleven different sized poly(stearylmethacrylate)$_{30}$-poly(benzylmethacrylate)$_{X}$ polymers were synthesised in mineral oil

  These polymers were prepared via a one-pot RAFT dispersion polymerisation using the acid group PETTC RAFT agent to generate a polar capping of the nanoparticles. These polymer chains will form nanospheres because the benzyl methacrylate block is insoluble within the mineral oil, and as such, the stearyl methacrylate block will wrap around the benzyl methacrylate core to form a stabilising block. Crosslinked versions of these nanoparticles were produced by adding ethylene glycol dimethacrylate to the core of the polymer nanoparticles; this should improve the stability of these

nanoparticles.

- Polymerisation was successful and nanoparticles were formed

  These polymer chains were synthesised with good control, as shown by GPC. The nanoparticles were highly ordered with slight variance in size distribution, as shown by DLS, TEM and SAXS. The size of these nanoparticles was shown to be controlled purely by altering the benzyl methacrylate block size, allowing for the size of the nanoparticles to be highly tuned. DLS in THF showed that crosslinking of the nanoparticles was successful and produced stable nanoparticles.

- Friction testing displays effective friction reduction by nanoparticles in particular in the boundary regime

  PCS MTM, TE54 and UMT testing demonstrated that these PSMA-PBzMA nanoparticles were able to reduce friction in the boundary lubrication regime across a variety of different contact environments including a linear contact at all sliding to rolling ratios as well as in a reciprocating contact.

- Smaller crosslinked $PSMA_{30}PBzMA_{X}PEGDMA_{X/10}$ (<30nm) nanoparticles can effectively reduce the friction across all contact environments tested.

  Across all contact types, rolling ratio and speeds the $PSMA_{30}PBzMA_{X}PEGDMA_{X/10}$ (<30nm) nanoparticles display a reduction in friction of the contact. With the non-crosslinked equivalent being effective in most contacts. These small polymer nanoparticles may be effective friction modifiers in an ICE.

- Larger $PSMA_{30}PBzMA_{X}EGDMA_{X/10}$ nanoparticles (>35nm) can effectively reduce friction in the boundary regime but show a significant increase in friction at higher contact speeds.

  This friction reduction in the boundary regime is present in most contacts both linear and reciprocating, the exception being at high sliding to rolling ratio continuous contacts. The non-crosslinked similarly sized nanoparticles display the same trend in some contacts but with smaller friction reduction in the boundary regime, however, this friction reduction is inconsistent.

- Nanoparticles have no effect on other tribological properties

  Studies into the effects of these nanoparticles on other tribological properties, i.e. wear of contact and viscosity of oil, show they have no effect from pure mineral oil, indicating that these nanoparticles will not have adverse effects on other functions of the motor oils. These results suggest that small crosslinked PSMA-PBzMA nanoparticles may be effective long term friction modifiers for an ICE.

- Nanoparticles are stable upon completion of tribological testing

  Testing was undertaken using viscosity, DLS and GPC to establish if the nanoparticles were still stable upon completion of tribological testing. These showed the presence of stable nanoparticles within the oil, indicating that any friction reduction due to these nanoparticles is long term.

- Nanoparticles form a stable tribofilm which can then compress, results in an ultra-low friction film between the contacting surfaces, and as a result, this friction is reduced.

  An understanding of the mechanism by which these nanoparticles reduce friction within a contact was undertaken. Film analysis of the nanoparticle tribofilm was undertaken by MTM spacial layer imaging and quartz crystal microbalance. These show a thick stable tribofilm being formed immediately upon the contact surface. The tribofilm is larger when the nanoparticle is larger and crosslinking is present, with larger nanoparticles forming a more stable tribofilm. These larger nanoparticles, however, display a large maximum film thickness. This film thickness is likely the result of nanoparticles stacking, which is likely what results in oil starvation of the contact. Nanoindentor SEM analysis showed these nanoparticles can be highly compressed within a contact while being soft and easily sheared. Upon removal of compression, these nanoparticles then elastically rebound and reform their original shape. These film and compression results mean that these nanoparticles are likely reducing friction via a dual mechanism.

- Water based nanoparticles show same effect indicating a universal friction reducing

capability

Testing of water-based PDMAC-PDAAM nanoparticles confirms that these findings are not specific to one particular chemistry nanoparticle and are likely universal across all block copolymer nanoparticles. With low pH tests, where the stabilising block will be uncharged, showing that having a charged stabilising block that will attract to the contact surface dramatically improves the friction-reducing capability.

These results show that block copolymer nanoparticles can be effective friction modifiers within motor oils. This friction is most effective with small (<30nm), crosslinked particles and where the outer block is attracted to the contacting surface. This friction reduction was shown to be the result of forming a soft, easily compressed and easily sheared tribofilm. This effect should be universal across all block copolymer PISA nanoparticles, and as such, the development of an ideal commercially viable friction modifier can take into account a wide variety of factors such as effectiveness, cost, ease of synthesis etc.

10.2 Future Work

While providing the basis to demonstrate how these PISA nanoparticles may be used as friction modifiers, much more work is required to fully understand the effectiveness and the mechanism by which these nanoparticles work as friction modifiers.

- Further testing in different contact environments is required.

  The majority of the tests undertaken were performed at similar contact pressures and temperatures. Understanding the effectiveness of these nanoparticles in other environments is necessary, e.g. are they also effective in low or ultra-high pressures, are they effective at engine start-up when oil is cold. Also, no testing has been undertaken on a reciprocating contact with some rolling within the contact. Understanding the friction modifier performance in the wide variety of environments that can occur within an ICE is vital for understanding if they can be effective.

- Further testing on other contact materials

These experiments were also only undertaken on a bearing steel contact. While steel is the most common material within an internal combustion engine, other materials are often present, e.g. coatings on components such as DLC. The steel components are also likely not as well machined and polished as the samples tested so far, and understanding the effectiveness of these nanoparticles in these contacts is essential.

- Fully formulated oil tests need to be undertaken

  No work has been undertaken to establish if these nanoparticles still reduce friction within fully formulated motor oils and ensure they do not negatively affect the performance of other oil additives. This is important as negatively affecting the performance of some additives, e.g. preventing the formation of ZDDP films to prevent wear, can have catastrophic effects on an ICE. Also, the nanoparticle additives will never be the only additive in the same way these tests have been, and as such, their ability to reduce friction has to be present with other additives present.

- Full in-engine tests

  The ultimate test to establish these nanoparticles as friction modifiers would be an in-engine test; this would allow for the most unambiguous indication as to the effectiveness of these nanoparticles. In-engine tests would allow for a full evaluation of their long term friction reducing ability and any other effects of their addition within the engine, e.g. potential soot removal from the oil similar to what was potentially observed with the TE54 samples after testing.

- Further testing of nanoparticle stability

  Further evaluation of the nanoparticle stability within the solution should be undertaken via a drip-fed system. Here all nanoparticles will be drawn through the contact, rather than potentially remain in the oil reservoir like the tests undertaken in this thesis. This testing would mean that any breakdown of the nanoparticle or polymer chain within the contact would be observable via viscosity, DLS or GPC measurements.

- Further tribofilm analysis

The mechanistic analysis of these nanoparticles detailed in this thesis details that a film is being formed, but it does not establish how it is formed. X-ray photoelectron spectroscopy (XPS) would establish the chemical bonding occurring at the surface and how these nanoparticles form the film. Further investigations into the chemistry of the tribofilm should also be undertaken such as Raman or IR spectroscopy. The potential to investigate the mechanical properties of the tribofilm using AFM to allow for an understanding of the effects of contact upon the tribofilm. XPS was attempted as part of this thesis, but this technique requires removing all the oil from the surface, and a cleaning technique could not be found that removes the oil without removing any nanoparticle film. These experiments could also be difficult to undertake due to the relatively low concentration of nanoparticle within the solution and as such the wear scar. As such experiments may be required using a greater concentration of nanoparticle in order to form a greater tribofilm.

- Compressive testing with lateral forces

  Analysis of the effects of physical pressures upon the nanoparticle film was also only undertaken by the compression tests detailed; this does not replicate a contact well as no lateral forces are applied. Testing with lateral forces could be undertaken using the nanoindenter SEM or with atomic force microscopy (AFM). This type of testing would require the formation of a film before removing oil present for testing; this again requires the issue of cleaning the samples similarly to the XPS tests detailed above.

- In-situ mechanism testing

  Most of the mechanistic analysis undertaken in this thesis was undertaken ex-situ, where the sample is removed from a regular contact for analysis. In situ analysis would allow for a clearer understanding of the nanoparticles mechanism within the contact. Film analysis would be possible using an elastohydrodynamic test rig, this works similarly to the MTM-SLIM, but instead, the light is shined through a glass disc contact. The film is measured as the ball is in contact with the disc, and so it is possible to observe how this contact affects the film. Analysis of the nanoparticle

in situ could also be performed by using a tribometer exposed to a syncatron light source, such as at the diamond light source. Here high energy electrons would be shined through the contact; the nanoparticles will scatter these electrons within the contact and, as such, would allow for imaging of the nanoparticles within the contact. This testing would allow for imaging of the effects of the contact upon the nanoparticles and confirm the mechanism by which they reduce friction.

Bibliography

Abdel-Hameed, H., Ahmed, N., and Nassar, A. (2015). *Some Ashless Detergent/Dispersant Additives for Lubricating Engine Oil*. PhD thesis, Ain Shams University, Cairo.

Askwith, T. C., Cameron, A., and Crouch, R. F. (1966). Chain length of additives in relation to lubricants in thin film and boundary lubrication. Technical Report 1427, Imperial College London.

Barnhill, W. C., Qu, J., Luo, H., Meyer, H. M., Ma, C., Chi, M., and Papke, B. L. (2014). Phosphonium-organophosphate ionic liquids as lubricant additives: Effects of cation structure on physicochemical and tribological characteristics. *ACS Applied Materials and Interfaces*, 6(24):22585–22593.

Battez, A. H., González, R., Viesca, J. L., Blanco, D., Asedegbega, E., and Osorio, A. (2009). Tribological behaviour of two imidazolium ionic liquids as lubricant additives for steel/steel contacts. *Wear*, 266(11-12):1224–1228.

Bercea, M. and Bercea, M. (2009). Friction reduction in rolling bearing by using polymer additives. *Lubrication Science*, 21:321–330.

Blanazs, A., Madsen, J., Battaglia, G., Ryan, A. J., and Armes, S. P. (2011). Mechanistic insights for block copolymer morphologies: How do worms form vesicles? *Journal of the American Chemical Society*, 133(41):16581–16587.

Bogunovic, L., Zuenkeler, S., Toensing, K., and Anselmetti, D. (2015). An Oil-Based Lubrication System Based on Nanoparticular TiO2 with Superior Friction and Wear Properties. *Tribology Letters*, 59(2):1–12.

Boodhoo, K. V. and Jachuck, R. J. (2000). Process intensification: Spinning disk reactor for styrene polymerization. *Applied Thermal Engineering*, 20(12):1127–1146.

Brinkhuis, R. P., Rutjes, F. P., and Van Hest, J. C. (2011). Polymeric vesicles in biomedical applications.

Brittain, W. J. and Minko, S. (2007). A structural definition of polymer brushes. *Journal of Polymer Science Part A: Polymer Chemistry*, 45(16):3505–3512.

Byard, S. J., Williams, M., McKenzie, B. E., Blanazs, A., and Armes, S. P. (2017). Preparation and Cross-Linking of All-Acrylamide Diblock Copolymer Nano-Objects via Polymerization-Induced Self-Assembly in Aqueous Solution. *Macromolecules*, 50(4):1482–1493.

Cameron, A. and Crouch, R. F. (1963). Interaction of hydrocarbon and surface-active agent. *Nature*, 198(4879):475–476.

Cann, P. M. (1996). Starvation and reflow in a grease-lubricated elastohydrodynamic contact. *Tribology Transactions*, 39(3):698–704.

Chevron (2022). Viscosity Modifiers | Chevron Oronite (Global).

Chinas, F., Vicent, J., and Spikes, H. A. (2003). Mechanism of Action of Colloidal Solid Dispersions. *Tribology Transactions*, 125:552–557.

Choo, J.-H., Forrest, A. K., and Spikes, H. A. (2007). Influence of Organic Friction Modifier on Liquid Slip: A New Mechanism of Organic Friction Modifier Action. *Tribology Letters*, 27(2):239–244.

Coffey, T. A., Forster, G. D., and Hogarth, G. (1996). Molybdenum(VI) imidodisulfur complexes formed via double sulfur-carbon bond cleavage of dithiocarbamates. *Journal of the Chemical Society - Dalton Transactions*, 2(1):183–193.

Colucci, W. and Fricke, K. (2007). Methods to improve the low temperature compatibility of amide friction modifiers in fuels and amide friction modifiers.

Cosimbescu, L., Robinson, J. W., Zhou, Y., and Qu, J. (2016). Dual functional star polymers for lubricants. *RSC Advances*, 6(89):86259–86268.

Cousseau, T., Björling, M., Graça, B., Campos, A., Seabra, J., and Larsson, R. (2012). Film thickness in a ball-on-disc contact lubricated with greases, bleed oils and base oils. *Tribology International*, 53:53–60.

De Barros'bouchet, M. I., Martin, J. M., Le-Mogne, T., and Vacher, B. (2005). Boundary lubrication mechanisms of carbon coatings by MoDTC and ZDDP additives. *Tribology International*, 38:257–264.

De Laurentis, N., Cann, P., Lugt, P. M., and Kadiric, A. (2017). The Influence of Base Oil Properties on the Friction Behaviour of Lithium Greases in Rolling/Sliding Concentrated Contacts. *Tribology Letters*, 65(4):1–16.

Derry, M. J., Fielding, L. A., and Armes, S. P. (2015). Industrially-relevant polymerization-induced self-assembly formulations in non-polar solvents: RAFT dispersion polymerization of benzyl methacrylate. *Polym. Chem.*, 6(16):3054–3062.

Derry, M. J., Fielding, L. A., and Armes, S. P. (2016a). Polymerization-induced self-assembly of block copolymer nanoparticles via RAFT non-aqueous dispersion polymerization. *Progress in Polymer Science*, 52:1–18.

Derry, M. J., Fielding, L. A., Warren, N. J., Mable, C. J., Smith, A. J., Mykhaylyk, O. O., and Armes, S. P. (2016b). In situ small-angle X-ray scattering studies of sterically-stabilized diblock copolymer nanoparticles formed during polymerization-induced self-assembly in non-polar media. *Chem. Sci.*, 7(8):5078–5090.

Derry, M. J., Mykhaylyk, O. O., and Armes, S. P. (2017). A Vesicle-to-Worm Transition Provides a New High-Temperature Oil Thickening Mechanism. *Angewandte Chemie International Edition*, 56:1746–1750.

Derry, M. J., Mykhaylyk, O. O., Ryan, A. J., and Armes, S. P. (2018). Thermoreversible crystallization-driven aggregation of diblock copolymer nanoparticles in mineral oil. *Chemical Science*, 9(17):4071–4082.

Derry, M. J., Smith, T., O'Hora, P. S., and Armes, S. P. (2019). Block Copolymer Nanoparticles Prepared via Polymerization-Induced Self-Assembly Provide Excellent Boundary Lubrication Performance for Next-Generation Ultralow-Viscosity Automotive Engine Oils. *ACS Applied Materials and Interfaces*, 11(36):33364–33369.

Desanker, M., He, X., Lu, J., Liu, P., Pickens, D. B., Delferro, M., Marks, T. J., Chung, Y. W., and Wang, Q. J. (2017). Alkyl-Cyclens as Effective Sulfur- and Phosphorus-Free Friction Modifiers for Boundary Lubrication. *ACS Applied Materials and Interfaces*, 9(10):9118–9125.

Discher, D. E. and Eisenberg, A. (2002). Polymer vesicles.

Doig, M., Warrens, C. P., and Camp, P. J. (2014). Structure and friction of stearic acid and oleic acid films adsorbed on iron oxide surfaces in squalane. *Langmuir*, 30(1):186–195.

Domingos Alves, E., Assis Oliveira, L. B., and Guilherme Colherinhas (2019). Understanding the stability of polypeptide membranes in ionic liquids: a theoretical molecular dynamics study. *New Journal of Chemistry*, 43(25):10151–10161.

Donnell, M. L., Lyon, A. J., Mormile, M. R., and Barua, S. (2016). Endotoxin hitchhiking on polymer nanoparticles. *Nanotechnology*, 27(28):285601.

Dowson, D. and Higginson, G. R. (1959). A Numerical Solution to the Elasto-Hydrodynamic Problem:. *Journal of Mechanical Engineering Science*, 1(1):6–15.

Erdemir, A. (2008). Boron-Based Solid Nanolubricants and Lubrication Additives. In *Nanolubricants*, pages 203–223. John Wiley & Sons, Ltd, Chichester, UK.

Eriksson, K. (2014). *Fatty Amines as Friction Modifiers in Engine Oils Correlating Adsorbed Amount to Friction and Wear Performance*. PhD thesis, Chalmers University of Technology Gothenburg.

Fan, J., Müller, M., Stöhr, T., and Spikes, H. A. (2007). Reduction of friction by functionalised viscosity index improvers. *Tribology Letters*, 28(3):287–298.

Feldman, Y., Frey, G. L., Homyonfer, M., Lyakhovitskaya, V., Margulis, L., Cohen, H., Hodes, G., Hutchison, J. L., and Tenne, R. (1996). Bulk synthesis of inorganic fullerene-like MS_2 (M = Mo, W) from the respective trioxides and the reaction mechanism. *Journal of the American Chemical Society*, 118(23):5362–5367.

Fischer, D., Mues, H., Jacobs, G., and Stratmann, A. (2019). Effect of Over Rolling Frequency on the Film Formation in Grease Lubricated EHD Contacts under Starved Conditions. *Lubricants 2019, Vol. 7, Page 19*, 7(2):19.

Ghaednia, H., Babaei, H., Jackson, R. L., Bozack, M. J., and Khodadadi, J. M. (2013). The effect of nanoparticles on thin film elasto-hydrodynamic lubrication. *Applied Physics Letters*, 103(26):263111.

Ghaednia, H., Hossain, M. S., and Jackson, R. L. (2016). Tribological Performance of Silver Nanoparticle–Enhanced Polyethylene Glycol Lubricants. *Tribology Transactions*, 59(4):585–592.

Ghaednia, H. and Jackson, R. L. (2013). The Effect of Nanoparticles on the Real Area of Contact, Friction, and Wear. *Journal of Tribology*, 135(4):041603.

Ghaednia, H., Jackson, R. L., and Khodadadi, J. M. (2015). Experimental analysis of stable CuO nanoparticle enhanced lubricants. *Journal of Experimental Nanoscience*, 10(1):1–18.

Gould, B., Demas, N. G., Pollard, G., Rydel, J. J., Ingram, M., and Greco, A. C. (2019). The Effect of Lubricant Composition on White Etching Crack Failures. *Tribology Letters*, 67(1).

Graham, J., Spikes, H., and Korcek, S. (2001). The friction reducing properties of molybdenum dialkyldithiocarbamate additives: part i — factors influencing friction reduction. *Tribology Transactions*, 44(4):626–636.

Grossiord, C., Varlot, K., Martin, J. M., Le Mogne, T., Esnouf, C., and Inoue, K. (1998). MoS 2 single sheet lubrication by molybdenum dithiocarbamate. *Tribology International*, 31(12):737–743.

Guegan, J., Kadiric, A., Gabelli, A., and Spikes, H. (2016). The Relationship Between Friction and Film Thickness in EHD Point Contacts in the Presence of Longitudinal Roughness. *Tribology Letters*, 64(3):1–15.

Guegan, J., Southby, M., and Spikes, H. (2019). Friction Modifier Additives, Synergies and Antagonisms. *Tribology Letters*, 67(3).

Hamley, I. W. (2000). The effect of shear on ordered block copolymer solutions. *Current Opinion in Colloid and Interface Science*, 5(5-6):341–349.

Hamley, I. W. (2001). Structure and flow behaviour of block copolymers. *Journal of Physics: Condensed Matter*, 13(33):R643–R671.

Hamley, I. W., Pople, J. A., Fairclough, J. P., Terrill, N. J., Ryan, A. J., Booth, C., Yu, G. E., Diat, O., Almdal, K., Mortensen, K., and Vigild, M. (1998). Effect of shear on cubic phases in gels of a diblock copolymer. *Journal of Chemical Physics*, 108(16):6929–6935.

Haque, T., Morina, A., Neville, A., Kapadia, R., and Arrowsmith, S. (2009). Effect of oil additives on the durability of hydrogenated DLC coating under boundary lubrication conditions. *Wear*, 266(1-2):147–157.

Hardy, W. B. and Doubleday, I. (1922). Boundary Lubrication. The Paraffin Series. *Proceedings of the Royal Society A: Mathematical, Physical and Engineering Sciences*, 100(707):550–574.

Hatton, F. L., Park, A. M., Zhang, Y., Fuchs, G. D., Ober, C. K., and Armes, S. P. (2019). Aqueous one-pot synthesis of epoxy-functional diblock copolymer worms from a single monomer: new anisotropic scaffolds for potential charge storage applications. *Polymer Chemistry*, 10(2):194–200.

Henriquez, C., Bueno, C., Lissi, E. A., and Encinas, M. V. (2003). Thiols as chain transfer agents in free radical polymerization in aqueous solution.

Herdan, J. M. (2000). Friction modifiers in engine and gear oils. *Lubrication Science*, 12(3):265–276.

Hernández Battez, A., González, R., Viesca, J., Fernández, J., Díaz Fernández, J., Machado, A., Chou, R., and Riba, J. (2008). CuO, ZrO2 and ZnO nanoparticles as antiwear additive in oil lubricants. *Wear*, 265(3-4):422–428.

Hertz, H. (1881). On the Contact of Elastic Solids. *Crelle's Journal*, 92:156–171.

Hill, D. J., O'Donnell, J. H., and O'Sullivan, P. W. (1985). Analysis of the Mechanism of Copolymerization of Styrene and Maleic Anhydride. *Macromolecules*, 18(1):9–17.

Holmberg, K., Andersson, P., and Erdemir, A. (2012). Global energy consumption due to friction in passenger cars. *Tribology International*, 47:221–234.

Hoshino, K., Kawai, H., and Akiyama, K. (1998). Fuel efficiency of SAE 5W-20 friction modified gasoline engine oil. In *SAE Technical Papers*. SAE International.

Hu, C., Bai, M., Lv, J., Liu, H., and Li, X. (2014). Molecular dynamics investigation of the effect of copper nanoparticle on the solid contact between friction surfaces. *Applied Surface Science*, 321:302–309.

Huang, G., Yu, Q., Ma, Z., Cai, M., and Liu, W. (2017). Probing the lubricating mechanism of oil-soluble ionic liquids additives. *Tribology International*, 107:152–162.

Huang, H., Hu, H., Qiao, S., Bai, L., Han, M., Liu, Y., and Kang, Z. (2015). Carbon quantum dot/CuSx nanocomposites towards highly efficient lubrication and metal wear repair. *Nanoscale*, 7(26):11321–11327.

Hutchings, I. M. and Shipway, P. (2017). *Tribology : friction and wear of engineering materials*. Butterworth-Heinemann, London, 2nd edition.

Ilavsky, J. and Jemian, P. R. (2009). Irena: Tool suite for modeling and analysis of small-angle scattering. *Journal of Applied Crystallography*, 42(2):347–353.

Ito, K. (1969). Effect of viscosity on termination rate constant in radical polymerization at low conversion. *Journal of Polymer Science Part A-1: Polymer Chemistry*, 7(9):2707–2710.

Jahanmir, S. (1985). Chain length effects in boundary lubrication. *Wear*, 102(4):331–349.

Johnson, K., Kendall, K., and Roberts, A. (1971). Surface energy and the contact of elastic solids. *Proceedings of The Royal Society A Mathematical Physical and Engineering Sciences*, 324(1558):301–313.

Johnson, M. D., Jensen, R. K., and Korcek, S. (1997). Base oil effects on friction reducing capabilities of molybdenum dialkyldithiocarbamate containing engine oils. In *SAE Technical Papers*. SAE International.

Joly-Pottuz, L., Bucholz, E. W., Matsumoto, N., Phillpot, S. R., Sinnott, S. B., Ohmae, N., and Martin, J. M. (2010). Friction properties of carbon nano-onions from experiment and computer simulations. *Tribology Letters*, 37(1):75–81.

Joly-Pottuz, L., Matsumoto, N., Kinoshita, H., Vacher, B., Belin, M., Montagnac, G., Martin, J. M., and Ohmae, N. (2008). Diamond-derived carbon onions as lubricant additives. *Tribology International*, 41(2):69–78.

Joo, Y., Agarkar, V., Sung, S. H., Savoie, B. M., and Boudouris, B. W. (2018). A nonconjugated radical polymer glass with high electrical conductivity. *Science*, 359(6382):1391–1395.

Kano, M. (2006). Super low friction of DLC applied to engine cam follower lubricated with ester-containing oil. *Tribology International*, 39(12):1682–1685.

Kasrai, M., Cutler, J. N., Gore, K., Canning, G., Bancroft, G. M., and Tan, K. H. (1998). The chemistry of antiwear films generated by the combination of zddp and modtc examined by x-ray absorption spectroscopy. *Tribology Transactions*, 41(1):69–77.

Kenbeek, D., Buenemann, T., and Rieffe, H. (2000). Review of Organic Friction Modifiers - Contribution to Fuel Efficiency? *SAE Technical Paper*.

Khadom, A. A., Hassan, A. F., and Abod, B. M. (2015). Evaluation of environmentally friendly inhibitor for galvanic corrosion of steel-copper couple in petroleum waste water. *Process Safety and Environmental Protection*, 98(1):93–101.

Khalkar, S., Bhowmick, D., and Pratap, A. (2013). Synthesis and Effect of Fatty Acid Amides as Friction Modifiers in Petroleum Base Stock. *Journal of Oleo Science*, 62(11):901–904.

Khare, V., Pham, M. Q., Kumari, N., Yoon, H. S., Kim, C. S., Park, J. I., and Ahn, S. H. (2013). Graphene-ionic liquid based hybrid nanomaterials as novel lubricant for low friction and wear. *ACS Applied Materials and Interfaces*, 5(10):4063–4075.

Kheireddin, B. A., Lu, W., Chen, I. C., and Akbulut, M. (2013). Inorganic nanoparticle-based ionic liquid lubricants. *Wear*, 303(1-2):185–190.

Klein, J., Kumacheva, E., Mahalu, D., Perahia, D., and Fetters, L. J. (1994). Reduction of frictional forces between solid surfaces bearing polymer brushes. *Nature*, 370(6491):634–636.

Klein, J., Kumacheva, E., Perahia, D., and Fetters, L. J. (1998). Shear forces between sliding surfaces coated with polymer brushes: the high friction regime. *Acta Polymerica*, 49(10-11):617–625.

Klumperman, B. (2010). Mechanistic considerations on styrene-maleic anhydride copolymerization reactions.

Kogovšek, J., Remškar, M., Mrzel, A., and Kalin, M. (2013). Influence of surface roughness and running-in on the lubrication of steel surfaces with oil containing MoS_2 nanotubes in all lubrication regimes. *Tribology International*, 61:40–47.

Lahouij, I., Bucholz, E. W., Vacher, B., Sinnott, S. B., Martin, J. M., and Dassenoy, F. (2012). Lubrication mechanisms of hollow-core inorganic fullerene-like nanoparticles: Coupling experimental and computational works. *Nanotechnology*, 23(37).

Lahouij, I., Dassenoy, F., De Knoop, L., Martin, J. M., and Vacher, B. (2011). In situ TEM observation of the behavior of an individual fullerene-like MoS 2 nanoparticle in a dynamic contact. *Tribology Letters*, 42(2):133–140.

Langmuir, I. (1920). The mechanism of the surface phenomena of flotation. *Transactions of the Faraday Society*, 15:62–74.

Lee, K., Hwang, Y., Cheong, S., Choi, Y., Kwon, L., Lee, J., and Kim, S. H. (2009). Understanding the role of nanoparticles in nano-oil lubrication. *Tribology Letters*, 35(2):127–131.

Li, B., Wang, X., Liu, W., and Xue, Q. (2006). Tribochemistry and antiwear mechanism of organic-inorganic nanoparticles as lubricant additives. *Tribology Letters*, 22(1):79–84.

Li, X., Deng, G., Zhang, Y., and Wang, J. (2019). Rapid removal of copper ions from aqueous media by hollow polymer nanoparticles. *Colloids and Surfaces A: Physicochemical and Engineering Aspects*, 568:345–355.

Li, Y., Zhang, S., Ding, Q., Li, H., Qin, B., and Hu, L. (2018a). Understanding the synergistic lubrication effect of 2-mercaptobenzothiazolate based ionic liquids and Mo nanoparticles as hybrid additives. *Tribology International*, 125:39–45.

Li, Z., Ma, S., Zhang, G., Wang, D., and Zhou, F. (2018b). Soft/Hard-Coupled Amphiphilic Polymer Nanospheres for Water Lubrication. *ACS Applied Materials and Interfaces*, 10(10):9178–9187.

Liati, A., Schreiber, D., Dimopoulos Eggenschwiler, P., and Arroyo Rojas Dasilva, Y. (2013). Metal particle emissions in the exhaust stream of diesel engines: An electron microscope study. *Environmental Science and Technology*, 47(24):14495–14501.

Lin, J., Wang, L., and Chen, G. (2011). Modification of graphene platelets and their tribological properties as a lubricant additive. *Tribology Letters*, 41(1):209–215.

Lovell, M. R., Kabir, M. A., Menezes, P. L., and Higgs, C. F. (2010). Influence of boric acid additive size on green lubricant performance. *Philosophical Transactions of the Royal Society A: Mathematical, Physical and Engineering Sciences*, 368(1929):4851–4868.

Mahrova, M., Pagano, F., Pejakovic, V., Valea, A., Kalin, M., Igartua, A., and Tojo, E. (2015). Pyridinium based dicationic ionic liquids as base lubricants or lubricant additives. *Tribology International*, 82(PA):245–254.

Malhotra, B. D. and Ali, M. A. (2018). Functionalized Carbon Nanomaterials for Biosensors. In *Nanomaterials for Biosensors*, pages 75–103. Elsevier.

Martin, J. M., Grossiord, C., Varlot, K., Vacher, B., and Igarashi, J. (2000). Synergistic effects in binary systems of lubricant additives: A chemical hardness approach. *Tribology Letters*, 8(4):193–201.

Masilela, S. R. and De Vaal, P. L. (2019). The tribological characteristics of selected base oils under oscillatory sliding conditions. *STLE 2019 - 74th Annual Meeting and Exhibition of the Society of Tribologists and Lubrication Engineers*.

Mezghani, S., Demirci, I., Yousfi, M., and El Mansori, M. (2013). Running-in wear modeling of honed surface for combustion engine cylinderliners. *Wear*, 302(1-2):1360–1369.

Miklozic, K. T., Graham, J., and Spikes, H. (2001). Chemical and physical analysis of reaction films formed by molybdenum dialkyl-dithiocarbamate friction modifier additive using Raman and atomic force microscopy. *Tribology Letters*, 11(2):71–81.

Miller, A. L., Stipe, C. B., Habjan, M. C., and Ahlstrand, G. G. (2007). Role of Lubrication Oil in Particulate Emissions from a Hydrogen-Powered Internal Combustion Engine. *Environmental Science and Technology*, 41(19):6828–6835.

Minami, I. and Mori, S. (2007). Concept of molecular design towards additive technology for advanced lubricants. *Lubrication Science*, 19(2):127–149.

Mitchell R.Dorfman (2012). *Handbook of Environmental Degradation of Materials:Thermal Spray Coatings*, volume 19. Elsevier Inc.

Morina, A. and Neville, A. (2007). Understanding the composition and low friction tribofilm formation/removal in boundary lubrication. *Tribology International*, 40(10-12 SPEC. ISS.):1696–1704.

Muller, M., Jingyan, F., and Spikes, H. (2008). Design of functionalized PAMA viscosity modifiers to reduce friction and wear in lubricating oils. *Journal of ASTM International 4*, 10:116–125.

Müller, M., Topolovec-Miklozic, K., Dardin, A., and Spikes, H. A. (2006). The design of boundary film-forming pma viscosity modifiers. *Tribology Transactions*, 49(2):225–232.

Okubo, H., Tadokoro, C., Sumi, T., Tanaka, N., and Sasaki, S. (2019). Wear acceleration mechanism of diamond-like carbon (DLC) films lubricated with MoDTC solution: Roles of tribofilm formation and structural transformation in wear acceleration of DLC films lubricated with MoDTC solution. *Tribology International*, 133:271–287.

Padgurskas, J., Rukuiza, R., Prosyčevas, I., and Kreivaitis, R. (2013). Tribological properties of lubricant additives of Fe, Cu and Co nanoparticles. *Tribology International*, 60:224–232.

Parsaeian, P., Van Eijk, M. C., Nedelcu, I., Neville, A., and Morina, A. (2017). Study of the interfacial mechanism of ZDDP tribofilm in humid environment and its effect on tribochemical wear; Part I: Experimental. *Tribology International*, 107:135–143.

Patterson L Zakin J M Rodriguez, K. J. (1969). DRAG REDUCTION Polymer Solutions, Soap Solutions and Solid Particle Suspensions in Pipe Flow. *Industrial and Engineering Chemistry Research*, 61(1):31.

PCS Instruments (2005). MTM2 Mini-Traction Machine. Technical report, PCS Instruments.

Pedersen, J. S. and Gerstenberg, M. C. (1996). Scattering Form Factor of Block Copolymer Micelles. *Macromolecules*, 29(4):1363–1365.

Philippon, D., De Barros-Bouchet, M. I., Lerasle, O., Le Mogne, T., and Martin, J. M. (2011). Experimental simulation of tribochemical reactions between borates esters and steel surface. *Tribology Letters*, 41(1):73–82.

Pople, J. A., Hamley, I. W., and Diakun, G. P. (1998). An integrated Couette system for in situ shearing of polymer and surfactant solutions and gels with simultaneous small angle x-ray scattering. *Review of Scientific Instruments*, 69(8):3015–3021.

Qu, J., Bansal, D. G., Yu, B., Howe, J. Y., Luo, H., Dai, S., Li, H., Blau, P. J., Bunting, B. G., Mordukhovich, G., and Smolenski, D. J. (2012). Antiwear performance and mechanism of an oil-miscible ionic liquid as a lubricant additive. *ACS Applied Materials and Interfaces*, 4(2):997–1002.

Qu, J., Barnhill, W. C., Luo, H., Meyer, H. M., Leonard, D. N., Landauer, A. K., Kheireddin, B., Gao, H., Papke, B. L., and Dai, S. (2015). Synergistic Effects between Phosphonium-Alkylphosphate Ionic Liquids and Zinc Dialkyldithiophosphate (ZDDP) as Lubricant Additives. *Advanced Materials*, 27(32):4767–4774.

Rapoport, L., Bilik, Y., Feldman, Y., Homyonfer, M., Cohen, S. R., and Tenne, R. (1997). Hollow nanoparticles of WS_2 as potential solid-state lubricants. *Nature*, 387(6635):791–793.

Rapoport, L., Fleischer, N., and Tenne, R. (2003). Fullerene-like WS_2 Nanoparticles: Superior Lubricants for Harsh Conditions. *Advanced Materials*, 15(78):651–655.

Ratoi, M., Niste, V. B., Alghawel, H., Suen, Y. F., and Nelson, K. (2014). The impact of organic friction modifiers on engine oil tribofilms. *RSC Adv.*, 4(9):4278–4285.

Reynolds, O. (1886). On the Theory of Lubrication and Its Application to Mr. Beauchamp Tower's Experiments. *Proceedings of Royal Society of London.*

Risdon, T. J. and Gresty, D. A. (1975). An historical review of reductions in fuel consumption of United States and European engines with MoS_2. In *SAE Technical Papers*. SAE International.

Rivera, N., Blanco, D., Viesca, J. L., Fernández-González, A., González, R., and Battez, A. H. (2019). Tribological performance of three fatty acid anion-based ionic liquids (FAILs) used as lubricant additive. *Journal of Molecular Liquids*, 296:111881.

Robinson, J. W., Zhou, Y., Bhattacharya, P., Erck, R., Qu, J., Bays, J. T., and Cosimbescu, L. (2016a). Probing the molecular design of hyper-branched aryl polyesters towards lubricant applications. *Scientific Reports*, 6(1):18624.

Robinson, J. W., Zhou, Y., Qu, J., Bays, J. T., and Cosimbescu, L. (2016b). Highly branched polyethylenes as lubricant viscosity and friction modifiers. *Reactive and Functional Polymers*, 109:52–55.

Rodriguez, F. (1971). Drag Reduction by a Polymeric Aluminium Soap. *Nature Physical Science*, 230(15):152–153.

Rong-Hua, J. (1985). Effects of the composition and fibrous texture of lithium soap grease on wear and friction. *Tribology International*, 18(2):121–124.

Saccomando, D. J., Vickerman, R. J., and Patterson, S. M. (2012). Amine Derivatives as Friction Modifiers in Lubricants.

Samy, A. M., Mahmoud, M. M., Khashaba, M. I., and Ali, W. Y. (2007). Friction of rubber sliding against ceramics part II1: Influence of oil and oil-water lubrication. Technical Report 12, KGK.

Sarin, R., Tuli, D. K., Sureshbabu, A. V., Misra, A. K., Rai, M. M., and Bhatnagar, A. K. (1994). Molybdenum dialkylphosphorodithioates: synthesis and performance evaluation as multifunctional additives for lubricants. *Tribology International*, 27(6):379–386.

Savins, J. G. (1967). A stress-controlled drag-reduction phenomenon. *Rheologica Acta 1967 6:4*, 6(4):323–330.

Scarano, S., Mariani, S., and Minunni, M. (2016). Label free Affinity sensing: Application to food analysis. *Acta IMEKO*, 5(1):36–44.

Shah, F. U., Glavatskih, S., and Antzutkin, O. N. (2012). Novel alkylborate-dithiocarbamate lubricant additives: Synthesis and tribophysical characterization. *Tribology Letters*, 45(1):67–78.

Shah, F. U., Glavatskih, S., and Antzutkin, O. N. (2013). Boron in Tribology: From Borates to Ionic Liquids. *Tribology Letters 2013 51:3*, 51(3):281–301.

Shah, F. U., Glavatskih, S., Höglund, E., Lindberg, M., and Antzutkin, O. N. (2011). Interfacial antiwear and physicochemical properties of alkylborate- dithiophosphates. *ACS Applied Materials and Interfaces*, 3(4):956–968.

Somers, A. E., Khemchandani, B., Howlett, P. C., Sun, J., Macfarlane, D. R., and Forsyth, M. (2013). Ionic liquids as antiwear additives in base oils: Influence of structure on miscibility and antiwear performance for steel on aluminum. *ACS Applied Materials and Interfaces*, 5(22):11544–11553.

Song, W., Yan, J., and Ji, H. (2019). Fabrication of GNS/MoS 2 composite with different morphology and its tribological performance as a lubricant additive. *Applied Surface Science*, 469:226–235.

Song, X., Zheng, S., Zhang, J., Li, W., Chen, Q., and Cao, B. (2012). Synthesis of monodispersed ZnAl2O4nanoparticles and their tribology properties as lubricant additives. *Materials Research Bulletin*, 47(12):4305–4310.

Song, Z., Liang, Y., Fan, M., Zhou, F., and Liu, W. (2014). Ionic liquids from amino acids: Fully green fluid lubricants for various surface contacts. *RSC Advances*, 4(37):19396–19402.

Spengler, G. and Weber, A. (1959). Über die Schmierfähigkeit organischer Molybdänverbindungen. *Chemische Berichte*, 92(9):2163–2171.

Spikes, H. (2015). Friction Modifier Additives. *Tribology Letters*, 60(1).

Spikes, H. A. (1989). Additive-additive and additive-surface interactions in lubrication. *Lubrication Science*, 2(1):3–23.

Spikes, H. A. (2003). The half-wetted bearing. Part 1: Extended Reynolds equation. Technical Report 1, Imperial College.

Stolte, S., Steudte, S., Areitioaurtena, O., Pagano, F., Thöming, J., Stepnowski, P., and Igartua, A. (2012). Ionic liquids as lubricants or lubrication additives: An ecotoxicity and biodegradability assessment. *Chemosphere*, 89(9):1135–1141.

Studt, P. (1989). Boundary lubrication: adsorption of oil additives on steel and ceramic surfaces and its influence on friction and wear. *Tribology International*, 22(2):111–119.

Tanaka, N., Fukushima, A., Tatsumi, Y., and Saito, Y. (1997). Lubricating oil composition.

Tang, H.-Z. and Jao, T.-C. (2013). Detergent Additives. In *Encyclopedia of Tribology*, pages 720–726. Springer, Boston, MA.

Tannous, J., Dassenoy, F., Bruhács, A., and Tremel, W. (2010). Synthesis and Tribological Performance of Novel $Mo_xW_{1-x}S_2$ ($0 \leq x \leq 1$) Inorganic Fullerenes. *Tribology Letters*, 37(1):83–92.

Tenne, R., Margulis, L., Genut, M., and Hodes, G. (1992). Polyhedral and cylindrical structures of tungsten disulphide. *Nature*, 360(6403):444–446.

Tevet, O., Von-Huth, P., Popovitz-Biro, R., Rosentsveig, R., Wagner, H. D., and Tenne, R. (2011). Friction mechanism of individual multilayered nanoparticles. *Proceedings of the National Academy of Sciences of the United States of America*, 108(50):19901–19906.

Topolovec-Miklozic, K., Lockwood, F., and Spikes, H. (2008). Behaviour of boundary lubricating additives on DLC coatings. *Wear*, 265(11-12):1893–1901.

Trent, J. S. (1984). Ruthenium Tetraoxide Staining of Polymers: New Preparative Methods for Electron Microscopy. *Macromolecules*, 17(12):2930–2931.

Tsuchida, E. and Tomono, T. (1971). Discussion on the mechanism of alternating copolymerization of styrene and maleic anhydride. *Die Makromolekulare Chemie*, 141(1):265–298.

Tynik, R. J., Donnelly, S. G., and Karol, T. J. (2010). Molybdenum dialkyldithiocarbamate compositions and lubricating compositions containing the same.

Van Egmond, J. W. (1998). Shear-thickening in suspensions, associating polymers, wormlike micelles, and poor polymer solutions. *Current Opinion in Colloid and Interface Science*, 3(4):385–390.

Vengudusamy, B., Green, J. H., Lamb, G. D., and Spikes, H. A. (2012). Behaviour of MoDTC in DLC/DLC and DLC/steel contacts. *Tribology International*, 54:68–76.

Wells, H. M. and Southcombe, J. E. (1920). *The theory and practice of lubrication: the "Germ" process.* Central House.

Windom, B. C., Sawyer, W. G., and Hahn, D. W. (2011). A raman spectroscopic study of MoS 2 and MoO 3: Applications to tribological systems. *Tribology Letters*, 42(3):301–310.

Winer, W. O. (1967). Molybdenum disulfide as a lubricant: A review of the fundamental knowledge. *Wear*, 10(6):422–452.

Wu, Y. Y. and Kao, M. J. (2011). Using TiO2/DN nanofluid additive for engine lubrication oil. *Industrial Lubrication and Tribology*, 63(6):440–445.

Xu, Y., Peng, Y., Zheng, X., Dearn, K. D., Xu, H., and Hu, X. (2015). Synthesis and tribological studies of nanoparticle additives for pyrolysis bio-oil formulated as a diesel fuel. *Energy*, 83:80–88.

Yamamoto, Y., Gondo, S., Kamakura, T., and Konishi, M. (1987). Organoamine and organophosphate molybdenum complexes as lubricant additives. *Wear*, 120(1):51–60.

Yang, J., Zhang, H., Chen, B., Tang, H., Li, C., and Zhang, Z. (2015). Fabrication of the g-C3N4/Cu nanocomposite and its potential for lubrication applications. *RSC Advances*, 5(79):64254–64260.

Yang, L., Neville, A., Brown, A., Ransom, P., and Morina, A. (2014). Friction reduction mechanisms in boundary lubricated W-doped DLC coatings. *Tribology International*, 70:26–33.

Yazawa, S., Minami, I., and Prakash, B. (2014). Reducing Friction and Wear of Tribological Systems through Hybrid Tribofilm Consisting of Coating and Lubricants. *Lubricants*, 2:90–112.

Ye, C., Liu, W., Chen, Y., and Yu, L. (2001). Room-temperature ionic liquids: A novel versatile lubricant. *Chemical Communications*, 21(21):2244–2245.

Yilmaz, A. C. (2020). Tribological Enhancement Features of Various Nanoparticles as Engine Lubricant Additives: An Experimental Study. *Arabian Journal for Science and Engineering*, 45(2):1125–1134.

Zhang, J. and Spikes, H. (2016). On the Mechanism of ZDDP Antiwear Film Formation. *Tribology Letters*, 63(2):1–15.

Zhang, M., Wang, X., Liu, W., and Fu, X. (2009). Performance and anti-wear mechanism of Cu nanoparticles as lubricating oil additives. *Industrial Lubrication and Tribology*, 61(6):311–318.

Zhang, Y., Park, A., Cintora, A., McMillan, S. R., Harmon, N. J., Moehle, A., Flatté, M. E., Fuchs, G. D., and Ober, C. K. (2017). Impact of the synthesis method on the solid-state charge transport of radical polymers. *Journal of Materials Chemistry C*, 6(1):111–118.

Zhang, Y., Tang, H., Ji, X., Li, C., Chen, L., Zhang, D., Yang, X., and Zhang, H. (2013). Synthesis of reduced graphene oxide/Cu nanoparticle composites and their tribological properties. *RSC Advances*, 3(48):26086–26093.

Zhang, Z., Yan, W., Chen, Q., Zhou, N., and Xu, Y. (2019). The relationship between exposure to particulate matter and breast cancer incidence and mortality: A meta-analysis. *Medicine*, 98(50).

Zhao, H., Neville, A., Morina, A., Vickerman, R., and Durham, J. (2012). Improved anti-shudder performance of ATFs-Influence of a new friction modifier and surface chemistry. *Tribology International*, 46(1):62–72.

Zheng, J., Zhou, C., Yu, M., and Liu, J. (2012). Different sized luminescent gold nanoparticles. *Nanoscale*, 4(14):4073.

Zheng, R. H., Liu, G. J., Devlin, M., Hux, K., and Jao, T. C. (2010). Friction Reduction of Lubricant Base Oil by Micelles and Crosslinked Micelles of Block Copolymers. *Tribology Transactions*, 53(1):97–107.

Zhou, Y., Dyck, J., Graham, T. W., Luo, H., Leonard, D. N., and Qu, J. (2014). Ionic liquids composed of phosphonium cations and organophosphate, carboxylate, and sulfonate anions as lubricant antiwear additives. *Langmuir*, 30(44):13301–13311.

Copyright Permissions

Figure 4.11: Fan, J., Müller, M., Stöhr, T., and Spikes, H. A. (2007). Reduction of friction by functionalised viscosity index improvers. *Tribology Letters*, 28(3):287–298. Reprinted with permission ©2007 Springer Science Business Media, LLC.

Figure 4.12: Bercea, M. and Bercea, M. (2009). Friction reduction in rolling bearing by using polymer additives. *Lubrication Science*, 21:321–330. Reprinted with permission ©2009 John Wiley & Sons, Ltd.

Figure 4.13: Robinson, J. W., Zhou, Y., Bhattacharya, P., Erck, R., Qu, J., Bays, J. T., and Cosimbescu, L. (2016a). Probing the molecular design of hyper-branched aryl polyesters towards lubricant applications. *Scientific Reports*, 6(1):18624. Adapted with permission ©CC BY 4.0, https://creativecommons.org/licenses/by/4.0/legalcode

Figure 4.15: Huang, G., Yu, Q., Ma, Z., Cai, M., and Liu, W. (2017). Probing the lubricating mechanism of oil-soluble ionic liquids additives. *Tribology International*, 107:152–162. Reprinted with permission ©2016 Elsevier Ltd.

Figure 4.16: Qu, J., Barnhill, W. C., Luo, H., Meyer, H. M., Leonard, D. N., Landauer, A. K., Kheireddin, B., Gao, H., Papke, B. L., and Dai, S. (2015). Synergistic Effects between Phosphonium-Alkylphosphate Ionic Liquids and Zinc Dialkyldithiophosphate (ZDDP) as Lubricant Additives. *Advanced Materials*, 27(32):4767–4774. Reprinted with permission ©2015 Wiley-VCH Verlag GmbH & Co. KGaA, Weinheim.

Figure 4.17: Grossiord, C., Varlot, K., Martin, J.M., Le Mogne, T., Esnouf, C., and Inoue, K. (1998). MoS_2 single sheet lubrication by molybdenum dithiocarbamate. *Tribology International*, 31(12):737–743. Reprinted with permission ©1999 Elsevier Science Ltd.

Figure 4.18: Grossiord, C., Varlot, K., Martin, J.M., Le Mogne, T., Esnouf, C., and Inoue, K. (1998). MoS_2 single sheet lubrication by molybdenum dithiocarbamate. *Tribology International*, 31(12):737–743. Reprinted with permission ©1999 Elsevier Science Ltd.

Figure 4.19: Spikes, H. (2015). Friction Modifier Additives. *Tribology Letters*, 60(1). Reprinted with permission ©2015 Springer Science Business Media New York.

Figure 8.17: Lee, K., Hwang, Y., Cheong, S., Choi, Y., Kwon, L., Lee, J., and Kim, S. H. (2009). Understanding the role of nanoparticles in nano-oil lubrication. *Tribology Letters*, 35(2):127–131. Reprinted with permission ©2009 Springer Science Business Media, LLC.

Figure 4.21: Malhotra, B. D. and Ali, M. A. (2018). Functionalized Carbon Nanomaterials for Biosensors. In *Nanomaterials for Biosensors*, pages 75–103. Reprinted with permission ©2018 Elsevier Inc.

Figure 4.23: Lahouij, I., Bucholz, E. W., Vacher, B., Sinnott, S. B., Martin, J. M., and Dassenoy, F. (2012). Lubrication mechanisms of hollow-core inorganic fullerene-like nanoparticles: Coupling experimental and computational works. *Nanotechnology*, 23(37). Reprinted with Permission ©2012 IOP Publishing Ltd.

Figure 4.24: Joly-Pottuz, L., Bucholz, E. W., Matsumoto, N., Phillpot, S. R., Sinnott, S. B., Ohmae, N., and Martin, J. M. (2010). Friction properties of carbon nano-onions from experiment and computer simulations. *Tribology Letters*, 37(1):75–81. Reprinted with permission ©2009 Springer Science Business Media, LLC.

Figure 4.25: Li, B., Wang, X., Liu, W., and Xue, Q. (2006). Tribochemistry and anti-wear mechanism of organic-inorganic nanoparticles as lubricant additives. *Tribology Letters*, 22(1):79–84. Reprinted with permission ©2006 Springer Science Business Media, Inc.

Figure 4.26: Hernández Battez, A., González, R., Viesca, J., Fernández, J., Díaz Fernández, J., Machado, A., Chou, R., and Riba, J. (2008). CuO, ZrO2 and ZnO nanoparticles as antiwear additive in oil lubricants. *Wear*, 265(3-4):422–428. Reprinted with permission ©2007 Elsevier B.V.

Figure 4.27: Padgurskas, J., Rukuiza, R., Prosyčevas, I., and Kreivaitis, R. (2013). Tribological properties of lubricant additives of Fe, Cu and Co nanoparticles. *Tribology International*, 60:224–232. Reprinted with permission ©2012 Elsevier Ltd.

Figure 4.28: Hu, C., Bai, M., Lv, J., Liu, H., and Li, X. (2014). Molecular dynamics investigation of the effect of copper nanoparticle on the solid contact between friction surfaces. *Applied Surface Science*, 321:302–309. Reprinted with permission ©2014 Elsevier B.V.

Figure 4.29: Joly-Pottuz, L., Matsumoto, N., Kinoshita, H., Vacher, B., Belin, M., Montagnac, G., Martin, J. M., and Ohmae, N. (2008). Diamond-derived carbon onions as lubricant additives. *Tribology International*, 41(2):69–78. Reprinted with permission ©2007 Elsevier Ltd.

Figure 4.30: Zhang, Y., Tang, H., Ji, X., Li, C., Chen, L., Zhang, D., Yang, X., and Zhang, H. (2013). Synthesis of reduced graphene oxide/Cu nanoparticle composites and their tribological properties. *RSC Advances*, 3(48):26086–26093. Reprinted with permission ©2011, Royal Society of Chemistry.

Figure 4.31: Kheireddin, B. A., Lu, W., Chen, I. C., and Akbulut, M. (2013) Inorganic nanoparticlebased ionic liquid lubricants. *Wear*, 303(1-2):185–190. Reprinted with permission ©2013 Elsevier B.V.

Figure 4.34: Derry, M. J., Smith, T., O'Hora, P. S., and Armes, S. P. (2019). Block Copolymer Nanoparticles Prepared via Polymerization-Induced Self-Assembly Provide Excellent Boundary Lubrication Performance for Next-Generation Ultralow-Viscosity Automotive Engine Oils. *ACS Applied Materials and Interfaces*, 11(36):33364–33369. Reprinted with permission ©CC-BY, https://creativecommons.org/licenses/by/2.0/legalcode

Figure 4.36: Fischer, D., Mues, H., Jacobs, G., and Stratmann, A. (2019). Effect of Over Rolling Frequency on the Film Formation in Grease Lubricated EHD Contacts under Starved Conditions. *Lubricants 2019*, Vol. 7, Page 19, 7(2):19. Reprinted With Permission ©CC-BY 4.0., https://creativecommons.org/licenses/by/4.0/legalcode

Figure 4.37: Li, Z., Ma, S., Zhang, G., Wang, D., and Zhou, F. (2018b). Soft/Hard-Coupled Amphiphilic Polymer Nanospheres for Water Lubrication. *ACS Applied Materials and Interfaces*, 10(10):9178–9187. Reprinted with permission ©2018 American Chemical Society.

Figure 6.1: Gould, B., Demas, N. G., Pollard, G., Rydel, J. J., Ingram, M., and Greco, A. C. (2019). The Effect of Lubricant Composition on White Etching Crack Failures. *Tribology Letters*, 67(1). Reprinted with permission ©2019 Springer Science & Business Media, LLC. PCS Instruments (2005). MTM2 Mini-Traction Machine. Technical report, PCS Instruments. Reprinted with permission ©2005 PCS Instruments.

Figure 6.6: PCS Instruments (2005). MTM2 Mini-Traction Machine. Technical report, PCS Instruments. Reprinted with permission ©2005 PCS Instruments.

Figure 6.7: Scarano, S., Mariani, S., and Minunni, M. (2016). Label free Affinity sensing: Application to food analysis. *Acta IMEKO*, 5(1):36–44. Reprinted with permission ©2016 CC-BY-3, https://creativecommons.org/licenses/by/3.0/legalcode

Figure 7.4: Chinas, F., Vicent, J., and Spikes, H. A. (2003). Mechanism of Action of Colloidal Solid Dispersions. *Tribology Transactions*, 125:552–557. Reprinted with permission ©2003 ASME.